SINGLE VOXEL PROTON MAGNETIC RESONANCE SPECTROSCOPY OF CHILDHOOD BRAIN TUMOURS

by

SIMRANDIP KAUR GILL

**A thesis submitted to the
University of Birmingham
for the degree of
DOCTOR OF PHILOSOPHY**

I

<u>Abstract</u>

Conventional magnetic resonance imaging (MRI) is essential for the management of childhood brain tumours. However, it is increasingly being supplemented with functional techniques such as magnetic resonance spectroscopy (MRS). This thesis investigates how pre-treatment single voxel MRS can aid in diagnosis and surveillance of paediatric brain tumours and identify prognostic biomarkers. Data from multiple centres, scanners from three leading manufacturers and field strengths of 1.5 T and 3 T are incorporated. MRS was analysed using TARQUIN software with metabolite peaks fitted using a simulated basis set to provide metabolite concentrations. Univariate and multivariate statistical tests were used to compare variables. Multi-scanner spectroscopy detected significant differences in common and rare paediatric brain tumours. Diagnostic metabolite profiles were able to confirm tumour on follow-up imaging. Elevated creatine and total choline determined good prognosis in medulloblastoma. Myo-inositol and citrate aided in the characterisation of diffuse pontine gliomas (DIPG). While conventional MRI was unable to identify prognostic markers for DIPG, elevated taurine was found to be significantly associated with a better prognosis. The results encourage the use of MRS as an adjunct to conventional MRI in routine clinical practice. For future studies, accurate assignment of biomarkers will be determined in tumour tissue using *in vitro* high-resolution spectroscopy methods.

<u>Dedication</u>

For my parents Gurdip Singh Gill and Harjeet Kaur Gill,

For your amazing love and support throughout

<u>Declaration</u>

I declare that work presented in this thesis is entirely my own.

The following aspects of this study were performed in collaboration:

1) The magnetic resonance spectroscopy protocol for paediatric brain tumours was decided by Professor Andrew Peet, Dr. Nigel Davies and Dr. Martin Wilson in close discussion with Children's Cancer and Leukaemia Function Imaging Group (CCLG FIG) members

2) MRI and MRS investigations were acquired by radiographers in the Radiology Department at Birmingham Children's Hospital. MRS data transfer and processing aided by the radiographers was performed by the Brain Tumour Research Group in particular Rachel Grazier.

3) MRI and MRS investigations were acquired by radiographers at Royal Marsden Hospital, Sutton, Great Ormond Street, London, Royal Liverpool Children's Hospital, Liverpool and Queen's Medical Centre, Nottingham were collated and made available by Jane Crouch and members of the CCLG FIG.

4) Dr. Martin Wilson developed TARQUIN and devised programming scripts that generated TARQUIN analysis of in vivo MRS for inclusion in the analysis.

5) Reporting of MRI and MRS data at the Birmingham Children's Hospital was done so by Consultant Radiology staff, in particular Dr Lesley Macpherson and Dr Katharine Foster.

6) The central radiological review of brain stem tumours was performed by Dr. Lesley MacPherson, Dr. Dawn Saunders and Dr. Tim Jaspan.

7) Dr. James Davison requested the MRS acquired on patients with inherited metabolic disorders

Acknowledgments

I would like to thank my supervisors Professor Andrew Peet and Dr. Theodoros Arvanitis for their encouragement, support and guidance and for always having faith in me! This work would not have been possible without them.

Thank you to the members of the Brain Tumour Research Group in particular Dr. Martin Wilson and Dr. Nigel Davies, my co-supervisors for their advice throughout specifically computing and statistics guidance and Martin for TARQUIN ☺. Also thank you to other members of the group, Dr. Eleni Orphanidou-Vlachou, Dr. James Davison, Dr. Yu Sun, Dr. Xiaoyan Pan, Rachel Grazier, Jane Crouch, Dr. Jan Novak and Lara Worthington for making me feel so welcome when I first joined and thank you to more recent members of the group Dr. Sarah Kohe, Dr. Ben Babourina-Brooks and Dominic Carlin. Thank you all for providing biscuits, tea and more recently coffee in addition to the friendly atmosphere and discussions. I have never once dreaded coming into work! Thank you to the members of the CCLG FIG for discussion and feedback at both technical and scientific meetings.

A huge thank you goes to the radiology department staff at the Birmingham Children's Hospital particularly the radiographers for acquiring the MRS data and consultant radiologists with special mention for Dr. Lesley Macpherson and Dr. Katherine Foster for providing time and expertise for research studies.

I would also like to thank staff at the tumour registry at Birmingham Children's Hospital and the clinical research nurses and radiology staff at Royal Marsden Hospital, Sutton, Great Ormond Street, London, Royal Liverpool Children's Hospital, Liverpool and Queen's Medical Centre, Nottingham.

Thank you to staff at the Henry Wellcome Building for NMR spectroscopy at the University of Birmingham for helping me understand the theory behind NMR.

An additional, thank you to the charities involved in the funding for my work including Cancer Research UK (CRUK), Engineering and Physical Sciences Research Council (EPSRC), Medical Research Council (MRC) and in particular the National Institute for Health Research (NIHR) for their invaluable funding for the 3 T MR research centre.

Thank you to my amazing mum and dad for always being supportive of every choice I've made and giving me so much love. I am who I am because of you. Love you both dearly and I hope I can continue to keep making you proud.

Thank you to my darling little sister, Pip and Grandma, Beeji Malkit Kaur for always keeping me laughing. Love you both so much! Last but not least, thank you to Aman for providing me with support and for always checking I was coping! ☺

Journal publications

<u>In Press</u>

S.K. Gill, M. Wilson, N.P. Davies, L. MacPherson, English M, T.N. Arvanitis, A.C. Peet. (2013) Diagnosing relapse in children's brain tumors using metabolite profiles. Neuro-oncology, In Press

Book Chapter

Simrandip K. Gill, Ashok Panigrahy, Theodoros N. Arvanitis, Andrew C. Peet, (2012). Magnetic Resonance Spectroscopy of Pediatric Brain Tumors. MR Spectroscopy of Pediatric Brain Disorders. Springer: 45-60.

Conference papers resulting from this work

First Author Oral Presentations

1) 16[th]Annual Scientific Meeting of the British Chapter of the ISMRM, Nottingham, September 2010; **S.K. Gill**, L.M. Harris, N.P. Davies, Y. Sun, K. Natarajan, L. MacPherson, T.N. Arvanitis, D. Hargrave, G.S. Payne, M.O. Leach, F.A. Howe, P.Morgan, D. Saunders, D.P. Auer, T. Jaspan, R.G. Grundy, A.C. Peet, O39-A multi-centre study of 1H magnetic resonance spectroscopy in the diagnosis and prognosis of brain stem tumours in children.

2) 17[th]Annual Scientific Meeting of the British Chapter of the ISMRM, Manchester, September 2011; **S.K. Gill**, M. Wilson, N.P. Davies, Y. Sun , K. Natarajan, L. MacPherson, T.N. Arvanitis, A.C. Peet, O27-1H magnetic resonance spectroscopy for characterising medulloblastomas in children.

3) 21st British Chapter ISMRM Postgraduate Symposium, Bristol, March 2012; **S.K. Gill**, M. Wilson, N.P. Davies, L. MacPherson, T.N. Arvanitis, A.C. Peet, O18-1H Magnetic Resonance Spectroscopy: Do metabolite profiles of brain tumours in children differ at diagnosis to those at first tumour relapse?

4) IPEM Conference 3 T or not 3 T?, Sheffield, March 2013; **S.K. Gill**, M. Wilson, N.P. Davies, L. MacPherson, T.N. Arvanitis, A.C. Peet, Single voxel proton MRS in the brain shows improved metabolite quantification at 3 T in paediatric patients.

Named Author Oral Presentations

IPEM conference on 'Advancements in Body MRI: Clinical Applications and New Techniques', London 2012; J.Novak, **S. K. Gill**, M. Wilson, P. R. Kearns ,T. N. Arvanitis , N.P. Davies, A. C. Peet, Towards combined 1H and 31P Magnetic Resonance Spectroscopy of Childhood tumours of the abdomen.

First Author Poster Presentations

1) 20th British Chapter ISMRM Postgraduate Symposium, Cambridge, March 2011; **S.K. Gill**, L.M. Harris, N.P. Davies, Y. Sun, K. Natarajan, L. MacPherson, T.N. Arvanitis, D. Hargrave, G.S. Payne, M.O. Leach, F.A. Howe, P.Morgan, D. Saunders, D.P. Auer , T. Jaspan , R.G. Grundy , A.C. Peet, P1-A multi-centre study of ^{1}H-Magnetic Resonance Spectroscopy in the characterisation of brain stem tumours in children compared with focal tumours in other parts of the brain using TARQUIN software.

2) 3rd Annual Cancer Research UK & EPSRC Cancer Imaging Conference, London, April 2012; **S.K. Gill**, M. Wilson, N.P. Davies, L. MacPherson, T.N. Arvanitis, A.C. Peet, ^{1}H Magnetic Resonance Spectroscopy Biomarkers of Prognosis for Localised Medulloblastoma in Children.

3) 15th International Symposium on Pediatric Neuro-Oncology (ISPNO), Toronto, June 2012; **S. K. Gill**, M. Wilson, N. P. Davies, L. MacPherson, T. N. Arvanitis and A. C. Peet, Non-Invasive Molecular Characterisation of Medulloblastomas in Children, *Neuro-Oncology*, 14(s1): i143, 2012.

4) 44th Congress of the International Society of Paediatric Oncology (SIOP), London, October 2012; **S.K. Gill**, M. Wilson, N. P. Davies, L. MacPherson, T. N. Arvanitis and A. C. Peet, Novel Biomarkers of Prognosis for Medulloblastoma Using ^{1}H Magnetic Resonance Spectroscopy, *Pediatric Blood and Cancer*, 59(6): 1087, 2012.

Named Author Poster Presentations

1) 15th International Symposium on Pediatric Neuro-Oncology (ISPNO), Toronto, June 2012; N. Davies, **S. Gill**, M. Wilson, L. MacPherson, T. Arvanitis and A. Peet, MRS Shows Metabolite Differences with Age in Children and Young People with Brain Tumours, *Neuro-Oncology*, 14(s1): i143, 2012.

2) 15th International Symposium on Pediatric Neuro-Oncology (ISPNO), Toronto, June 2012; J. Rossiter, T. Arvanitis, K. Natarajan, M. Wilson , N. Davies, **S. Gill**, R. Grazier, J. Crouch, D. Auer, C. Clark, R. Grundy, D. Hargrave, F. Howe, T. Jaspan, M. Leach, L. MacPherson, G. Payne, D. Saunders and A. Peet, A Clinical Trials e-Repository with Integrated Conventional and Imaging Data, *Neuro-Oncology*, 14(s1): i124, 2012.

3) ISMRM 21st Annual Meeting, Salt Lake City 2013; 0970- Effects of Age on Brain Tumour Metabolite Levels Measured by *In vivo* 1H MRS in Children and Young People Are Tumour Type Specific; N.P. Davies, **S. K. Gill**, L. MacPherson, T.N. Arvanitis, A.C. Peet

TABLE OF CONTENTS

X

LIST OF FIGURES

XIV

LIST OF TABLES

ABBREVIATIONS

2HG - 2-hydroxyglutarate

31P MRS - Phosphorous spectroscopy

Ala - Alanine

ANOVA - Analysis of variance

Asp - Aspartate

ATRT - Atypical Teratoid Rhabdoid tumour

BST - Brain stem tumour

Cit - Citrate

CNS PNET - Central nervous system primitive neuro-ectodermal tumour

CNS - Central nervous system

CPC - Choroid plexus carcinoma

CPP - Choroid plexus papilloma

Cranio - Craniopharyngioma

Cr - Creatine

CRLB - Cramer-Rao lower bounds

CT - Computed Tomography

DA - Diffuse astrocytomas

DIPG - Diffuse pontine glioma

EP - Ependymoma

FID - Free induction decay

FWHM - Full width half maximum

GABA - γ-Aminobutyric acid

GER - Germinomas

GG - Gangliogliomas

Glc - Glucose

Gln - Glutamine

Glth - Glutathione

Glu - Glutamate

Glx - Glutamate + Glutamine

Gly - Glycine

GPC - Glycerophosphocholine

Gua - Guanidinoacetate

HR-MAS - High resolution magic angle spinning

Lac - Lactate

LDA - Linear discriminant analysis

L - Lipids+Lactate

LMM - Lipids+ macromolecules

LMM0.9 - Lipids+ macromolecules at 0.9 ppm

LMM1.3 - Lipids+ macromolecules at 1.3 ppm

LMM2.0 - Lipids+ macromolecules at 2.0 ppm

LOOCV - Leave-one-out-analysis

MB - Medulloblastomas

Millimolar - mM

mIns - Myo-inositol
MR - Magnetic resonance
MRI - Magnetic resonance imaging
MRSI - Magnetic resonance spectroscopic imaging
MRS - Magnetic resonance spectroscopy
ms - milliseconds
NAAG - N-acetylaspartylglutamate
NF-1 - Neurofibromatosis type 1
NSA - number of averages
PA - Pilocytic astrocytoma
PCA - Principal Component Analysis
PC - Phosphocholine
PmA - Pilomyxoid astrocytoma
PNET - Primitive neuro-ectodermal tumour
Ppm - Parts per million
PRESS-Point resolved spectroscopy
QC - Quality Control
Q - Q Fit
ROI - Region of interest
sIns - Scyllo-inositol
SNR - Signal-to-noise
SVS - Single voxel spectroscopy
Tau - Taurine
tCho - Total choline
TE - echo time
tNAA or NAA - N-acetylaspartate
TPG - Tectal plate glioma
T - Tesla
WHO - World Health Organisation

CHAPTER 1: INTRODUCTION

CHAPTER 1

1   INTRODUCTION

1.1   Brain Tumours and the Importance of Magnetic Resonance Imaging and Magnetic Resonance Spectroscopy

Brain tumours are the most common solid tumour to present in children (Bleyer, 1999) with approximately 400 cases diagnosed each year within the United Kingdom (Northern Ireland Cancer Registry, 2011, ISD Scotland, 2011, Welsh Cancer Intelligence and Surveillance Unit, 2011, Office for National Statistics, 2010). Consequently, they are the leading cause of death from cancer in children accounting for around 32% of deaths (Stiller C, 2007). Rates of survival for brain tumours are now around 70% at five years compared to only 35% in the 1960s (Cancer Research UK) and while survival rates have significantly improved for other cancers, improvements for brain and spinal tumours have been comparatively steady. It should be noted that paediatric brain tumours consist of a diverse cohort thus improvements in survival are very tumour specific. Whilst some now have a very good prognosis, others have continued to present major challenges, highlighting the need for new techniques for investigation and management.

The emergence of high resolution imaging, firstly Computed Tomography (CT) followed by Magnetic Resonance Imaging (MRI), both non-invasive methods of tumour tissue characterisation, has been crucial to the improvement of the clinical management of children with brain tumours (Panigrahy and Bluml, 2009). MRI scans are now performed on these children at multiple time points in their clinical management: initially at presentation to confirm the presence of a mass and aid diagnosis; prior to a surgical intervention, if recommended for staging and planning; following surgery to assess the

extent of resection; at approximately 3 monthly intervals during adjuvant treatment to monitor effectiveness; and at similar intervals after the end of treatment for tumour surveillance (Gill et al., 2013). Although the use of conventional MRI has become extensive, there are a number of significant limitations with the information that it provides.

Diagnosis of a specific brain tumour at presentation is determined by its appearance on conventional MR images. The assessment of the anatomical and spatial information provided by MRI can pre-operatively reduce the number of possible diagnoses. However, it is not always tumour type or tumour grade specific and overlapping features are often seen in many of the heterogeneous tumours that present in children. Evidence has shown determining tumour grade can be difficult and studies in both adults and children have shown sensitivity of MRI can be limited (Law et al., 2003, Waldman, 2010, Panigrahy and Bluml, 2009, Hargrave et al., 2008). Changes in enhancement upon injection of a contrast agent and tumour appearances can aid in the assessment of tumour progression, however enhancement does not always reflect the changes in the underlying tumour. Alterations in enhancement can occur as a result of local tissue reaction to radiation therapy or 'pseudo-progression', as a result of the expansion of brain volume and changes in permeability of vessels caused by chemotherapeutic agents (Arthurs and Gallagher, 2011, Warren et al., 2000). Administration of chemotherapy can exhibit dramatic improvements in enhancement or 'pseudo-response' rather than true tumour response and differentiating between the two can be problematic (Clarke and Chang, 2009, Batchelor et al., 2007). Surveillance imaging performed at timely intervals is used to assess the extent of residual disease. This requires careful planning with treatment

schedules to avoid over and/or underestimation of disease but does not always provide a definitive diagnosis. The assessment of apparent adverse tumour features has shown limited prognostic significance (Hargrave et al., 2008, Liu et al., 2009). Identifying prognostic markers would be useful, particularly for tumours that are diagnosed on clinical and imaging grounds alone.

Although MRI is an essential tool for brain tumour assessment, the drawbacks outlined highlight that the benefits may be enhanced if supplemented with additional functional MR methods for example magnetic resonance spectroscopy (MRS). MRS can attempt to address the unanswered questions that conventional methods are unable to.

Proton magnetic resonance spectroscopy (1H MRS) is a non-invasive, *in vivo* method that measures the biochemical information within a region of interest (ROI) defined as a voxel(s). The voxel(s) samples a volume of tissue, measuring the chemicals present within it thereby providing information on cellular metabolism. In theory, the ROI of choice can be within any tissue of the body but the technique is predominantly performed in the brain. Localisation of chemical information termed metabolites can be performed using two approaches, either as a single voxel method, single voxel spectroscopy (SVS) or multi-voxel method, magnetic resonance spectroscopic imaging (MRSI). SVS acquires metabolite information from one voxel whereas MRSI acquires from multiple voxels thus providing chemical information across multiple regions in the tissue. The resultant output is a spectrum of peaks that correspond to the metabolites found in the tissue and each metabolite is determined by its position in the spectrum. A number of metabolites are commonly identified in the brain and these include n-acetylaspartate or NAA/tNAA,

4

(marker of neurons), creatine or Cr (marker of the energy state of cells), total choline or tCho (a marker of cell proliferation) and lactate or Lac (marker of abnormal energy metabolism). It should be noted that each signal peak can give rise to more than one metabolite, for example total choline is a sum of phosphocholine, glycerophosphocholine and free choline hence often referred to as total choline. Further details on these signals, their positions in spectrum and their roles are given in Chapter 3 (see section 3.5).

When interpreted alongside conventional MRI, MRS can add new information to many clinical situations. Non-invasive diagnosis using MRS has been the focus of many research studies (Panigrahy et al., 2006, Harris et al., 2011, Davies et al., 2008, Kovanlikaya et al., 2005) but is only the prelude to the improved characterisation of tumours. One of the most important strategies in the management of childhood cancer is the identification of prognostic factors, which have improved tumour characterisation and allow stratification of treatment according to risk (Zacharoulis and Moreno, 2009, Dufour et al., 2012). A number of prognostic MRS biomarkers have been discovered and await formal evaluation in a clinical trial setting (Wilson et al., 2013, Marcus et al., 2007). The non-invasive nature of MRS means scans can be performed at multiple time points, which is useful for monitoring the effectiveness of treatment. Identifying early markers of treatment response would be favourable and there is increasing evidence that MRS can provide these in some situations (Steffen-Smith et al., 2012, Laprie et al., 2005). Determining post-treatment residual masses on MRI can be challenging and there is promise that MRS could aid with this. Similarly, distinguishing radiotherapy related changes from recurrent tumour cannot always be achieved by conventional MRI and MRS could help provide extra valuable information.

1.2 Development of MR spectroscopy studies

The field of MR spectroscopy has evolved and developed over time and is now showing encouraging results in many clinical scenarios. The initial focus of early spectroscopy studies was on adults with brain tumours with few reports on paediatric cohorts. The rarity of brain tumours in children has hindered its application in paediatrics resulting in small cohort numbers for studies (Howe et al., 2003, Castillo et al., 2000, Hattingen et al., 2008a, Sibtain et al., 2007b, Wang et al., 1995). The tumours diagnosed in children and their clinical course differ from those that present in adults, with adult tumours often being more malignant (Jones et al., 2011). This prevents the application of the same spectroscopy findings in adult and paediatric cohorts (Porto et al., 2011, Jones et al., 2011).

With paediatric brain tumours most commonly located in the cerebellum, initial studies reported MRS findings for these tumours (Wang et al., 1995, Davies et al., 2008, Harris et al., 2008). MRS of rare tumours were reported as cases studies (Horská et al., 2001, Cirak et al., 2005). The main focus of initial studies was predominantly tumour diagnosis and characterisation with few studies focusing on prognosis. Studies probed the potential of spectroscopy to yield information during treatment monitoring, however this combined adult and paediatric cases into one (Weybright et al., 2005).
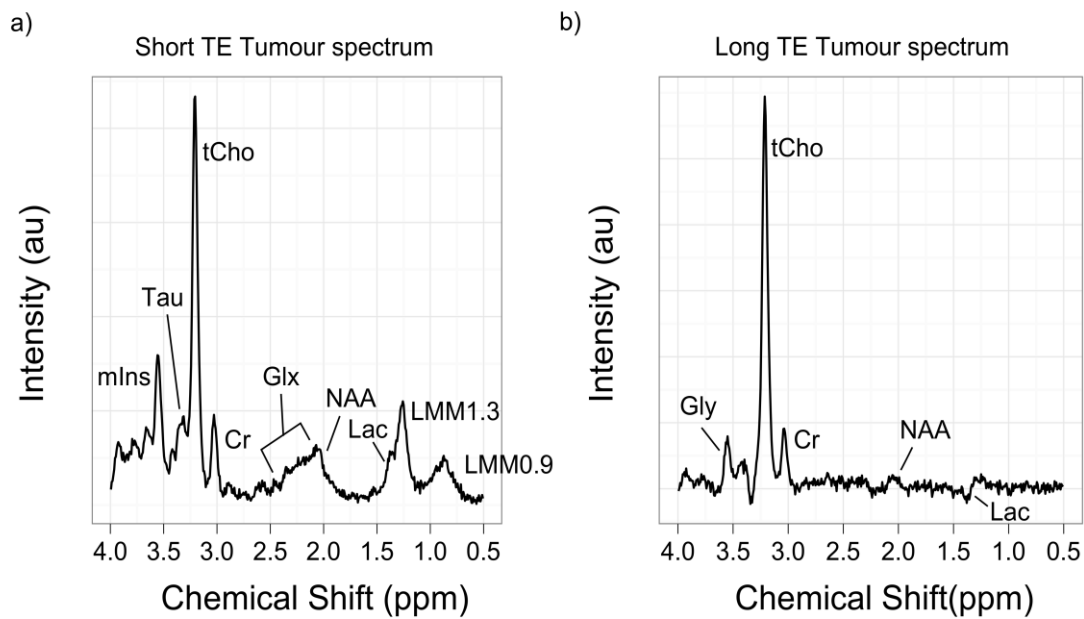
Figure 1.1 Comparison of MRS acquired pre-diagnosis at a) short TE and b) long TE from the same brain tumour patient (MB). Abbreviations: medulloblastoma, MB; mIns, myo-inositol; Tau, taurine; tCho, total choline; Cr, creatine; Glx, Glutamate+Glutamine; NAA, N-acetylaspartate; Lac, lactate; LMM0.9, lipids at 0.9 ppm; LMM1.3, lipids at 1.3 ppm

The signal intensity of metabolites seen in the spectrum can change as a result of alteration of the parameter called echo time (TE). For example long TE (approximately 135-270 ms) allows the detection of limited metabolites whereas short TE (approximately 20 to 40 ms) allows the detection of more metabolites as shown in Figure 1.1.

Despite the known benefits of short TE spectroscopy, initial studies were performed at long TE. This was because long TE provides metabolite profiles that are simpler to interpret with no dominance of lipids which are therefore easier to quantify (Figure 1.1) (Howe and Opstad, 2003, Panigrahy et al., 2010b). With improvements in metabolite quantitation, the value of short echo time spectroscopy is being highlighted. The increased metabolite information, reduces metabolite signal loss and increases signal-to-noise ratio (SNR) (Panigrahy et al., 2010b). This has enabled the identification of tumour

subtype specific markers for aiding characterisation that is not possible at long echo time (Kovanlikaya et al., 2005, Panigrahy et al., 2006, Peet et al., 2007b, Wang et al., 1995).

For the interpretation of results, simple methods such as peak height measurements were used initially. These were readily available and found to be effective (Wang et al., 1995, Harris et al., 2007). With radiologists often not having access to spectroscopy analysis tools, this method can be easily applied using standard scanner manufacturer software. A study by Harris et al. (2007) demonstrated a flow scheme by which the spectroscopy of paediatric cerebellar tumours could aid diagnosis by measuring the peak heights determined by manufacturer software (Harris et al., 2007). The reproducible results obtained from multiple users illustrated the robustness of the technique. This could be useful for particular tumour types and while peak heights are easy to use they are only surrogates for metabolite concentrations as many metabolites do not consist of a single peak in one position but instead a number of overlapping peaks (Helms, 2008, Tong et al., 2004, Hattingen et al., 2008a). It is peak area determined by integration rather than peak height that is proportional to metabolite concentration. Early studies reported peak area findings relative to a metabolite in the spectrum. While ratios allow immediate inferences to be made, they eliminate determining the usefulness of the metabolite used as the denominator and assume it remains unchanged (Helms, 2008, Jansen et al., 2006). A number of studies have utilised Cr as a denominator assuming it to be stable in both normal brain and pathological states. However, this has now been shown to alter significantly resulting in confounding observations (Li et al., 2003). Fewer peaks are sufficient to aid diagnosis on a general level, but for complex analyses where comparisons are made between different subjects, tumour types, scanners and sequence

protocols this method is less useful. These pitfalls encouraged the move towards apparent absolute metabolite quantitation.

Quantitation analysis software is often complex and very technical with a choice of different packages available to use. This often makes it difficult for an inexperienced spectroscopist to decide on the software to use and how to interpret the findings. Improved metabolite quantitation is seen when the MR spectrum is fit to a set of individual metabolite spectra, which can be acquired experimentally or be simulated (Wilson et al., 2010). The whole spectrum can be fitted automatically to produce a list of metabolites and their relative concentrations. The most commonly used software available commercially for this is LCModel (Provencher, 2001). The combination of metabolite fitting and using the water signal (acquired from an additional water scan taken at time of acquisition) as a concentration reference is proving to be a powerful technique for the automated processing of single voxel spectroscopy (SVS) data and is essential for consistency within and between studies (Tong et al., 2004).

Simple statistical methods for assessing differences in metabolite information between tumours, although promising, do not use the information acquired to the full potential. This has led to the introduction of simple pattern recognition methods (Preul et al., 1998). The main aim of these is to extract information from several input features to classify tumours. The most commonly used statistical tests include principal component analysis (PCA) and/or linear discriminant analysis (LDA) with some using the approach of a series of statistical tests to extract features from MRS data (Hagberg, 1998). Further

detail on these is given in chapter 4. Pattern recognition techniques are more powerful with large datasets.

1.3   Advances in MRS

Following an increase in the body of work on brain tumour diagnosis and characterisation, paediatric studies have become more focused on identifying prognostic information (Blüml et al., 2011, Yamasaki et al., 2011, Steffen-Smith et al., 2011). This is of particular interest in diffuse pontine glioma (DIPG), a tumour of the brain stem because it is diagnosed on clinical and imaging grounds alone (Hargrave et al., 2008). Tumours of the brain stem are extremely rare, accounting for 10-25% of brain tumours in children (Hargrave et al., 2006). MRS of a large cohort of brain stem tumours from a multi-centre cohort is investigated in this thesis. Larger cohort numbers are important to establish enough cases for a robust statistical analysis. Publications highlighting the benefits of using MRS have led to large studies including rare tumour types (Harris et al., 2011) and this has been further explored to establish distinguishing features of rare tumour types to aid pre-operative diagnosis. The introduction of higher field strength scanners, the strength of which is determined in units of Tesla, is now on the increase. There is an increasing interest in how high field 3 Tesla (3 T) will provide benefits over 1.5 T in clinical practice. Although theoretical benefits of the technique including increased SNR and peak separation are known, it is less well known how this translates in practice (Dagia and Ditchfield, 2008). While spectroscopy at 1.5 T is useful in many clinical scenarios there is still the need for an improved discrimination between different brain pathologies. A number of groups have performed comparisons with spectroscopy data collected at 1.5 T and 3 T to evaluate its use (Kim et al., 2006, Barker et al., 2001) but

paediatric studies making this comparison have not yet been published to our knowledge and this has been investigated in this body of work.

Pattern recognition methods have become very popular with research groups for the classifying of brain tumours using MRS. They give excellent accuracy rates for tumour diagnosis but are not currently available for use in routine clinical settings. PCA and LDA can be performed on either the whole MR spectrum or a list of parameters which have been extracted from it, for example; metabolite concentrations (Davies et al., 2008, Hao et al., 2009). More complex methods, such as artificial neural networks and support vector machines, have also been used and shown to have high accuracy (Hao et al., 2009). Spectroscopy classifiers can be further implemented with imaging, clinical and other information to increase the robustness and accuracy of the analysis to develop multimodal classifiers (Graves et al., 2001). This will become increasingly more important in clinical practice with the increasing implementation of functional imaging to support conventional sequences. Classification using these methods is most effective when a small number of diagnoses are being considered and the effect of combining tumour groups to give smaller numbers of larger classes has proven an effective strategy (Davies et al., 2008). A recent study by Vicente et al. (2013) has illustrated excellent diagnostic accuracy for a multicentre cohort of paediatric brain tumours and this has also been explored in this thesis (Vicente et al., 2013). The next focus for spectroscopy studies would be optimisation in search for prognostic markers.

The current understanding of cancer pathogenesis is that genetic events, for example gain of functional genes termed oncogenes, lead to cancer cell transformation. This is a

multistep process where accumulation of genetic aberrations increases over time. Oncogenes are involved in signalling transduction cascades that are related to growth, division and survival of cells (Dang, 2012, Moestue et al., 2011). This has led to the discovery that oncogene targeted therapies can inhibit cancer signalling cascades and be used to treat cancer (Leitner et al., 2011). Monitoring these changes using MRS particularly at 3 T where spectral dispersion is greater, will prove useful as major metabolic pathways are regulated by oncogenic signalling pathways. A preliminary investigation of how the metabolic changes seen in medulloblastoma spectra can be explained by the signalling pathways identified has been explored. This is of particular interest as four molecular subgroups of the disease with varying prognoses have been identified. Each subgroup is speculated to have different dominant signalling pathway that aids pathogenesis (Taylor et al., 2012).

The diagnosis of brain tumours on histopathology is determined using the World Health Organisation (WHO) grading scheme from I to IV (Louis et al., 2007). Mutations in two genes; isocitrate dehydrogenase I and II (IDH1 and IDH2), have been found to be prevalent in WHO grade II and III gliomas in adults (Yan et al., 2009, Balss et al., 2008). This led to the discovery that IDH mutant enzymes produce high levels of metabolite 2HG (2-hydroxyglutarate). 2HG is not easily measured using standard spectroscopy protocols but through manipulation of spectroscopy parameters the metabolite can be identified and measured. A study by Choi et al. (2012) was the first to show spectroscopy was able to identify a direct metabolic consequence of a genetic mutation in a cancer cell (Choi et al., 2012). It is hoped that a similar methodology can be applied to other tumour types

and that manipulating spectroscopy parameters will enable sequences to be optimised for a more tailored approach during treatment monitoring.

Most applications of spectroscopy in paediatrics have been for brain tumours and brain lesions. In adults spectroscopy has been well studied in breast and prostate lesions (Morse et al., 2009, Costello et al., 1999) but these very rarely occur in children. With the introduction of high field scanners, researchers have worked on addressing the pitfalls of performing spectroscopy on body lesions, such as renal and liver masses to develop the technique for use in clinical practice. Technical issues for example motion artefacts associated with diaphragm and/or heart and ineffective water suppression need to be addressed (Fischbach and Bruhn, 2008, Katz-Brull et al., 2005). With the practical drawbacks of the technique, the method is currently being developed as a research tool before its application in a clinical setting.

1.4   Aims and Objectives

Overall Aims

The aims of this work were to investigate how single voxel MRS can non-invasively aid in diagnosis, prognosis and surveillance of brain tumours in children. The research focuses on the use of multi-centre and multi-scanner data, analysis of tumour subgroups and the incorporation of data at the higher field strength of 3 T.

Objectives

1. To compare *in vivo* mean metabolite profiles of brain tumours in children with the inclusion of both common and rare types at 1.5 T and 3 T

2. To investigate the use of metabolites and metabolite profiles as diagnostic aids in paediatric brain tumours

3. To determine how metabolite profiles of brain tumours differ from diagnosis to first relapse and investigate how this can help to accurately diagnose and characterise tumour relapse or progression

4. To investigate the variability of *in vivo* metabolite profiles within subgroups of brain tumours, in particular medulloblastoma and brain stem tumours

5. To establish biomarkers of prognosis in medulloblastoma and diffuse intrinsic pontine glioma

6. To determine whether the higher field strength of 3 T demonstrates an improvement in metabolite determination and quality of data acquired in paediatric patients

1.5   Thesis organisation and contributions

The classification of paediatric brain tumours and a comprehensive review of the current published MRS literature for these tumours have been summarised in chapter 2. The theory of MRS pertinent to the research is outlined in chapter 3 and followed by a summary of the statistical methodology used to analyse the spectroscopy data in chapter 4.

Chapter 5 focuses on characterising metabolite profiles in a large cohort of paediatric brain tumours obtained on multiple scanners at multiple centres including 1.5 T and 3 T. Mean metabolite concentrations are determined and compared for various tumour groups and an investigation into the use of metabolites in tumour diagnosis undertaken, meeting objectives one and two. Multi-centre studies in the MRS of childhood brain tumours are lacking and there are none which are large enough to investigate the rarer tumours or report results at two field strengths. These weaknesses have failed to show the robustness of the technique thus this chapter aims to overcome this.

To meet objective three, Chapter 6 presents a study in which paired comparisons of metabolites at diagnosis and first tumour relapse are made within a heterogeneous cohort of malignant tumours. The use of metabolite profiles in diagnosing tumour relapse is explored. Previous studies of tumour MRS at diagnosis and relapse have focused on adults and used single metabolites or their ratios. Brain tumours in children have a different spectrum of disease to those in adults and the tumours have varied metabolite profiles highlighting the importance of paediatric specific studies. This work has been presented as an oral presentation at the 16th Annual Scientific meeting of the British Chapter of the ISMRM, 2010 and poster presentation at the 20th British Chapter ISMRM Postgraduate, 2011.

Chapter 7 uses metabolite concentrations to identify markers of prognosis in medulloblastoma and makes comparisons with other clinical factors related to prognosis and used in treatment stratification to meet objective 4. Unlike previous analyses that have identified metabolites of prognostic significance in heterogeneous cohorts of brain tumours, this study is the first to present markers specific to a subtype, medulloblastoma. This is of particular interest in light of recent reports that medulloblastoma consists of four different molecular subgroups with varying prognoses. Part of this work has been previously presented as an oral presentation at the 17th Annual Scientific meeting of the British Chapter of the ISMRM, 2011. This work has also been presented as a poster at 3rd Annual Cancer Research UK and EPSRC Cancer Imaging conference, 2012 and at the 44th Congress of the International Society of Paediatric Oncology (SIOP) the abstract of which is now printed in Paediatric Blood and Cancer.

Chapter 8 investigates MRS of brain stem tumours. Spectroscopy is potentially valuable for these tumours as they are often diagnosed on clinical and imaging grounds alone and commonly the cause of diagnostic dilemmas. This multi-centre analysis investigates both diagnostic and prognostic markers in these tumours meeting objectives four and five. This study of rare tumours is large compared to previous analyses and is supported by the inclusion of multi-centre data. This work was presented as an oral presentation at the 21st British Chapter ISMRM Postgraduate Symposium, 2012 and is currently *In Press* for publication in Neuro-oncology.

Chapter 9 details the analysis of spectroscopy data acquired at a higher field strength of 3 T and compares it to 1.5 T data, objective six. To the best of our knowledge this is the first analysis that aims to determine whether the higher field strength of 3 T shows any benefits for spectroscopy in terms of metabolite determination and quality of data acquired in a paediatric population of patients. This is particularly important with the increasing introduction of higher field strengths in clinical practice. This work has been previously presented as an oral presentation at IPEM conference, "3 T or not 3 T?", 2013. The final chapter includes the conclusions drawn from this work and discusses future work.

CHAPTER 2: PAEDIATRIC BRAIN TUMOURS AND THE APPLICATION OF MAGNETIC RESONANCE SPECTROSCOPY

CHAPTER 2

2 PAEDIATRIC BRAIN TUMOURS AND THE APPLICATION OF MRS

2.1 Brain tumours in children and adults

Brain tumours comprise of approximately 20-25% of all cancer diagnoses in children between 0-14 years of age, with approximately 10% of tumours occurring in 15-19 year olds (Gurney and Bondy, 2006). Adults and children's brain tumours are known to be different with those in children found to be more heterogeneous (Slavc, 2011). Adult brain tumours are either WHO grade III astrocytoma, anaplastic astrocytoma (AA) or glioblastoma multiforme (GBM, grade IV) whereas paediatric brain tumours consist of WHO grades I to IV with pilocytic astrocytoma (PA, grade I), medulloblastoma (MB, grade IV) and ependymoma (EP, grade II or III) being the most common. The majority of tumours in children occur infratentorially in the cerebellum, whereas in adults most occur supratentorially (Vézina, 2005). The therapeutic strategies for adults and children also vary. The role of chemotherapy in children has been found to be more effective than in adults and radiotherapy is mostly administered to children above the age of three due to the expected long-term side effects. In general the outcome of children with brain tumours is more favourable than in adults however, this does vary between tumour types (Pollack, 1999). Environmental risk factors as a cause of cancer in children are rare and only previous exposure to ionizing radiation has been confirmed to be linked (McKinney, 2004). Evidence has shown that many childhood cancers occur as a result of aberrations in early developmental processes (Gurney and Bondy, 2006). There are a small number of genetic risk factors that predispose children to brain tumours. These include neurofibromatosis type 1 and 2 (pilocytic astrocytoma, low-grade gliomas,

ependymoma), Turcot syndrome (medulloblastoma and high-grade glioma), Li-Fraumeni

syndrome, Gorlin syndrome, and von Hippel-Lindau syndrome (hemangioblastoma) but

these account for only a small proportion of tumours (Dubuc et al., 2010, Carlotti et al.,

2008).

2.2 Classification of childhood brain tumours

For children who have surgery, their brain tumour is classified by histopathology and

graded using the 2007 WHO Classification of Tumours of the Central Nervous system

(Louis et al., 2007). For those who do not have surgery, the tumours are diagnosed on

characteristic clinical and imaging findings. Figure 2.1 summarises the approximate

incidence of common CNS tumours in children (Gurney and Bondy, 2006)
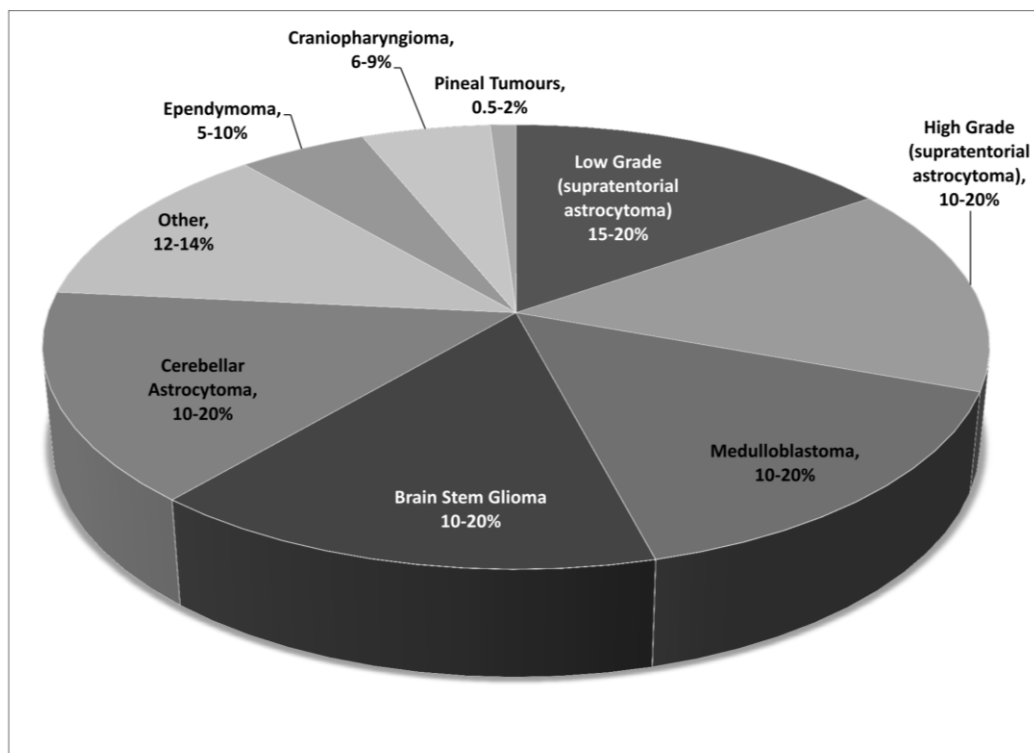
Figure 2.1 Pie chart demonstrating the approximate incidence of common central nervous system tumours in children. The figure includes both those diagnosed on histopathology and clinical and imaging grounds (Gurney and Bondy, 2006).

2.2.1 Glial

Glial tumours make up approximately 60% of brain tumours in children. Pilocytic astrocytoma (PA) and ependymoma (EP) are the most common subtypes diagnosed from this diverse group (Gurney and Bondy, 2006).

<u>Astrocytomas</u>

Astrocytomas are the most commonly occurring glial tumours in children, making up, approximately 50% of all brain tumours. Their behaviour and treatment depend greatly on their grade. PA, classified as WHO grade I tumour with a low mitotic rate, rarely infiltrates the surrounding brain. It can occur in various locations in the brain but is particularly common in the cerebellum and optic pathway (Gan and Haas-Kogan, 2010). Children with mutations in the neurofibromatosis 1 (NF-1) gene have an increased risk of developing PA, particularly in the optic pathway (Listernick et al., 2007). The prognosis of patients diagnosed with PA is generally very good with some studies reporting a five-year survival of 100% and 10 year survival of 95.8%, following diagnosis (Burkhard et al., 2003). Cerebellar tumours have an excellent prognosis but supratentorial tumours of the optic pathway and thalamus are more difficult to treat. Those in the optic pathway often present with visual loss and preserving vision is a major challenge (Gurney and Bondy, 2006). Some PA metastasise and a recent more aggressive variant, pilomyxoid astrocytoma, has been recognised by the WHO classification (Komotar et al., 2004). Identifying these more aggressive variants by non-invasive imaging is the current goal.

Diffuse astrocytomas (DA, grade II) have a more varied course, with some having a very poor prognosis. These tumours can be heterogeneous and often consist of high grade

areas within the tumour resulting in the progression of the whole tumour to a higher grade lesion (Broniscer et al., 2007). The clinical course of these patients and progression of tumour is difficult to predict based on MRI (Wessels et al., 2003). High grade (grade III and IV) astrocytomas including AA (III) and GBM (IV) are aggressive tumours with a poor prognosis (Piette et al., 2008).

EP makes up approximately 6-10 % of brain tumour diagnoses with over half of cases diagnosed below the age of 5 (Smyth and Rubin, 2010, Blaney et al., 2006). The majority are located in the intracranial region with two thirds arising in the posterior fossa. Metastases are rare but the management of the tumour in the primary site is often challenging. They are classified as either WHO grade II or III. The current treatment strategy for these tumours is surgical resection, followed by radiotherapy if the child is old enough and chemotherapy in the very young (Mack and Taylor, 2009, Zacharoulis and Moreno, 2009). Overall survival ranges from 39% to 64% at 5 years (Kilday et al., 2009).

2.2.2 Embryonal

Embryonal tumours are highly malignant tumours seen predominantly in children. Primitive neuroectodermal tumours are the largest subgroup of embryonal tumours.

<u>Primitive Neuroectodermal Tumours (PNET)/Medulloblastoma (MB)</u>

PNET are composed of poorly differentiated neuroepithelial cells (Sandberg and Stone, 2008). Distinct subgroups are seen, characterised by their location with those found in the cerebellum termed medulloblastoma and those found elsewhere as supratentorial PNET (CNS PNET). Whilst closely related histologically, they have been shown to form separate groups on gene expression analysis (Pomeroy et al., 2002). The five-year survival

rate for the group as a whole is around 40-70% but differs between the groups and also varies with stage and age at diagnosis (Sandberg and Stone, 2008). Multiple signalling pathways have been associated with the growth and development of MB. Some of the developmental pathways include WNT (Wingless-related integration site), c-Met, erB2, SHH (Sonic Hedgehog), Notch and Chromosome 17 abnormalities. There is an interest in using these prognostic groups and their pathways as targets for new therapy (Guessous et al., 2008) .

2.2.3 Rare tumour types

<u>Atypical Teratoid Rhabdoid (ATRT)</u>

ATRT is a rare embryonal tumour with a highly malignant nature. The tumour is classified as WHO grade IV with a poor prognosis and arises in very young children. The true incidence is unknown as it has only recently been identified as a separate entity but is speculated to be around 1-2% (Heck et al., 2013). ATRT was the first tumour for which a candidate tumour suppressor gene was found. INI1 gene is found to be either mutated or deleted in ATRT (Reddy, 2005, Heck et al., 2013) .

<u>Choroid Plexus tumours</u>

Choroid plexus tumours represent 3% of brain tumours in children and are often diagnosed below the age of five. Two of the more commonly occurring choroid plexus tumours are choroid plexus papilloma (CPP) and choroid plexus carcinoma (CPC) of which CPP is WHO grade I and CPC is WHO grade III. This is reflected in the poor five-year survival of CPC which is around only 26%. Surgery is usually the treatment of choice although this can prove problematic in CPC due to its high vascularity (Due-Tønnessen et

al., 2001). More recently difficulties in distinguishing between CPP and CPC on histopathology have resulted in an additional intermediate WHO grade choroid plexus tumour, atypical choroid plexus papilloma (WHO grade II) being identified (Wrede et al., 2009).

Pineal Tumours

Pineal tumours are those defined as arising from the pineal body and surrounding structures. Although the overall incidence of tumours in this region is rare (0.5-2%) the different types that present are diverse. The incidence of pineal tumours depends on the age and ethnicity of the patient (Echevarría et al., 2008). Germ cell tumours, germinomas (GER) are the most common and have a long term survival rate of over 90% (Konovalov and Pitskhelauri, 2003) whereas pineoblastomas, a category of supratentorial primitive neuroectodermal tumours (sPNETs) found in the pineal gland are highly malignant with varying prognosis dependent on age (Gilheeney et al., 2008, Tate et al., 2012). The infrequent presentation of these tumours makes them difficult to diagnose and manage (Packer et al., 2000).

Neuronal and mixed

Ganglioglioma(GG)

Gangliogliomas (GG) are WHO grade I tumours composed of a mixed histology of astrocytes and atypical ganglion cells. The tumours can occur in any region of the brain and have an incidence of 2-10%. The primary treatment strategy is surgical resection following which prognosis is good (Rocco and Tamburrini, 2006, Castillo, 1998).

Craniopharyngioma (Cranio)

Craniopharyngioma (Cranio) is a non-glial intracranial tumor derived from embryonal tissue. The tumour is relatively rare representing 6-9% of all childhood brain tumours. Cranio (WHO grade I) are slow growing tumours and symptoms often present 1-2 years prior to a formal diagnosis being made. The overall five-year survival in children is around 85% (Muller, 2008, Garnett et al., 2007).

2.2.4   Classification of tumours with no histopathology

Many childhood brain tumours are diagnosed without histopathology and instead diagnosed based on clinical and imaging grounds alone. Improving the diagnosis of these tumours using a non-invasive method is of great interest.

Brain Stem Tumours (BST) and Diffuse Pontine Gliomas (DIPG)

Brain stem gliomas account for 10-20% of CNS tumours among children (Donaldson et al., 2006). They are usually diagnosed using clinical criteria and conventional MRI characteristics, with a biopsy only being performed if the diagnostic criteria are not met. The majority of brain stem gliomas are made up of DIPG. DIPG historically have a very poor prognosis partially because of the location of the tumour but also because of its poor response to adjuvant treatment. The median time for progression is around 5-6 months with mean survival under 12 months (Hargrave et al., 2006). Very few studies have performed biopsies on these patients; however it is now becoming apparent that the lack of biopsy material is hindering the advances in treatment for these patients resulting in a limited understanding of the biology of these tumours. The studies that have presented cases where DIPG have been biopsied found the majority to be

astrocytomas, usually of grade II or III (Hargrave et al., 2006). A different study found at autopsy the majority of these tumours were GBM (Remke et al., 2011). Key differences in MRS have been previously reported for DIPG and other astrocytomas (Panigrahy et al., 2008). The remaining 20% of brain stem tumours are focal and are either low grade or high grade astrocytomas (Sanai and Prados, 2010). NF-1 positive patients are also prone to developing diffuse brain stem lesions, which are less aggressive but often result in diagnostic dilemmas on conventional sequences (Listernick et al., 2007) .

Optic Pathway Gliomas

Tumours of the optic pathway, particularly in children with NF-1 are commonly not biopsied due to the risks posed to vision and also because they are invariably PA (Gan and Haas-Kogan, 2010).

Germ Cell Tumours

Germ cell tumours can be located anywhere in the midline of the brain with the pituitary and pineal glands being the most common sites. Surgical resection is not part of the management for most malignant germ cell tumours and therefore a non-invasive diagnosis could entirely avoid surgery. For secreting germ cell tumours, a non-invasive diagnosis is already achieved using serum markers, however non-secreting tumours require a biopsy (Kendi et al., 2004, Blaney et al., 2006).

2.3   Application of magnetic resonance spectroscopy in paediatric brain tumours

2.3.1   Non-invasive diagnosis and characterisation

The most studied application of SVS is its use as a non-invasive diagnostic aid. A review of MR reports compared with final pathology at Los Angeles Children's Hospital found that 83% of cases were correctly diagnosed by radiologists between January 2005 and November 2007 after the introduction of MRS, compared with only 63% of cases between June 2001 and January 2005, a result that was statistically significant. To prove this was not simply a learning effect, the older set of cases were re-reviewed and an improvement from 63% to 71% was seen. Although this partially attributed to more thorough imaging workup, the accuracy is still short of that seen in the group where MRS is available. This provides evidence for the importance of MRS in aiding diagnosis and characterisation of brain tumours as an adjunct to MRI (Panigrahy et al., 2010b). The use of MRS with statistical tests and pattern recognition methods using metabolites is a powerful method of yielding accurate and robust results. The metabolic features of normal paediatric brain and common paediatric brain tumours have been reported in a number of studies and a summary of the current literature has been reported below.

A number of metabolites are commonly identified in brain and brain tumour spectra. The mostly commonly identified and their roles are listed below. These include:

- Total Choline (tCho), peak at ~3.2 ppm, marker of cell turnover

- Creatine (Cr), peaks at ~3.02,3.94 ppm, marker of abnormal energy metabolism

- N-acetylaspartate (NAA/tNAA), peak at ~2.0 ppm, presence of neurons

- Myo-inositol (mIns), peak at 3.6 ppm, involved in the activation and proliferation of glial cells

- Glutamine (Gln), Glutamate (Glu) and Glutamate+Glutamine (Glx), peaks around 2.0-2.6 ppm. Gln is the storage form of Glu, involved in every metabolic task of proliferating tumour cells and Glu is an excitatory neurotransmitter

- Taurine (Tau), ~3.3 ppm, role as osmolyte and apoptotic marker

- Glucose (Glc), peaks at ~ 3.43, 3.80 ppm, provides energy for all proliferating cells

- Lactate (Lac), peak at ~1.3 ppm, marker of anaerobic metabolism and aerobic glycolysis

- Citrate (Cit), ~2.6 ppm, marker of malignant progression

- Glycine (Gly), ~ 3.6 ppm, inhibitory neurotransmitter and antioxidant

- Scyllo-inositol (sIns), ~3.34 ppm, precursor of mIns and related to membrane synthesis

- Lipids and macromolecules (LMM), peaks at ~0.9, 1.3, 2.0 ppm, marker of membrane degradation, apoptosis and necrosis

- Guanidinoacetate (Gua), ~3.78 ppm, precursor of creatine

- Alanine (Ala), ~1.48 ppm, non-essential amino acid

Further detail on these metabolites is given in 3.5.

Normal paediatric brain

Features of normal brain spectroscopy include elevated NAA, decreased tCho, decreased lipids at 0.9 ppm and 1.3 ppm (Davies et al., 2008).

It should be noted that metabolites are not homogenously distributed across all structures of the brain. The regional variation in the concentration of metabolites within the brain in children has been previously studied using single voxel MRS (Pouwels et al., 1999).

Single voxel MRS was performed on 97 children who were either healthy or suffered from mental retardation, movement disorders, epilepsies, neoplasm, or vascular malformation. Metabolite quantitation was performed in the cortical grey and white matter, cerebellum, thalamus and basal ganglia in six age groups from infancy to adulthood and measured metabolites included NAA, Cr , tCho, mIns, Glu, Gln and Tau. Results show NAA is elevated in the grey matter, cerebellum and thalamus particularly during the first few years of life and remains constant in the white matter and basal ganglia. Creatine is highest in the cerebellum, followed by the basal ganglia, thalamus, grey matter and white matter. Choline containing compounds are highest in cerebellum and the lowest in the grey matter. Concentrations of mIns remain constant in most brain regions except for the cerebellum where the highest levels are observed. Glu and Gln are on the whole constant throughout the brain. However, a 50% reduction in Gln is seen in white matter from early childhood to adulthood. Tau is found to decrease with age in both the grey matter and the cerebellum, with the highest concentrations in infancy. Lower concentrations of Tau are seen in the white matter and thalamus and again

decrease with age whereas concentrations remain constant in the basal ganglia (Pouwels et al., 1999).

Pilocytic Astrocytoma (PA)

Spectroscopy studies include comparisons of PA with normal brain, ependymoma (EP), medulloblastoma (MB), and all other childhood brain tumours (All Other), respectively. A comparative study has also been performed between childhood and adult PA.

PA versus uninvolved brain

A study by Davies *et al.* (2008) compared 12 PA spectra with four control spectra acquired from four patients, in remission, for posterior fossa tumours where SVS was performed on non-involved brain. Qualitative analysis of the PA mean spectra showed very low Cr at 3.0 ppm with a high tCho/Cr and moderate levels of lipids and Lac. In addition, a discernible tNAA peak was seen (Davies et al., 2008).

PAs vs. All other tumours

Panigrahy *et al.* (2006) compared PA from all locations in the brain with all other brain tumours (All Other). No difference between PA located supratentorially (n=6) and infratentorially (n=11) was seen, resulting in a pooled analysis forming a single group. The analysis revealed the most significant differentiators between PA and All Other, were low mean levels of Cr, mIns, Tau and tCho. Evaluation of concentration ratios demonstrated low Cr/tCho was the most significant differentiator of PAs from All Other. Mean levels of Glutamate+Glutamine (Glx)/Cr, NAA/Cr, NAA/tCho and Gln/tCho in PA were significantly

higher than in All Other. The ratios of mIns/tCho, Tau/tCho and Tau/ Cr were significantly lower in PA (Panigrahy et al., 2006).

PA vs. EP and MB

Davies *et al.* (2008) compared PA, EP and MB. Myo-inositol was shown to be the only significantly different metabolite between the three tumours when performing three pair-wise comparisons, with highest mean values in EP and lowest in PA. Significantly lower Cr and higher NAA were found in PA when compared to MB and EP. Tau, phosphocholine (PCh) and Glu were significantly lower and Gln significantly higher in PA when compared to MB. Lipids+macromolecule (MMs) peaks at 1.3 and 2.0 ppm were significantly lower in PA compared to MB (Davies et al., 2008).

PA in adults vs. PA in children

While PA is relatively common in children (25%), their incidence in adults is very rare (2%). Although classified as WHO grade I in both, their clinical course varies (Porto et al., 2010b) with adult PA exhibiting a more aggressive nature (Johnson et al., 2012). It is unclear why this difference is seen but is speculated to be due to differences in tumour biology, for example paediatric low grade gliomas do not possess the same molecular abnormalities as those in adults. Tumour suppressor gene P53 is found to be frequently mutated in adult tumours but is rare in paediatric patients (Sievert and Fisher, 2009).

A study by Porto *et al.* (2010) investigated the differences in MRS between PAs in adults (n=5) and children (n=11). The analysis demonstrated a trend towards higher mean tCho

in adults and higher mean Cr in paediatric PAs, although not significant. It should be noted the study consisted of a very small cohort of patients (Porto et al., 2010b).

PA in different locations of the brain

A study by Harris *et al.* (2008) compared MRS of PA on the basis of location. The presence of a peak at 3.65 ppm due to mIns and Gly was the most prominent difference when qualitatively comparing the mean spectra from nine infratentorial and 12 supratentorial PA. Long TE spectra acquired from three supratentorial PA suggested the contributions from glycine were small; attributing the difference due to mIns. A more pronounced broad peak of Glx (around 2.0-2.5 ppm) and lipids+MMs were also seen in the supratentorial cases. Significantly higher mIns and Glx was observed in supratentorial PAs. A trend towards lower Cr was seen in cerebellar PAs. Orphanidou-Vlachou *et al.* (2013) found significantly higher Cr , sIns , Tau and mIns in supratentorial PAs with optic pathway gliomas when compared with infratentorial PAs (Orphanidou-Vlachou et al., 2013). Harris *et al.* (2008) confirmed the difference in mIns was not due to regional differences in uninvolved brain (Harris et al., 2008).

Medulloblastoma (MB)

Studies have used MRS to identify and characterise MB, compared with normal brain, other childhood brain tumours and common cerebellar tumours.

MB versus uninvolved brain

Qualitative analysis of MB mean spectra (n=18) compared to four control spectra revealed high tCho, very low NAA and a small Tau peak. A large variability is seen in the lipids+MMs and Lac region (Davies et al., 2008).

PNET vs. All other tumours

Kovanlikaya *et al.* (2005) investigated whether the quantitation of Tau could improve the differentiation of PNET from other common brain tumours in paediatric patients. From a cohort of 29 patients, 13 of which were PNET, elevated Tau was found to be most significant discriminator between PNET and All Other with the exception of a patient with a GER. Significantly elevated levels of tCho were also seen in PNET. Evaluation of metabolite ratios demonstrated significantly elevated Tau/tCho and Tau/Cr and significantly reduced NAA/tCho in PNET compared to All Other (Kovanlikaya et al., 2005).

Panigrahy *et al.* (2006) also found Tau to be the most prominent signal in MB spectra. Mean tCho, Ala and Gua were found to be significantly elevated in MB compared to All Other. Significantly decreased NAA/tCho , Gln/tCho , Glx/tCho and Gln/Cr were also seen in MB compared to All Other (Panigrahy et al., 2006).

MB vs. PA and EP

A significantly narrower choline peak width was seen at 3.2 ppm in MB when compared with both PA and EP. Tau, PCh and Glu were significantly higher, while Gln was significantly lower in MB. Lipids+MMs peaks were in general higher in MB when compared to PA and EP. However, this was only significant for the components at 1.3 and

2.0 ppm, when compared with PA, and the component at 0.9 ppm, when compared to EP (Davies et al., 2008).

Ependymoma (EP)

MRS of ependymomas in children has been investigated in a number of studies including comparisons with uninvolved brain and other tumour types.

EP versus uninvolved brain

EP demonstrates a prominent mIns peak and low levels of NAA. Lac and lipids+MMs were found to vary considerably (Davies et al., 2008).

EP vs. All Other

Panigrahy *et al.* (2006) found a large range of mIns concentrations when comparing EP and anaplastic ependymomas (A-EP) providing evidence for the spectral heterogeneity between tumours (Panigrahy et al., 2006). Davies et al. (2008) also found a high variability of mIns shown by the reported standard deviation (Davies et al., 2008).

Despite the differences seen by Panigrahy *et al.* (2006) EP spectra were pooled due to small numbers. Reduced mean NAA was the most significant differentiator between EP+A-EP and All Other. Evaluation of concentration ratios demonstrated significantly reduced NAA/Cr and NAA/tCho (Panigrahy et al., 2006). Davies *et al.* (2008) found mIns to be significantly higher in EP compared to all tumours and EP with a significantly lower LMM0.9 when compared to MB (Davies et al., 2008).

Low grade gliomas (LGG)

A large study of low grade gliomas (n=69) demonstrated significant subtle differences between closely related subtypes. Comparison of glial with glioneuronal tumours showed significantly increased Cr and significantly decreased LMM0.9 and LMM1.3 in glioneuronal tumours. Significantly higher Cr, NAA and mIns and significantly lower Lac were seen in DA when compared with PAs+optic pathway gliomas (Orphanidou-Vlachou et al., 2013).

More rare tumour types

Pilomyxoid Astroyctomas

Pilomyxoid astrocytomas (PmA), a more aggressive variant of PA is currently indistinguishable from PA on conventional imaging. A study by Cirak *et al.* (2005) compared two PmA with two PAs using magnetic resonance spectroscopic imaging (MRSI). Total choline was higher in PA compared to the PmA, an unexpected finding in a less malignant tumour however, the cohort was too small to draw firm conclusions (Cirak et al., 2005).

Anaplastic astrocytoma (AA)

Very few studies have reported MRS of anaplastic astrocytomas due to their rarity. Panigrahy *et al.* (2006) comparison of AA with low grade astrocytomas found highly variable concentrations of tCho. Significantly lower mean Gua, LMM0.9 and LMM1.3 were seen in AA plus low grade astrocytomas when compared with All Others. Significantly reduced Glu/Cr and Gua/Cr were also observed (Panigrahy et al., 2006).

Citrate (Cit) was found to be a prominent feature of some AA (Blüml et al., 2011, Seymour et al., 2008).

Glioblastoma Multiforme (GBM)

GBM is a relatively uncommon tumour in children and is often difficult to differentiate on conventional imaging. Chang *et al.* (2003) performed a multimodal MR study on 11 patients with GBM, of which three had SVS. Analysis of spectra by determining area under peak demonstrated a reduction in the amplitude of NAA and elevation of tCho. A low NAA/Cho ratio was found to be a valuable aid for precise targeting of stereotactic biopsies. However, these findings were only observational (Chang et al., 2003).

Choroid Plexus tumours

Although choroid plexus tumours are relatively rare, case studies have looked at metabolic features of these tumours in order to differentiate the diagnosis of choroid plexus papilloma (CPP) and choroid plexus carcinoma (CPC). Choroid plexus tumours have also been compared to other brain tumours. Results should be interpreted with caution, as these studies consist of small cohort numbers.

Choroid plexus tumours vs. All Other

Choroid plexus tumours demonstrate spectra with low levels of metabolite information. The main peaks observed in both tumours are tCho and mIns.

Choroid plexus papilloma (CPP) vs. All Other

Myo-inositol was the most prominent feature of CPP on qualitative analysis with significantly elevated concentrations. CPP also demonstrated reduced mean tCho, Cr, Gln, LMM0.9 and LMM1.3 when compared with All Other.

Choroid plexus carcinoma (CPC) vs. All Other

Significantly reduced mean NAA, Glx, Cr and no sIns was seen in CPC compared to All Other. Mean tCho was high when compared with All Other, but did not reach significance. Reduced NAA/tCho was the most significant discriminators of CPC from All Other. Other significant ratios included reduced Cr/tCho, NAA/Cr, mIns/tCho, Glu/tCho and Glx/tCho (Panigrahy et al., 2006).

CPP vs. CPC

The most striking feature seen on qualitative analysis comparing the two tumours was the presence of a prominent mIns peak in the three patients with CPP, not seen in CPC (Panigrahy et al., 2006).

Horska *et al.* (2001) included spectroscopy results from only two patients, one patient with CPP and the other with CPC. Both cases had low NAA but CPC possessed higher levels of tCho than the CPP in keeping with its more malignant course (Horská et al., 2001).

Germ cell tumours

For germ cell tumours located in deep midline structures in the brain, commonly the pineal gland, a non-invasive diagnosis would be advantageous. The location makes it difficult to biopsy and more than 90% are curable without surgery.

Pineal Germinoma vs. All Other

Increased LMM1.3, prominent tCho and Tau were seen on qualitative analysis of a typical GER spectrum. GER showed significantly reduced mean tCho and mIns compared to All Other. Significantly elevated Glx/tCho and Glu/tCho and significantly reduced mIns/Cr and NAA/Cr were also observed (Panigrahy et al., 2006).

Harris *et al.* (2011) reported spectroscopy of germ cell tumours to be dominated by lipids+MMs and as a result making is difficult to distinguish other metabolite peaks. However, a small peak around 3.35 ppm attributed to Tau was seen (Harris et al., 2011).

2.3.2   Prognosis

Most spectroscopy studies that have searched for markers of prognosis have done so from a heterogeneous cohort of brain tumours with a particular focus on biomarkers for high and low grade tumours. Few studies have used spectroscopy to identify subtype specific markers.

Low vs. High grade

Lipids and tCho

Analysis of MRSI acquired from 23 high grade (III+IV) compared with 43 low grade (I+II) tumours, both of which were determined by histopathology, found tCho and lipids+lactate (L) to be significantly elevated in the high grade tumours.

For each case, metabolite signals in the tumour were normalised to the mean of the Cr signal in non-involved brain and intermediate echo time of 65 ms used to minimise the contribution of the Lac signal. A linear combination of tCho and 0.49 L was proposed as the best discriminator with a 91% accuracy for classifying tumour grade. Logistical regression revealed that both biomarkers to be significant independent predictors of tumour grade (Astrakas et al., 2004).

Glycine (Gly)

Glycine has been identified in a number of *in vitro* studies to increase with WHO grade (Lehnhardt et al., 2005, Carapella et al., 1997). The metabolite is often overlooked due to its strong overlap with the multiplet peak of mIns but at long TE MRS Gly is more readily identifiable.

 A study by Davies *et al.* (2009) identified Gly as a feature in paediatric brain tumours. The comparison 18 high grade (III or IV) with 17 low grade (I or II) paediatric brain tumours classified using the WHO criteria revealed high grade tumours possessed significantly increased levels of normalised Gly while no difference was seen between normalised mIns based on grading (Davies et al., 2009).

Whilst grade is strongly associated with prognosis, tumours with the same grade can behave very differently (Taylor et al., 2012) and studies of event free survival and overall survival are required to establish the accuracy of recognized prognostic biomarkers.

2.3.3   Survival

A study by Marcus *et al.* (2007) extended Astrakas' (2004) study to investigate whether the biomarkers of grade were also associated with survival in children with CNS tumours. MRSI was performed on a cohort of 76 children on a heterogeneous cohort of tumours including all WHO grades. Univariate analysis showed that tCho, L, tCho/NAA and tumour grade were significantly different between survivors (n=58) and non-survivors (n=18). Receiver operating characteristics (ROC) curve analysis found tCho (AUC=0.725) and L (AUC=0.687) to be good discriminators between the two cohorts. The combined index tCho + 0.1L were a more accurate and more specific predictor than tCho or tCho/NAA. Total Choline + 0.1L was the only independent predictor of survival (Marcus et al., 2007) .

A study by Wilson *et al.* (2013) found increased lipids at 1.3 ppm and sIns predicted poor survival and increased Gln and NAA predicted improved survival in a cohort of 115 pre-treatment paediatric brain tumours (Wilson et al., 2013).

2.3.4   Progression

MRSI performed on 27 children, during treatment for a neuroglial brain tumour, showed the percentage change in tCho was significantly greater in patients who had progressive examinations compared to stable disease. Total choline/NAA was determined to be the most important prognostic indicator of tumour progression with significantly higher

levels in patients with progressive outcomes. Probability of tumour progression was 55 times greater for patients with a 20% change in tCho/NAA (Tzika et al., 2004).

Another study evaluated MRSI on 27 recurrent brain tumours and found maximum tumour tCho/NAA ratio to be predictive of outcome in children with recurrent brain tumours (Warren et al., 2000).

Citrate (Cit)

A retrospective analysis by Seymour *et al.* (2008) of MRS from 85 paediatric brain tumour patients with 615 spectra from 469 subjects showed spectra from DIPG, an EP and an AA with a signal at 2.6 ppm consistent with citrate. Diffuse brain stem gliomas had the highest mean concentration of Cit compared to all tumours. Significantly lower levels of Cit were detected in MB and PA compared to diffuse brain stem gliomas (Seymour et al., 2008).

Bluml *et al.* (2011) analysis demonstrated grade II astrocytomas with disease progression in <2 years following diagnosis to have significantly higher levels of mean Cit compared to grade II astrocytomas that exhibited stable disease for >2 years. Significantly higher Cit/Cr and reduced NAA was seen in grade II astrocytomas with disease progression. However, Cit was only identified in a subgroup of paediatric grade II astrocytomas destined for aggressive behaviour, detecting a possible subgroup of tumours with a metabolically different course (Blüml et al., 2011).

Tumour type specific markers

Metastatic PA vs. non-metastatic infratentorial PA

Orphanidou-Vlachou *et al.* (2013) found trends towards higher tCho and Glx in metastatic PA at presentation (n=2) when compared with infratentorial PA (n=19) (Orphanidou-Vlachou et al., 2013).

Metastatic and non-metastatic MB

Peet *et al.* (2007) comparison of MRS of MB patients with localised (n=8) and metastatic disease (n=8) found those that presented with metastatic disease had increased tCho, decreased lipids and Lac. Total choline was found to be correlated positively with histopathological indicator of tumour cell proliferation, Ki67 index. These findings imply that tumours that have metastasised at diagnosis have a different biology to localised tumours, growing more rapidly and metastasising earlier (Peet et al., 2007a).

Diffuse pontine gliomas (DIPG)

Steffen Smith *et al.* (2011) evaluated changes in both SVS and MRSI of 38 DIPGs at first MRS and follow-up. Total choline/NAA was found to be the only variable predictive of patient survival on first MRS. Patients with higher SVS tCho/NAA values at their first scan were at greater risk of mortality. No predictive variables were seen with MRSI (Steffen-Smith et al., 2011).

Yamasaki *et al.* (2011) found the presence of Lac and a high tCho/NAA in DIPGs to be correlated with shorter overall survival. Citrate was speculated to be associated with a good prognosis in this cohort (Yamasaki et al., 2011).

2.3.5 Treatment monitoring

Tumour monitoring at present involves performing serial MRI scans to provide measurements of the size of the tumour. Scans are mostly performed at three-monthly intervals whilst on treatment and so significant delays in the detection of ineffective treatment are incurred. A number of studies have used MRS both SVS and/or MRSI at follow-up. The development of new non-invasive methods, which can provide surrogate biomarkers of early treatment response or failure, would be a major advance in the clinical management of brain tumours.

A comparison of pre-treatment MRS and first on treatment MRS in children with PA identified significant decreases in mIns in patients with tumour progression. The median time between the two MRS studies was 2.1 months compared with a median time to progression using conventional criteria of 12.2 months. This indicates MRS can identify early biomarkers of progression during treatment monitoring (Harris et al., 2008).

A comparison of Cit levels at baseline and follow-up in DIPG found levels had significantly decreased at baseline to final MRS (Seymour et al., 2008). Another study found DIPG patients with an increased tCho/NAA at follow-up were at greater risk of death compared to patients with stable or decreased levels. Increases in the variance of MRSI tCho/NAA was associated with decreased patient survival (Steffen-Smith et al., 2011).

These studies demonstrate that changes in metabolite profiles of tumours occur over time and could aid in treatment monitoring. In keeping with most studies investigating imaging in cancer, MRS was performed to coincide with conventional imaging, however, it may be that MRS can provide earlier biomarkers of treatment response but these would need testing in a study specifically designed to investigate this hypothesis (Arthurs and Gallagher, 2011).

2.3.6   Surveillance scans and the detection of recurrent disease

MRI monitoring of children with brain tumours following treatment is routine. One of the challenges that radiologists face are diagnosing the changes seen in the brain following radiation treatment and the presentation of new contrast enhancing lesions. Differentiating tumour recurrence and post radiation change is difficult and a number of studies have investigated whether MRS can be used to overcome this.

A study by Weybright *et al.* (2005) used 2D MRSI to evaluate new areas of contrast enhancement in patients with brain tumours that had been previously treated with conventional fractionated radiation therapy (Weybright et al., 2005). It should be noted that the study included both adults and children. 26 patients (age range 5-54 years) with a range of tumour diagnoses including 24 gliomas (grade I to IV) and a PNET, a MB, an EP and one case of acute promyelotic leukaemia were included in the study. The confirmation of tumour recurrence was seen in 16 patients and radiation changes in 12 patients based on follow-up imaging or histopathology results. MRS was performed on both the contrast enhancing lesion and normal appearing white matter and peak areas of metabolites in the same voxel were used to calculate metabolite ratios. Significantly

higher tCho/Cr was seen in those patients with recurrence or residual tumour compared to those with radiation injury. Those in the radiation injury group had significantly higher tCho/Cr ratios than normal appearing white matter. The lesions in the tumour group also had significantly higher tCho/NAA ratios than those in the radiation injury group and significantly higher tCho/NAA ratios than normal appearing white matter. NAA/Cr ratios were significantly lower in the lesion group compared to those in the radiation injury group. Analysis has shown that none of the lesions classified as radiation injury had tCho/Cr or tCho/NAA ratios above 1.8. Using tCho/Cr or tCho/NAA ratios with values above 1.8 as tumour recurrence enabled 27 out of 28 patients to be correctly classified with either recurrent tumour or radiation injury assuming radiation injury was diagnosed accurately (Weybright et al., 2005).

Smith *et al.* (2009) compared the spectroscopy of patients deemed to have tumour recurrence compared with radiation injury. Patients with tumour recurrence had significantly higher mean values of tCho/Cr and tCho/NAA) than those with radiation changes but lower mean values of NAA/Cr. Total choline/NAA was found to be predictive of tumour recurrence determined by using logistic regression and ROC curve analysis. Every unit increase in tCho/NAA was found to increase the odds of tumour recurrence by 13-fold (Smith et al., 2009).

It is to be noted that these studies have been performed on a cohort of both adults and children with a heterogeneous group of tumour types. Metabolite values are known to vary greatly between tumour types and this may need to be taken into account. Less than half of these patients have had a biopsy confirmed diagnosis of recurrence or radiation

injury so classification is dependent on clinical and imaging grounds only. However, these studies haves shown the potential for MRS to be an effective tool in discriminating between tumour recurrence and radiation change.

2.4 Summary

Children's tumours are known to be more heterogeneous, less aggressive and more responsive to treatment than those that present in adults. Their classification is performed either on histopathology or clinical and imaging grounds alone. The value of MRS in brain tumours has led to expansion of research in the field. The current published spectroscopy literature for paediatric brain tumours has been comprehensively reviewed.

CHAPTER 3: MAGNETIC RESONANCE SPECTROSCOPY

CHAPTER 3

3 MAGNETIC RESONANCE SPECTROSCOPY

3.1 Theory

This chapter outlines a brief overview of the theory behind magnetic resonance spectroscopy. More detailed information is available in a number of well-known MR textbooks (de Graaf, 2007b, Mukherji, 1998, Levit, 2001).

Proton magnetic resonance spectroscopy is a non-invasive, *in vivo* method that measures the biochemical information within a region of interest (ROI) termed voxel, thus providing information on cellular metabolism. Spectroscopy uses the signal from protons (1H) within chemicals observed in the ROI to produce a spectrum (Panigrahy et al., 2010b). The localisation of the signal can be performed using two approaches as either single voxel (SVS) or multi-voxel technique, MRSI. The theory for single voxel spectroscopy will be exclusively explored for this thesis.
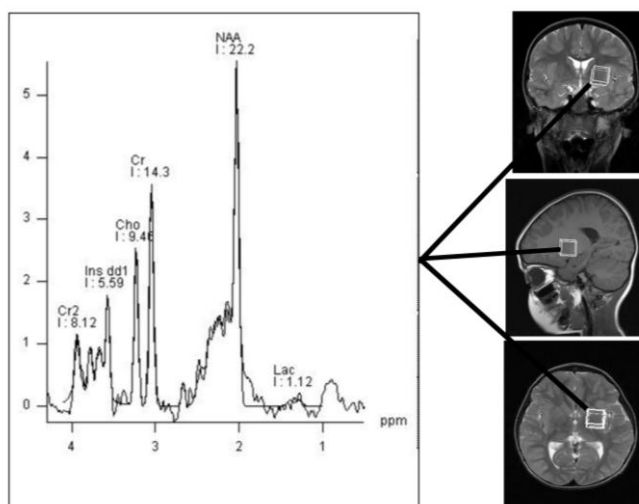
Figure 3.1 1H MR spectrum acquired from a single volume of interest in the brain. Voxel positions included to specify location from where spectrum was obtained. Abbreviations: Ins, myo-inositol; Cho, total choline; Cr, creatine; Cr2, 2nd Creatine peak ; NAA, N-acetylaspartate; Lac, lactate; ppm, parts per million.

47

Following conventional MRI, a voxel is placed on a ROI that covers a volume that pre-defines where the spectra are acquired from (example given in Figure 3.1 specific to a ROI in a brain tumour). The resulting spectrum consists of two axes. The x-axis, known as the chemical shift axis, is the measure of the signal or metabolite position in the spectrum relative to a fixed reference. The chemical shift axis can be reported in either Hz or ppm. Hz determines the frequency at which the protons precess and this differs at different field strengths making it difficult to compare spectral profiles. To overcome this, metabolite peak positions are reported in ppm, a scale independent of field strength. To express chemical shift in ppm the following calculation is applied, where δ is chemical shift (ppm), ν and νref are the resonant frequencies of the compound under investigation and the reference compound respectively, measured in Hz (Figure 3.2) (de Graaf, 2007a)

$$\delta = \frac{\nu - \nu\,ref}{\nu\,ref} \times 10^6$$

Figure 3.2 An equation representing the definition of chemical shift, where δ is chemical shift, ν is the resonant frequency of the compound being investigated, νref is the resonant frequency of the reference compound multiplied by 10^6 (de Graaf, 2007a).

Most *in vivo* MR spectra range from 0.5 to 9.0 ppm but the lack of metabolite information observed downfield of 4.7 ppm results in this being rarely shown. Instead spectra extend from 0.5 ppm to around 4.5 ppm as shown on the MR scanner output in Figure 3.1.

The y-axis measures the signal intensity which is proportional to the apparent concentration of the chemical seen in the ROI (Figure 3.1) (Panigrahy et al., 2010b).

The positioning of each peak in the spectrum is a result of chemical shift. The nucleus of an atom consists of both protons and neutrons, surrounded by orbiting electrons. When

the atom is placed in an externally applied magnetic field (B_0), protons precess and induce their own local magnetic field known as the effective magnetic field (B_{eff}). The density of electrons surrounding each nucleus can vary and as a result the B_0 plus B_{eff} can differ at each nucleus which results in the phenomenon known as chemical shift (Kwock, 1998). Chemicals usually have more than one proton and each proton gives an MR detectable signal. Protons within the same chemical environment experience the same magnetic field resulting in identical chemical shifts. This results in a spectrum consisting of a collection of peaks at different radiofrequencies representing proton nuclei in different chemical environments.

Nuclei in close proximity to one another influence each other's B_{eff}. Nuclei experiencing the same chemical shift are termed equivalent and those experiencing different chemical shifts, nonequivalent. Equivalent nuclei produce no observable peak splitting. However, if there is more than one proton in a molecule and these protons are nonequivalent, then a coupling between these occurs, called spin-spin coupling or J coupling (de Graaf, 2007a) causing resonance peaks to split. Instead of one signal as would be seen for the equivalent nuclei, signals at two or more resonant frequencies are observed (Klose, 2008).

3.2   Spectroscopy acquisition

3.2.1   Select region of interest

It is important to ensure that the voxel is placed fully over the ROI to obtain a good quality spectrum that is representative of the pathology being assessed. To assess accurate voxel positioning the ROI is placed using imaging from planes of all three axes

(Figure 3.1). Voxel placement should be away from bone, scalp and air interfaces and should not be dominated by normal brain.

3.2.2   PRESS

A number of single volume localisation sequences can be used for acquisition of MRS data. The acquisition method use for the studies in this thesis was **P**oint-**RES**olved **S**pectroscopy (PRESS) (Bottomley, 1987). The PRESS acquisition is based on a spin echo sequence with a 90° radiofrequency pulse (RF) followed by two 180° RF pulses so that the primary spin echo is refocused again by the third pulse. As demonstrated in the Figure 3.3 from the paper by Klose (2008) the volume is excited in a stepwise method with each pulse having a slice selective gradient on one of the three principal axes (x,y,z). The initial 90° radiofrequency pulse is applied in the z-axis depicted in Figure 3.3a followed by the first 180° pulse in the y-axis in Figure 3.3b and final 180° pulse in x-axis depicted in Figure 3.3c. The order of the gradients used is given as an example and can be altered (Klose, 2008). The aim of slice selective gradient is to ensure that only the protons located in the ROI experience the three RF pulses. It should be noted that contributions to the signal from the border of the ROI can still occur. This is overcome by the use of spoiler gradients also depicted in Figure 3.3.
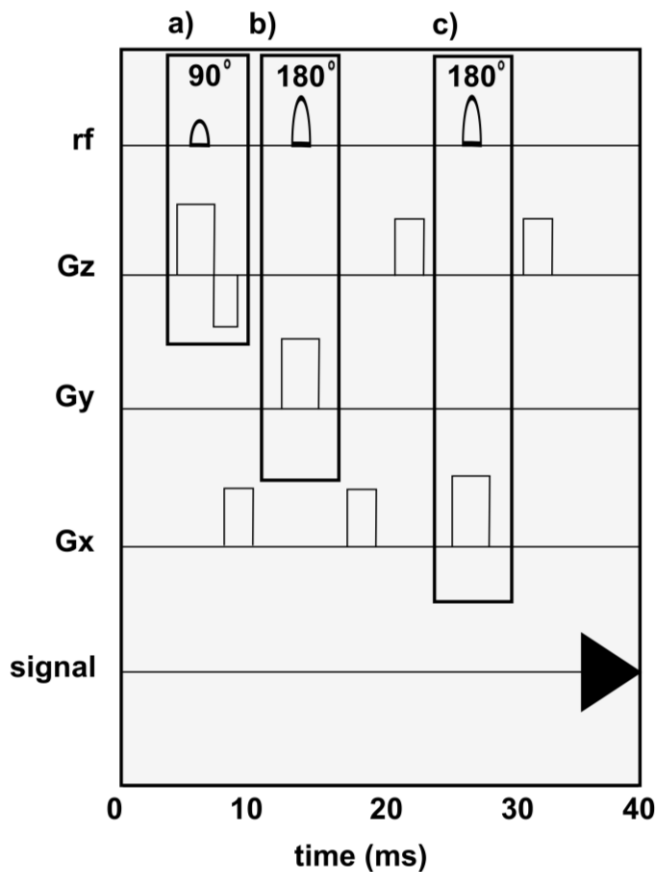
Figure 3.3 Volume selection using the PRESS sequence with three simultaneously applied radiofrequency pulses. a) The first 90°radiofrequency pulse is applied in the z axis followed by b) 180° radiofrequency pulse in the y and finally an c) 180° radiofrequency pulse in the x. The three radiofrequency pulses within the sequence are marked and the selected regions after each pulse are shown for a cubic object. Redrawn from Klose (Klose, 2008). Abbreviations: rf, radiofrequency pulse; Gz, field gradient along z axis; Gy, field gradient along y axis; Gx , field gradient along x axis; ms, milliseconds.

3.2.3   Shimming

The purpose of shimming is to produce a homogenous magnetic field over the ROI. This ensures equivalent nuclei experience the same magnetic field. A good shim results in good peak resolution and high SNR. Whereas, a poor shim results in broad metabolite peaks or spectral linewidth. An approximation of this can be determined by measuring the full-width-half-maximum (FWHM) of the peak. The greater the value the more

difficult it is to distinguish nearby peaks for example overlapping Cr and tCho peaks. The

FWHM of the water peak is a good determinant of field homogeneity (Kwock, 1998).

3.2.4   Water suppression
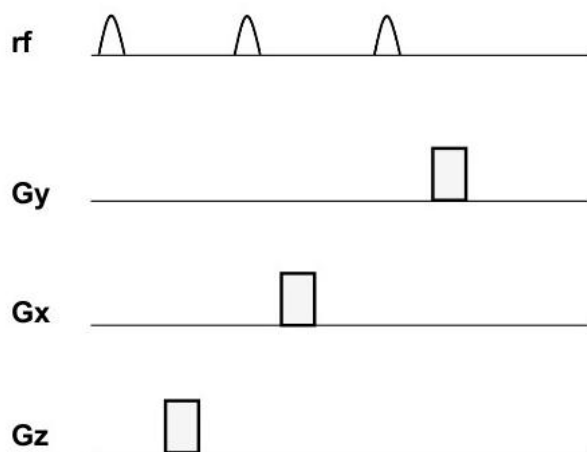
Figure 3.4 The Gaussian chemical shift selective (CHESS) pulse sequence

The water signal (4.7 ppm) is 10,000-fold greater than the metabolite signals seen in the

spectrum. This results in an over dominance of the water and limited metabolite

information (Castillo et al., 1996) which can be overcome by employing water

suppression. The two most commonly used methods are chemical shift selective (CHESS)

and the water elimination Fourier transform technique (WEFT) although CHESS is more

frequently used. CHESS consists of a 90° frequency selective pulse centred over the

proton water resonance frequency (Figure 3.4) whereas WEFT consists of a 180° pulse.

The pulses in both methods are applied before the implementation of the PRESS

sequence (Kwock, 1998).

3.2.5   Acquiring a water spectrum

Following data acquisition from the lesion, an additional water spectrum (unsuppressed water spectrum) is obtained from the same volume. This is used as an internal reference signal for quantitation of metabolite signal intensities (Graaf, 2010). A number of studies have reported differences in water content in different pathologies. Brain tumours, for example exhibit an increased water content compared to healthy tissues (Jansen et al., 2006). This analysis does not account for differences in water content in the ROI, instead the water unsuppressed spectrum is referenced assuming the water concentration of white matter (35.88 mol/L) (Baker et al., 2008). While it is known the water concentration varies for grey and white matter, it is often assumed this difference is small. There are few studies that investigate pathology specific changes. A more in- depth discussion regarding the assumptions made are described by Ernst et al. and Gasprovic et al. (Ernst et al., 1993, Gasparovic et al., 2006).

3.3   Pre-processing

The acquired signal is obtained in the form of a free induction decay or FID. The time dependence of the signal intensity is called the FID (de Graaf, 2007a). Analysis of data is divided into two main stages, pre-processing and quantitation both of which can be performed in either the time domain or frequency domain (Mandal, 2012). The time domain is the raw data domain, so the same as the measured signal (FID), whereas the frequency domain is that of the processed signal so once the FID has been Fourier transformed to obtain a spectrum of peaks (Poullet et al., 2008). Several software packages are available for analysis of spectroscopy data including LCModel (Provencher, 2001), QUEST (Mansson et al., 2006) and TARQUIN (Wilson et al., 2011). The analysis of

raw data in this thesis was performed using TARQUIN software (Wilson et al., 2011) thus, the pre-processing and quantitation methods described below are specific for the analysis of data with TARQUIN.

The pre-processing steps the data undergoes are as follows:

3.3.1 Water removal by Hankel Singular Value Decomposition (HSVD)

As previously discussed the signal of the water peak is significantly larger than that of the metabolites. Using HSVD model (Barkhuijsen et al., 1987), the water signal is constructed and subtracted from the FID to remove the residual water peak thus leaving only metabolite information for analysis.

3.3.2 Zero and first order phase correction

Phase correction is applied to avoid inverted or out-of-phase peaks. These are corrected using zero and first order correction. The initial estimate for phase correction is performed by comparing the phase of the data to the magnitude spectra. This enables easier inspection of the spectral peaks and enables the quality of the spectroscopy to be assessed reliably (Wilson et al., 2011).

3.3.3 Automatic referencing

Although the resonance of the water signal is known, minor frequency shifts due to small inhomogeneities in the applied magnetic field can occur and determining this accurately is essential for the fitting of peaks. To overcome this, cross correlation between the absolute value of acquired spectrum and reference spectrum is determined. The reference spectra used in this analysis included peaks at 2.01, 3.22 and 3.03 assigned to

NAA, tCho and Cr respectively expected in brain spectra and extended to lipid peaks at 1.28 and 0.9 ppm for brain tumour data (Wilson et al., 2011).

3.3.4   Basis set simulation

The metabolite basis set used in the analysis is simulated from previously reported chemical shift and J-coupling values (Govindaraju et al., 2000). Lipids and MMs are added to basis set using particular parameters – taken from LCModel (Provencher, 2001) (ppm, FWHM in ppm and amplitude (au)).

3.3.5   Signal model

Signal modelling in TARQUIN uses the approach of modelling the experimental data as a linear combination of modified simulated basis signals.

3.3.6   Fitting with constraints

The first points of the FID typically contain distortions and broad signals with the last points containing a high contribution of noise (de Graaf, 2007a). Both can be difficult to model and as a result are removed. Removing the elements that cause baseline interferences, eliminates the need for baseline correction (Wilson et al., 2011).

3.4   Peak fitting and quantitation

The quantitation of metabolites using TARQUIN is also performed in the time domain. Short TE spectra can often be complex with overlapping peaks that can be difficult to determine separately and as a consequence challenging to accurately quantitate. To overcome this, the whole spectrum is fit to a set of individual metabolite spectra acquired by simulation. Fitting can be applied automatically resulting in a list of quantifiable metabolites and their relative concentrations. The combination of metabolite fitting and

use of the water signal as a concentration reference is proving to be a powerful technique for the automated processing of SVS data and allows a set of metabolite concentrations to be expressed in standard units of millimolar (mM). The spectrum is then Fourier transformed for visualisation.

3.5   Interpretation of the metabolites measured using 1H MRS

In vivo spectroscopy contains three different components; water, metabolites (<2000Da and concentration >1mM) and lipids and macromolecules (Hajek and Dezortova, 2008). The resulting spectrum acquired from a human brain consists of approximately 18-20 metabolites and nine lipid and macromolecular components. It should be noted that the metabolite profiles alter in different pathologies including differences between normal brain and brain pathology and between different pathologies themselves often resulting in the presence and absence of different metabolites (Figure 3.5) (Panigrahy et al., 2010b). The main metabolites observed in brain spectra and their roles in the brain and/or brain pathology are given in detail below.
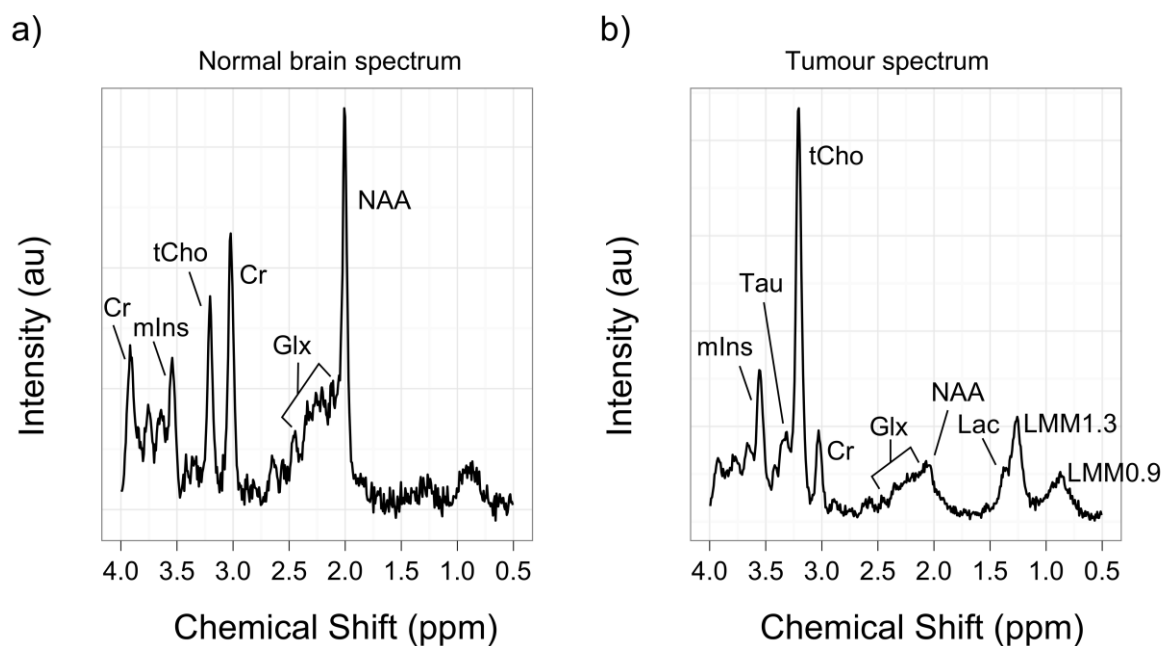
Figure 3.5 Comparison of MRS acquired from a) normal brain and b) brain tumour (MB) at short echo time. Abbreviations: MB, medulloblastoma; mIns, myo-inositol; Tau, taurine; tCho, total choline; Cr, creatine; Glx, Glutamate+Glutamine; NAA, N-acetylaspartate; Lac, lactate; LMM0.9, lipids at 0.9 ppm; LMM1.3, lipids at 1.3 ppm.

N-acetyl aspartate (NAA)

NAA, seen around 2.0 ppm is the one of the most abundant metabolites present in normal brain. It is known marker of neuronal and axonal integrity and the most reliable biomarker of pathological disease in the brain with decreased levels found in all brain related disease spectra including brain tumours (Gujar et al., 2005).

N-acetylaspartylglutamate (NAAG) found on the shoulder of the NAA peak, around 2.04 ppm is very closely linked with NAA. Reductions in NAA levels correspond to reductions in NAAG or an underestimation of NAA levels with NAAG levels remaining unvaried (Moffett et al., 2007).

Creatine (Cr)

Cr is made of at least two compounds , creatine and phosphocreatine with peaks at 3.02 ppm and 3.94 ppm respectively (Rosen and Lenkinski, 2007). The main role of Cr is in energy storage and transmission where Cr through phosphocreatine provides phosphate for ATP. In early studies, Cr has often been taken as a reference metabolite as its levels remain relatively stable in normal brain and were thought to be relatively unchanged in diseases states. However, Cr is now known to vary in pathology therefore it should be interpreted with caution when used in metabolite ratios (Nasrallah et al., 2010, Vigneron et al., 2001).

Glutamate (Glu), glutamine (Gln) and Glutamate+Glutamine (Glx)

Glu and Gln, often reported as a sum, Glx, are a broad group of resonances found between 2.0-2.6 ppm. The complex spectral overlap between the two metabolites makes it difficult to separate the two signals below 3 T and consequently, resulting in them being measured as one entity.

Glu has many roles including as an excitatory neurotransmitter. Gln is an amino acid precursor and a storage form of glutamate (Panigrahy et al., 2010a). They have been found to be indicators of altered brain tumour metabolism in adults (Howe and Opstad, 2003).

Myo-inositol (mIns)

Myo-inositol is a simple sugar that resonates at 3.6 ppm. The metabolite is an osmolyte and astrocyte marker, however its functions are not well understood (Panigrahy et al.,

2010a, Castillo et al., 2000). Myo-inositol is known to be involved in cell membrane and myelin sheet structures and increased membrane turnover or damage to myelin sheets can result in increased levels. It is also associated with an activation of glial cells. For glial tumours, the increased mIns may reflect the cellular density of reactive astrocytes but is also increased in membrane turnover of highly proliferating tumour cells (Hattingen et al., 2008b). Brain tumours exhibit varying concentrations of mIns speculated to be because of altered membrane metabolism (Harris et al., 2008, Panigrahy et al., 2006, Callot et al., 2008, Panigrahy et al., 2010a).

Total choline (tCho)

Choline is a complex peak assigned around 3.2 ppm that consists of major contributions from three components; free choline, glycerophosphocholine and phosphocholine. The peak is often referred to as total choline (tCho) due to the difficulty in separating the contributions of individual metabolites. Choline is involved in membrane synthesis and breakdown with increasing levels associated with cell proliferation. There is increasing evidence of elevated choline levels, when compared to normal brain, being representative of malignancy (Peet et al., 2007b, Marcus et al., 2007, Astrakas et al., 2004, Ronen et al., 2001, Smith et al., 2009, Spampinato et al., 2007).

Glucose (Glc)

Glc has a complex spectral pattern with two *in vivo* peaks assigned at 3.43 ppm and 3.80 ppm. However, the close overlap with other metabolites often makes it difficult to determine the contribution of Glc. Glc provides energy for all proliferating cells and is expected to decline in malignant cells (Panigrahy et al., 2006).

Lactate (Lac)

Lac forms a doublet peak at 1.3 ppm. The metabolite is a marker of anaerobic metabolism and aerobic glycolysis. The various possible origins makes the interpretation of Lac levels difficult. It is present in very low concentrations in normal brain and elevated concentrations in brain pathologies (Panigrahy et al., 2010a). The increase of Lac levels following hypoxia, are of great interest in clinical MRS studies particularly where blood flow is impaired for example following stroke, trauma or formation of a tumour. Lac levels are variable in brain tumours (Govindaraju et al., 2000, Astrakas et al., 2004, Davies et al., 2008).

Taurine (Tau)

Tau, found around 3.3 ppm is a less commonly detected metabolite. Due to the close overlap with a number of metabolites it can be difficult to identify. The role of Tau is not fully understood but it is speculated to have a number of roles including as an osmoregulator and modulator of the action of neurotransmitters. There is evidence to suggest that an intracellular accumulation of osmolytes such as Tau is a key factor in protecting cells from hyperosmotic stress. Hyperosmolarity triggers cell shrinkage, oxidative stress, DNA damage amongst other affects that render cells susceptible to apoptosis (Brocker et al., 2012). Taurine also has a role as a neuro-protective chemical that prevents the accumulation of free radicals again preventing DNA damage. Both roles of Tau provide a cell survival advantage for tumour cells (Blüml et al., 2013). Tau has been detected in increased levels in a number of brain tumours (Moreno-Torres et al.,

2004, Panigrahy et al., 2006, Opstad et al., 2009, Kovanlikaya et al., 2005, Harris et al., 2011).

Scyllo-inositol (sIns)

Scyllo-inositol is a less commonly observed metabolite that forms a singlet peak at 3.34 ppm. A positive correlation of sIns with mIns both in normal controls and pathology implies a relationship between the two metabolites although its role is poorly understood (Swanson et al., 2003). Scyllo-inositol has been detected in a number of brain tumours (Kaiser et al., 2005, Govindaraju et al., 2000).

Glycine (Gly)

Glycine, Gly, a singlet peak at 3.55 ppm is better observed at long TE due to its close overlap with mIns. The roles of Gly include as an inhibitory neurotransmitter and antioxidant (Govindaraju et al., 2000, Davies et al., 2009). Gly has been found to be increased in brain tumours particularly increased with WHO grade (Davies et al., 2009, Lehnhardt et al., 2005, Carapella et al., 1997).

Citrate (Cit)

Citrate, Cit, an intermediate product of the tricarboxylic acid cycle (TCA cycle) resonates around 2.6 ppm. The concentrations of this metabolite are found to be low in the human brain with possible causes of accumulation thought to be metabolic, pathological or both. Citrate has been reported to be involved in malignant progression (Seymour et al., 2008). The peak has also been observed in various paediatric brain tumours and has been found to be prominent in DIPG spectra (Costello et al., 1999, Seymour et al., 2008).

Lipids and macromolecules (LMM)

Lipids and macromolecules consist of broad resonances. The main lipid assignments are found around 0.9 ppm, 1.3 ppm and 2.0 ppm. Lipid levels seen in normal brain are very low but are known to increase in brain tumours. The observed increases in signal can be as a result of membrane degradation, necrosis and/or apoptosis (Tzika et al., 2003, Tzika et al., 2002). Macromolecule assignment is more difficult to determine as they become masked by lipid signals. Their presence is considered to be due to cytosolic proteins or lipids (Barker and Gillard, 2005, Panigrahy et al., 2010a). Lipid levels observed in metabolite profiles have been found to be indicators of tumour growth and can vary in response to treatment (Peet et al., 2007b, Astrakas et al., 2004).

Assessment of lipid signals in suspected tumour spectra should be conducted with caution. It is important to ensure that the voxel positioning before acquiring MRS was correct, as an increase in lipid can also be a result of out of volume lipid contamination from proximity to bone for example skull or from cysts (Rosen and Lenkinski, 2007).

Guanidinoacetate (Gua)

Guanidinoacetate, Gua, forms a peak around 3.78 ppm although its assignment is currently tentative. The peak has been identified in many brain tumour spectra but its role unknown (Panigrahy et al., 2006). Gua is a precursor of Cr synthesis and is closely associated with Cr (Longo et al., 2011).

<u>Alanine (Ala)</u>

Alanine, Ala, forms a doublet around 1.48 ppm similar to that of Lac. There are very few reports of Ala in paediatric brain tumours. However, it has previously been identified as a feature in adult meningiomas (Howe et al., 2003).

3.6 Summary

The resonances detected in MRS occur as a result of two phenomena, chemical shift and coupling. This chapter summarises the brief theory behind NMR with signposting to key texts for further detail. The PRESS acquisition sequence has become the most frequently used method for single voxel data in a clinical environment. The raw data in this thesis has been processed using TARQUIN software, listing the pre-processing steps used prior to obtaining metabolite concentrations. Accurate peak fitting and quantitation is challenging but with automated methods, MRS is becoming increasingly powerful in the assessment of brain tumours. The metabolites seen in *in vivo* brain spectra, including their identified roles have been summarised.

CHAPTER 4: METHODS

CHAPTER 4

4 METHODS

4.1 MRS acquisition

Multicentre ethical approval was given for all the studies and parental consent obtained. Single voxel proton MRS was performed between July 2003 and October 2012 on a paediatric population of patients (Age range: 0.1 to 16.4 years) during routine MRI scans for a suspected brain tumour that identified a tumour lesion, prior to treatment. The analysis also included a small cohort of paediatric patients with inherited metabolic disorders. MRS was performed after conventional MRI which included T1 weighted and T2 weighted sequences for the inherited metabolic disorder patients and after additional T1 weighted post contrast sequences for the brain tumour cohorts (Blaney et al., 2006). Spectroscopy data was acquired from 5 different centres including Birmingham Children's Hospital, Birmingham (BCH), Royal Marsden Hospital, Sutton (RMH), Great Ormond Street, London (GOS), Royal Liverpool Children's Hospital, Liverpool (RLC) and Queen's Medical Centre, Nottingham (QMC) at both 1.5 T and 3 T. Data was acquired from six different scanners from three different manufacturers including 1.5 T Siemens Symphony, 1.5 T Siemens Avanto, 1.5 T GE Signa Excite, 1.5 T Phillips Intera, 1.5 T Phillips Achieva and a 3 T Phillips Achieva TX. Data was incorporated into the different analyses where deemed appropriate and as a result the studies consisted of multi-scanner analyses from single or multiple centres. Three studies consisted of data from multiple centres (Chapter 5, 8 and 9) and remaining were single centre analyses because of the lack of available follow-up data. Spectroscopy was performed using a point-resolved spectroscopy sequence (PRESS) in all cases with short TE ranging from 23-37 ms and long TE 135-144

ms at 1.5 T with a TR 1500 ms and a range of signal averages (NSA) from 128 to 256 depending on voxel size. The ROI for each acquisition ranged from 3.38 cm^3 to 8 cm^3. At 3 T the core protocol for short eco time comprised of TE 37-41 ms and at long echo time 135-144 ms with a TR 2000 ms and 96-128 NSA. The ROI for each of these acquisitions varied from 2.2 cm^3 to 8 cm^3. Voxel placement was entirely within the tumour as delineated by the conventional MRI with the enhancing component maximised, or over brain pathology (in the cases of metabolic disease) in the left basal ganglia or the right parietal white matter. A water unsuppressed MR spectrum (16 NSA) was acquired following the acquisition using the same parameters. It is important for the voxel size for both the metabolite and water unsuppressed spectrum, for the same voxel position to correspond. Referencing to the water allows for comparisons between different volume acquisitions to be made.

4.2 Processing

Raw spectroscopy data was exported from the scanner and analysed using TARQUIN software (Wilson et al., 2011). It was chosen over other spectroscopy analysis packages for its use of simulated basis sets to fit metabolites. Simulated basis sets are generated computationally from the knowledge of the chemical properties of each metabolite and the pulse sequence parameters. The advantages of using simulated basis sets are that they can be generated very quickly for each metabolite in each experiment particularly where pulse sequence parameters have been altered. The small variations in echo time and repetition time for the data acquisitions on different scanners is more easily accounted for and less time consuming using a simulated method, than repeating single metabolite solution experiments for input into the experimental basis set each time a

parameter is changed. This is particularly advantageous for the data analysed in this thesis because of the combination of two field strengths (Wilson et al., 2010). The acquired raw data was fit to a linear combination of 25 metabolite basis functions generated at the correct field strength and echo time (see APPENDIX 1). In some analyses the extended basis set was used to include more recently reported metabolites, glycine and citrate (Davies et al., 2009, Seymour et al., 2008, Wilson et al., 2011). The uncertainty of the metabolite fits was assessed using Cramer-Rao Lower Bounds (CRLBs) (Cavassila et al., 2001). CRLB determine the precision of the fit of individual metabolites in the spectra calculated by standard deviation in mM. This is an important parameter to observe, as meaningless fit results that have extremely high estimated errors can as a consequence give false results. This is often seen with less well determined metabolites. The area under the unsuppressed water peak was used as an internal reference signal for quantitation of metabolite signals with concentrations reported in mM, assuming the water content of white matter (Jansen et al., 2006).

4.3   Quality control

All spectra in the analyses were assessed using the set quality control (QC) criteria (Davies et al., 2008). These included having conventional MRI and voxel location available for each case. Accurate voxel positioning was confirmed using the three imaging planes (example given in Figure 4.1) and voxel placement was verified to be >3mm away from bone, scalp and air and not dominated by normal brain. Spectra acquired from voxels that encompassed cyst and/or necrotic areas were excluded. In addition to this, spectra were required to meet TARQUIN quality control values for three parameters which were (1) full-width half-maximum (FWHM), a determinant of spectral width; (2) signal-to-noise

ratio (SNR), calculated as either SNR from the spectral residual or SNR MAX from spectral noise; and (3) Q, a measure of fit quality. Spectra were required to have a FWHM of <0.150 ppm, a SNR >5 and Q determined for each spectrum to be <2.5. Visual inspection of baseline abnormalities and major artefacts were also performed.
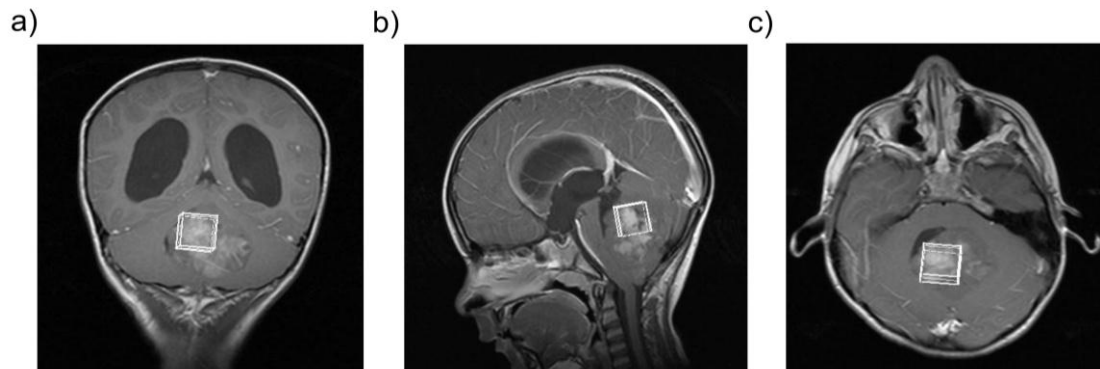
Figure 4.1 Example of voxel positioning over a medulloblastoma tumour in the a) coronal, b) sagittal and c) axial MRI plane

It should be noted that voxel placement is important for the assessment of spectra. Voxel placement over low or high grade elements within the same tumour will result in different spectral characteristics. This is likely to impact the results obtained. To overcome this, the voxel is aimed to be placed to maximise the solid enhancing component which expected to correspond to the most malignant part of the tumour. To reduce the number of variables that affect the spectra, a common protocol particularly across multiple centres is used. However, if the voxel is required to be placed in the same position on follow-up for longitudinal studies this may be problematic (Ricci et al., 2000). This is less likely to be an issue for tumour spectroscopy data as the clinical question will vary at different time points in MR imaging follow-up that will consequently result in a varied voxel placement.

4.4 Statistical analysis

All statistical analysis was performed with R Statistical Software (R Development Core Team, 2011) (Version 2.13.1) on the metabolite concentrations (mM) quantified using TARQUIN (Wilson et al., 2011). The version of TARQUIN, with the specific use or not of the extended basis set for each analysis, has been noted in each chapter. This varies for each study, because the analyses were performed over a three-year period. TARQUIN is periodically updated to accept new data formats, fix bugs, include new metabolites and improve user interaction. As result the most up-to-date version available was used at the start of each study's analysis. Although determination of CRLB for all metabolites across spectra was not formally tested in this body of work, metabolites Asp and GABA with previously reported high CRLB were excluded (Davies et al., 2008). Lipids and macromolecules at 0.9 ppm (LMM0.9), 1.3 ppm (LMM1.3) and 2.0 ppm (LMM2.0) were reported mostly as combined signals unless specified. A P value of <0.05 was considered to be statistically significant. Corrections for multiple comparisons are not usually applied in MRS studies (Panigrahy et al., 2006). However, other studies have demonstrated that these corrections are essential to control Type I error thus highlighting the importance of accounting for significant differences observed due to chance (Streiner and Norman, 2011). In this thesis the Bonferroni correction (significance value divided by the number of variables being tested) was used to calculate P values where large numbers of variables were tested and reported in their respective chapters. The conservative method assumes all variables are independent which for metabolites is unlikely to be true. As a result Bonferroni corrected P values were calculated but not applied (Bland and Altman, 1995). It should be noted that results that demonstrate P values greater than the

Bonferroni corrected value may be less significant. Power analysis has been performed for small cohorts that demonstrated no significant differences.

Paired and unpaired Student's t-test (Student, 1908), Mann-Whitney U-test (Mann and Whitney, 1947) and Wilcoxon signed ranked test (Wilcoxon, 1945) were used to compare means and probability of differences in metabolite concentrations or two imaging variables between two tumour types. Student's t-test's were used to compare means where analysis included variables that followed a normal distribution. Mann-Whitney U-test (Mann and Whitney, 1947) was used for independent tumour cohorts and Wilcoxon signed ranked test for paired analyses with both tests making no assumption regarding the distribution of the data (Wilcoxon, 1945).

For comparisons between more than two means, greater than two tumour groups (independent samples), ANOVA (Speed, 1987) was used where variables followed a normal distribution and Kruskal Wallis test where this had not been established (Kruskal and Wallis, 1952).

Principal component analysis (PCA) (Pearson, 1901) was used to determine the variability of the pre-treatment metabolite profiles of the tumour groups that had been selected as inputs. PCA was used an unsupervised method where the maximum number of principal components (i.e. the principal metabolites) was reached when 95% of the cumulative variance or the minimum group size -1, if the number of components that reached 95% exceeded this. Each point on a PCA plot represents a single case and those with similar metabolite profile characteristics will cluster together (Pearson, 1901, Harris et al., 2008). Linear Discriminant Analysis (LDA), a supervised dimension reduction method was applied

to the PCA scores (the point given to each case on the PCA plot) to produce diagnostic classifiers (Fisher, 1936). Leave-one out analysis (LOOCV) (Geisser, 1975) based on the LDA was used as a cross validation technique for the classifier. A posterior probability was outputted for each classification group per tested case to determine how likely it was that the case fell into the given groups. The classification with the highest probability was taken as the predicted classification group. Cases with > 80% posterior probability were deemed as good quality and reliable classifications.

A receiver operating characteristics (ROC) (Egan, 1975) curve is a method of visualising and determining cut-offs for classifiers (Fawcett, 2006). The curve is constructed with the sensitivity on the y-axis plotted against (1-specificity) on the x-axis for each possible cut-off value. The inputs for the plot were either metabolite concentrations for each case for a single metabolite as prognostic markers, or a combinatory model of metabolites. The accuracy of a diagnostic test from an ROC curve can be determined by the area under the curve or the AUC. An AUC of 0.5 corresponds to random chance and the perfect classification produces a curve up to the top left corner or an AUC of 1.0. Using the curve, a combination of specificity and sensitivity is used to select an optimal cut-off value (Linnet et al., 2012). This optimal cut-off was then used to evaluate the classifiers and visualise their performance using Kaplan-Meier curves.

Kaplan-Meier curves were constructed to compare the survival of different tumour cohorts over time using censoring to account for current patient status at the point of last follow-up (Kaplan and Meier, 1958). By censoring the data, cases lost during follow-up, or those that die or survive before the end of the study can be accounted for (Rich et al.,

2010). These were constructed using metabolite concentrations where ROC curves determined the cut-off or using discreet variables. This method was employed to identify markers of prognosis. The difference between the two curves, so difference in survival between the two groups, was tested for using a log-rank test (Mantel, 1967, Cox, 1972).

Cox-Regression analysis was performed to investigate the effect of variables on the survival of patients by determining a hazard ratio (Cox, 1972). This method was used confirm the significance of prognostic metabolite markers identified using Kaplan-Meier curves.

4.5 Summary

This chapter initially summarises the cohort and the centres involved in the studies in the chapters to follow. The core acquisition protocol used including TE, TR, the number of averages and size of ROI are given and specific details for each study have been expanded in their respective chapters. TARQUIN data is processed with the use of a simulated basis sets, shown to have a number of advantages over experimental basis sets. For an accurate interpretation of analysed spectroscopy data, it is important that it is assessed using a quality control criterion and this is common for all the data assessed in this thesis. With many metabolites quantitated and in some cases subtle changes observed, univariate and multivariate statistical methods are employed to use all the information obtained and to determine significant differences.

CHAPTER 5:
CHARACTERISATION OF
METABOLITE PROFILES OF
PAEDIATRIC BRAIN TUMOURS

CHAPTER 5

5 CHARACTERISATION OF METABOLITE PROFILES OF PAEDIATRIC BRAIN TUMOURS

5.1 Introduction

For over 20 years, Magnetic Resonance Imaging (MRI) has been the primary method of choice for the non-invasive diagnosis and characterisation of brain tumours in adults and children (Poussaint, 2001, Kuperman, 2000, Bryant et al., 2010). Although this modality illustrates exceptional anatomical and spatial information, conventional sequences are unable to provide functional understanding (Rao, 2008). Conventional MRI gives limited indication of tumour type and grade and provides no prognostic or treatment monitoring markers. This often leads to diagnostic dilemmas, where an accurate pre-operative diagnosis is essential for the clinical management of patients.

Preliminary studies of single voxel spectroscopy, published around 20 years ago were shown to aid in the characterisation of adult brain tumours (Bruhn et al., 1989, Langkowski et al., 1989). The potential of the technique lead to an interest in its use in paediatric neuro-oncology (Sutton et al., 1992). Early spectroscopy studies were performed at long echo time with limited metabolite information, mainly tCho, Cr, possibly tNAA and Lac. It soon became evident that short echo time spectroscopy was a more useful characterisation tool because it provided more metabolite information and had a greater SNR (Panigrahy et al., 2006). Results were mostly reported as trends of increases or decreases in metabolites relative to a reference metabolite, mostly Cr (Horská et al., 2001, Wang et al., 1995, Howe et al., 2003). However, the use of these

relative quantitation methods has demonstrated a number of disadvantages hindering its application to potentially useful clinical scenarios.

Firstly, the use of ratio based reporting results in the elimination of a potentially useful metabolite in the spectrum. Secondly, the most commonly used metabolite Cr, initially assumed to be stable in pathological states, has now been shown to alter significantly, resulting in confounding observations (Li et al., 2003). Reporting of ratios does not reveal whether changes are occurring in the numerator, denominator or even both (Jansen et al., 2006).

This has been overcome by using water as an internal reference for robust absolute metabolite quantitation, expressed in standard units of mM. This is achieved by taking an additional water reference scan from the same voxel. Analysis is now preferentially performed using automated software packages containing metabolite fitting methods, using basis sets in combination with the water as a reference metabolite. This demonstrates a powerful method of processing SVS data (Provencher, 2001, Wilson et al., 2011). As a result, subsequent studies have been able to differentiate between closely related metabolite profiles of brain tumours and have allowed the detection of tumour specific markers (Kovanlikaya et al., 2005, Panigrahy et al., 2006).

More recently, pattern recognition methods have become very popular with researchers for the classification of brain tumours using MRS. They often give excellent accuracy rates for tumour diagnosis but are not currently available for use in a routine clinical setting. Pattern recognition methods commonly used are based on multivariate statistics and can be performed on either the whole MR spectrum or a list of parameters for example

metabolite concentrations extracted from it (Davies et al., 2008, Hao et al., 2009). The most commonly used multivariate techniques include PCA and LDA (Opstad et al., 2007). Classification using these methods is most effective when a small number of potential diagnoses are being considered. The effect of combining tumour groups to give smaller numbers of larger classes has proven an effective strategy (Davies et al., 2008).

Despite the developments that have been made in MRS, the majority of studies are single centre and single scanner based consisting of small cohort numbers. This makes it difficult to demonstrate how robust the technique is and the benefits of using it. Cohorts often consist of common subtypes with spectroscopy of rarer tumours merely reported as case reports (Horská et al., 2001, Porto et al., 2010a, Chang et al., 2003).

The aims of this chapter were to measure metabolite concentrations of common and rare paediatric brain tumours using short-echo time spectroscopy and to establish distinguishing features from a large multi-scanner cohort of paediatric brain tumours in order to aid in their pre-operative diagnosis as an adjunct to conventional MRI.

5.2 Method

5.2.1 Patients

This is a retrospective analysis from a study in which single voxel 1H MRS was performed on children between July 2003 and October 2012 during routine MRI for a suspected brain tumour that identified a tumour lesion, prior to treatment. All spectra were checked for QC (section 4.3). Following this, a cohort of good quality spectra for inclusion in the study was established. Cases were subdivided into corresponding diagnostic subtypes (Table 5.1-5.5) and were included in the analysis if full diagnostic information

was available to determine the tumour group. Full diagnostic information included classification and grading of tumour tissue following surgery (biopsy or surgical resection) by histopathology performed using the 2007 WHO Classification of Tumours of the Central Nervous system (Louis et al., 2007). For those cases that did not have surgery, tumours were diagnosed on clinical and imaging findings alone. No tumour grade was determined for these tumours. To ensure spectral profiles were representative of the tumour types been investigated, diagnostic subgroups with only three or more cases available were included. Two cases had more than one good quality pre-treatment spectrum available. For these the earliest spectrum was used in the analysis. The cases were divided into the two different field strengths and further subdivided into echo times. Flow diagrams for patients included in the study at 1.5 T (Figure 5.1) and 3 T (Figure 5.2) are given. At 1.5 T, all spectroscopy was performed on five different scanner models from three different scanner manufacturers at five centres (BCH, QMC, RMH, RLC and GOS). These included the Siemens Symphony, Siemens Avanto, GE Signa Excite, Phillips Intera and Phillips Achieva. At 3 T all spectroscopy was performed on the Phillips Achieva at two centres (QMC and RLC).
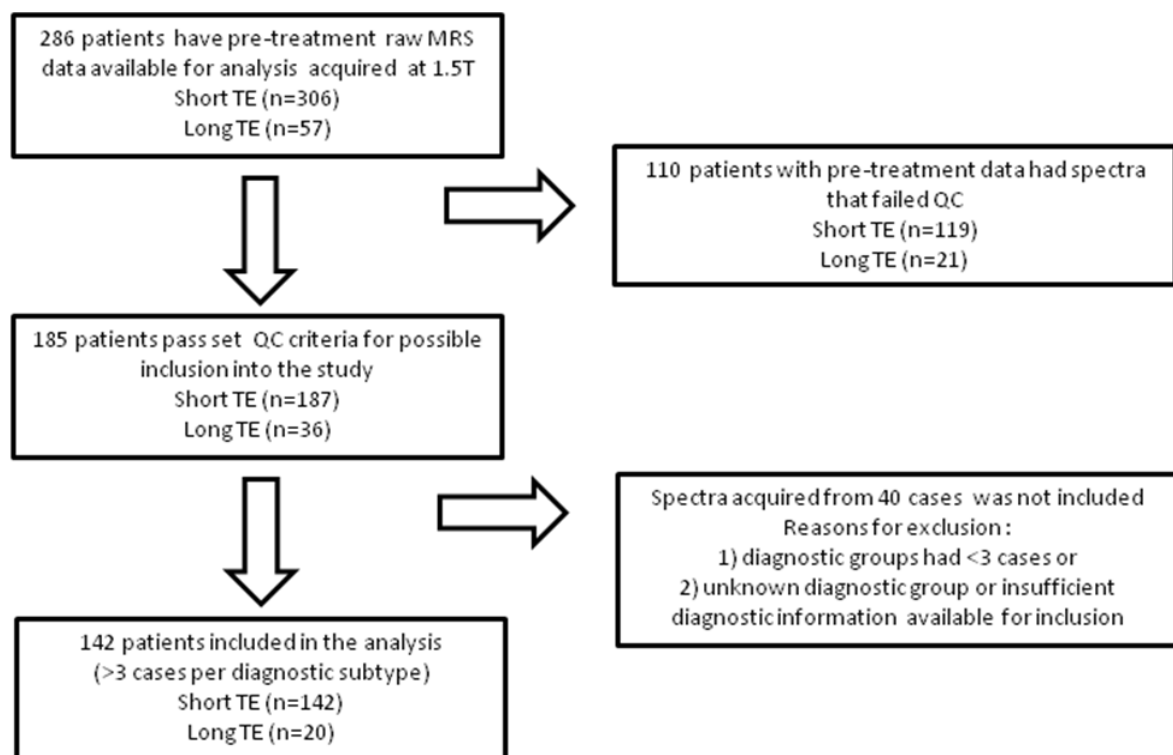
Figure 5.1 Flow diagram of patients studied at 1.5 T.
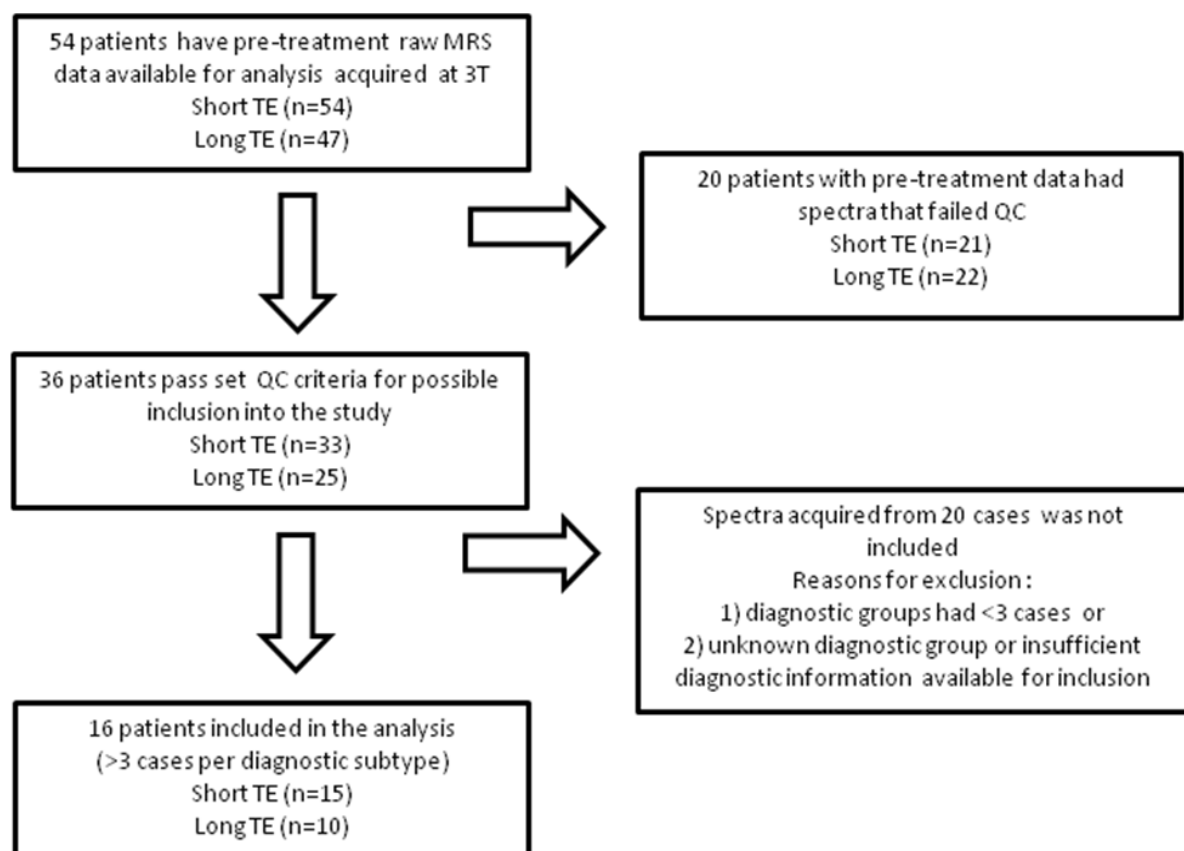
Figure 5.2 Flow diagram of patients studied at 3 T.

Table 5.1 Patient demographics of the most common paediatric brain tumours (>10) in the cohort with short echo time MRS at 1.5 T.

	Subjects	WHO grade	Age (mean ± SD)	Sex (F/M)
All Cases	142	I-IV	7.4 ± 4.5	55 / 87
Tumour Type				
Pilocytic Astrocytoma (PA) *****	35	I/II	7.2 ± 4.3	17/18
Medulloblastoma (MB) ****	42	IV	6.9 ± 3.6	12/30
Ependymoma (E) ***	10	II/III	5.1 ± 5.7	4/6
Diffuse Pontine Glioma (DIPG)	12	N/A	6.8 ± 3.4	7/5

Note: -
*** includes tanycytic and anaplastic
**** includes classic, desmoplastic and large cell
***** includes pilomyxoid
N/A not diagnosed on the basis of histopathology so no WHO grading available

Table 5.2 Patient demographics of the rare paediatric brain tumours (<10) in the cohort with short echo time MRS at 1.5 T.

Tumour Type	Subjects	WHO grade	Age (mean ± SD)	Sex (F/M)
Anaplastic Astrocytoma (AA)	3	III	9.5 ± 5.8	2/1
Atypical Teratoid Rhabdoid Tumour (ATRT)	5	IV	1.6 ±1.6	2/3
Choroid plexus Papilloma (CPP)	3	I	3.0 ± 2.6	0/3
CNS Primitive Neuroectodermal Tumour (CNS PNET)	3	IV	8.3 ± 5.5	2/1
Craniopharyngioma (CRANIO) *	3	I	7.4 ± 2.3	2/1
Diffuse astrocytoma (DA)**	5	II/III	11.0 ± 6.6	4/1
Ganglioglioma (GG)	5	I	11.8 ± 4.6	3/2
Germinoma (GER)	7	N/A	12.9 ± 2.2	1/6
Glioblastoma Multiforme (GBM)	9	IV	8.4 ± 4.5	2/7

Note: -
* includes classic and adamantinomatous
** includes classic, fibrillary and gemistocytic
N/A not diagnosed on the basis of histopathology so no WHO grading available

Table 5.3 Patient demographics of the cohort with long echo time MRS at 1.5 T.

	Subjects	WHO grade	Age (mean ± SD)	Sex (F/M)
All Cases	20	I and IV	7.9 ± 3.7	8/12
Tumour Type				
Pilocytic Astrocytoma (PA)	10	I	9.1 ± 4.1	6/4
Medulloblastoma (MB)	10	IV	6.8 ± 2.7	2/8

Table 5.4 Patient demographics of the cohort with short echo time MRS at 3 T.

	Subjects	WHO grade	Age (mean ± SD)	Sex (F/M)
All Cases	15	I and IV	6.7 ± 3.2	8/7
Tumour Type				
Pilocytic Astrocytoma (PA)	8	I	8.5 ± 2.4	4/ 4
Medulloblastoma (MB)	7	IV	4.5 ± 3.0	4/3

Table 5.5 Patient demographics of the cohort with long echo time MRS at 3 T

	Subjects	WHO grade	Age (mean ± SD)	Sex (F/M)
All Cases	10	I and IV	9.6 ± 4.4	6/4
Tumour Type				
Pilocytic Astrocytoma (PA)	5	I	9.1 ± 4.2	2/3
Medulloblastoma (MB)	5	IV	10 ± 5.0	4/1

5.2.2 MRS acquisition and quantitation of metabolite concentrations and lipid intensities

MRS was performed following conventional MRI. The spectroscopy protocol at 1.5 T consisted of short TE ranging from 23-37 ms and long TE 135-144 ms with a TR 1500 ms and a range of averages 128-256 depending on voxel size. At 3 T, short echo time comprised of TE 37-41 ms and at long echo time 135-144 ms with a TR 2000 ms and 128 averages. All spectra were analysed using TARQUIN (version 4.2.4 with extended basis set) fitting to a linear combination of 25 metabolite basis functions generated at the correct field strength and echo time (see APPENDIX 1) (Wilson et al., 2011). All spectra were assessed using the quality control (QC) criteria (section 4.3).

5.2.3 Statistical analysis

Asp and GABA were excluded due to their high CRLBs. Lipids and macromolecules at 0.9 ppm (LMM0.9), 1.3 ppm (LMM1.3) and 2.0 ppm (LMM2.0) were reported as combined signals. The Mann-Whitney U-test (Mann and Whitney, 1947) was performed to compare 1.5 T short echo time spectroscopy of low (WHO grade II and II) with high grade (WHO

grade III and IV) tumours. This comparison was made between the cases in the final analysis that had a confirmed WHO grade classification only. Mann-Whitney U-tests were also performed to compare one tumour type with all other tumours pooled (All Other) and for comparing between tumour types that are often included in a differential diagnosis on conventional MRI sequences. Comparisons between MB and PA at 1.5 T long TE were also undertaken. Mann-Whitney U-tests were also used to compare PA with MB at 3 T at both short and long TE. With 18 variables tested, a Bonferroni corrected significance of 0.002 ($P<0.002$) was calculated. A diagnostic classifier for discriminating between the three most common tumour subtypes, MB, PA and EP was constructed from the available short TE 1.5 T data. Metabolite concentrations and lipids+MM were first inputted into the PCA (Pearson, 1901) to reduce the number of variables, followed by LDA on the PCA scores for each case (Fisher, 1936). The maximum number of principal components (PCs) was reached when 95% of the cumulative proportion of variance was accounted for resulting in nine PCs as inputs. Accuracy of the classifier was determined using leave-one-out cross-validation (LOOCV) (Geisser, 1975). Spectroscopy data acquired at short TE 1.5 T from MB cases on four different scanners (Siemens Symphony, Siemens Avanto, GE Signa Excite, Phillips Intera) was compared using a Kruskal Wallis test (Kruskal and Wallis, 1952). Metabolite concentrations and standard deviations (SD) have been reported for each of diagnostic subtypes.

5.3 Results

5.3.1 Metabolic features of common childhood brain tumours
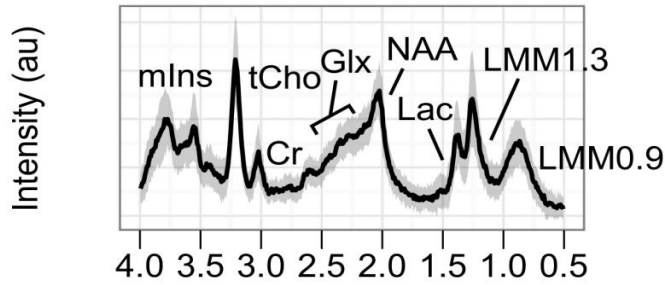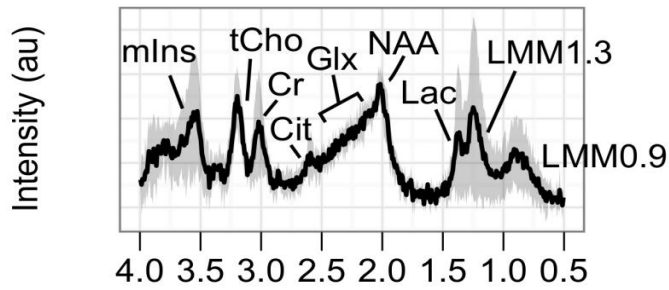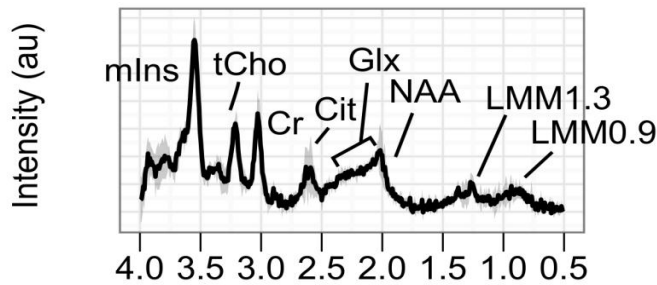
Figure 5.3 Mean spectra for a) pilocytic astrocytomas (n=35), b) diffuse astrocytomas (n=5), c) anaplastic astrocytomas (n=3) and d) glioblastoma multiforme (n=9). The solid black line depicts the mean with SD indicated by the shaded region (1.5 T and short TE).

Table 5.6 Mean absolute concentrations (mM) ± SD of short echo time pre-treatment paediatric brain tumours at 1.5 T compared using Mann-Whitney U-test.

Metabolites (mM ± SD)	AA (n=3)	ATRT (n=5)	CPP (n=3)	CNS PNET (n=3)	CRANIO[A] (n=3)	DA[B] (n=5)	DIPG (n=12)	E[C] (n=10)	GG (n=5)	GER (n=7)	GBM (n=9)	MB[D] (n=42)	PA[E] (n=35)	All Other (n=142)
Ala	0.14±0.2	0.21±0.5	0.98±1.3	0.38±0.5	0.11±0.2	0.12±0.2	0.33±0.4	0.21±0.4	0.46±0.3	0.04±0.1	0.25±0.5	0.49±0.9	0.39±0.7	0.36±0.7
Cit	2.07±1.6	0.45±0.3	0.33±0.4	0.29±0.3	0.12±0.1	0.62±0.6	**1.03±0.6****	0.73±0.4	0.49±0.5	0.76±0.4	0.61±0.5	0.59±0.4	**0.40±0.3****	0.60±0.5
Cr	**4.17±1.8***	1.48±2.2	0.76±1.3	0.59±0.5	**0.22±0.1****	2.18±1.5	**2.85±1.4***	**4.37±2.4****	2.35±0.7	1.26±0.4	1.24±0.9	**2.87±1.3******	**0.92±0.8******	2.10±1.7
tCho	1.22±0.4	1.87±1.7	2.24±2.3	1.63±1.5	**0.28±0.3****	0.94±0.4	**1.16±0.6***	2.00±1.1	1.32±0.5	1.19±0.6	1.82±1.3	**3.57±1.5******	**1.05±0.4******	1.99±1.5
Glc	**3.49±1.0***	2.71±4.4	3.25±0.8	0.01±0.02	0.9±0.9	1.41±1.8	**2.67±1.5***	1.06±1.2	1.28±1.3	2.55±1.6	1.38±1.5	**0.62±1.0******	**2.81±1.9******	1.74±1.9
Gln	3.01±1.0	2.03±2.4	1.41±1.8	2.22±0.1	2.22±1.5	3.21±1.1	3.65±4.2	3.15±1.9	4.02±1.8	3.14±2.1	4.08±3.0	2.86±2.6	3.53±1.9	3.17±2.4
Glu	4.11±2.5	2.44±2.1	2.71±1.7	2.10±2.6	**0.37±0.7***	1.81±1.4	1.95±1.3	2.77±1.8	3.14±1.1	**4.93±1.4*****	**1.17±1.6***	3.03±2.2	**1.68±1.4***	2.44±2.0
Glx	7.11±1.7	4.47±2.7	4.12±2.6	4.32±2.5	**2.60±0.9***	5.02±1.7	5.60±3.8	5.92±3.4	7.16±2.6	**8.06±2.5***	5.25±3.2	5.89±3.4	5.20±2.2	5.61±2.9
Gly	**0***	0.87±1.2	3.32±3.3	1.60±2.8	0.54±0.6	**0.04±0.1***	1.17±2.1	3.44±3.3	1.59±1.1	1.41±1.6	1.31±1.0	**3.45±2.3******	**0.63±1.1*****	1.87±2.2
Gua	0.41±0.4	1.36±2.7	0.42±0.7	0.51±0.9	0.97±0.9	0.38±0.5	0.66±2.1	0.61±1.0	0.47±0.4	0.49±1.3	0.42±0.7	**1.14±1.1******	**0.23±0.5***	0.67±1.1
mIns	**11±2.0****	1.07±1.8	**8.11±9.7***	1.91±2.8	0	2.83±2.3	**5.95±3.3******	**6.14±4.9****	1.28±1.9	1.19±1.3	0.74±0.9	**0.8±2.0******	0.70±0.9	2.07±3.4
Lac	**0.64±0.6***	3.43±2.3	2.67±3.6	4.76±3.0	3.74±1.5	1.73±1.4	**0.71±0.9******	1.60±1.0	1.85±0.7	2.84±4.6	**5.24±4.0****	2.67±1.8	2.32±1.9	2.50±2.3
LMM0.9	2.98±1.7	10.4±4.4	7.53±8.3	6.30±2.3	6.16±3.0	3.65±2.8	**2.21±1.7******	4.96±3.5	2.92±1.0	5.04±4.2	**9.13±5.1***	**6.9±3.3******	**4.29±2.3***	5.55±3.7
LMM1.3	3.62±2.1	**41±25****	12.6±18	15±14	9.37±7.0	5.40±6.2	**2.99±2.3******	15±16	**2.92±2.1***	18±22	14±6.1	**17±13******	**6.1±4.3******	12±13
LMM2.0	7.94±1.3	12±5.7	5.79±3.0	7.19±2.6	5.69±2.0	9.90±6.4	**6.02±3.0*****	12.±7.5	8.43±2.6	9.38±3.2	**12±2.4***	**11±3.0******	**6.54±2.8******	9.07±4.2
tNAA	1.54±1.7	1.12±0.9	**0.29±0.5***	1.18±0.4	1.00±0.7	1.81±0.5	**2.52±1.1*****	1.07±0.7	1.79±0.9	1.23±0.7	1.02±0.9	1.25±0.8	1.55±0.8	1.42±0.9
sIns	0.18±0.2	0.10±0.2	0.37±0.5	0.16±0.2	0	0.08±0.08	0.27±0.3	**0.47±0.4***	0.09±0.2	0.29±0.4	0.07±0.1	**0.49±0.5******	**0.05±0.1******	0.26±0.4
Tau	1.39±1.4	1.36±2.1	0.95±0.9	0.43±0.7	0.41±0.4	0.23±0.4	0.40±0.5	0.89±1.3	0.35±0.4	1.86±1.5	**0.1±0.3****	**2.68±2.3******	0.64±1.0	1.28±1.79

Note: - * *P*<0.05, ** *P*<0.01, *** *P*<0.001, **** *P*<0.0001, versus All Other tumours

A. includes classic and adamantinomatous B. includes classic, fibrillary and gemistocytic C. includes tanycytic and anaplastic D. includes classic, desmoplastic and large cell E. includes pilomyxoid
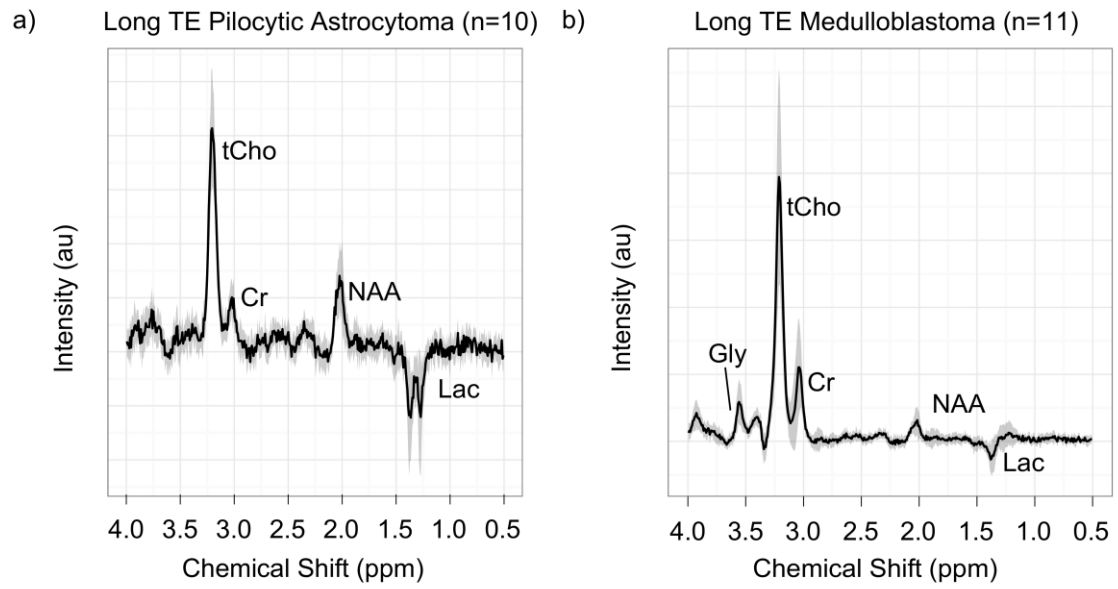
Figure 5.4 Mean spectra for a) pilocytic astrocytomas (n=10) and b) medulloblastomas (n=11). The solid black line depicts the mean with SD indicated by the shaded region (1.5 T and long TE).
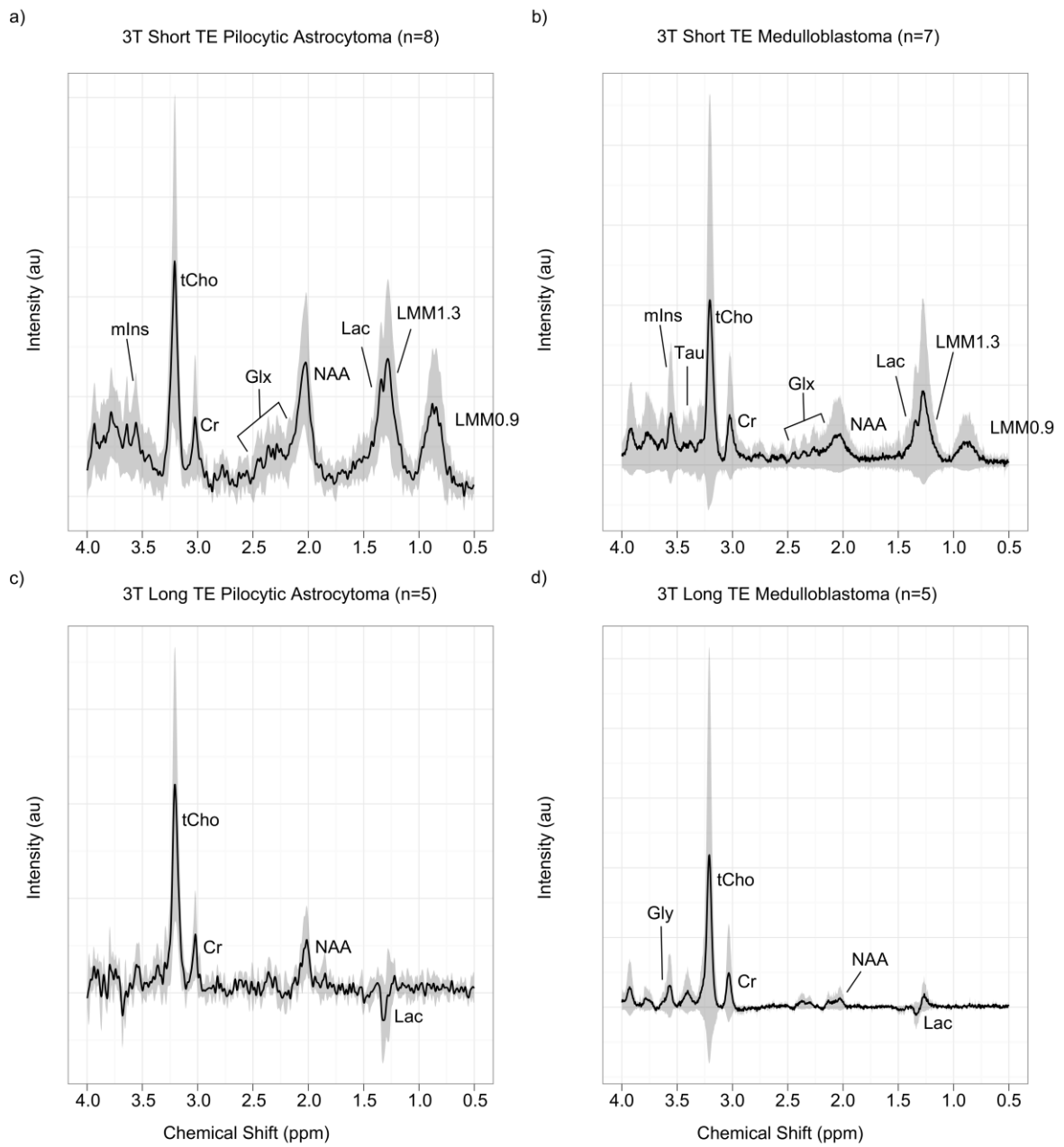
Figure 5.5 Mean spectra for a) pilocytic astrocytomas (n=8), b) medulloblastoma at short TE (n=7), c) pilocytic astrocytoma (n=5) and d) medulloblastoma at long TE (n=5). The solid black line depicts the mean with SD indicated by the shaded region (3 T and short and long TE).

Table 5.7 Mean absolute concentrations (mM) ± SD of long echo time pre-treatment paediatric brain tumours at 1.5 T with *P* values determined using Mann-Whitney U-test.

Metabolite concs (mM ± SD)	MB (n=10)	PA (n=10)
Ala	0.99±0.8	0.37±0.5
Cit	1.46±1.3	0.61±0.7
Cr	**7.96±6.2**	**0.90±0.8 ****
tCho	**10.4±5.9**	**1.52±0.9 ****
Gly	**3.83±2.5**	**0.36±0.5 ****
Lac	2.62±2.2	2.09±1.7
tNAA	2.23±1.8	1.10±0.5

Note: - * *P*<0.05, ** *P*<0.01

Table 5.8 Mean absolute concentrations (mM) ± SD of short echo time pre-treatment paediatric brain tumours at 3 T with *P* values determined using Mann-Whitney U-test.

Metabolites concs (mM ± SD)	MB (n=7)	PA (n=8)
Ala	0.31±0.5	3.3±4.2
Cit	0.47±0.2	0.78±0.5
Cr	**3.80±1.3**	**1.55±1.2 ****
tCho	**4.99±2.0**	**2.11±1.1 ****
Glc	**6.37±4.5**	**2.57±2.0 ***
Gln	2.39±1.6	2.72±1.7
Glu	3.38±0.6	4.99±4.0
Glx	5.77±1.9	7.71±5.2
Gly	**3.79±2.5**	**0.57±0.6 ****
mIns	0.69±1.7	2.08±2.5
Lac	2.14±2.5	1.91±1.6
LMM0.9	5.24±1.8	6.09±2.4
LMM1.3	**25.3±7.0**	**13.5±6.7 ****
LMM2.0	10.1±4.6	7.85±3.2
tNAA	**0.78±0.3**	**2.33±1.0 *****
sIns	0.46±0.7	0.08±0.1
Tau	**6.65±6.0**	**1.91±1.6 ***

Note: - * *P*<0.05, ** *P*<0.01, *** *P*<0.001, **** *P*<0.0001

Table 5.9 Mean absolute concentrations (mM) ± SD of long echo time pre-treatment paediatric brain tumours at 3 T with *P* values determined using Mann-Whitney U-test.

Metabolite concs (mM ± SD)	MB (n=5)	PA (n=5)
Ala	0.74±0.7	1.17±0.7
Cit	0	0
Cr	**10.1±3.1**	**2.85±1.9 ****
tCho	**13.4±5.7**	**3.99±3.0 ***
Gly	5.27±4.6	0.52±0.7
Lac	3.54±3.1	1.86±1.3
tNAA	1.86±0.9	1.73±1.1

Note: - * *P*<0.05, ** *P*<0.01

Pilocytic Astrocytoma (PA)

Histopathological subtypes of PA occurring in different locations in the brain were pooled as one group in this analysis.

Characteristic features of the PA spectra (Figure 5.3a) were readily detectable Lac, decreased Cr and increased tNAA. Compared with All Other, PA had significantly decreased mean Cit (*P*<0.01), Cr (*P*<0.0001), tCho (*P*<0.0001), Glu (*P*<0.05), Gly (*P*<0.001), LMM0.9 (*P*<0.05), LMM1.3 and LMM2.0 (*P*<0.0001) and sIns (*P*<0.0001) and significantly increased Glc (*P*<0.0001) (Table 5.6). At long TE significantly less Cr, tCho and Gly (*P*<0.01) was observed in PA than was found in MB (Figure 5.4a and Table 5.7). At 3 T short TE PA had significantly lower Cr (*P*<0.01), tCho (*P*<0.01), Glc (*P*<0.05), Gly (*P*<0.01), LMM1.3 (*P*<0.01) and Tau (*P*<0.05), and significantly higher tNAA (*P*<0.001) when compared to MB (Figure 5.5a and Table 5.8). At 3 T long TE MRS demonstrated significantly lower Cr (*P*<0.01) and tCho (*P*<0.05) in PA than MB (Figure 5.5c and Table 5.9)
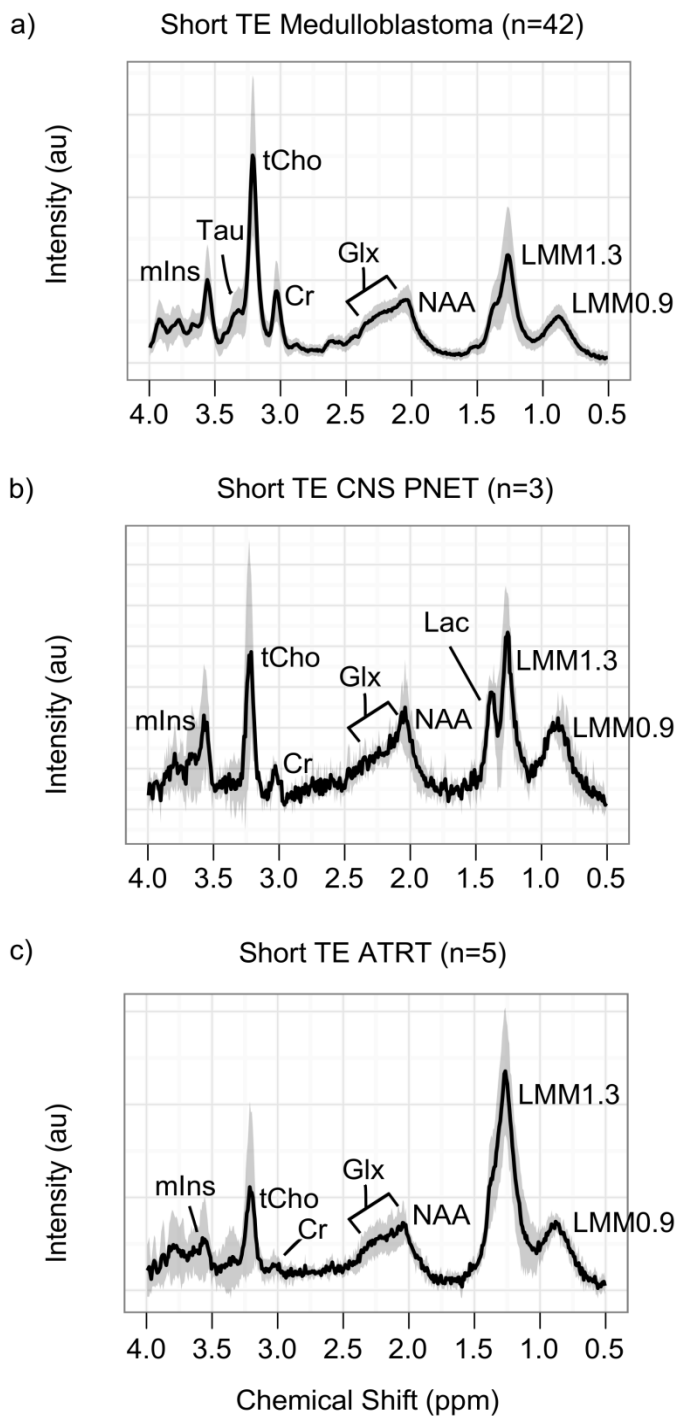
Figure 5.6 Mean spectra for a) medulloblastomas (n=42), b) central nervous system primitive neuroectodermal tumours (n=3) and c) atypical teratoid rhabdoid tumours (n=5). The solid black line depicts the mean with SD indicated by the shaded region (1.5 T and short TE)

Medulloblastoma (MB)

The most prominent feature of the MB mean spectra (Figure 5.6a) was Tau. Other features include elevated tCho, decreased mIns and elevated lipids+MMs at 1.3 ppm. On comparison with All Other subtypes, MB exhibited the most difference in metabolites and lipids+MMs and with the highest significance. MB spectra demonstrated significantly elevated concentrations of mean Cr, tCho ,Gly, LMM0.9, LMM1.3 and LMM2.0, sIns and Tau and decreased mean Glc and mIns ($P<0.0001$ for all) (Table 5.6). Significantly increased Cr, tCho and Gly ($P<0.01$) were seen at long TE when compared to PA (Figure 5.4b and Table 5.7)

MB spectra acquired at short TE at 3 T had significantly higher Cr, tCho, Gly, LMM1.3 ($P<0.01$), Glc and Tau ($P<0.05$) and significantly lower tNAA ($P<0.001$) compared to PA (Figure 5.5b & Table 5.8). Significantly higher Cr ($P<0.01$) and tCho ($P<0.05$) was seen at long TE at 3 T in MB (Figure 5.5c and Table 5.9)
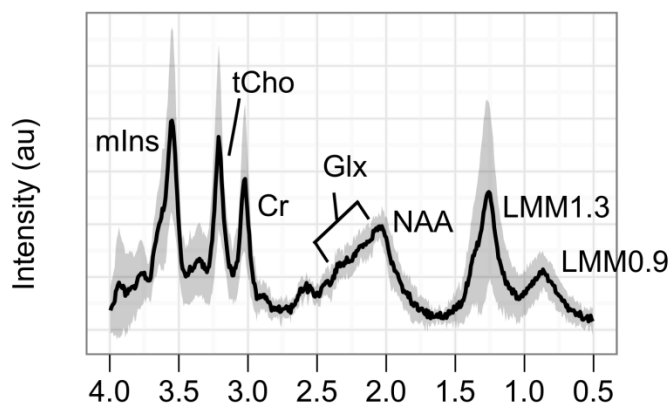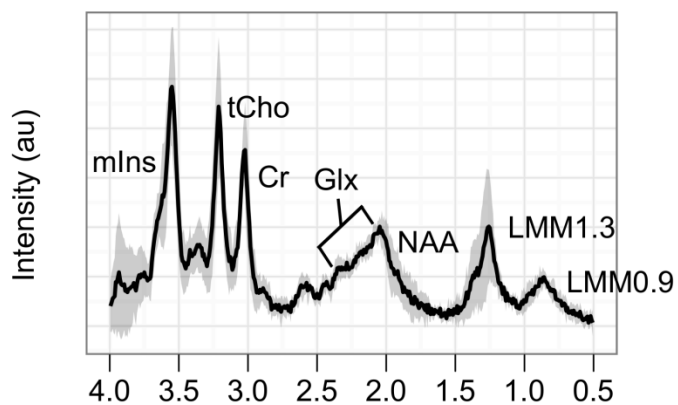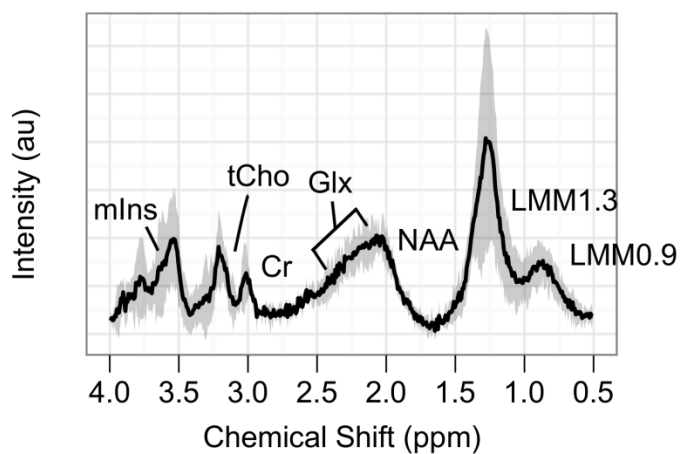
Figure 5.7 Mean spectra for a) all ependymomas (n=10), b) WHO grade II ependymomas (n=7) and c) WHO grade III ependymomas (n=3). The solid black line demonstrates the mean with SD indicated by the shaded region (1.5 T and short TE).

Ependymoma (EP)

Qualitative analysis of the EP mean spectra (Figure 5.7a) showed highly elevated mIns and elevated Cr. Comparison of EP grade II (Figure 5.7b) and grade III (Figure 5.7c) on qualitative analysis show an increase in LMM1.3 and decrease of mIns with increasing grade. Compared to All Other, EP had significantly elevated mean concentrations of mIns, Cr ($P<0.01$) and sIns ($P<0.05$) (Table 5.6).
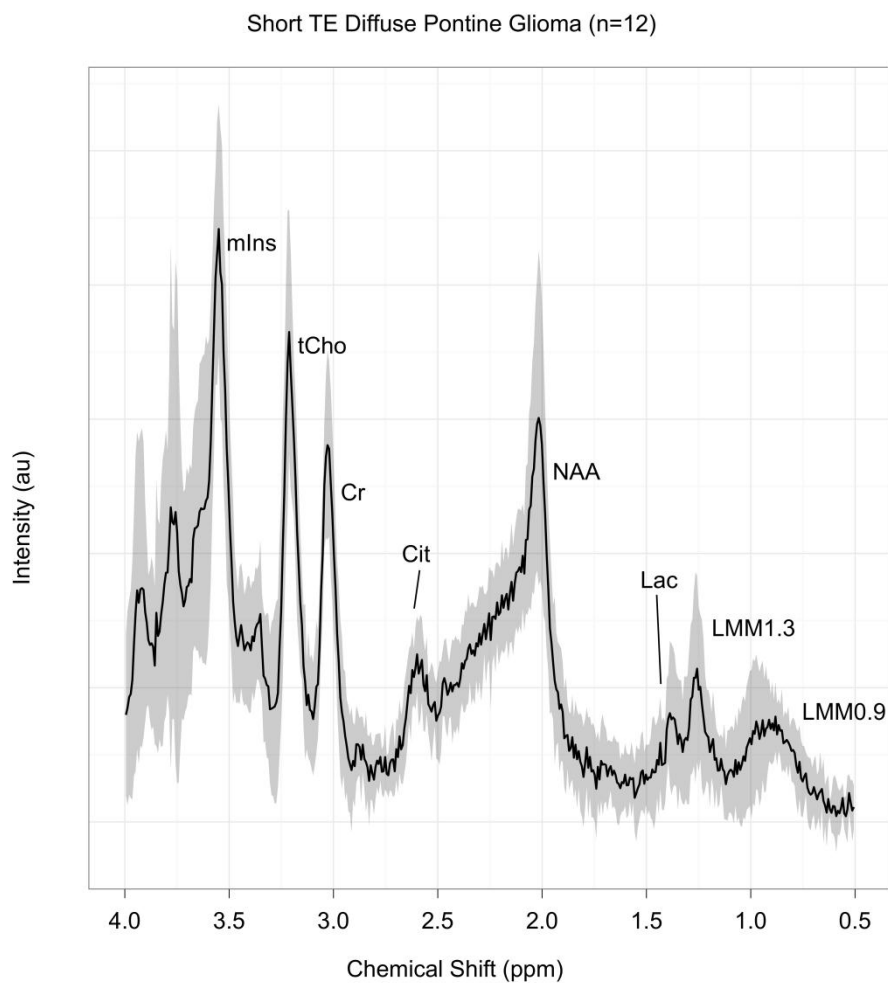
Figure 5.8 Mean spectra for diffuse pontine gliomas (n=12). The solid black line depicts the mean spectra with SD indicated by the shaded region (1.5 T and short TE).*

* The additional two patients included in the mean spectra had no water files so were not included in the statistical analysis

Diffuse Intrinsic Pontine Glioma (DIPG)

The DIPG mean spectra (Figure 5.8) possessed a prominent Cit, increased Cr, mIns and tNAA and decreased Lac, LMM0.9 and LMM1.3. Significantly elevated mean Cit ($P<0.01$), Cr, Glc ($P<0.05$), mIns ($P<0.0001$) and tNAA ($P<0.001$) and decreased mean tCho ($P<0.05$), Lac, LMM0.9, LMM1.3 and LMM2.0 ($P<0.0001$) were found in DIPG when compared to All Other (Table 5.6).
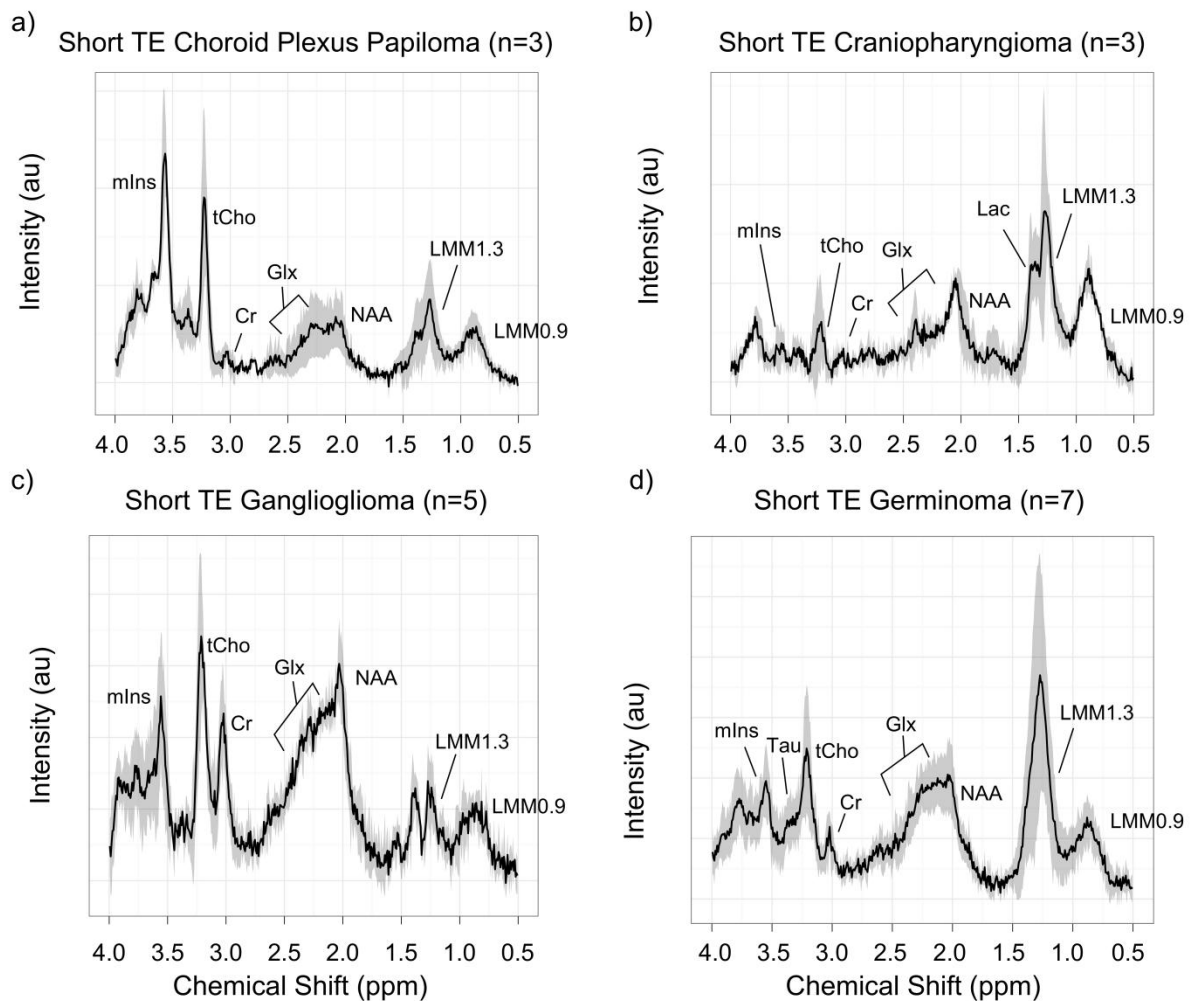
Figure 5.9 Mean spectra for a) choroid plexus papilloma (n=3), b) craniopharyngioma (n=3), c) ganglioglioma (n=5) and d) germinoma (n=7). The solid black line depicts the mean with SD indicated by the shaded region (1.5 T and short TE).

5.3.2 Metabolic features of rare childhood brain tumours

<u>Anaplastic Astrocytoma (AA)</u>

On qualitative analysis the AA mean spectra (Figure 5.3c) showed low LMM0.9 and LMM1.3, prominent Cit and high mIns. Compared with All Other, AA had significantly increased mean Cr, Glc ($P<0.05$) and mIns ($P<0.01$) and decreased Lac ($P<0.05$). No Gly ($P<0.05$) was quantified in these tumours (Table 5.6).

<u>Atypical Teratoid Rhabdoid Tumour</u>

ATRT mean spectra (Figure 5.6c) exhibited elevated LMM1.3 which was found to be significantly different to All Other ($P<0.01$, 40.9 vs. 12.0) (Table 5.6).

<u>Choroid Plexus Papilloma (CPP)</u>

The most prominent features of the CPP mean spectra (Figure 5.9a) were low Cr and high mIns. Compared with All Other, CPP demonstrated significantly increased mean mIns and decreased tNAA ($P<0.05$).

<u>CNS Primitive Neuroectodermal Tumour (CNS PNET)</u>

Qualitative analysis demonstrated high levels of LMM1.3 (Figure 5.6b). No significantly different metabolites or lipids+MMs ($P>0.05$) were identified when compared to All Other (Table 5.6).

<u>Craniopharyngioma (Cranio)</u>

The tumour mean spectra consisted of low levels of metabolites and high lipids+MMs (Figure 5.9b). This is consistent with All Other comparisons where significantly decreased

mean Cr ($P<0.01$), tCho ($P<0.01$), Glu ($P<0.05$) and Glx ($P<0.05$) were observed (Table 5.6). It should be noted that low metabolite levels was not characteristics for all Cranio and overlap with PA spectra has been previously observed.

Diffuse astrocytoma (DA)

Qualitative analysis demonstrated readily detectable Cit and high tNAA (Figure 5.3b). Significantly decreased mean Gly ($P<0.05$) was the only differentiator from All Other (Table 5.6).

Ganglioglioma (GG)

On qualitative analysis elevate Glx was seen (Figure 5.9c). GG had significantly lower LMM1.3 ($P<0.05$) when compared with All Other (Table 5.6).

Germinoma (GER)

GER mean spectra demonstrated readily detectable Tau and elevated LMM1.3 (Figure 5.9d). Compared with All Other, GER consisted of significantly increased mean Glu ($P<0.05$) and Glx ($P<0.05$) (Table 5.6).

Glioblastoma Multiforme (GBM)

A characteristic spectral feature of GBM was high LMM1.3 (Figure 5.3d). Significantly high mean Lac ($P<0.01$), LMM2.0 ($P<0.05$) and low Glc ($P<0.05$) and Tau ($P<0.01$) were seen when compared to All Other (Table 5.6).

<u>Low (WHO grade I and II) vs. high grade tumours (WHO grade III and IV)</u>

Statistical analysis comparing low (n=65) and high grade (n=58) tumours demonstrated significantly higher Cr, tCho, Gly, Gua, LMM0.9, LMM1.3, LMM2.0, sIns (*P*<0.001 for all), Cit (*P*<0.01), Tau (*P*<0.01) and Lac (*P*<0.05) and significantly lower Glc (*P*<0.001) and mIns in high grade tumours (Table given in APPENDIX 2).

5.3.3 Comparison of tumour types that are often included in a differential diagnosis

Table 5.10 Differentiation between tumour metabolite profiles at 1.5 T comparing those that are often included in differential diagnoses on conventional radiology using Mann-Whitney U-test with *P* values reported.

	ATRT (n=5)	E[A] (n=10)	PA[B] (n=35)
MB (n=42)	↑ Cr *	↓ Cr *	↑ Cit**
	↑ Gly **	↑ tCho **	↑ Cr ****
	↓ LMM0.9 *	↓ mIns ***	↑ tCho ****
	↓ LMM1.3 *	↑ LMM0.9 *	↓Glc ****
	↑ sIns *	↑ Tau **	↑ Glu **
			↑ Gly ****
			↑ Gua ****
			↑ mIns *
			↑ LMM0.9 ****
			↑ LMM1.3 ****
			↑ LMM2.0 ****
			↑ sIns ****
			↑Tau ****
	DA[c] (n=5)	GBM (n=9)	
DIPG (n=12)	↑m Ins*	↑ Cit*	
		↑ Cr ***	
		↑ mIns ***	
		↓ Lac ***	
		↓ LMM0.9 ***	
		↓ LMM1.3 ****	
		↓ LMM2.0 ***	
		↑ tNAA **	
		↑ Tau *	

Note: - * *P*<0.05, ** *P*<0.01, *** *P*<0.001, **** *P*<0.0001

A. includes tanycytic and anaplastic B. includes pilomyxoid C. includes classic, fibrillary and gemistocytic D. includes classic, desmoplastic and large cell

Distinguishing MB from ATRT showed MB to have significantly higher Cr ($P<0.05$), Gly ($P<0.01$) and sIns and significantly decreased LMM0.9 and LMM1.3 ($P<0.05$). Comparisons between MB and EP demonstrated MB to have significantly increased tCho ($P<0.01$), LMM0.9 ($P<0.05$) and Tau ($P<0.01$) with significantly decreased Cr ($P<0.05$) and mIns ($P<0.001$). Compared with PA, MB had a number significantly higher metabolites including Cr, tCho, Gly, Tau, LMM0.9, LMM1.3 and LMM2.0 ($P<0.0001$) excluding Glc that was significantly lower ($P<0.0001$) (Table 5.10).

The only discriminator between DIPG and DA was mIns with DIPG having significantly higher concentrations ($P<0.05$). To distinguish metabolite profiles of GBM from DIPG, DIPG was found to have significantly increased Cit ($P<0.05$), Cr ($P<0.001$), mIns ($P<0.001$), tNAA ($P<0.01$) and Tau ($P<0.05$) with significantly decreased Lac, LMM0.9, LMM1.3 and LMM2.0 ($P<0.001$) (Table 5.10).
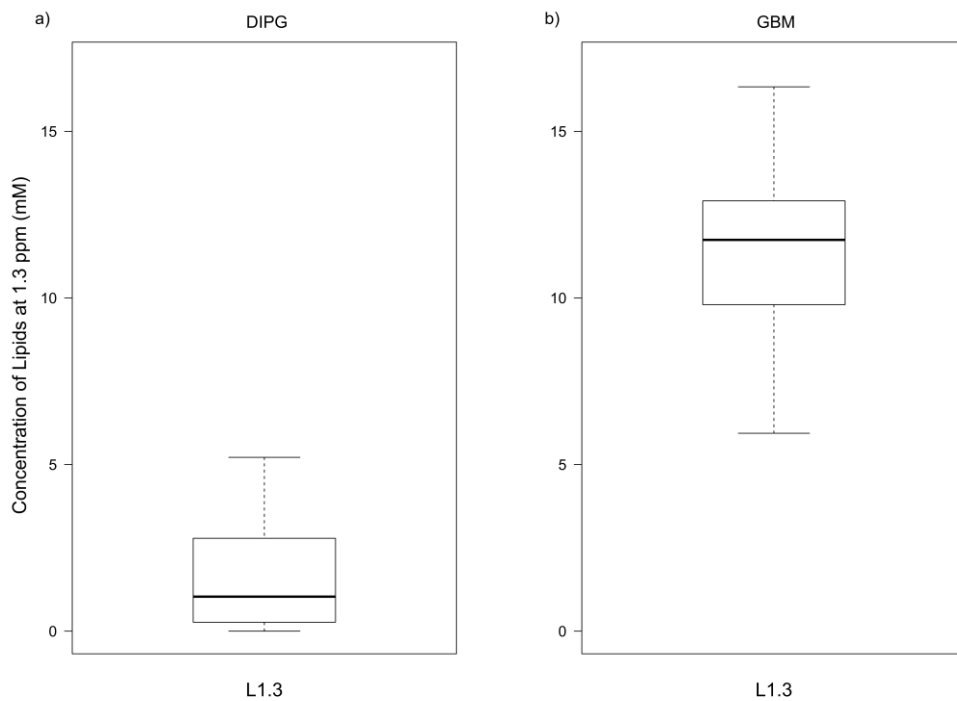
Figure 5.10 Box and whisker plot comparing levels of lipids at 1.3 ppm (L1.3) in DIPG and GBM

Box and whisker plots analysis comparing tumour types that often result in differential diagnosis on MRI exhibited no discriminatory metabolites or lipids+MMs. A comparison of lipids (lip1.3a+lip1.3b) alone at 1.3 ppm (L1.3) was found to discriminate GBM from DIPG (Figure 5.10) with higher levels found in GBM.

5.3.4 Classification of common brain tumours by metabolite profile
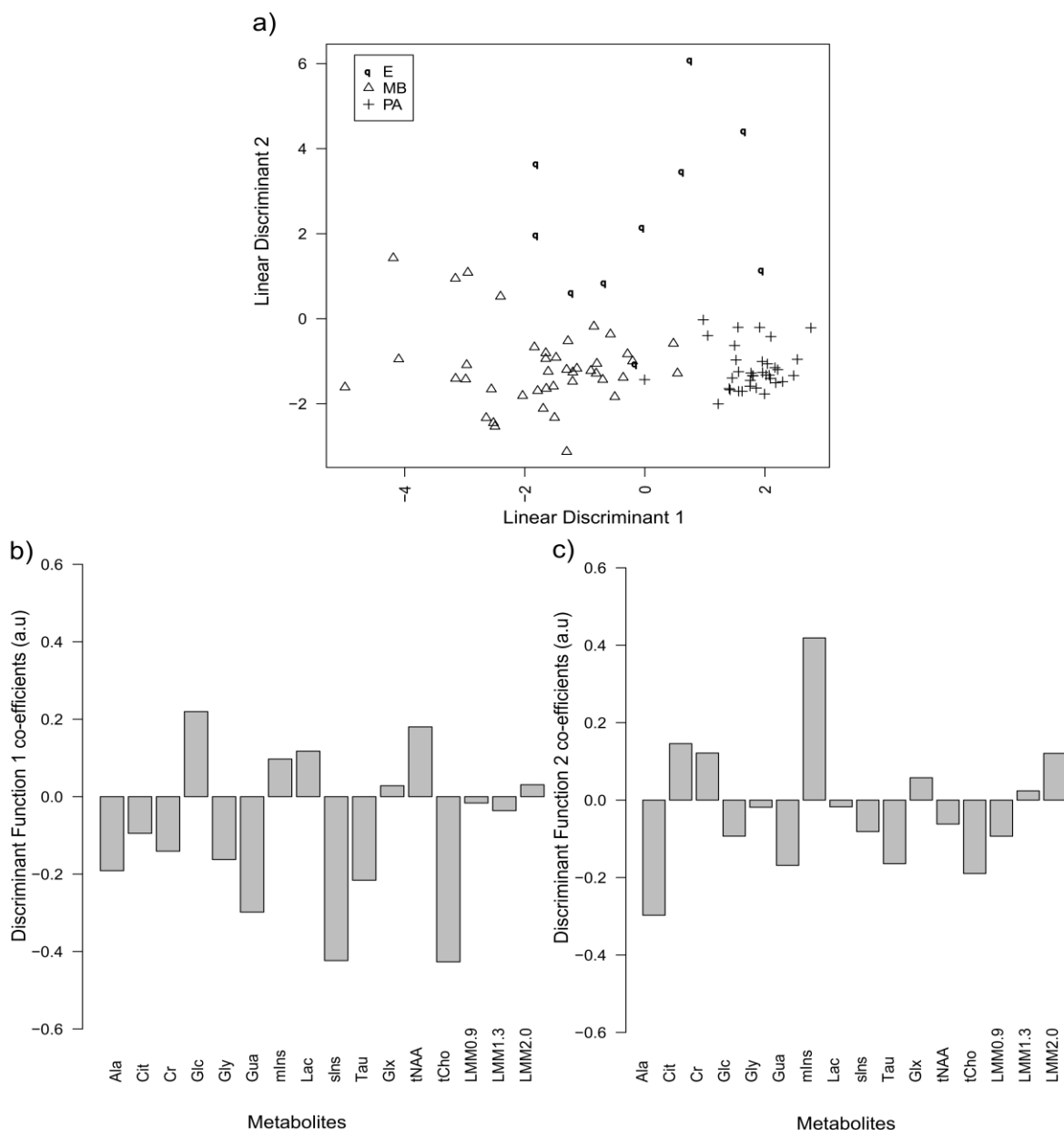
Figure 5.11 Results of the three way classifier between MB, PA and EP showing a a) scatter plot of the discriminant function scores for each tumour type b) discriminant function 1 coefficients and c) discriminant function 2 coefficients of the standardised metabolite profile.

The diagnostic three way classifier showed a good separation between the three tumour types with highly clustered regions seen for each tumour (Figure 5.11a). MB scored highly in discriminant function 1, characterised by high tCho, sIns, Gua and Tau and PA with high tNAA and Lac (Figure 5.11b). PA was distinguished from EP by high tNAA with EP

characterised by high mIns (Figure 5.11c). LOOCV demonstrated a success rate of 86% with the correct classification of 71 out of 83 cases all with a posterior probability above 80%.

5.3.5 Scanner comparisons

Table 5.11 Mean absolute concentrations (mM) ± SD of short echo time MB spectra acquired on 4 different scanners at 1.5 T prior to treatment with comparisons made using Kruskal-Wallis test.

Metabolite concs (mM ± SD)	P value	GE Signa Excite	Phillips Intera	Siemens Symphony	Siemens Avanto
Cr	**0.03**	3.68±0.34	1.99±1.11	2.76±1.40	3.52±0.65
Gua	**0.008**	3.32±1.06	0.87±0.91	0.85±0.70	1.23±0.84

Cr and Gua were the only significant metabolites found when comparing metabolite concentrations measured in MB from spectra acquired on four different scanner models at 1.5 T (Siemens Symphony (n=27), Siemens Avanto (n=6), GE Signa Excite (n=4), Phillips Intera (n=5) (Table 5.11).

5.4 Discussion

5.4.1 Metabolite profiles for characterising paediatric brain tumours

Mean metabolite concentrations of common and rare paediatric brain tumours determined by quantitative short echo time spectroscopy were shown to differ from one tumour type to another. The reported differences show MRS has the potential to aid in diagnosis and characterisation. The variations in *in vivo* concentrations of metabolite pathway intermediates observed in MRS are likely to be explained by differences in tumour biology. Although the number of metabolites which can be quantified by *in vivo* MRS is limited, many have been linked to important processes in the pathogenesis of cancer. Establishing how these are linked may provide an insight into the favoured pathways for pathogenesis.

Total choline (tCho)

The highest levels of tCho were seen in MB and CPP and lowest levels in Cranio, DA and PA mostly in agreement with previous studies with the exception of CPP (Panigrahy et al., 2006, Davies et al., 2008, Vicente et al., 2013). Higher grade tumours have shown significantly elevated tCho levels as previously reported (Astrakas et al., 2004).

Activated choline metabolism is a known metabolic hallmark of cancer (Glunde et al., 2011). Elevated levels of choline containing compounds are associated with cell proliferation and malignant transformation with a role in cell membrane synthesis and breakdown (Glunde et al., 2011). The expected elevated levels of tCho seen in MB (grade IV) and lower levels in Cranio (grade I), DA (grade II) and PA (grade I) are consistent with the association of tumour malignancy. The unexpected increased levels seen in CPP (grade I) is likely to be an effect of small group size (n=3).

The metabolism of choline is influenced by changes in the tumour microenvironment (Glunde et al., 2011). An increase in metabolic activity of tumour cells results in a hypoxic environment that acidifies extracellular pH (Gillies et al., 2002). These changes result in an decrease of GPC and an increase in PCh in brain tumours compared to normal brain tissue (Usenius et al., 1994). Many studies have shown an increase in the expression and activity of choline kinase α, an enzyme that regulates the conversion of PCh from free choline to be directly associated with cell proliferation and malignancy. GPC is responsible for contributing to the production of PCh (Glunde et al., 2011). Thus choline metabolism is controlled by the interplay of enzymes involved in the Kennedy pathway modulated by oncogenic signalling. The deregulation of these pathways is a common

feature in cancer and the differences in the pathway affected, results in differences in tumour pathogenesis (Glunde et al., 2011, Righi et al., 2009). However, the close overlap between *in vivo* measurements of choline containing compounds makes it difficult to infer which genes are involved in mediation of the pathway for targeted therapies (Tzika et al., 2007).

Alternatively, phosphorous spectroscopy or 31P MRS enables the measurement of the relative concentrations of PCh and GPC due to the greater chemical shift separation between the two metabolites (reported values of 0.007 ppm using proton vs. 0.13 ppm using phosphorous) (Loening et al., 2005). The method is currently limited by low sensitivity and abundance of phosphorus metabolites, however with the availability of high field scanners the technique looks promising in aiding the investigation of tumour biology (Qiao et al., 2006).

Creatine (Cr)

High levels of Cr were seen in EP and AA and low levels in Cranio, CNS PNET, CPP and PA. High grade tumours possessed higher Cr levels. Previous studies have reported high levels in EP and AA (Panigrahy et al., 2006). Cr was also found to be low in PA compared to other cerebellar tumours (Davies et al., 2008).

Creatine is an essential component of energy metabolism and is thereby a marker of the energy state of cells (Martinez-Bisbal and Celda, 2009). It is responsible for energy storage and transmission where Cr, through phosphocreatine provides phosphate for ATP (Nasrallah et al., 2010, Vigneron et al., 2001). This process is catalysed by creatine kinase and it is hypothesised that the downregulation of the enzyme is responsible for the

decrease in Cr suggesting a likely pathway of choice in these tumours for pathogenesis (Patra et al., 2012). The current understanding is that highly malignant, active tumours exhibit a high metabolic rate of activity resulting in the depletion of energy stores and a hypoxic environment. A marker of these changes is decreased levels of Cr in tumours (Rao, 2008, Tzika et al., 2001). This cohort demonstrates low levels of Cr in low grade tumours, with the exception of CNS PNET. Other studies have shown that there is no specific trend associated with malignancy when comparing spectroscopy of brain tumours (Panigrahy et al., 2006).

N-acetylaspartate (tNAA)

Total N-acetylaspartate in the brain tumours was variable but generally low. The highest tNAA was seen in DIPG and lowest concentrations in CPP. Previous studies have found higher tNAA in PA compared to other cerebellar tumours, although not significant (Davies et al., 2008).

Total N-acetylaspartate is a known marker of neuronal and axonal integrity and most reliable marker of pathological disease in the brain (Gujar et al., 2005). It does not appear to provide information on tumour metabolism and instead mostly used as a cell type marker. For example increased tNAA in DIPG is likely to be due to the diffuse nature of the tumour (Hargrave et al., 2008). However, the contribution of tNAA in *in vivo* metabolite profiles of PA requires further investigation. Decreased tNAA did not aid brain tumour differentiation in this cohort.

<u>Myo-inositol (mIns)</u>

Myo-inositol was increased in AA and CPP and also a prominent feature of DIPG and EP. It has been previously reported as prominent feature of EP (Davies et al., 2008, Panigrahy et al., 2006) and studies have demonstrated trends in higher mIns in low grade tumours and lower in high grade tumours , also seen in this analysis (Castillo et al., 2000).

The role of mIns in brain tumours is not fully understood but it is believed to be involved in the synthesis of cell membranes and myelin sheets. The increased mIns seen in tumours is thought to be as a result of the activation and proliferation of glial cells (Hattingen et al., 2008b, Callot et al., 2008). Myo-inositol, synthesised from glucose is involved in various signalling cascades (Downes and Macphee, 1991). It contributes to the formation of a phosphorylated form of phosphatidylinositol which is broken down to form secondary messengers, diacylglycerol and inositol 1,4,5-triphospate. The resulting diacylglycerol activates protein kinase C and a cascade of proteolytic enzymes that regulate a diverse set of cellular processes including proliferation, apoptosis, cell survival and migration all of which contribute to tumourigenesis. Inositol 1,4,5-triphospate activates a calcium (Ca^{2+}) signalling system control mechanism that also controls cellular processes including cell proliferation. It also forms inositol 3,4,5-triphosphate that is involved in generating membrane lipids (Wymann and Schneiter, 2008, Castillo et al., 2000).

The elevated levels of mIns seen in EP, particularly grade II and CPP is consistent with the expected findings in low grade tumours. The high standard deviation (6.14±4.9) of mIns seen in EP demonstrates the variability seen in the same tumour type. Myo-inositol

103

transportation is said to be facilitated by the choroid plexus and the presence of a CPP limits the ability of transportation hence the accumulation of mIns. Choroid plexus carcinomas are thought to have a less efficient uptake of mIns explaining the reason why this is not seen as a feature (Panigrahy et al., 2006). The elevated levels also seen in AA and DIPG do not fit the expected trend, but interestingly both tumours have features of prominent mIns and low lipid+MMs. With mIns known to be involved in the generation of membrane lipids, does this eliminate this pathway of tumourigenesis in these tumours thereby eliminating a pathway for targeted treatment? Are grade III EP tumours using mIns to generate membrane lipids hence the accumulation of lipids+MMs seen? Further work is warranted to establish whether these pathways are upregulated in those tumours that demonstrate low levels of the metabolite and explore their potential as targets for novel agents.

Glutamine (Gln), Glutamate (Glu) and Glutamate+Glutamine (Glx)

The quantitation of Gln and Glu can be determined independently with use of simulated basis sets (Kanowski et al., 2004). This is particularly useful at low field strengths where they closely overlap. However, the use of various quantitation methods in spectral analysis has resulted in the metabolites being reported as a sum, Glx.

Gln was seen at similar concentrations across all tumour types. The lowest levels were observed in CPP and highest in GBM. Glu was highest in GER and AA with low levels seen in Cranio and GBM. Low levels of Gln has been previously reported in CPP (Panigrahy et al., 2006). Significantly lower Glu and significantly higher Gln have been observed in PA when compared to MB (Davies et al., 2008).

Gln is an amino acid precursor and storage form of Glu (Panigrahy et al., 2010a) and is involved in every metabolic task of proliferating tumour cells including bioenergetics, supporting cell defences against oxidative stress and complementing glucose metabolism (DeBerardinis and Cheng, 2010). Glu is known to activate a number of processes via its roles as a major excitatory neurotransmitter (Prickett and Samuels, 2012).

Gln provides energy for tumours and is involved in the process of glutaminolysis, where Gln is converted to Glu. Glu then either enters the TCA cycle or is a precursor for other metabolic intermediates. The use of Gln provides a less efficient process of energy production but is favoured by cancer cells because it not only provides ATP but a number of by-products such as lipids, fatty acids, NADPH, Cit and amino acids including Gly that aid in tumour cell proliferation (Teicher et al., 2012, Lu et al., 2010). Myc, an oncogene known to be dysregulated in many cancers including MB is a major regulator of Gln metabolism. It is speculated that multiple signalling pathways activated by Gln contribute to tumour growth (Daye and Wellen, 2012, Guessous et al., 2008).

Glu has recently been shown to aid rapid proliferation of malignant gliomas and accelerate destruction of normal brain tissue (Sontheimer, 2008). Manipulating the activation of multiple signalling nodes has been found to be responsible for glioma pathogenesis (de Groot and Sontheimer, 2011).

The pivotal role of Gln and Glu and their close association makes it difficult to determine the role of these metabolites in individual tumours. With GBM possessing high levels of Gln, but low levels of Glu, it can be speculated that an alternative energy source is being utilised to aid tumour proliferation. There is a large body of evidence that GBM possess

areas of hypoxia particularly in adults but also seen in paediatrics (Yang et al., 2012, Donovan et al., 2012). There is evidence to suggest that that these cells preferentially use aerobic glycolysis known as the 'Warburg effect', to survive and rapidly proliferate, a possible explanation for the increase Gln levels observed (Wolf et al., 2010).

Taurine (Tau)

Taurine is observed to be highest in MB and GER with low concentrations seen in GBM and ATRT. Tau has been previously identified as a differential marker of MB (Kovanlikaya et al., 2005) and a marker of malignancy (Peeling and Sutherland, 1992). It has also been observed as a feature in germinomas (Harris et al., 2011).

Tau has been speculated to be correlated with apoptosis in gliomas (Opstad et al., 2009) but also been found to decrease in the stages of apoptosis (Valonen et al., 2005). It has also been shown to have an important role in osmoregulation and volume regulation in the central nervous system (Vitvitsky et al., 2011). Tau is generated from Glc through the diversion of the glycolytic intermediate 3-phosphoglycerate (3PG) into the serine synthesis pathway where serine is converted to cysteine. Cysteine is then converted to a number of intermediates before being made into Tau. The high level of Tau in MB (WHO IV) correlates with malignancy as expected but does not explain the low levels seen in GBM and ATRT. The mechanisms of Tau in tumour pathogenesis are poorly understood, in particular the link with apoptosis, thereby requiring further work for clarification.

Glucose (Glc)

High Glc was observed in AA, DIPG and PA and low levels observed in CNS PNET and Cranio. High Glc levels have been reported in MB, in disagreement with this study's findings (Panigrahy et al., 2006).

Glc provides energy for all proliferating cells. Low Glc concentrations found in malignant tumours is speculated to be due to the large energy requirements of tumour cells for rapid proliferation (Panigrahy et al., 2006). This affects closely related metabolites including the levels of Lac. The data shows no correlation of low Glc for more malignant tumours.

Lactate (Lac)

Lactate was found to be high in GBM and CNS PNET and low in DIPG and AA. Lac is a known feature of pathology (Panigrahy et al., 2010b) and has been detected in many tumours including PA (Davies et al., 2008, Panigrahy et al., 2006). It should be noted that although the use of a basis set accounts for the different components of the spectrum, there will be an overlap between LMM1.3 and Lac if the lipid component dominates. This can make it difficult to quantitate Lac reliably. To overcome this some studies perform long TE spectroscopy where the short T2 of lipids results in a decay of the lipid signals and an inverted Lac peak is observed (Graaf, 2010).

Lac production is a known feature of abnormal glucose metabolism. Multiple pathways result in the production of Lac that explains the variability seen in different tumours (Hirschhaeuser et al., 2011). The elevated concentrations of Lac in GBM are in keeping

with the tumours favouring aerobic glycolysis of which Lac is a by-product. The decreased Lac seen in DIPG and AA could be inferred as the tumours favouring other energy sources for proliferation. Evidence has shown that when DIPG are biopsied, a rarely performed procedure for these tumours, the largest histopathological grouping is found to be anaplastic astrocytomas (30%) demonstrating their close association (Perez-Gomez et al., 2010).

Tumour cells undergo a cyclic variation in hypoxic and aerobic conditions that results in the differences in Lac levels. It is the adaptation of tumour cells to their regional environment that enables them to continue proliferating. Excess Lac used by aerobic cells generates 18 ATP (Teicher et al., 2012) via oxidative phosphorylation. Under hypoxic conditions Glc conversion to Lac is highly upregulated by HIF-1 (Semenza, 2008) resulting in two ATP (Teicher et al., 2012). The acidic environment created by the presence of Lac provides several growth advantages for tumours (Munoz-Pinedo et al., 2012). Hypoxic tumours have been found to be more resistant to treatment resulting in a poor prognosis for the patient (Semenza, 2008).

Citrate (Cit)

Citrate is present at high concentrations in AA and DIPG. Low levels of the metabolite are detected in the other tumour types. Literature findings support the presence of a prominent citrate peak in DIPG (Costello et al., 1999, Seymour et al., 2008). It is also reported to increase in grade II astrocytomas that show malignant progression (Blüml et al., 2011).

In cancer cells, de novo lipid and sterol synthesis is known to be enhanced with the support of citrate making it a key regulator of energy production (Icard et al., 2012, Teicher et al., 2012). However, under hypoxic conditions tumours increase glycolytic energy production and decrease mitochondrial function thereby favouring glycolysis which may explain the observed accumulation of citrate (Blüml et al., 2011).

The close association of citrate with lipid synthesis supports the accumulation of citrate and low levels of lipids+MM seen in both DIPG and AA. This however suggests aerobic glycolysis is favoured rather than glutaminolysis but observed Lac levels for these tumours are low demonstrating an unclear observation.

Glycine (Gly)

Glycine was seen to be highest in MB and lowest in DA and PA. Reports of Gly in paediatric tumours are limited, however Davies et al. (2009) identify the peak as a feature of paediatric brain tumours with increasing levels found to be correlated with WHO grade. MB and GBM were found to possess the highest concentrations (Davies et al., 2009). This cohort also demonstrates significantly elevated levels in high grade tumours.

Gly functions as an inhibitory neurotransmitter and antioxidant (Govindaraju et al., 2000, Davies et al., 2009). Like Tau, Glc metabolism is diverted via 3PG for the conversion of serine to Gly providing several advantages for cell growth including limiting production of ATP and TCA cycle intermediates that may contribute to tumour pathogenesis (Locasale et al., 2011). The elevated levels of Gly seen in MB and its close association with Tau, suggests glucose is favoured as an energy source in these tumours.

<u>Scyllo-inositol (sIns)</u>

Scyllo-inositol was found to be low in most tumours. The highest concentrations were seen in MB and EP. Scyllo-inositol has been previously identified as a feature in brain tumour spectra but not specific for any tumour type (Panigrahy et al., 2006). It has also been found to be associated with a poor prognosis in brain tumours (Wilson et al., 2013). The role of sIns is mostly unknown. Most findings in the literature report mIns as a precursor of sIns and so speculate it to be related to membrane synthesis and/or to the function of inositol phosphates as secondary messengers in cellular signal transduction (Swanson et al., 2003). This suggests a positive correlation between the two metabolites thus the findings are often reported in the context of myo-inositol metabolism (Kaiser et al., 2005). Evidence in the literature demonstrates sIns as a marker of poor prognosis (Wilson et al., 2013) whereas mIns has been found to be a marker of good prognosis (Castillo et al., 2000) which does not fit with the suggested positive correlation of two metabolites. Pearson's correlation analysis, testing the relationship between the sIns and mIns in the 1.5T cohort of tumours identified no relationship (r=0.22), where 1 determines a strong positive correlation and 0 no correlation. It could be speculated that these metabolites have different roles in different tumours, hence the discrepancy in correlation seen in cohorts of pooled heterogeneous tumours.

<u>Alanine (Ala)</u>

Alanine was detected in low levels in most brain tumours and elevated in CPP (with high variability) and MB. There are very few reports of Ala in paediatric brain tumours, it is however a known feature of adult meningiomas (Howe et al., 2003).

Ala is synthesised via two different routes either from glucose through the diversion of 3PG to pyruvate and finally Ala (Locasale et al., 2011) or in the absence of glucose from Gln (Le et al., 2012). The elevated Ala seen in tumours is speculated to be as a result of the use of Gln as an energy substrate rather than glucose (Howe et al., 2003). The catabolism of Gln to Lac has been demonstrated to be accompanied by secretion of Ala. Re-routing metabolism via Gln was found to provide survival advantage for cells (DeBerardinis et al., 2007). Elevated Ala seen in MB is in keeping with favouring of glucose as an energy source.

Guanidinoacetate (Gua)

Guanidinoacetate was highest in MB and ATRT with low levels in PA. Gua has been previously seen as a feature in brain tumours. Panigrahy et al. also reported high levels of the metabolite in MB (Panigrahy et al., 2006).

Gua is a precursor of Cr synthesis and its link with Cr associates increased Gua with malignant progression (Longo et al., 2011). While the assignment of Cr in brain tumour spectra is tentative, some studies have acquired spectra from patients with creatine deficiency syndromes. Studies have found while Cr in these patients is markedly decreased, a peak around 3.8 ppm speculated to be assigned to Gua is elevated demonstrating its close association (Bianchi et al., 2007, Schulze et al., 1997). The elevated Gua seen in two highly malignant tumours, MB and ATRT and decreased levels in a low grade tumour PA support the association with malignancy.

111

<u>Lipids+MMs (LMM)</u>

Elevated levels of lipid+MMs were found in GBM and ATRT with ATRT having a particularly elevated peak at 1.3 ppm. Low level lipids+MMs were seen in DIPG and PA. Interestingly, the increase in LMM1.3 seen in EP from grade II to grade III was also observed (Figure 5.7b and c). A number of studies have identified the association of elevated lipid levels with high grade tumours and poor prognosis but they have also been reported as highly variable in the same tumours (Wilson et al., 2013, Panigrahy et al., 2006). Reports in literature demonstrate high levels of mobile lipids to correlate with malignancy in paediatric brain tumours (Astrakas et al., 2004).

Lipid synthesis occurs as a result of using Gln as an energy source, particularly under hypoxic conditions. The inverse correlation between intra-cellular Gln and mobile lipids has provided evidence for the link between Gln and lipogenesis (Wilson et al., 2013, Teicher et al., 2012). A number of metabolites including elevated Glc, increased Gln and decreased Glu and increase Cit link with aerobic glycolysis and in turn explain the elevated lipids+MMs seen in GBM and ATRT. The presence of lipids in tumour spectra have been identified as markers of both necrosis (Catalaa et al., 2006, Tzika et al., 2002) and apoptosis (Blankenberg et al., 1997, Tzika et al., 2003). Studies have demonstrated links to Sonic Hedgehog (SHH) pathway, which activates the Rb/E2F tumour suppressor complex that promotes lipogenesis (Teicher et al., 2012).

An increasing body of evidence demonstrates that paediatric brain tumours can be stratified by the molecular subgroups. With the current focus on MB, it will become increasingly more important to link metabolic changes with genetic alterations to aid the

understanding of tumour pathogenesis (Taylor et al., 2012). Monitoring these metabolites may help in the future for the evaluation of treatment strategies.

5.4.2 MRS as a diagnostic tool

The use of conventional MRI in the pre-operative diagnosis of brain tumours, although key, is often challenging and can result in a number of differential diagnoses (Panigrahy et al., 2006, Panigrahy and Bluml, 2009). This highlights the need for MRI to be supplemented with additional methods such as MRS to aid in diagnosis.

Significant differences in mean metabolite concentrations are seen between tumours. However, box and whisker plot analysis identifies no discriminatory variables differentiating any of the tumours often included in the differential diagnoses on MRI. The large number of differences in mean concentrations quantitated demonstrates paediatric brain tumours consist of a heterogeneous population of tumour types. While these findings highlight the important metabolite features of specific tumours, there is a great overlap in metabolite means and for some metabolites a high variability in concentrations within groups. This emphasises the difficulty in using this information to discriminate between tumour types, findings that have been a previously reported by a number of studies (Panigrahy et al., 2006). This provides evidence for the infectiveness of using single metabolites for diagnosis. Interestingly Tau, a known marker of differentiation between MB and All Other (Kovanlikaya et al., 2005) does not discriminate between MB and PA or MB and EP when using a box and whisker plot of Tau levels in this analysis. This is likely to be explained by the fact Tau is not observed and quantified in every MB in this cohort so although the presence of Tau proposes MB as a probable

diagnosis when assessing spectroscopy of new cases, the absence of the metabolite does not rule out MB as a diagnosis. This demonstrates the disadvantage of using single variables for discrimination.

An alternative approach using measured concentrations plotted against either other metabolite concentrations or concentration ratios has been employed in other studies (Harris et al., 2007, Panigrahy et al., 2006). However, ratios eliminate determining the usefulness of metabolite used as the denominator and assume it remains unchanged. With more than one metabolite being used to aid discrimination it was envisaged that this would be a more successful method for classification. However, this has been less well integrated into clinical practice and practicality of the method requires testing.

The use of simple pattern recognition methods with metabolite profiles for classification has proven to be a useful method for discriminating tumour groups. The success of multivariate analysis techniques is shown by the high classification accuracy achieved, thus exhibiting MRS to be more useful if all the metabolite information is used. The LDA plot (Figure 5.11c) provides a visual diagnostic aid showing how well cases fit in with other profiles of the same tumour type and the posterior probability determines how well the case fits with the classified group. A number of studies have used similar classification methods of brain tumours and reported classification accuracies (Vicente et al., 2013, Davies et al., 2008), for example over 80% in paediatric posterior fossa tumours (Davies et al., 2008).

In a clinical setting, radiologists often qualitatively assess new patient spectra against a cohort of mean spectra. This has been particularly applied to the three most common

brain tumours (MB, PA and EP) but is increasingly being supplemented for rare tumours. The use of mean spectra given in the analysis may prove to be a useful diagnostic aid for radiologists but needs to be formally tested to prove the benefits.

5.4.3 Scanner comparisons and quality control

Two metabolites were found to be significantly different between the four scanners, one of which Gua, is a less well determined metabolite at 1.5 T. The second metabolite Cr, was found to be significantly higher in MB spectra acquired on the Siemens Avanto and GE Signa Excite. Recent evidence has shown that MB consist of heterogeneous subgroups that differ in prognosis (Taylor et al., 2012). With the small number of cases seen in these two groups, it is possible that some subtypes may have predominated on particular scanners and the unknown bias in the case mix may be resulting in the differences in Cr observed. This requires further investigation and has been preliminarily investigated and discussed in Chapter 7. The similarity in metabolite concentrations seen between scanners provides justification for combining multi-scanner datasets for increasing cohort numbers for analysis.

The analysis demonstrates MRS from a heterogeneous group of tumours with varying concentrations of metabolites seen in each tumour type. However, evidence has shown that metabolite profiles between different brain tumours can overlap and spectral regions of the same brain tumour type can also vary (Panigrahy et al., 2006, Davies et al., 2008). A number of studies have shown that differences in metabolic information can be explained by tumour location and prognosis (Wilson et al., 2013, Harris et al., 2008). It should be noted, for example that although PA in this analysis has been pooled as one

group, there are reported differences in metabolites when comparing tumour location and NF-1 status (Orphanidou-Vlachou et al., 2013, Harris et al., 2008).

Out of a total of 464 spectra, 183 spectra from 130 cases were excluded from this study based on seven main categories of quality control. These included SNR (n=104), artefact or distorted peaks (n=29), Q fit (n=23), voxel positioning (n=17), broad peaks (n=8) and FWHM (n=2). Over half the cases (n=66) that were excluded on SNR were acquired from tumours that are known to exhibit a low cellularity (PA and Cranio and low grade gliomas). Voxel positioning was mostly problematic in PA and low grade gliomas resulting in 11 out of 17 being excluded for normal brain contamination or incorrect placement and 12 of the 29 spectra excluded as result of distortions and/or artefact peaks were acquired on the GE scanner.

The experience of collecting spectroscopy data over 9 years has shown that spectra that fail QC do not necessarily fail as a limitation of the technique, the characteristics of the tumour also play a role in the results obtained. In total 66 of the cases that failed QC were either PA or pilomyxoid astrocytoma. PA seems to be a particularly challenging tumour to obtain spectra from both in terms of voxel placement due to its highly cystic properties and small solid components (Gan and Haas-Kogan, 2010). The low cellularity of low grade tumours results in spectra of low SNR making it difficult to assess the metabolite profile, previously also reported in a number of studies (Gupta et al., 2000, Harris et al., 2008). When speculating the diagnosis of low grade tumours these factors should be taken into consideration to determine tumour diagnosis rather than assuming the spectra are of no value. While having less stringent QC criteria would include these

cases, determining metabolite peaks would become inherently more difficult. Inevitably this would affect metabolite concentrations and introduce error into the analyses. It is important to note that MRS cannot be interpreted in isolation and should be used in combination with conventional MRI sequences.

5.5   Conclusions

This analysis consists of a large cohort of common and rare paediatric brain tumours where spectroscopy has been acquired pre-diagnosis on multiple scanners. The study includes a large range of tumour types where spectroscopy has been acquired at short and long echo time and two field strengths (1.5 T and 3 T). It has been established that single metabolite variables are unable to discriminate reliably between brain tumours whereas pattern recognition methods incorporating all available metabolite information are superior. The similarity of MB metabolite profiles has shown multi-scanner analyses to be a robust method for increasing cohort size. Qualitative assessment of mean spectra may also be a useful diagnostic aid for radiologists. The mean spectra, metabolite concentrations and classifier analysis constructed for brain tumours using statistical analysis methods provides diagnostic information that can be used alongside conventional MRI sequences. It should be noted that MRS should be used in combination with MRI. Single voxel spectroscopy is shown to be a valuable characterisation tool for use in paediatric brain tumours.

CHAPTER 6: DIAGNOSING RELAPSE IN CHILDREN'S BRAIN TUMOURS USING METABOLITE PROFILES

CHAPTER 6

6 DIAGNOSING RELAPSE IN CHILDREN'S BRAIN TUMOURS USING METABOLITE PROFILES

6.1 Introduction

Brain tumours are the most common solid tumours in children (Bleyer, 1999) . Whilst some brain tumours have a very good prognosis, others continue to present major challenges and brain tumours are now the leading cause of death from cancer in children (Stiller C, 2007). Children who relapse following treatment for a malignant brain tumour commonly have a very poor prognosis. The diagnosis of relapse is made by using the indications from clinical course of the disease and by examining changes on imaging without a biopsy. However, it is well documented that changes can occur on an MRI as a result of treatment that may not represent tumour recurrence or progression (van den Bent et al., 2011). A more accurate non-invasive diagnosis of relapse would enhance the clinical management of these tumours (van den Bent et al., 2011, Mehta et al., 2011, Quant and Wen, 2011, Sundgren, 2009, Warren et al., 2000).

The Macdonald criteria, where an increase in the size of an enhancing tumour on consecutive MRI scans, together with clinical assessment, has been used to determine tumour recurrence (Clarke and Chang, 2009, Macdonald et al., 1990). However, not all tumours enhance and changes in enhancement can result from treatment effects, in particular radiotherapy. These treatment related changes are often referred to as pseudo-progression and are due to secondary oedema and vessel permeability changes (Hygino da Cruz et al., 2011). Further challenges have arisen with the introduction of new therapeutic agents which alter the permeability of the blood-brain barrier and

demonstrate a dramatic improvement in enhancement, rather than a true tumour response or 'pseudo-response' (Batchelor et al., 2007). The recognition of pseudo-progression, particularly in adults with high grade glioma, led to the agreement of the Response Assessment in Neuro-oncology criteria or RANO criteria which have also been extended to low grade gliomas in adults (Wen et al., 2010, van den Bent et al., 2011). The RANO criteria provide an improved assessment of disease progression and treatment response by addressing the limitations of the Macdonald criteria. However, they are still restricted in their ability to diagnose relapse accurately and there are currently no similar guidelines for diagnosing relapse which are specific to children and a need for these has been identified (Warren et al., 2013).

As discussed previously, MRS has been used extensively in the assessment of brain tumours (Peet et al., 2012). MRS in adults has investigated the methods for diagnosis and evaluating tumour recurrence (Tate et al., 2006, García-Gómez et al., 2009, Julià-Sapé et al., 2012, Smith et al., 2009). Brain tumours in children have a different spectrum of disease to those diagnosed in adults (Jones et al., 2011). Potentially, MRS could be used to aid the identification of tumour at suspected relapse, however, the diversity of metabolite profiles seen across tumour types ensures that simple rules based on single metabolites or ratios of metabolites are unlikely to be successful in identifying relapsed tumour in all children (Panigrahy et al., 2006). One approach would be to use the metabolite profile of the tumour at diagnosis to inform the interpretation of MRS during surveillance but it is unknown how the metabolite profiles of brain tumours in children differ between diagnosis and relapse. As it is known that alterations in the biology of tumour cells can occur between diagnosis and relapse, for example chromosomal

changes accumulate in ependymomas (Puget et al., 2009) , large changes in the MRS

profile could potentially occur and this possibility needs to be investigated.

The main purpose of this chapter is to determine whether large changes occur in

metabolite profiles of malignant childhood brain tumours from diagnosis to relapse and if

so to identify these. A secondary aim was to confirm that significant differences do exist

between the MRS of tumours at diagnosis and non-tumour lesions observed in the same

patients at follow-up. The potential of MRS to aid the confirmation of relapse when

added to conventional MRI and clinical course was explored.

6.2   Method

6.2.1   Patients

This is a retrospective analysis from a study in which single voxel MRS was performed on

children between July 2003 and July 2011 during routine MRI for a suspected brain

tumour prior to treatment and at subsequent MRI where a lesion was identified. The

inclusion criteria for this study were all children with a histologically diagnosed grade II-IV

brain tumour that demonstrated progression or relapse and had good quality MRS.

Diffuse pontine gliomas were excluded due to the known difficulties of identifying

progression on conventional MRI (Hargrave et al., 2008) and the previously reported

evolution of MRS with subsequent disease progression (Panigrahy et al., 2008). 19

patients were identified (Table 6.1). The cohort consisted of seven different tumour types

with a mean age of 7 years and included four glioblastoma multiforme (four male, mean

age 11 years), 4 medulloblastomas (three male, one female, mean age 5.6 years), four

diffuse astrocytomas (four male, mean age 8.6 years), three ependymomas one of which

was an anaplastic ependymoma (two male, one female, mean age 1.8 years) , two central nervous system primitive neuroectodermal tumours (CNS PNETs) (two male, mean age 5.6 years), one atypical teratoid rhabdoid tumour (ATRT) (male, age 0.1 years) and one patient with gliomatosis cereberi (male, age 16.3 years) giving a total of 15 male and four female patients.

Table 6.1 A summary of clinical data from a cohort of 19 cases included in the MRS study. Abbreviations: GTR, gross total resection; SR, subtotal resection, Status D=died, A=alive

No.	Sex	Diagnosis	Treatment (prior to relapse)	Surgery at diagnosis	Relapse site	Surgery at relapse	Status	No. of days follow-up
1	M	Glioblastoma	Focal radiotherapy and chemotherapy	SR	Distant	None	D	676
2	M	Glioblastoma	Chemotherapy	GTR	Local	None	D	194
3	M	Glioblastoma	Focal radiotherapy and chemotherapy	SR	Local	None	D	282
4	M	Glioblastoma	Focal radiotherapy and chemotherapy	SR	Local	None	D	483
5	M	Ependymoma	Focal radiotherapy and chemotherapy	GTR	Local	SR	D	935
6	F	Ependymoma	Focal radiotherapy	SR	Local	4 surgeries SR	D	1074
7	F	Anaplastic Ependymoma	Chemotherapy	SR	Local	None	D	576
8	M	Atypical Teratoid Rhabdoid Tumour	Chemotherapy	SR	Local	None	D	213
9	F	Medulloblastoma	Focal radiotherapy and chemotherapy	SR	Local	None	D	1245
10	M	Medulloblastoma	Cranio-spinal radiotherapy and chemotherapy	SR	Distant	None	D	816
11	M	Medulloblastoma	Chemotherapy	GTR	Distant	None	D	539
12	F	Large Cell Anaplastic Medulloblastoma	Cranio-spinal radiotherapy and chemotherapy	GTR	Local	None	D	764
13	M	CNS Primitive Neuroectodermal Tumour	Focal radiotherapy and chemotherapy	SR	Distant	SR	D	465
14	M	Supratentorial Primitive Neuroectodermal Tumour	Chemotherapy	Biopsy	Distant	None	D	596
15	M	Diffuse Astrocytoma	Focal radiotherapy and chemotherapy	Biopsy	Local	None	D	571
16	M	Diffuse Astrocytoma	Chemotherapy	SR	Local	None	A	2268
17	M	Diffuse Astrocytoma	Focal radiotherapy and chemotherapy	Biopsy	Distant	None	D	756
18	M	Diffuse Astrocytoma	Chemotherapy	SR	Local	None	D	170
19	M	Gliomatosis Cerebri	Radiotherapy and chemotherapy	Biopsy	Distant	None	D	227

Following the MRI at presentation, all patients underwent surgery. Following surgery, an MRI scan was performed within one to three days and formal radiological reporting together with review in a multi-disciplinary team meeting was used to determine the extent of tumour excision (gross total or subtotal resection). Four had a gross total resection by surgical opinion and post-operative MRI, 11 had a subtotal resection and four had a biopsy for diagnosis alone. All children underwent adjuvant treatment with either focal or craniospinal radiotherapy and/or chemotherapy depending on their tumour type and prognostic stratification (Table 6.1).

6.2.2 Assessment of disease progression

Disease progression confirmation in the cohort was taken as the decision made by the neuro-oncology multi-disciplinary team from a combination of clinical and radiological features. The criteria were that progression is diagnosed if there is an increase in the size of the tumour of more than 25% measured in two dimensions on the MRI scan; the appearance of tumour in a previously uninvolved area or clear clinical evidence of disease progression in combination with an equivocal MRI. Follow-up scans were then performed every one to three months depending on case scenario to determine patient status. MRS was performed if a lesion, either local or distant to the tumour identified at diagnosis, was large enough for SVS (>1.5 cm^3). During suspected tumour relapse, MRS processed by the scanner was made available to the clinical multi-disciplinary team and qualitatively analysed by them. However, a quantitative comparison with the diagnostic MRS was not made available. If the consensus decision was that the patient demonstrated tumour relapse, optimal treatment strategies were discussed. Neurosurgery at relapse was only performed if it was felt to be beneficial to the patient taking account of outcome and

quality of life. Only three cases had surgical intervention at first relapse for comparison with histopathological diagnosis at presentation. In all cases, the histology was in keeping with that at diagnosis. At the end of the study 18 patients had died of disease progression and one patient was alive with stable disease. The mean time from diagnosis to relapse was 15 months and mean time from diagnosis to death was 19 months.

6.2.3 MRS acquisition and quantitation of metabolite concentrations and lipid intensities

MRS was carried out on a 1.5 T MR scanner (GE Excite, Siemens Symphony or Siemens Avanto) after conventional MRI. A single voxel MRS protocol was used with PRESS localisation, TE time of 30 ms and TR of 1500 ms. A water unsuppressed acquisition was also acquired as a concentration reference. Cubic voxels were used with either 2 cm or 1.5 cm side length and 128 or 256 repetitions acquired, respectively. Voxel placement was entirely within the tumour as delineated by the conventional MRI with the enhancing component maximised. Local relapses were at the site of the primary tumour, whilst distant relapses were taken to be at any other location. All spectra were assessed using the QC criteria (section 4.3). In addition to the 19 cases included, one case was excluded due to unstable baseline on the relapse MRS.

6.2.4 Statistical analysis

Metabolite concentrations (mM) were quantified using TARQUIN (version 3.2.2) (Wilson et al., 2011). Statistical analysis excluded aspartate and GABA. The lipid and macromolecular components were included in the analysis as both individual components so lipids at 1.9 ppm (L0.9), sum of lipids at 1.3 ppm so lip1.3a+lip1.3b (L1.3), lipids at 2.0 ppm (L2.0) and as combined components with macromolecules at 0.9

ppm (LMM0.9), 1.3 ppm (LMM1.3) and 2.0 ppm (LMM2.0). A power analysis calculation

showed that 19 samples would detect a large effect size (Cohen d=0.68) for a two tailed

paired t-test at a significance level of 0.05 with a power of 0.8. Paired Student's t-tests

were performed to investigate differences between metabolite profiles at diagnosis and

relapse. The comparison was also performed separately for local and distant relapse. Box

and whisker plots were constructed for differences between absolute concentrations of

variables at diagnosis and relapse. Line plots were constructed to visualise differences

between levels of four main variables (tCho, mIns, NAA and lipids at 1.3 ppm) at diagnosis

and relapse. Wilcoxon signed rank test was used for the paired analysis of metabolites in

non-tumour lesions at follow-up and tumours at diagnosis due to the smaller numbers of

cases and lack of information on the Gaussian nature of the distribution.

6.3 Results

Table 6.2 Mean metabolite concentrations for diagnosis vs. relapse (n=19), diagnosis vs. local relapse (n=12) and diagnosis vs. distant relapse (N=7), showing no significant differences between any of the three groups using a two-tailed Student's t-test (n.s, not significant).

		Mean metabolite concentrations(mM)		
Metabolite	*P* values	Diagnosis vs. relapse at any location	Diagnosis vs. local relapse	Diagnosis vs. distant relapse
Ala	n.s	0.27 vs. 0.37	0.32 vs. 0.48	0.20 vs. 0.18
Cit	n.s	0.64 vs. 1.10	0.79 vs. 1.32	0.39 vs. 0.71
Cr	n.s	2.73 vs. 3.14	2.53 vs. 2.66	3.08 vs. 3.96
PCh + GPC	n.s	1.98 vs. 1.99	1.78 vs. 1.73	2.31 vs. 2.45
GPC	n.s	1.25 vs. 1.24	1.16 vs.1.19	1.39 vs. 1.34
PCh	n.s	0.73 vs. 0.75	0.62 vs. 0.54	0.92 vs. 1.11
Glc	n.s	1.82 vs. 1.31	1.74 vs. 1.28	1.97vs. 1.35
Gln	n.s	3.19 vs. 3.02	3.88vs. 3.21	2.01 vs. 2.72
Glu	n.s	2.16 vs. 2.84	2.22 vs. 2.42	2.01 vs. 3.57
Glu + Gln	n.s	5.35 vs.5.87	6.10 vs. 5.62	4.06 vs. 6.29
Gly	n.s	2.20 vs. 2.11	2.42 vs. 2.33	1.83 vs. 1.74
Gua	n.s	0.61 vs. 0.68	0.62 vs. 0.70	0.59 vs. 0.65
mIns	n.s	2.81 vs.3.01	2.75 vs. 3.87	2.90 vs. 1.54
Lac	n.s	2.16 vs.1.67	2.62 vs. 2.35	1.37 vs. 0.51
sIns	n.s	0.30 vs. 0.35	0.31 vs. 0.36	0.28 vs. 0.32
Tau	n.s	1.02 vs. 0.94	0.55 vs. 0.74	1.83 vs. 1.28
NAA+NAAG	n.s	1.27 vs. 1.54	1.15 vs. 1.25	1.48 vs. 2.03
LMM0.9	n.s	6.61 vs.7.95	7.30 vs. 8.90	5.43 vs. 6.33
L 0.9	n.s	3.32 vs. 3.78	4.01 vs. 3.98	2.13 vs. 3.44
MM 0.9	n.s	3.29 vs. 4.17	3.29 vs. 4.91	3.30 vs. 2.90
LMM1.3	n.s	15.32 vs. 19.13	19.83 vs. 22.69	7.60 vs. 13.52
L1.3	n.s	13.32 vs.16.44	17.30 vs. 18.52	6.50 vs. 12.87
MM 1.3	n.s	2.00 vs. 2.88	2.53 vs. 4.17	1.01 vs. 0.65
LMM2.0	n.s	10.30 vs. 9.66	11.28 vs. 9.44	8.63 vs. 10.05
L2.0	n.s	3.70 vs. 3.07	4.48 vs. 2.94	2.36 vs. 3.28
MM 2.0	n.s	6.61 vs. 3.36	6.80 vs. 6.49	6.27 vs. 6.77

No significant differences in metabolites or lipids and macromolecules were found between diagnosis and relapse (n=19) (P>0.05, paired Student's t-test). Sub-group analyses of local relapse (n=12) and distant relapse (n=7) also showed no significant

differences in metabolites or combined and individual macromolecules and lipid components in either of these two groups (P>0.05, paired Student's t-test). However, lipids at 1.3 ppm were close to significance (6.5 vs. 12.9, P=0.07) in the group where MRS was of a distant relapse (Table 6.2)

In addition, no significant differences (Student's t-test, P>0.05) were found when comparing MRS at diagnosis and relapse in specific tumour types. The tumour types tested were those that had four or more cases per tumour type, glioblastomas (n=4), medulloblastomas (n=4) and diffuse astrocytomas (n=4).
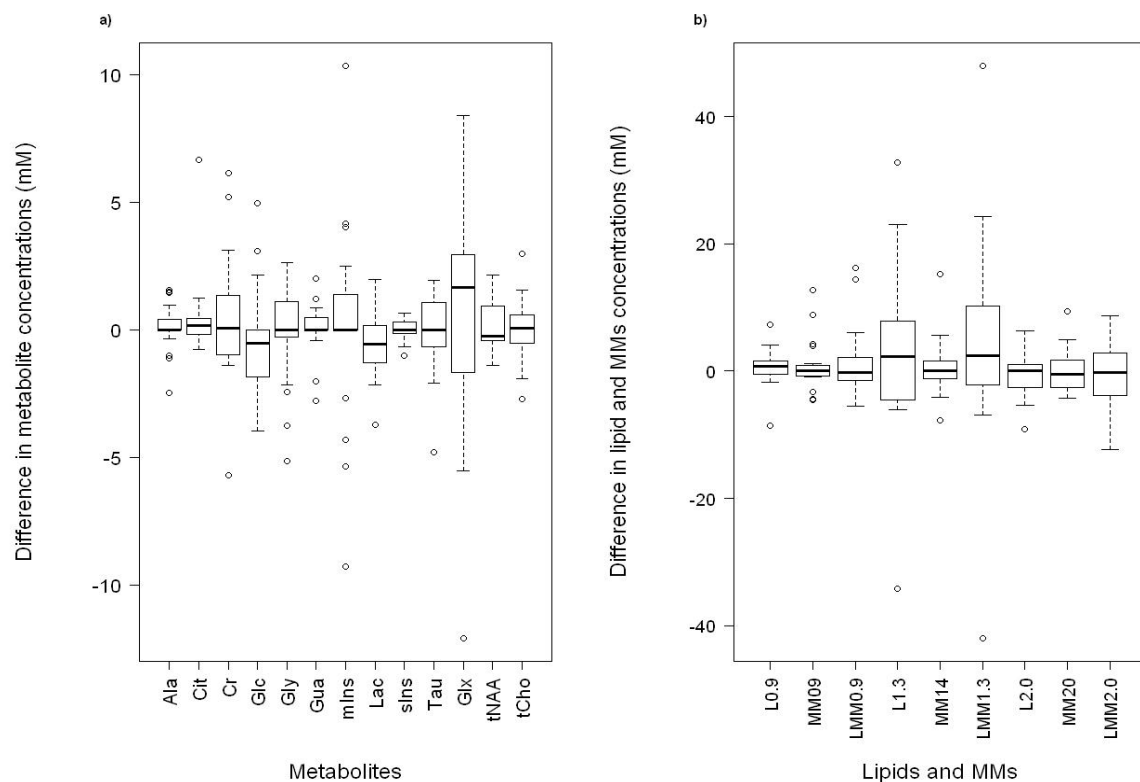
Figure 6.1 Box and whisker plots of a) the differences in metabolite concentration at diagnosis and relapse and b) difference in lipid and macromolecular concentrations at diagnosis and relapse (n=19).

Differences in metabolite, lipid and MM levels at diagnosis and relapse are demonstrated in Figure 6.1 as a box and whisker plot. Although there are some metabolites which

change by a large amount from diagnosis to first relapse, there are no tumours for which this occurs for several metabolites, lipids or macromolecules indicating that for all tumours, the majority of the MRS profile is the same at relapse as at diagnosis.
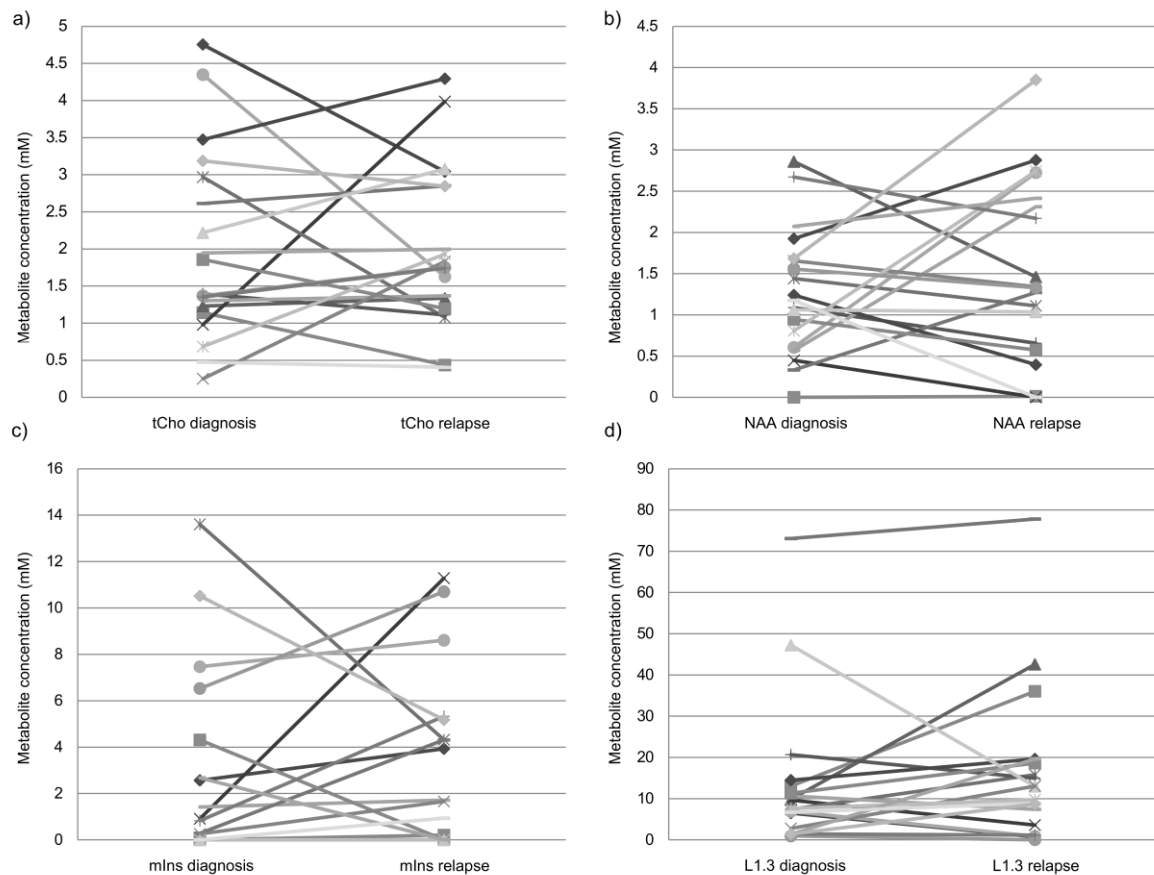
Figure 6.2 Line plots of changes in metabolite concentration levels at diagnosis and relapse for individual patients a) tCho b) NAA c) mIns and d) lipids at 1.3 ppm.

Figure 6.2 shows changes in metabolite concentrations from diagnosis to relapse for four main variables, tCho, NAA, mIns and lipids at 1.3 ppm. Again, for most cases there is little change in the levels of these metabolites between diagnosis and relapse. However, for a small number of cases there is a large change in a specific metabolite.

For five of the cases, the MRS indicated the presence of tumour prior to a diagnosis of relapse being made by the multi-disciplinary team using clinical information, conventional MRI and histology where available. The median time from MRS indicating the presence of

tumour to diagnosis of relapse was three months in these five cases. Four of the cases were astrocytomas and one was an ependymoma.
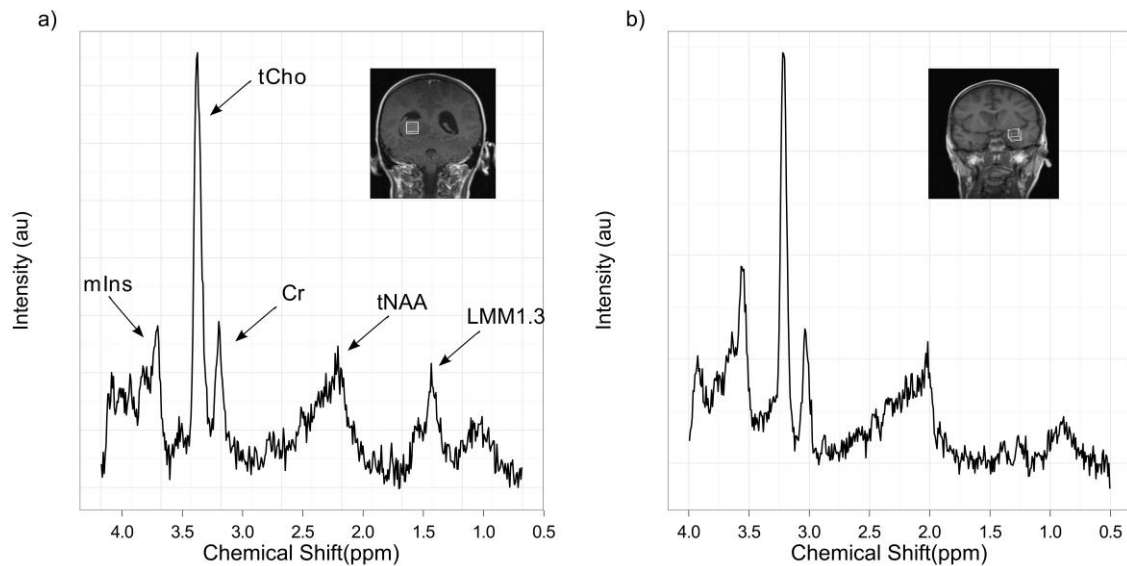
Figure 6.3 Comparison of MRS acquired from a brain tumour a) pre-diagnosis with an insert of a coronal T1 weighted image showing the voxel location and b) MRS obtained from the same tumour at relapse from a distant site with an insert of a T1 weighted imaging showing the voxel location (Case 1).

Figure 6.3 demonstrates the similarity of MRS at diagnosis and distant relapse in a patient with glioblastoma multiforme who had two surgical resections followed by radiotherapy. Tumour progression was seen at 536 days. An additional MRI was performed following radiologically confirmed progression at 654 days at two different distant tumour sites.
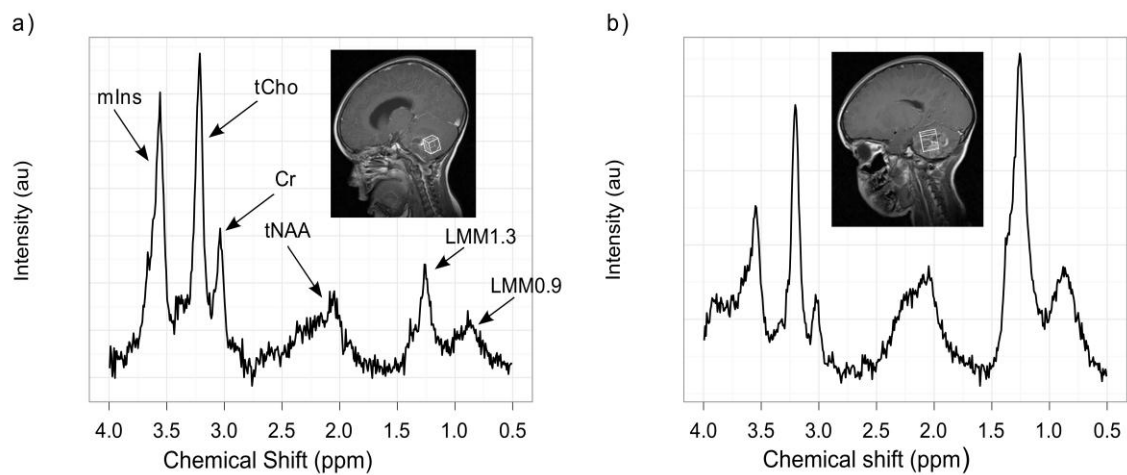
Figure 6.4 Evolution of MRS of an ependymoma at a) diagnosis and b) after subsequently confirmed relapse with inserts of a sagittal MRI images including voxel location for both spectra (Case 6).

Figure 6.4 illustrates spectra from a patient with multiply relapsed ependymoma. After diagnosis, the patient underwent surgical resection followed by focal radiotherapy but later developed local tumour progression. This patient had four surgical resections, two at diagnosis, one at first relapse and another at a subsequent relapse. Diagnosis at initial presentation was grade II ependymoma, but at first and second relapse the tissue samples were increasingly cellular and demonstrated an increasing proliferative rate. The final sample was suggestive of an anaplastic ependymoma (grade III). Spectroscopy was performed at each relapse with the last 908 days after diagnosis. The spectra show high levels of mIns and low levels of lipids at first relapse in keeping with the MRS at diagnosis (Figure 6.4a) but a decline in mIns and an increase in lipids on the last spectrum (Figure 6.4b).
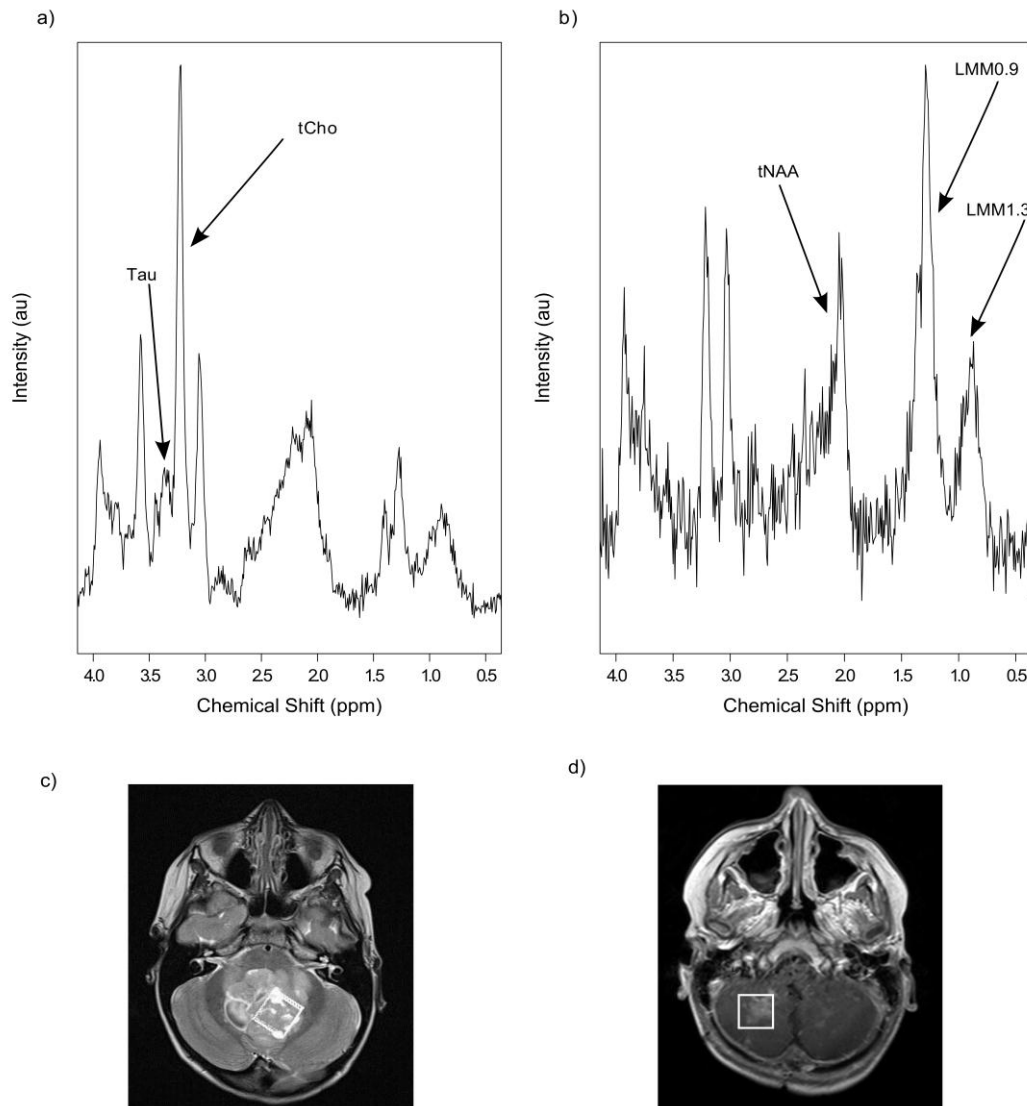
Figure 6.5 Comparison of MRS acquired from a patient with a classic medulloblastoma a) pre-diagnosis showing elevated tCho and Tau and b) from the same patient after completion of treatment with surgery, chemotherapy and radiotherapy in a region with pseudoprogression with a c) T1 weighted post contrast axial image showing location of voxel corresponding to spectrum in 5a and d) T1 weighted post contrast axial image showing an enhancing lesion in the posterior fossa with the position of the voxel indicated which corresponds to spectrum 5b.

In addition to the cases where relapse occurred, a further five cases had MRS at diagnosis and of a lesion which appeared post treatment but where extended follow-up confirmed that they were not relapsed tumour. The MRS in all these cases was very different on visual inspection from the MRS at diagnosis. An example is presented in Figure

6.5.Analysis of nine MRS profiles during surveillance paired with the MRS at initial diagnosis showed a significantly higher tCho, Gly, Lac and Tau at initial diagnosis (Wilcoxon signed rank test, $P<0.05$).

6.4   Discussion

This analysis investigated metabolite profiles of childhood brain tumours at diagnosis and suspected first relapse at either local and/or distant sites using short echo time MRS and found no significant differences in any metabolite, lipid or macromolecule level with a paired Student's t-test. In five cases there was diagnostic uncertainty based on the clinical and conventional MRI appearances with relapse only being confirmed one to six months later. MRS profiles of brain tumours recorded at diagnosis for these cases helped to confirm relapse prior to MRI and therefore has the potential to aid the diagnosis of relapse.

In adults with gliomas, simple ratios of metabolites such as tCho/Cr or tCho/tNAA are used to identify tumour (McKnight et al., 2007). However, paediatric neuro-oncology practice is not dominated by one single tumour type and a number of studies characterising metabolite profiles of paediatric brain tumours have identified key differences depending on the diagnostic subtype (Davies et al., 2008, Panigrahy et al., 2006, Harris et al., 2008). This study implies that for paediatric brain tumours, the MRS at diagnosis would be a useful aid in identifying tumour on follow-up scans. In any given case, a small number of metabolite values may change substantially from diagnosis to relapse but the overall pattern of metabolite levels tends to be very similar.

Whilst this study shows that metabolite profiles are similar at first relapse to diagnosis, there are some indications that alterations towards a more aggressive metabolite phenotype can occur in some circumstances. It might be expected that the greatest changes are seen in the distant relapses and there is a tendency towards higher lipids in these cases although this is not significant (P=0.07). The tendency for the MRS changes to be small from diagnosis to relapse even when the relapse is at a distant site are illustrated by case 1 which had both a local and a distant relapse (Figure 6.3). It may be expected that changes in tumour metabolite profiles accumulate over time and there is evidence for this in case 6 (Figure 6.4) which had subsequent relapses and showed evolving changes in the MRS profiles mirroring changes in histology. The decreasing mIns and increasing lipids at subsequent relapses are consistent with this evolution of grade. MRS of grade II ependymoma (Figure 5.7b) tend to have a prominent mIns peak seen at 3.6 ppm, in keeping with studies of adults with gliomas where there are trends towards lower levels of mIns at higher grade (Figure 6.4) (Castillo et al., 2000, Harris et al., 2008, Davies et al., 2008, Panigrahy et al., 2006). In addition, a number of previous studies have investigated the levels of lipids in paediatric brain tumours and found mobile lipids to correlate with malignancy across a range of paediatric brain tumours and associated them with necrosis, which is a histological characteristic of high grade tumours (Peet et al., 2007a, Sibtain et al., 2007a, Astrakas et al., 2004). Similar changes in MRS are likely to occur in tumours which are known to change from low to high grade as the disease progresses and this is consistent with findings for diffuse intrinsic pontine glioma (Panigrahy et al., 2008).

Whilst this study has established that the MRS of relapsed children's brain tumours is very similar to that at diagnosis, the degree of certainty with which MRS can be used to diagnose relapse also depends on the MRS characteristics of other lesions in the brain occurring in these patients. It is therefore reassuring that significant differences were seen in several metabolites between the MRS of tumours at diagnosis and non-tumour lesions observed in the same patients at follow-up. The feature of elevated lipids observed is likely to be as a result of radiation necrosis (Tzika et al., 2003).Caution does need to be taken when interpreting the spectra in these circumstances, in particular it is important to ensure that the voxel does not contain significant amounts of normal brain and that the spectra meet the quality control criteria.

It is encouraging that MRS was able to detect recurrent tumour in several cases where the clinical scenario and the conventional MRI were not able to diagnose relapse with confidence. The spectra was made available to the multidisciplinary team as part of their clinical information during the study and it may be that there were cases where MRS aided the diagnosis of relapse, although data was not collected systematically on this. It is interesting that none of the cases where MRS indicated the presence of tumour early were medulloblastomas or other primitive neuroectodermal tumours. Certainly, diagnostic dilemmas following treatment have been best documented in gliomas and it may be that post treatment abnormalities which mimic tumour on conventional MRI are rarer in primitive neuroectodermal tumours although this may change with increasing intensity of treatment in those with high risk disease (van den Bent et al., 2011, Clarke and Chang, 2009).

Analysis of MRS which includes the comparison of MRS at follow-up with that at diagnosis is now routinely used to inform the clinical decision making for these patients at the Birmingham Children's Hospital in combination with clinical information and conventional MRI. The role of other modalities such as perfusion imaging also warrant investigation although this technique is not as well established in children as it is in adults. The optimum combination of imaging techniques is yet to be formally established.

6.5 Conclusions and future investigations

This chapter's analysis found that the MRS metabolite profile of a child's brain tumour (grade II-IV) was not significantly different at first relapse to that at diagnosis, therefore aiding the confirmation of the presence of tumour on follow-up MRI. This finding is particularly relevant to the clinical management of these children given that radiotherapy and chemotherapy are known to cause abnormalities on MRI which are difficult to distinguish from recurrent tumour. A large multi-centre study should be undertaken to clearly define the role of MRS in distinguishing tumour relapse from treatment related effects and its added value compared with conventional MRI and other imaging modalities.

CHAPTER 7: NOVEL BIOMARKERS OF PROGNOSIS FOR MEDULLOBLASTOMA USING 1H MAGNETIC RESONANCE SPECTROSCOPY

CHAPTER 7

7   NOVEL BIOMARKERS OF PROGNOSIS FOR MEDULLOBLASTOMA USING 1H MAGNETIC RESONANCE SPECTROSCOPY

7.1   Introduction

Medulloblastoma (MB), a common primitive neuroectodermal tumour arising from the cerebellum is a major cause of morbidity and mortality in paediatric neuro-oncology. The classification of MB is performed on histopathology with five main variants of the disease including classic medulloblastoma, desmoplastic/nodular medulloblastoma, medulloblastoma with extensive nodularity, anaplastic medulloblastoma and large cell medulloblastoma with the last two more commonly grouped as one. Since 1969 these tumours have additionally been staged through the Chang classification, from M0 to M4. M0 describes a local tumour expansion with no evidence of metastases; M1 includes identification of tumour cells in the cerebrospinal fluid; M2 describes spread to other CNS areas; M3 includes gross nodular seeding in the spinal cord and finally M4 includes widespread metastases in particular outside the CNS (Kim et al., 2011) thus demonstrating a heterogeneous population of tumours. This staging and subsequent risk stratification is crucial in the management of MB.

Current MB risk stratification identifies three clinical characteristics associated with prognosis; patient age at diagnosis, extent of surgical resection and evidence of metastatic disease (de Haas et al., 2008). Patients below the age of three years, with residual disease greater than 1.5 cm^3 and metastatic disease are associated with high risk and poor prognosis. However, patients older than three years with minimal or no residual disease and no evidence of metastatic disease are associated with lower risk and a more

favourable prognosis (Kim et al., 2011, Carlotti et al., 2008). Histopathologically, it has long been known that the desmoplastic variant of medulloblastoma is associated with a better prognosis, whereas a large-cell anaplastic variant is associated with a shorter survival. In addition, a number of molecular markers have been identified over the last decade that has lead to further work and interest into medulloblastoma risk-stratification with a biological basis (Monje et al., 2011).

More recently, wide scale genomic and gene expression analysis have identified multiple signalling pathways to be associated with the growth and development of MB providing evidence for a genetically heterogeneous population (Carlotti et al., 2008, Taylor et al., 2012). The current consensus is that MB falls into four main molecular subgroups; WNT, SHH, Group 3 and 4 named after the signalling pathway thought to play a dominant role in the pathogenesis of the group. Each subgroup differs by patient demographic, genetics and clinical outcome. The WNT subgroup of MBs, thought to driven by the WNT signalling pathway is the best understood. The subgroup is mostly associated with a classic morphology and a very good prognosis when compared to the other groups. The SHH subgroup initiated by the Sonic Hedgehog pathway consists mainly of desmoplastic/nodular MB with a good to intermediate prognosis. Group 3 demonstrates a high expression of MYC amplification and consists of classic MB but pre-dominantly large cell MB. The group is associated with metastatic disease and increased disease recurrence thereby a poor prognosis. Group 4 has a less clear molecular pathology and is the least understood out of the subgroups however demonstrates enough difference to be grouped separately. Those that fall in this group demonstrate an intermediate risk. Multiple publications have recognised an increased expression of genes involved in

neuronal differentiation and neuronal development (Guessous et al., 2008, Gilbertson et al., 2001, Taylor et al., 2012). There is increasing interest in understanding how changes in metabolite profiles are correlated with genetic alterations and how they are related to metabolic pathways and provide information on tumour pathogenesis.

Generating a more accurate and precise stratification system will allow for greater discrimination between high-risk and standard-risk groups. Magnetic resonance spectroscopy is known to provide non-invasive biomarkers of tumour aggressiveness but studies are lacking in elaborating on specific tumour types and with long term follow-up for survival. This chapter investigates whether metabolite differences in children with MB can identify prognostic biomarkers by investigating metabolite differences as a function of survival time.

7.2   Method

7.2.1   Patients

Single voxel 1H MRS was performed on 42 children between January 2003 and July 2011 during routine MRI scans for a suspected brain tumour prior to treatment at the Birmingham Children's Hospital. Following QC (section 4.3), the cohort included three of the medulloblastoma variants: classic MB (n=32), desmoplastic/nodular MB (n=2) and large cell MB (n=2). The cohort consisted of Chang stages M0 to M3 of which 18 patients were staged as M0, four as M1, four as M2 and 10 as M3. The mean age at diagnosis for the whole cohort was 7±3.7 years (mean ± SD) (Figure 7.3). Maximum patient follow-up was 8.5 years with an average of follow up of three years.

Table 7.1 Patient demographics of the medulloblastoma cohort. Abbreviations: M, Male; F, Female; MB, medulloblastoma; DN MB, desmoplastic nodular medulloblastoma; LC MB, large cell medulloblastoma; D, died; A, alive; U, unknown.

Case	Sex	Diagnosis	Chang stage	Age at diagnosis	Status	No. of days follow up	Tumour size(cm^3)
1	F	MB	M0	8.5	A	501	12.2
2	M	MB	M0	7	A	2287	U
3	M	MB	M0	4.6	U	U	100
4	F	DN MB	M0	2	A	511	44.1
5	M	MB*	M0	4.9	D	477	12.16
6	M	MB	M0	4.1	D	279	84.28
7	M	MB	M0	13.8	D	932	62.8
8	F	MB	M0	7.1	D	1245	97.02
9	M	MB	M0	10.9	A	1985	88.9
10	M	MB	M0	6.1	A	414	124.2
11	M	MB	M0	10.1	A	1025	100.8
12	M	MB	M0	12.4	A	823	36.2
13	M	MB	M0	4	A	389	U
14	F	MB	M0	1.75	A	366	76.5
15	M	DN MB	M0	12.75	A	1514	U
16	F	MB	M0	4	A	2723	32.19
17	M	MB	M0	2.4	D	790	77.57
18	F	LC MB	M0	8.4	D	764	70
19	M	MB	M1	2.8	D	416	70.84
20	M	MB	M1	3.4	A	1724	U
21	M	MB	M1	5.4	A	2532	52
22	M	MB	M1	3.25	D	307	12.67
23	M	MB	M2	10.4	D	1155	U
24	M	MB	M2	12	D	1561	12.16
25	F	LC MB	M2	15	D	736	62.58
26	M	MB	M2	8.1	D	2436	33
27	M	MB	M3	8.5	A	364	94
28	M	MB	M3	11	D	464	23.6
29	F	MB	M3	11.4	A	3103	U
30	M	MB	M3	5.75	D	1737	103.68
31	F	MB	M3	6.3	A	1769	74.8
32	M	MB	M3	5.9	A	1624	U
33	M	MB	M3	5	D	727	U
34	M	MB	M3	4.9	D	550	70.17
35	F	MB	M3	2.5	A	595	U
36	F	MB	M3	4	D	507	16.9

Note: - * Medulloblastoma with Rhabdomyoblastic Differentiation

7.2.2 MRS acquisition and quantitation of metabolite concentrations and lipid intensities

Single voxel MRS was carried out after conventional MRI prior to treatment on a 1.5 T MR system (GE Excite, Siemens Symphony or Siemens Avanto). Core protocol consisted of TE 30 ms and TR 1500 ms. Cubic voxels were either 2 cm or 1.5 cm side length with 128 or 256 repetitions acquired respectively. Voxel placement delineated using conventional MRI was on the primary tumour.

Metabolite concentrations were determined using TARQUIN (version 3.2.2 with extended basis set) (Wilson et al., 2011). The lipid and macromolecular components were included in the analysis as individual components with the lipids at 1.3 ppm as lip1.3a+lip1.3b (L1.3) summed and as combined components at 0.9 ppm (LMM0.9), 1.3 ppm (LMM1.3) and 2.0 ppm (LMM2.0). All spectra were assessed using the QC criteria (section 4.3). From the 42 MRS studies performed, 36 met the quality control criteria with two cases failing due to inappropriate voxel location and four for distortions within the spectra.

7.2.3 Statistical Analysis

35 out of the 36 cases had follow-up data available. 17 of these patients developed tumour progression and subsequently died as a result. The mean time from diagnosis to last follow-up or death was 1123 days. Mann-Whitney U-test (Mann and Whitney, 1947) was performed to compare metabolite concentrations of MB patients currently alive (n=18) with those that had progressed and died (n=17). With 23 variables tested, a Bonferroni corrected significance of 0.002 (P<0.002) was calculated. Survival analysis (using R package survival) was performed using Cox-Regression modelling (Cox, 1972)

using a multivariate and univariate approach. Cox-Regression was performed on each quantified metabolite and using a multivariate model of survival with model simplification performed using backward elimination. Following this, the most significant metabolites from the univariate analysis were used to construct a model based on the linear co-efficients and an optimal cut-off determined using a ROC curve. The AUC was also reported for each ROC curve (Egan, 1975). Kaplan-Meier curves (Kaplan and Meier, 1958) were constructed for significant metabolites in the univariate analysis and the combined model using a ROC cut-off. Each Kaplan-Meier curve was tested using a log-rank test (Mantel, 1966) for significant differences in survival.

Cox-Regression analysis was performed on other factors in particular those that are used in treatment stratification. These included testing patient gender (male vs. female), extent of resection (complete resection vs. near complete resection (<1.5 cm^3) vs. incomplete resection (>1.5 cm^3), age at diagnosis (< 5 years vs. > 5 years) and Chang stage (M0 vs. M1-M3 and M0 vs. M1 vs. M2 vs. M3 and M0-M1 vs. M2-M3) for prognostic variables. These were also tested using Kaplan-Meier curve analysis and log-rank test for significance.

7.3 Results

7.3.1 Spectral features
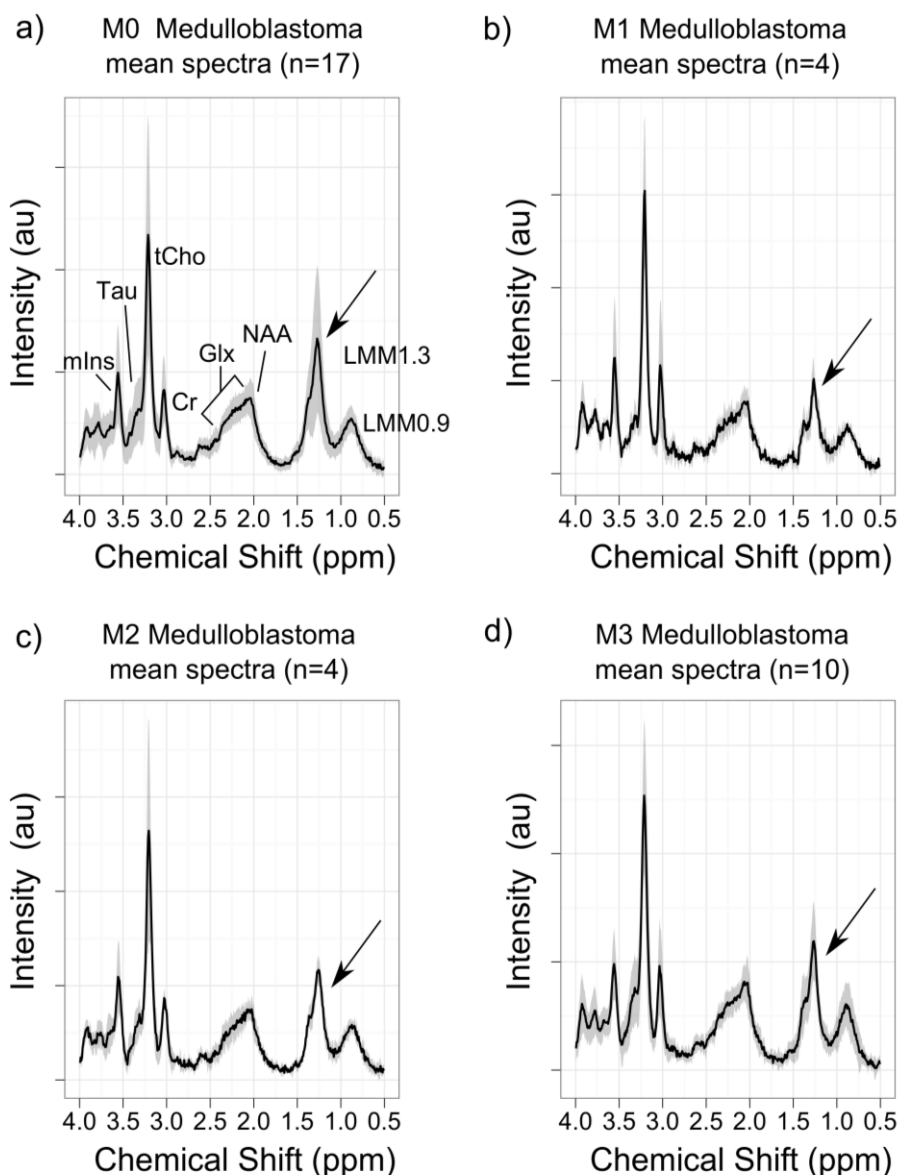
Figure 7.1 Mean spectral profiles for a) M0 MB (n=17) b) M1 MB (n=4) c) M2 MB (n=4) d) M3 MB (n=10) with standard deviations indicated by the shaded regions. Embedded arrow indicates variable LMM1.3 region.

Figure 7.1 illustrates mean spectra from the whole cohort split into their respective Chang stages, M0 to M3. The spectra, in general, exhibit very similar metabolite profiles but there are a few differences to be noted that could be of interest. For example, the

M0 spectra exhibit a more variable metabolite profile compared to the other Chang stages, which is shown by high standard deviations indicated by the shaded region. In addition to this the LMM1.3 region of the spectra appears to differ between Chang stages.
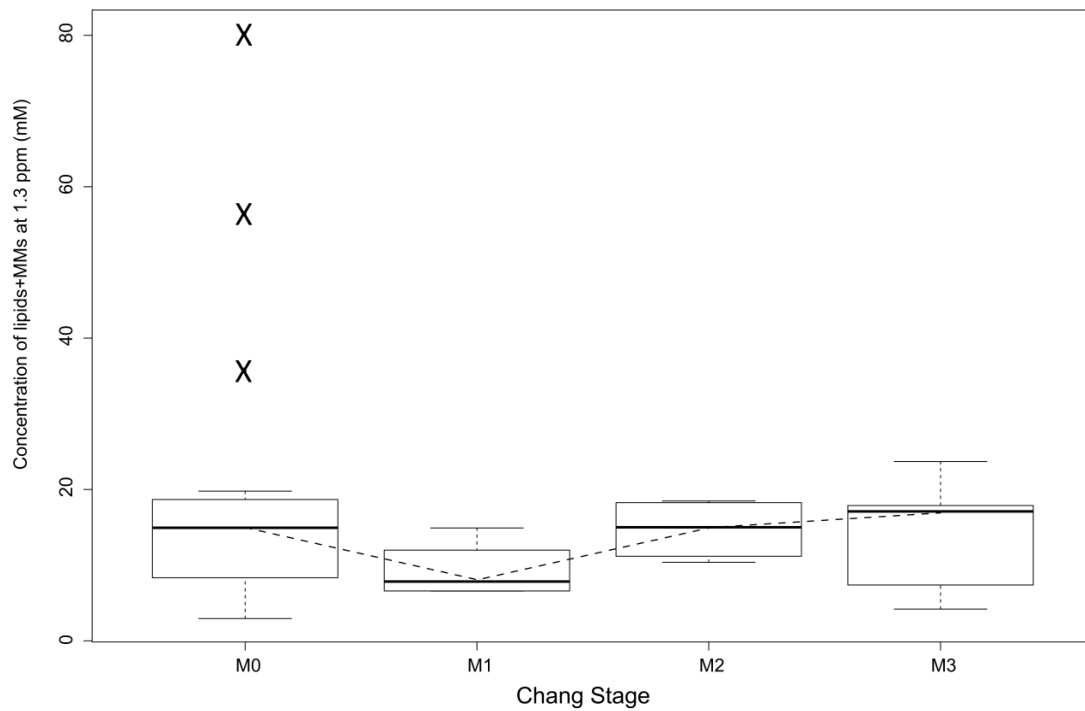
Figure 7.2 Box and whisker plot of levels of lipid+MMs at 1.3 ppm (LMM1.3) for Chang stages M0-M3

Figure 7.2 demonstrates Chang stages M0 to M3 to have similar levels of LMM1.3. Interestingly, the M0 cohort consists of three cases with very high levels of LMM1.3, represented as outliers on the box and whisker plot. All three patients developed tumour progression soon after diagnosis and died within a short follow-up period.

7.3.2   Univariate analysis

Table 7.2 A summary of mean metabolite concentrations (mM ± SD) comparing MB currently alive and MB that died of tumour progression using Mann-Whitney U-test. Significant metabolites are highlighted in bold.

Metabolites (mM)	p values	MB currently alive (n=18)	MB died (n=17)
Cr	**0.02**	**3.42±1.5**	**2.56±1.0**
tCho	0.15	3.98±1.7	3.16±1.4
Gua	**0.04**	**1.24±0.9**	**0.67±0.6**

Significantly lower levels of Cr and Gua were seen in those patients that developed tumour progression and died as a result (Mann Whitney U-test analysis, P=0.02 and P =0.04 respectively). No other metabolites were significant including tCho (P=0.15) (Table 7.2).

7.3.3   Survival Analysis

Table 7.3 A summary of univariate survival hazard ratios and p values of those metabolites that were significant when tested using a likelihood ratio test (P<0.05).

Metabolite	Hazard ratio	P value
tCho	0.611	0.008
MM20	0.724	0.02
Cr	0.64	0.03

Table 7.4 A summary of metabolites included in the final stepwise Cox-Regression model with survival hazard ratios and significance values. The likelihood ratio test was used for testing the significance of the model.

Metabolite	Hazard ratio	P value
Cr	0.602	0.03
tCho	0.580	0.01
Likelihood ratio test p value=0.002		

Cr, tCho and macromolecules (MMs) at 2.0 ppm from the univariate model were found to be significant predictors of survival based on the likelihood ratio test. Subjects with higher values of the variables were associated with a lower hazard (Table 7.3). Cr and tCho were the only significant metabolites in the stepwise Cox-Regression model with

higher values associated with lower hazard *P*=0.002 for the final model (Table 7.4). The combination of Cr, tCho and MMs at 2.0 ppm yielded a highly significant model when tested using the likelihood ratio test (*P*=0.003). The area under the ROC curve (AUC) for Cr, tCho, MMs at 2.0 ppm and combined model was 0.73, 0.64, 0.61 and 0.76 respectively.
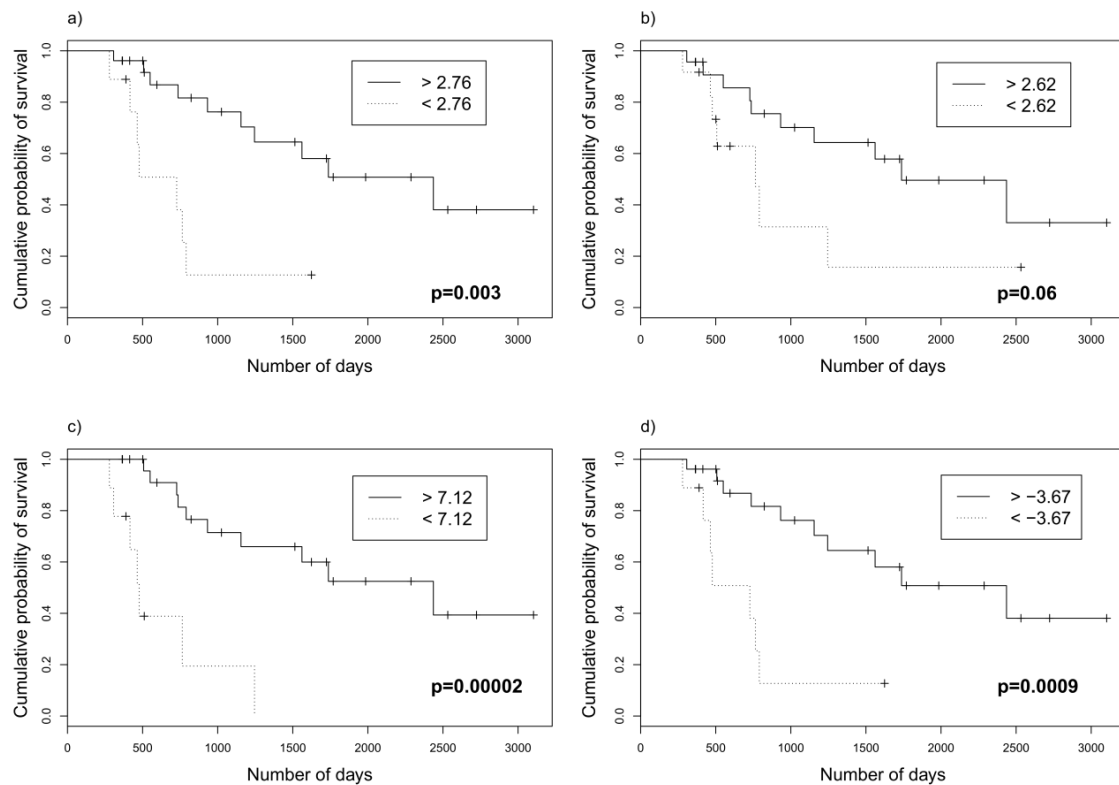
Figure 7.3 Kaplan-Meier survival distributions for a) Cr b) tCho c) MM at 2.0 ppm and d) a combined model of the linear co-efficients of Cr, tCho and MM at 2.0 ppm. Cut-offs were determined using ROC curves and significance values (*P)* tested using a log-rank test.

The corresponding Kaplan-Meier curves demonstrated significant differences in survival for Cr (*P*=0.003), MMs at 2.0 ppm (*P*=0.00002) and near significance for tCho (*P*=0.06) with lower values of the three variables having a worse survival. A combined model of metabolites was also significant (*P*=0.0009) (Figure 7.3).
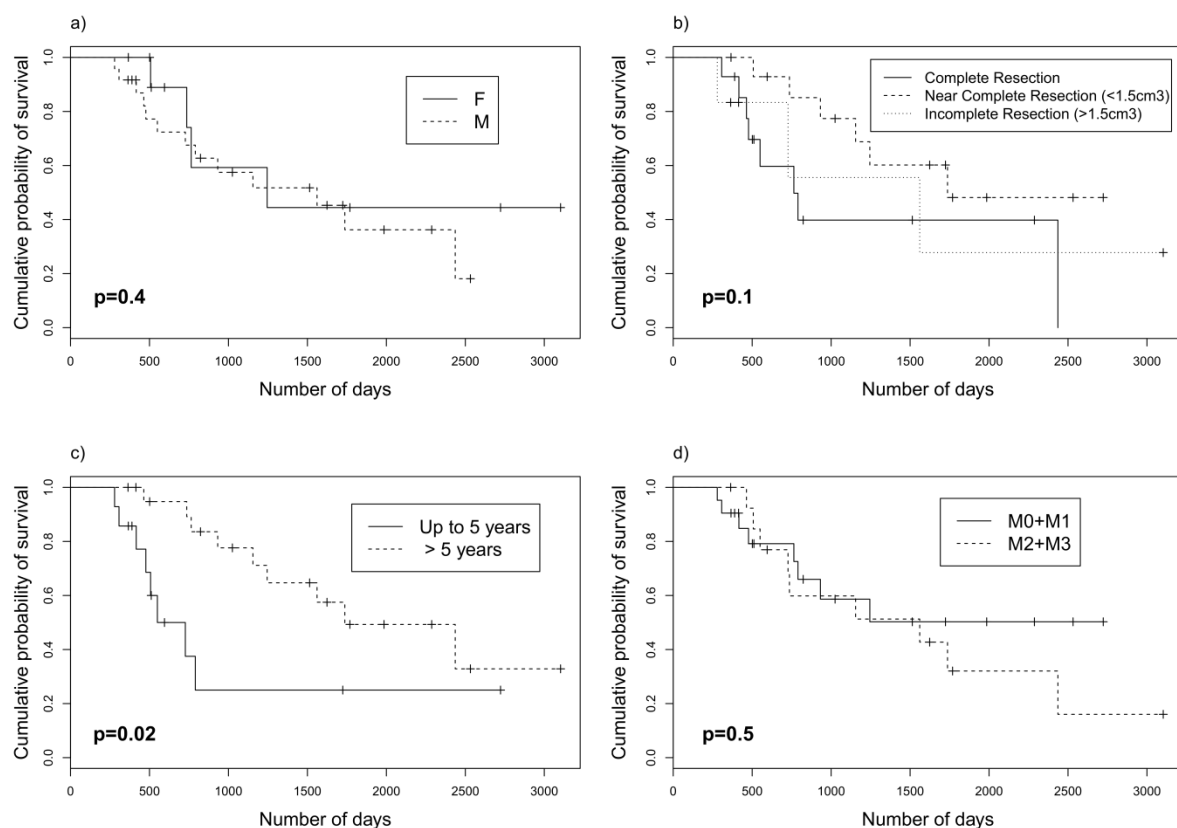
Figure 7.4 Kaplan-Meier survival distributions for a) patient gender (F vs. M) b) extent of tumour resection (complete resection vs. near complete resection (<1.5 cm^3) vs. incomplete resection (>1.5 cm^3) c) age of patient at diagnosis (≤5 vs. >5) and d) Chang stage ((M0+M1) vs. (M2+M3)). Significance values were tested using log-rank test. Abbreviations: F, Female; M, Male.

Cox-Regression modelling of clinical characteristics exhibited no significant variables when comparing gender, extent of resection and Chang stage. Age at diagnosis was the only significant variable (≤5 years vs. >5 years, likelihood ratio test, *P*=0.03). Kaplan-Meier curve analysis confirmed no significant variables amongst patient gender (*P*=0.4), extent of resection (*P*=0.1) and Chang stage (M0 vs. M1-M3, p=0.8 and M0 vs. M1 vs. M2 vs. M3, *P*=0.5 and M0-M1 vs. M2-M3, *P*=0.5). Age at diagnosis was significant (*P*=0.02) with young patients below the age of five doing worse (Figure 7.4). Patients below the age of five had significantly lower tCho (*P*=0.004) and Gly (*P*=0.03).

7.4 Discussion

This analysis has shown that metabolites detected non-invasively using 1H MRS are prognostic biomarkers in paediatric cohorts of patients with MB. Cr and tCho have been identified to be significant prognostic markers in these tumours with decreased levels associated with a poor prognosis. This study also found using a combinatorial model of metabolite markers Cr, tCho and MM at 2.0 ppm was able to predict survival of MB patients (Figure 7.3).

Creatine, often reported as tCr due to contributions from two compounds, creatine and phosphocreatine (PCr) is an organic acid that is an essential component of energy metabolism and marker of the energy state of cells (Martinez-Bisbal and Celda, 2009). Cr metabolism occurs through the creatine/creatine kinase system where Cr, through PCr, provides phosphate for ATP catalysed by the enzyme creatine kinase. It is hypothesised that the down regulation of creatine kinase is responsible for the decrease in creatine in tumours and therefore is the likely pathway utilised in tumourgenesis (Patra et al., 2012).

There is reported evidence of low creatine concentration in several malignant cell types (Davies et al., 2008, Martinez-Bisbal and Celda, 2009, Panigrahy et al., 2006). Yerli et al. demonstrated that tCr levels tended to be lower in high grade populations (Yerli et al., 2007). Tzika et al. found tCr to be the strongest predictor of active tumour in their study (Tzika et al., 2001). The current understanding is that very malignant active tumours have a high metabolic rate of activity that results in hypoxia and depletion of energy stores which results in decreased levels of creatine in tumours (Rao, 2008, Tzika et al., 2001). However, it is difficult to differentiate Cr and PCr using the field strength of clinical

scanners. It is unclear from the measure of tCr whether this mechanism is driven by increased expression of creatine kinase or decreased creatine kinase as either will result in the decrease of one metabolite and increase of another (Patra et al., 2012) .

The tCho signal resonances seen in MRS consist of three major components; phosphocholine (PCh), glycerophosphocholine (GPC) and free choline. It is well known that choline containing compounds are involved in cell membrane synthesis and breakdown and during malignant transformation this process becomes abnormal (Astrakas et al., 2004). Tumours that exhibit high levels of tCho are usually associated with increased cell proliferation, aggressive tumours and poor outcome. Previous literature MRS studies have demonstrated increased levels of tCho to be associated with increased tumour grade (Astrakas et al., 2004, Loening et al., 2005) but not always for example paediatric optic pathway gliomas despite being low grade tumours exhibit elevated tCho (Orphanidou-Vlachou et al., 2013). Though an increased tCho concentration is usually associated with a poor prognosis, this result does not fit the expected trend. However, it should be noted that the field strength of clinical scanners cannot separate out the major peak components and it is the proportion of contribution of these metabolites that better explains the results observed. Previous literature findings have demonstrated that tumours with a greater contribution of PCh than GPC seen for the tCho peak are correlated with oncogenic and malignant transformation and as a result have a more aggressive course (Hattingen et al., 2008a, Podo, 1999).

The assignment of MMs at 2.0 ppm as a prognostic marker although of importance, is difficult to determine accurately. This region of the spectra *in vivo* overlaps highly with

other metabolites for example Glu, Gln, lipids and macromolecules. The accurate assignment of the prognostic marker in this region will be best determined using *in vitro* high-resolution spectroscopy methods such as magic angle spinning (HR-MAS) (Wilson et al., 2009a).

ROC curves are often used in medical diagnostics to develop clinical decision making tools. Previous studies have reported results using this method for MRS to aid diagnosis, prognosis and treatment monitoring in paediatric brain tumours (Harris et al., 2007, Orphanidou-Vlachou et al., 2013, Smith et al., 2009, Astrakas et al., 2004, Marcus et al., 2007). The advantage of using this method is that it provides a numeric threshold that can be interpreted alongside conventional MRI. An ideal test would identify survivors and non-survivors from the ROC curve cut-off demonstrating no overlap of metabolite concentrations between the two groups. However, overlap is inevitable and can result in the mis-classification of cases. While the AUC provides a value for the diagnostic accuracy of the test thus assessing the sensitivity and specificity, it does no assess the selected cut-off value demonstrating advantages and disadvantages of using this method like many tests. A future approach of validating the findings would be to assess the biomarkers established from the retrospective cohort on a prospective cohort of patients with the disease (Zou et al., 2007, Linnet et al., 2012).

There are very few studies in the literature that have investigated the metabolic changes seen in subgroup specific tumours. To aid the understanding of tumour pathogenesis and treatment requires the development of tumour mouse models. A recent study demonstrated the development of a MB SMO mouse, SMO a receptor in the SHH

pathway seen to be highly activated in SHH tumours (Hatton et al., 2008). The mutations in the patched (Ptch) gene in the SHH pathway contribute to SMO mice developing subclinical MB by two months of age. High resolution *in vitro* spectroscopy was performed on the tumour tissue excised from the SMO mouse and results demonstrated decreased NAA and elevated levels of tCho, taurine and glycine. The elevated levels of metabolites observed are in agreement with an aggressive and highly malignant tumour (Hekmatyar et al., 2010). While there is currently no evidence in the literature for the metabolic changes observed for a WNT tumour to our knowledge, the WNT pathway plays a role in cancer progression, including tumour initiation, tumour growth, cell senescence, cell death, differentiation and metastasis (Anastas and Moon, 2013). It is known that tumours belonging to this subgroup have a good prognosis and it can be speculated that elevated tCho levels is likely be observed but vary in the contribution of components to the peak in comparison to SHH pathway tumours. A greater contribution of GPC to PCh maybe observed for the less malignant tumour.

With the confirmation of molecular subgroups of MB, the next challenge has been to develop rapid diagnostics tests to accurately determine grouping (Li et al., 2013). The combination of histopathology methods, immunohistochemistry and cytogenetics of new cases has recently been used at BCH to determine a limited number of genetic aberrations. The high variability of the LMM1.3 and high standard deviations seen in MB spectra provides preliminary evidence for subgroups of MB existing particularly within the M0 Chang stage. Interestingly, the three outliers seen in Figure 7.2 that exhibited high levels of LMM1.3 all had a poor survival. Currently no retrospective cytogenetic analysis has been performed in these cases so no genetic information is available. Analysis in

Chapter 5 identified Cr to be significantly different between spectroscopy acquired on different scanners in a cohort of MB with the highest levels measured on the GE and Siemens Avanto. Interestingly, the group acquired on the Siemens Avanto consisted of five out of six patients with no MYC or MYCN amplification (1 had no information available) suggesting a cohort of patients with good prognosis (Taylor et al., 2012). A combination of retrospective and prospective confirmation of genetic subgroups would be intriguing to establish in future studies. Evaluation of MB spectra results in the majority of cases passing the set QC criteria. It should be noted that a small number of cases fail due to low spectral SNR. However, it has been previously identified that low SNR in spectra acquired from tumours can be as result of low cellularity (Harris et al., 2007). This is particularly true of desmoplastic nodular medulloblastoma that exhibits a less aggressive clinical course and is known to have a better prognosis compared to other MB subtypes (Gulino et al., 2008). As a result their pre-diagnostic spectra are often noisy and consist of low metabolite levels thus failing the set QC criteria. Additionally the study does not capture spectroscopy on every MB that presents at the centre. Patients that present initially at a different centre, present acutely unwell or have an MRI scan under a scanner operator whose experience of MRS is limited are less likely to have a spectroscopy sequence performed. Consequently this study demonstrates a study bias eliminating a few cases including those inherently known to have a better prognosis and speculatively those with more aggressive tumours.

For future studies it may be beneficial to also perform 31P spectroscopy to measure the relative concentrations of PCh and GPC because of the greater chemical shift separation between the two metabolites (Loening et al., 2005). There is an increasing body of

evidence demonstrating the benefits of high field scanners for imaging and spectroscopy and 31P looks like a promising aid in the investigation of the biology of tumour cell proliferation (Qiao et al., 2006) but is hindered by low SNR (Albers et al., 2005). An alternative method for validating these findings would be to confirm the *in vivo* results with ex-vivo HR-MAS data. A recent study found a good correlation between metabolite quantities detected by HR-MAS and *in vivo* MRS for brain tumours (Wilson et al., 2009b). With the increased spectral resolution of HR-MAS it would be easier to determine the components of the significant peaks.

7.5   Conclusions and future investigations

In conclusion, this analysis has demonstrated the MRS detection of increased levels of Cr and tCho to be biomarkers of good prognosis in MB. Recent evidence supports the existence of four main molecular subgroups of MB that differ in prognosis thus providing interesting preliminary findings of a possible association. These non-invasive biomarkers may help in the future to stratify treatment in patients. However further work including analysis of tumour tissue and confirmation of biological subgroups is required to validate this work.

CHAPTER 8: A MULTI-CENTRE STUDY OF 1H MAGNETIC RESONANCE SPECTROSCOPY IN THE CHARACTERISATION OF BRAIN STEM TUMOURS IN CHILDREN

CHAPTER 8

8   A MULTI-CENTRE STUDY OF 1H MAGNETIC RESONANCE SPECTROSCOPY IN THE CHARACTERISATION OF BRAIN STEM TUMOURS IN CHILDREN

8.1   Introduction

Brain stem tumours (BST) account for 10-25% of brain tumours in children. The management of brain stem tumours is particularly challenging for clinicians as tumours in this region are usually unresectable and difficult to biopsy (Hargrave et al., 2006). Four main tumour types are found in the brain stem, and fall into two major categories of either diffuse or focal. The most common tumour of the brainstem is diffuse intrinsic pontine glioma (DIPG), which make up 80% of all brain stem gliomas (Donaldson et al., 2006). These tumours are not biopsied and have a particularly poor prognosis with a median survival of only nine months. Over the past 30 years, while the prognosis and survival time for many cancers including other brain tumours has considerably improved, this has remained unchanged for DIPG and they are now a major cause of death by brain tumour in children (Hargrave et al., 2006). However, amongst these cases there are a few long term survivors of DIPG but currently no conventional imaging characteristics that are able to identify this good prognostic group at diagnosis (Liu et al., 2009). The lack of available biopsy material from this tumour hinders the opportunity to determine biological markers for prognosis (Leach et al., 2008). Tectal plate gliomas (TPG) are also diagnosed solely on imaging with no biopsy performed but demonstrate an indolent course. If the tumours are focal or not typical of DIPG or TPG they are biopsied and most are diagnosed as high grade glioma, low grade glioma and occasionally other rarer types. Due to the difficulty of obtaining tumour tissue in these regions of the brain and the risks

of sampling error from small biopsies, improved non-invasive methods, which can give diagnostic, prognostic and biological information, would provide a significant advance in their management.

With the importance of imaging in brain stem tumours, spectroscopy holds promise as a diagnostic modality. As these tumours are extremely rare, very few studies have been focused on childhood brain stem lesions thereby requiring a multi-centre approach to obtain enough cases for robust statistical analysis. However, the difficulties arise when standardising data acquisition and analysis across different scanners demonstrating the need for MRS to developed and tested across multi-centre cohorts (Vicente et al., 2013, García-Gómez et al., 2009). The low incidence of focal tumours in the brain stem presents a challenge in specifying the MRS profile of these tumours. However, an approach where comparisons have been made with MRS of tumours with the same histology in other locations has been previously used and warrants further exploration (Panigrahy et al., 2008).

The increasing body of evidence of the poor correlation of conventional imaging markers with patient survival (Hargrave et al., 2008, Yamasaki et al., 2011, Liu et al., 2009) has resulted in an increasing interest in using MRS for determining prognosis. A number of studies have identified markers of prognosis for DIPG. High tCho/NAA values in a cohort of DIPGs was found to be associated with poor prognosis and an increase over subsequent scans was associated with greater risk of death compared to patients who had stable or decreased tCho/NAA (Steffen-Smith et al., 2011). An increased tCho/NAA at subsequent time points was predictive of shorter survival (Hipp et al., 2011).

A recently published study has identified lactate as a marker of poor prognosis in a cohort of DIPG that consisted mainly of children but also included adults (Yamasaki et al., 2011). These studies consist of data that has been acquired at long echo time so the number of quantifiable metabolites is restricted (Steffen-Smith et al., 2011, Yamasaki et al., 2011). Also there are currently no biomarkers for identifying the few long term survivors of DIPG. Short echo time MRS detects more metabolites and has successfully identified novel metabolite biomarkers of prognosis in children's brain tumours (Wilson et al., 2013). The use of short echo time MRS for investigating brain stem tumours in children may therefore give rise to distinct MRS profile differences and requires further investigation.

This chapter describes a study that is large compared with previous analyses. Whereas most published studies have collected and analysed data from a single centre, the work reported here is multi-centre data. A recent multi-centre study has shown that 1H MRS can yield high diagnostic accuracy in children's brain tumours and represents the first application of this strategy to brain tumours in children (Vicente et al., 2013). This chapter investigates potential diagnostic and prognostic metabolite differences in childhood brain stem tumours on a multicentre cohort. It examines the differences between diffuse and focal tumours diagnosed in both the brainstem and elsewhere in the brain. The analysis includes follow-up of patients to allow the determination of prognostic markers.

8.2   Method

8.2.1   Patients

Single voxel 1H MRS was performed on 35 children with brain stem tumours during routine MRI scans prior to treatment at four centres across the UK. These included BCH, QMC, GOS and RMH. All cases underwent central radiology review by three radiologists experienced in the review of children's brain tumours. Imaging characteristics of all tumours were documented including the presence of necrosis and/or haemorrhage. Diagnosis was made on the basis of central pathology review where tissue was available or central radiology review where there was no tissue. Only five patients were diagnosed on the basis of histopathology, one of which proved to be non-diagnostic. The diagnosis of DIPG was made without biopsy on the basis of clinical presentation and conventional imaging. Diagnostic criteria on MRI for DIPG included the tumour occupying at least 50% of the pons mostly with or without local tumour extension. In addition to this the T1 weighted MRI characteristics of the tumour were that of a hypointense lesion and homogenous on T2 weighted MRI. The cohort consisted of 14 DIPG (seven male and seven female, mean age 7 years), four focal low grade brain stem tumours (two male and two female, mean age 11 years), five focal high grade brain stem tumours (three male and two female, mean age 11 years) and six tumours of the brain stem with no definitive or consensus diagnosis (five male and one female, mean age 10 years). 29 cases were included in the final analysis with six cases failing spectral quality control (Table 8.1). MRS profiles of the brain stem cases was compared with those from 31 PA (17 male and 14 female, mean age 7 years) and eight HGG (six male and two female, mean age 8 years) outside the brain stem, all diagnosed on histopathology.

8.2.2 MRS acquisition and quantitation of metabolite concentrations and lipid intensities

MRS data was acquired prior to treatment on either a 1.5 T or 3 T MR scanner (echo time 30 ms or 38 ms; TR 1500 ms at 1.5 T and 2000 ms at 3 T). Raw spectroscopy data was processed using TARQUIN (Wilson et al., 2011). Metabolite levels were determined relative to a water reference spectrum. For cases where a water reference spectrum was not available, spectra were normalised to the sum of all metabolite levels. All spectra were assessed using the QC criteria (section 4.3).

Table 8.1 Brain stem tumour cohort characteristics

* Diagnosis made on the basis of histopathology

No.	Age (Yrs.)	Sex	Hospital	Tumour Site	Best Diagnosis (Central Pathology → Local Pathology → Central Radiology)	Differential diagnosis	Certainty of diagnosis	Imaging features
1	4.8	M	BCH	Pons	Diffuse pontine glioma	Astrocytoma grade 1 (25%)	75%	Non-enhancing
2	5.5	F	BCH	Pons	Diffuse pontine glioma	High grade glioma grade 1 (25%)	75%	Haemorrhage
3	14	M	BCH	Pons	Diffuse pontine glioma	-	99%	Haemorrhage
4	7.1	M	BCH	Pons	Diffuse pontine glioma	-	99%	Enhancing
5	4.1	M	BCH	Pons	Diffuse pontine glioma	-	99%	Non-enhancing
6	12.2	M	BCH	Pons	Glioblastoma multiforme*	Diffuse pontine glioma grade 3 (25%)	75%	Necrotic
7	6.1	M	BCH	Midbrain	Anaplastic astrocytoma*		99%	Haemorrhage, enhancing and necrotic
8	10.9	M	BCH	Tectal Plate	Tectal plate glioma	Primitive neuroectodermal tumour	90%	Enhancing
9	11	M	BCH	Midbrain/Tectum	Pilocytic astrocytoma	Pilomyxoid astrocytoma	99%	Enhancing
10	5.5	F	BCH	Pons	Diffuse pontine glioma		99%	Non-enhancing
11	15.5	M	BCH	Cerebello/ponto/ medullary	Diffuse astrocytoma*	Diffuse astrocytoma grade 3	99%	Non-enhancing

12	8	F	BCH	Pons	Diffuse pontine glioma	-	99%	Non-enhancing
13	4.8	F	BCH	Pons	Pilocytic astrocytoma	Astrocytoma grade 3	90%	Non-enhancing
14	4.5	F	BCH	Pons	Diffuse pontine glioma	-	99%	Non-enhancing
15	6.2	F	BCH	Pons	Diffuse pontine glioma	-	99%	Necrotic
16	4.8	M	BCH	Pons	Diffuse pontine glioma	-	99%	Non-enhancing
17	0.4	M	GOSH	Pons	Ependymoma	Low grade glioma (25%)/ High grade glioma (25%)	50%	Non-enhancing
18	5.1	F	GOSH	Pons	Diffuse pontine glioma			Enhancing
19	0.8	M	GOSH	Midbrain	Medulloblastoma	High grade glioma (25%)	75%	Enhancing
20	14.6	F	GOSH	Medulla	Glioblastoma multiforme	Pilocytic astrocytoma (25%)	75%	Enhancing
21	10.4	M	GOSH	Medulla	Pilocytic astrocytoma	No alternative	90%	Enhancing
22	14.5	M	GOSH	Pons	Diffuse pontine glioma		99%	Non-enhancing
23	13.2	F	GOSH	Pons	Glioblastoma multiforme	Pilocytic Astrocytoma (25%)	75%	Non-enhancing
24	7.7	F	QMC	Pons	Diffuse pontine glioma		99%	Non-enhancing
25	10.1	F	QMC	Pons	Ganglioglioma*	Diffuse glioma grade 3 (25%)	75%	Non-enhancing
26	6.1	M	QMC	Medulla	Diffuse pontine glioma		99%	Non-enhancing
27	10.3	F	RMH	Centred on Pons	Diffuse low grade glioma	Low grade glioma grade 1 (25%)	75%	Non-enhancing
28	22.2	M	RMH	Centred on Pons	50% DIPG grade 3 / 50% HGG grade 4	As best diagnosis	50%/50%	Necrotic
29	9.4	M	RMH	Centred on Pons	50% Diffuse astrocytoma / 50% HGG	As best diagnosis	50%/50%	Non-enhancing

8.2.3 Statistical Analysis

Metabolite quantitation was performed using TARQUIN (version 3.2.1) (Wilson et al., 2011). One way analysis of variance (ANOVA) and Student's t-tests were performed to assess the differences between DIPG, focal LGG and focal HGG within the brain stem. The known histopathology of focal tumours of the brain stem compares with histopathology of focal brain tumours found elsewhere and for this reason were seen as the ideal comparator group. ANOVA was also performed to compare DIPG, PA and HGG outside the brain stem. Student's t-tests were used to compare focal low and high grade tumours of the brain stem and also to compare PA and HGG outside the brain stem. With 23 variables tested, a Bonferroni corrected significance of 0.002 ($P<0.002$) was calculated. A diagnostic classifier for discriminating DIPG, PA and HGG was constructed using metabolite concentrations with lipids and MMs as separated variables, first as inputs into PCA followed by LDA of PCA scores. Accuracy of the classifier was determined using LOOCV (Geisser, 1975).

Survival data was available for the whole cohort of brain stem tumours with a minimum follow-up of three years from diagnosis. Analysis was performed separately on three groups, the DIPG cohort (14 patients), the unbiopsied brain stem cohort (25 patients) and the whole brain stem cohort (29 patients). Prognostic markers from characteristics seen on MR imaging and MRS variables were tested for using Mann Whitney U-tests comparing those patients that survived less than one year with those that survived more than one year for each of three groups. Optimal cut-offs for significant variables were determined using ROC curves for Kaplan Meier curve analysis. Significant differences in survival were assessed using a log-rank test.

8.3   Results

8.3.1   Spectral features
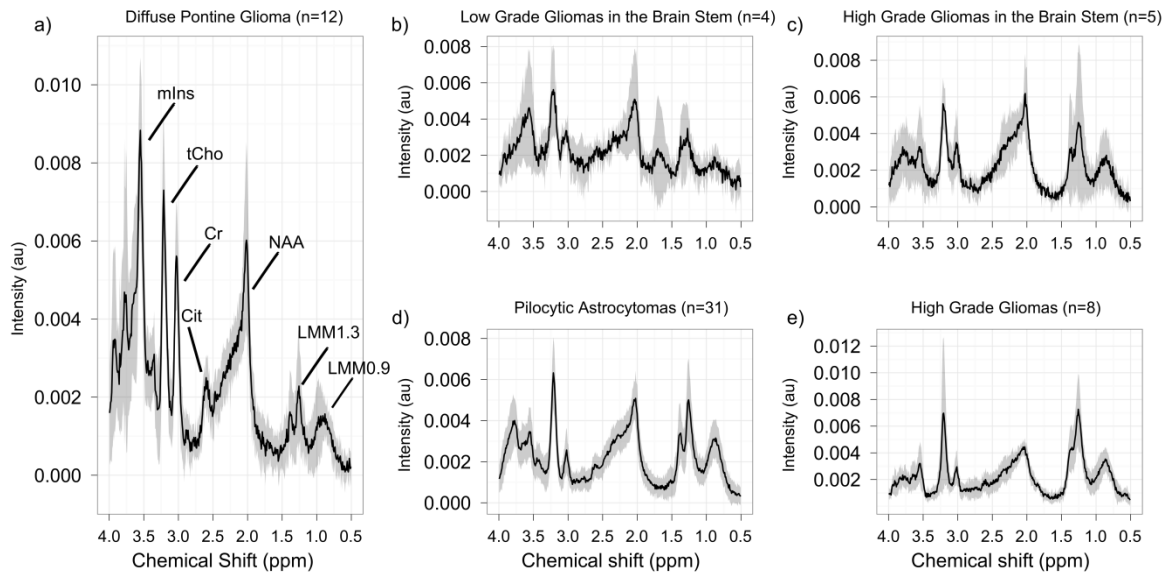
Figure 8.1 Mean spectral profiles for a) diffuse pontine gliomas (n=12) (b) low grade gliomas in the brain stem (n=4) (c) high grade gliomas in the brain stem (n=5) (d) pilocytic astrocytomas outside the brain stem (n=31) and (e) high grade gliomas outside the brain stem (n=8) with standard deviations indicated by the shaded regions.

Figure 8.1 shows mean spectra from the different tumours that were compared in the statistical analysis. The main features of the DIPG mean spectrum (Figure 8.1a) on qualitative analysis, that distinguished it from the spectra of other BST and non-BST was high mIns, prominent Cit and low LMM1.3 and LMM0.9. The brain stem low grade glioma (Figure 8.1b) and high grade glioma mean spectra (Figure 8.1c) exhibited low SNR as a result of small sized tumours. The increased metabolite variability seen at most positions can be explained by the small number of cases in each cohort. Spectral features that distinguished PA (Figure 8.1d) from HGG (Figure 8.1e) included detectable levels of NAA, readily detectable Lac and low Cr at 3.0 ppm. The main features of the HGG mean spectra (Figure 8.1d) were high tCho, low NAA and high lipids+MMs in particular at 1.3 ppm. The

highest variability in all tumour types appeared to be in the lipid+MMs area at 0.9 ppm

and 1.3 ppm.

The mean values of the metabolites and lipids and/or MM of most interest have been reported in Table 8.2 for the different tumour groups. Cit and sIns were the only two metabolites that were significantly different between all three tumour groups in the brain stem. The highest concentrations were seen in DIPG followed by focal LGG with focal HGG having the lowest concentrations (ANOVA, $P<0.01$, $P<0.05$ respectively). Significantly higher mIns in focal LGG of the brain stem was the only discriminator between focal HGG of the brain stem (Student's t-test; $P<0.05$). Significantly elevated tCho and decreased Gly were found in LGG in the brain stem compared to PA elsewhere in the brain (Student's t-test, $P<0.01$, $P<0.05$ respectively). Significantly decreased Cit, Lac and LMM2.0 concentrations were found in HGG in the brain stem compared to HGG found elsewhere in the brain (Student's t-test, $P<0.01$, $P<0.05$, $P<0.05$ respectively) (not reported in table). Significant differences in all major metabolites, lipids and macromolecules were found on comparison of DIPG, non-bst HGG and non-bst PA (ANOVA, $P<0.05$). Key discriminatory metabolites included Cit, Cr and mIns, all of which were significantly higher in DIPG than in HGG and lowest in PA. Lipids were seen to be significantly higher in HGG and lowest in DIPG.

8.3.2 Univariate analysis

Table 8.2 ANOVA and t-test analysis results with estimated metabolite concentrations of diffuse pontine gliomas, high grade and low grade gliomas of the brain stem with estimated metabolite concentrations of high grade gliomas and pilocytic astrocytomas found elsewhere in the brain.

Abbreviations: BST, brain stem cohort.

Metabolites	**ANOVA** DIPG vs. Focal BST (*P* value)	**ANOVA** DIPG vs. Focal outside BST (*P* value)	**Mean Concentration (mM)**					**T-test** Focal BST (*P* value)	**T-test** Focal outside BST (*P* value)
			Diffuse Pontine Glioma	focal tumours of the brain stem		focal tumours outside the brain stem			
				High Grade Gliomas (HGG)	**Low Grade Gliomas (LGG)**	**High Grade Gliomas (HGG)**	**Pilocytic astrocytomas (PA)**		
Cit	**<0.01**	**<0.0001**	0.89	0.23	0.67	0.68	0.34	<u>>0.05</u>	**0.05**
Cr	<u>></u> 0.1	**<0.0001**	2.96	2.11	2.21	1.42	0.88	<u>></u> 0.1	<u>></u> 0.1
GPC+PCh/ tCho	<u>></u> 0.1	**<0.01**	1.34	1.36	1.64	1.99	1.00	<u>></u> 0.1	<u>></u> 0.1
Gly	<u>></u> 0.05	**<0.001**	2.70	0.35	0.07	1.45	0.43	<u>></u> 0.1	**0.05**
mIns	<u>></u> 0.1	**<0.0001**	4.53	1.22	4.11	0.77	0.61	**<0.05**	<u>></u> 0.1
Lac	> 0.1	**<0.001**	0.84	1.20	1.61	3.91	2.12	<u>></u> 0.1	<u>></u> 0.1
sIns	**<0.05**	**<0.001**	0.26	0	0.18	0.09	0.04	<u>></u> 0.1	<u>></u> 0.1
Lipids at 0.9 ppm	<u>></u> 0.05	**<0.001**	0.79	1.71	1.70	2.84	1.65	<u>></u> 0.1	**<0.05**
MMs at 0.9 ppm	<u>></u> 0.1	**<0.0001**	1.34	2.77	1.99	5.72	2.70	<u>></u> 0.1	>0.05
Lipids at 1.3 ppm	0.1	**<0.0001**	1.87	6.03	4.48	11.98	5.25	<u>></u> 0.1	**<0.001**
Lipids at 2.0 ppm	<u>></u> 0.1	**<0.05**	0.94	1.85	3.61	3.85	2.12	<u>></u> 0.1	<u>></u> 0.1
MMs at 2.0 ppm	<u>></u> 0.1	**<0.001**	4.98	5.70	6.52	7.59	4.05	<u>></u> 0.1	**<0.0001**

8.3.3 Pattern classification
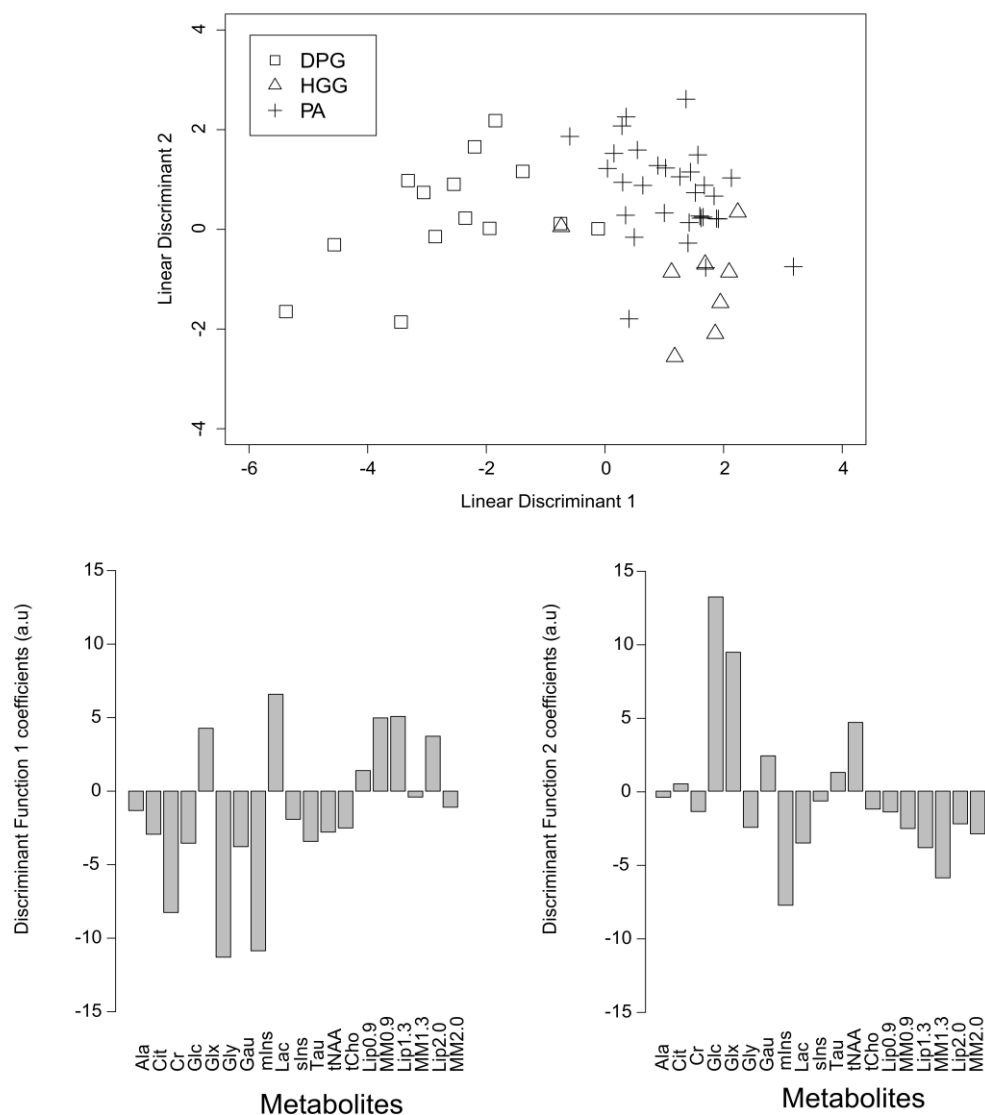
Figure 8.2 Three-way classifier between diffuse pontine gliomas and focal tumours outside the brain stem, pilocytic astrocytomas and high grade gliomas including a) a scatter plot of the discriminant function scores for each tumour type, b) discriminant function 1 coefficients and c) discriminant function 2 coefficients of the standardised metabolite profile

The three-way classifier showed a good separation between DIPG and the other tumours

with one overlapping HGG case (Figure 8.2). The cluster separation between the HGG and

PA although well overall, was less clear with, 1 HGG case clustering with the PA group and three PA clustering with the HGG group. DIPG scored highly in discriminant function 1, characterised by high mIns, Gly and Cr and low concentrations of Glx, Lac, LMM0.9, LMM1.3, and LMM2.0 (Figure 8.2b). Discriminant function 2 distinguished PA from HGG. PA were characterised by high Glc, NAA and Glx. HGG were characterised by higher LMM1.3 and also have a higher contribution of mIns than PA (Figure 8.2c). LOOCV used to evaluate the three-way classifier, demonstrated a success rate of 83% with the correct classification of 26 out of 31 all with a posterior probability above 80%.

8.3.4 Survival Analysis of conventional MRI characteristics
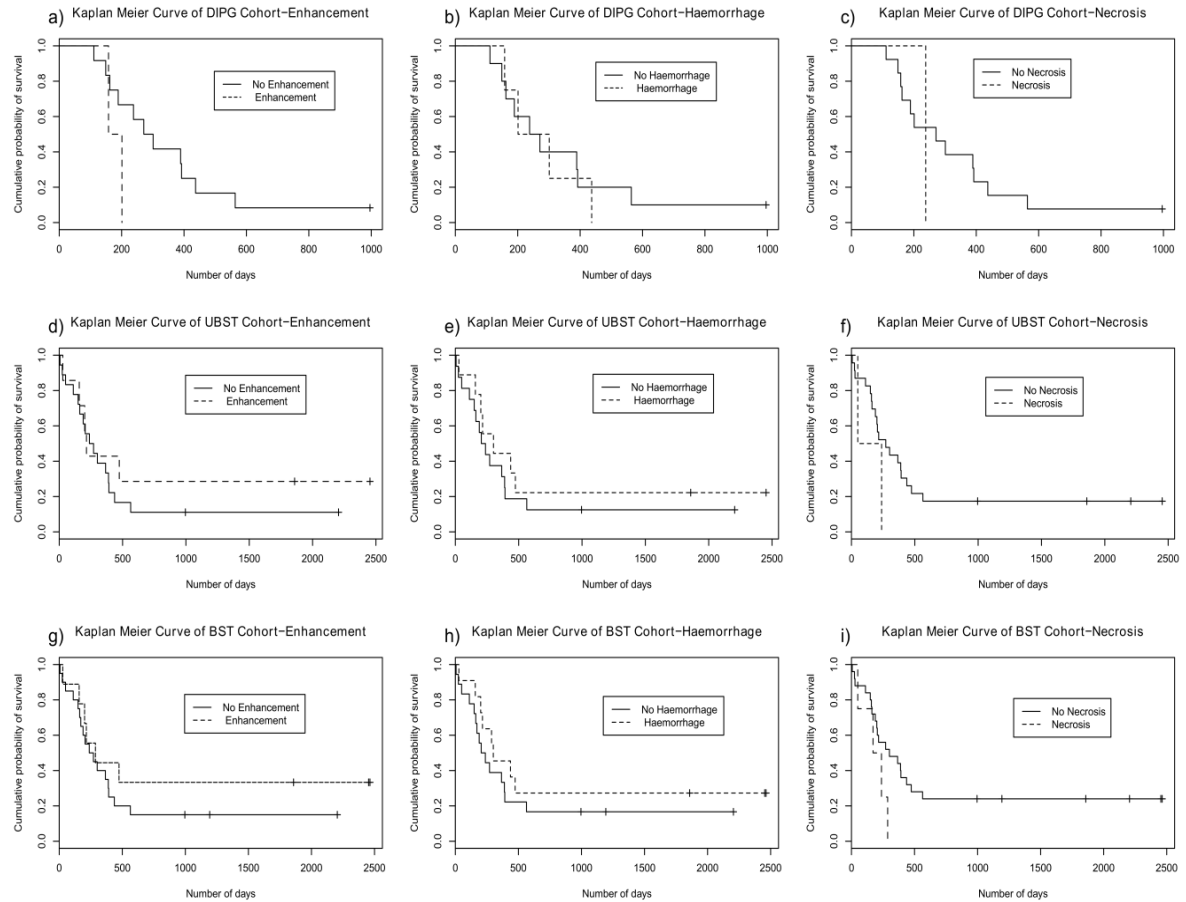
Figure 8.3 Kaplan-Meier survival distribution curves of a) enhancement b) haemorrhage and c) necrosis in DIPG and d) enhancement e) haemorrhage and f) necrosis in the unbiopsied brain stem cohort and g) enhancement h) haemorrhage and i) necrosis in whole brain stem cohort. Abbreviations: UBST, unbiopsied brain stem cohort; BST, brain stem cohort.

No significant differences were seen between those patients that demonstrated necrosis, haemorrhage or enhancement (Wilcoxon signed rank test, $P>0.05$) for the DIPG, unbiopsied brain stem and whole brain stem cohorts when comparing those patients that survived less than one year with those that survived more than one year. There was also no significant difference seen using Kaplan Meier survival curve analysis for the three imaging characteristics ($P>0.1$, log-rank test) (Figure 8.3).

8.3.5 Survival Analysis of metabolite profiles
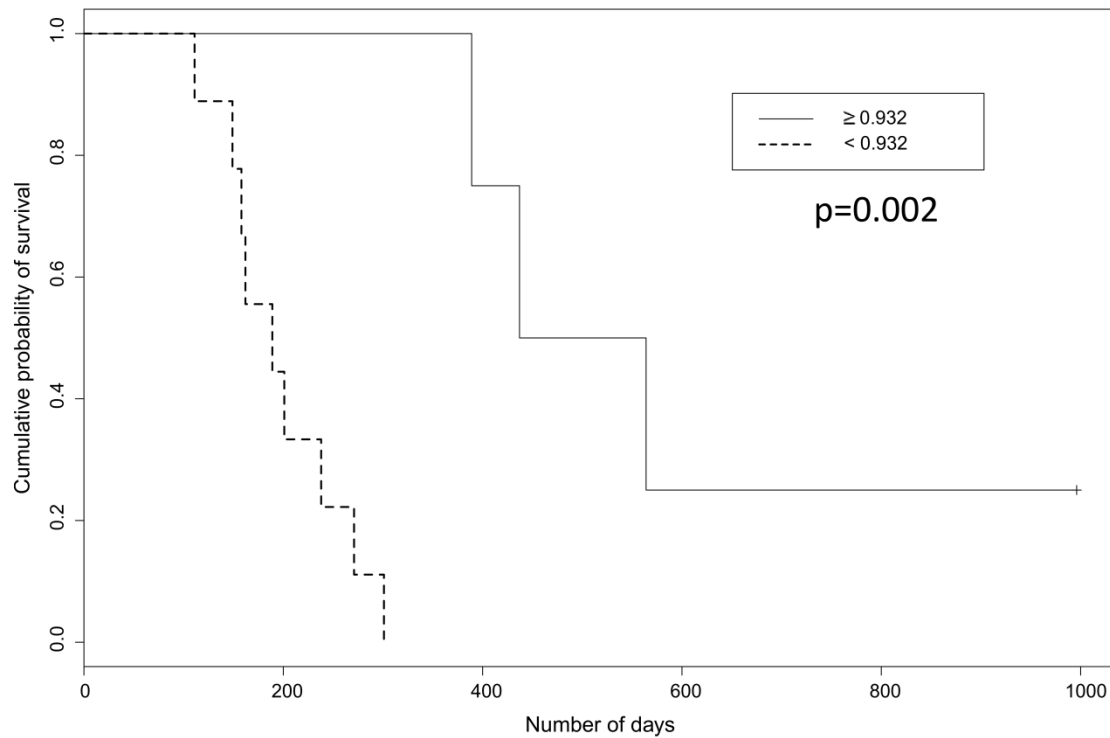
Figure 8.4 Kaplan-Meier survival distribution curve of Tau levels in the DIPG cohort. A cut-off of 0.932mM was determined using a ROC curve (ROC curve not shown) significance value tested using a log-rank test.

In the DIPG cohort, significantly higher Glx (5 vs. 3, P=0.05), Gln (3 vs. 0.7, P<0.05), LMM2.0 (6 vs. 4, P=0.05) and lower levels of Tau (0.1 vs. 1.2, P<0.05) were found in those cases surviving less than one year (Wilcoxon signed rank test). Kaplan-Meier curve survival analysis for Tau demonstrated a significant difference (P<0.01) in survival with a cut-off of 0.932 mM (Figure 8.4). There were no significant differences in metabolite variables for the whole brain stem cohort. The unbiopsied brain stem cohort showed significantly lower levels of Tau in those cases surviving less than one year (0.1 vs. 0.7, P =0.05). Two patients with MRS profiles which were substantially different from the DIPG

171

but who had diffuse pontine tumours, one biopsied diffuse astrocytoma and one in the DIPG cohort, were alive at three years.

8.4 Discussion

This analysis shows a successful collection and investigation of MRS data on a multi-centre cohort of important and rare tumours. MRS identified differences between metabolite levels in DIPG and focal high and low grade tumours of the brain stem and elsewhere in the brain. The presence of a prominent Cit peak and a high mIns are spectral characteristics of DIPG that can be readily identified in a clinical setting. The significant differences seen in the metabolite profiles of these tumour groups demonstrate spectroscopy to be a useful non-invasive diagnostic tool for brain stem tumours.

Citrate in particular was significantly different between the three groups of brain stem tumours, being highest in DIPG. In a previous study of 85 paediatric brain tumours, Cit was found to be highest in brain stem gliomas and concentrations were found to significantly declined over time in progressing brain stem gliomas (Seymour et al., 2008). Cit has also been found to be a marker of the malignant progression in astrocytomas in keeping with the characteristics and clinical course of DIPG (Blüml et al., 2011). The only DIPG survivor in this study had low levels of Cit at diagnosis. When comparing the DIPG with the focal tumours of the brain stem, Gly and sIns were also found to be high and these metabolites have been linked to high grade and poor prognosis in children's brain tumours (Davies et al., 2009, Wilson et al., 2013). The results show DIPG metabolite profiles at diagnosis are associated with aggressive tumours and poor prognosis, in

keeping with their subsequent behaviour. Focal LGG in the brain stem had higher levels of mIns than the brain stem HGG in keeping with studies of astrocytomas in adults (Castillo et al., 2000) and supratentorial pilocytic astrocytomas (Harris et al., 2008).

A small number of metabolites differed as a result of tumour location. Higher tCho in BST LGG than PA elsewhere in the brain was in keeping with their more aggressive nature. Reduced Lac and lipids seen in BST HGG compared to HGG elsewhere, metabolites associated with hypoxia and necrosis respectively, may reflect the larger tumour size of supratentorial tumours. Very few studies have investigated the differences between normal brain stem and other regions of the brain in paediatric patients. To the best of our knowledge these have been predominantly performed in adults (Tong et al., 2004, Hattingen et al., 2009). Spectroscopy is only likely to be acquired from the brain stem in paediatric patients if clinically indicated explaining the lack of studies. This could be an approach for a possible future multicentre study.

Panigrahy et al. (2008) reported comparisons of brain stem gliomas with anaplastic and grade IV astrocytomas elsewhere in the brain show significantly different levels of Cr, tCho and Glx but not mIns (Panigrahy et al., 2008). These metabolite differences may give an interesting insight into the biology of brain stem tumours and how it varies with tumour location. Overall, metabolite profiles were similar between tumours of the brain stem and their counterparts in other locations. In particular, the most discriminatory metabolite between HGG and LGG in the brain stem, mIns, was not significantly different

between brain stem tumours and similar tumours in other locations. These findings confirm that it is reasonable to interpret MRS of the brain stem by referring to MRS of tumours elsewhere in the brain. A diagnostic classifier based on MRS metabolite profiles and constructed using this approach, showed a good accuracy for diagnosing DIPG, HGG and PA and may provide a more formal aid to diagnosis than inspection of the spectra.

The three-way classifier demonstrated a number of interesting classifications. Case 7 was initially diagnosed from a tumour biopsy as a PA. As a result the patient was treated on a low grade tumour protocol but rapidly developed an increase in tumour size that resulted in the decision to perform a surgical resection. However, the diagnosis from the surgical tumour tissue was changed to anaplastic astrocytoma in keeping with the classifier result of HGG (80% posterior probability). This provides evidence that spectroscopy is able to identify features of a high grade tumour. Case 8 had imaging appearances in keeping with a high grade tectal plate lesion with a differential diagnosis of primitive neuroectodermal tumour. The case classified as a PA with a 92% probability and the patient is currently alive. Spectroscopy is shown to demonstrate low grade tumour features where conventional imaging is equivocal. None of the conventional MRI characteristics were related to survival demonstrating that MR imaging alone is unable to yield prognostic markers of brain stem tumours. This is in agreement with the findings of previous studies (Hargrave et al., 2008, Yamasaki et al., 2011).

Perez-Gomez et al. investigated the clinical features of paediatric patients that underwent stereotactic guided biopsy for brain stem tumours (Perez-Gomez et al., 2010). The histopathological entities of these tumours were either anaplastic astrocytomas (30%), or fibrillary and pilocytic types (25%) with low grade astrocytomas, high grade astrocytomas and even normal tissue. Clearly this needs to be studied with larger cohorts, but the mixed diagnoses identified confirms that brain stem tumours are not a single entity and do not all have the same prognosis. Several metabolites have been previously identified to be associated with prognosis in paediatric brain tumours. In this study, Tau was found to be a biomarker of good prognosis in the DIPG cohort. Tau is a diagnostic marker of primitive neuroectodermal tumours (Kovanlikaya et al., 2005). These tumours tend to respond to radiotherapy and have a better prognosis than HGG (Gottardo and Gajjar, 2008). Since the DIPG cohort was not biopsied, it is not possible to comment on whether any of the cases were primitive neuroectodermal tumours but it would be interesting to establish whether high Tau levels are associated with radiosensitivity across a range of tumours. Whilst Tau was the only individual metabolite which was significantly associated with improved survival, other metabolites undoubtedly have some association. Two patients surviving at three years with poor prognosis tumours had metabolite profiles which were different from the rest of the group as established in a PCA. One of the cases had the highest mIns in the group, which is further evidence for it being a marker good prognosis (Harris et al., 2008).

Small cohort numbers in the BST LGG (4 vs. 31) and spectra with a low SNR may explain the differences seen between focal non-BST and focal BST. Standard deviations at most metabolite positions in these spectra varied greatly making comparisons difficult particularly in the lipid, lactate and choline regions (Figure 8.1b and Figure 8.1c). Previous analyses have shown that lipid assignment in tumour types is extremely variable, also seen in the focal tumour spectra (Panigrahy et al., 2006). Previous studies investigating brain stem tumours in children have been few and have consisted of small cohorts and a multi-centre approach in this analysis has been used to overcome this. This multi-centre study highlights the importance of using MRS as an adjunct to conventional MRI and the role of Tau in DIPG warrants further understanding.

8.5   Conclusions and future investigations

Many tumours of the brain stem are diagnosed without a biopsy but it is often difficult to obtain a definitive consensus diagnosis. This analysis has been performed using a multi-centre approach to increase cohort numbers thereby increasing robustness of findings. MRS identifies key differences between tumours of the brain stem and can aid the characterisation of these tumours. In addition, whilst conventional MRI provides no markers of prognosis, Tau is significantly associated with a better prognosis in DIPG and metabolite profiles can also identify cases which become long term survivors. It has become apparent, that the lack of DIPG tumour tissue is hindering the understanding of tumour pathogenesis. In the future, high resolution *in vitro* spectroscopy methods

176

performed on tumour tissue may be able to confirm the presence of taurine and determine differences in long term survivors.

CHAPTER 9: SINGLE VOXEL PROTON MRS IN THE BRAIN SHOWS IMPROVED METABOLITE QUANTITATION AT 3 T IN PAEDIATRIC PATIENTS

CHAPTER 9

9   SINGLE VOXEL PROTON MRS IN THE BRAIN SHOWS IMPROVED METABOLITE QUANTITATION AT 3 T IN PAEDIATRIC PATIENTS

9.1   Introduction

With the increasing use of 3 T MRI scanners in clinical practice, there is an ever increasing interest in how 1H MRS at 3 T can provide improvements over 1.5 T. A higher field strength in theory should provide 100% increase in SNR and increase in spectral resolution enabling better quality data to be acquired in a shorter time period thus providing improved discrimination between different brain pathologies (Wardlaw et al., 2012).

Single voxel MRS is a promising technique that has been used in a number of studies to aid the characterisation of brain pathology in adults at 1.5 T (Smith et al., 2009, Howe and Opstad, 2003, Hattingen et al., 2008a) with more studies now being performed at 3 T (Wallis et al., 2007, Jeun et al., 2005, Hattori et al., 2002, Kim et al., 2006). The technique has also been well established in paediatric patients at 1.5 T (Harris et al., 2011, Panigrahy et al., 2010b, Davies et al., 2008, Kovanlikaya et al., 2005) with a limited number of studies performed at 3 T (Klomp et al., 2004). However, difficulties can arise when using the technique to differentiate between brain tumours as shown in chapter 5 and also between different brain pathologies (Hourani et al., 2006, Callot et al., 2008, Smith et al., 2009). The use of high field provides promise for aiding in these clinical scenarios. A number of groups have performed comparisons with spectroscopy data

collected at 1.5 T and 3 T to evaluate its use (Kim et al., 2006, Barker et al., 2001) but this comparison has not been performed in the paediatric population to our knowledge.

The purpose of the work presented in this chapter was to determine whether higher field strength of 3 T demonstrates an improvement in metabolite determination and quality of data acquired at 1.5 T in paediatric patients.

9.2   Method

Single voxel MRS was performed during September 2003 and October 2012 on 4 different cohorts of paediatric patients. Spectroscopy was acquired at 5 different centres.

9.2.1   MRS acquisition and quantitation of metabolite concentrations and lipid intensities

MRS data was acquired prior to treatment where the core acquisition protocol at 1.5 T for all cohorts comprised of TE 30 ms, TR 1500 ms and 128-256 NSA depending on voxel size and at 3 T TE 36-40 ms, TR 2000 ms and 96-128 NSA. All spectra were assessed using the QC criteria (section 4.3).

9.2.2   Statistical analysis

Metabolite quantitation was performed using TARQUIN (version 4.2.10 with extended basis set) (Wilson et al., 2011). Mann-Whitney U-tests (Mann and Whitney, 1947) were performed to compare five QC parameters calculated by TARQUIN. These included SNR, SNR max, water linewidth (Hz), water linewidth (ppm) and Q fit. SNR and SNR MAX per unit acquisition time were also compared between the two field strengths. The brain

tumour cohorts comprised of data acquired from different voxel volumes and as a result varying NSA. To account for these differences, SNR per unit voxel volume, SNR max per unit voxel volume and SNR per unit voxel volume per unit time and SNR max per unit voxel volume per unit time were also compared between the two field strengths. Metabolite concentrations (mM) and CRLB (SD) were compared using a Wilcoxon signed rank test where the analysis was paired and Mann-Whitney U-test for unpaired analyses (Mann and Whitney, 1947, Wilcoxon, 1945). Box and whisker plots were constructed to compare CRLB of metabolites at both 1.5 T and 3 T.

Table 9.1 A cohort summary of the paediatric patients included within the MRS study.

Cohort	Number of cases@1.5 T	Number of cases@3 T	Age range (years)	Mean age (years)	Paired Analysis?
1. Inherited metabolic disorders	7	7	1-7	3.6	Yes
2. Medulloblastoma	41	7	1.2-15	6.5	No
3. Pilocytic Astrocytoma	34	10	0.2-16.4	7.6	No
4. Low grade gliomas	6	6	06-8.9	3.3	Yes

9.3   Cohort 1: Inherited metabolic disorders

Cohort one consisted of seven paediatric patients (all male, Table 9.1) with inherited metabolic disorders all scanned at BCH. Patient diagnoses were either Methylmalonic acidaemia or X-linked adrenal leukodystrophy. The core acquisition protocol at 1.5 T comprised of TE 30 ms, TR 1500 ms and 128 NSA and at 3 T TE 38 ms, TR 2000 ms and 128 NSA. The ROI for each acquisition was 8 cm^3. Voxel locations for the patients were either located on the left basal ganglia or right parietal white matter with matched locations at both field strengths. All spectra acquired from patients with inherited metabolic disorders passed the set QC criteria.

9.3.1   Results
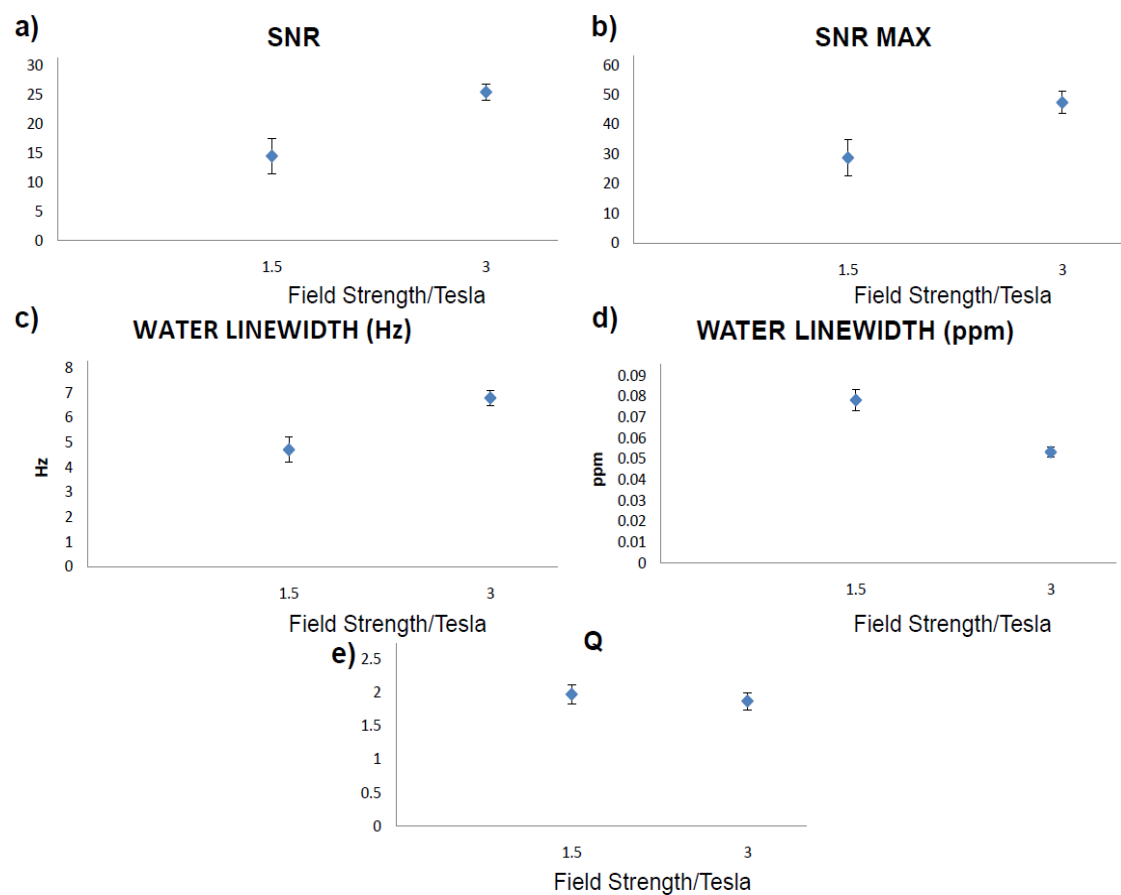
Figure 9.1 Quality control (QC) parameter plots show differences between 1.5 T and 3 T for a) SNR, b) SNR max, c) water linewidth (Hz), d) water linewidth (ppm) and e) Q fit.

Table 9.2 Wilcoxon signed rank test analysis comparisons for QC parameters calculated using TARQUIN.

QC parameters	*P* values	1.5 T	3 T
SNR	*	17.6	26.1
SNR max	*	28.7	47.4
water linewidth (Hz)	**	4.6	6.7
Water linewidth (ppm)	*	0.07	0.05
Q fit	n.s	1.9	2.0

Note: - n.s not significant, * $P<0.05$, ** $P<0.01$
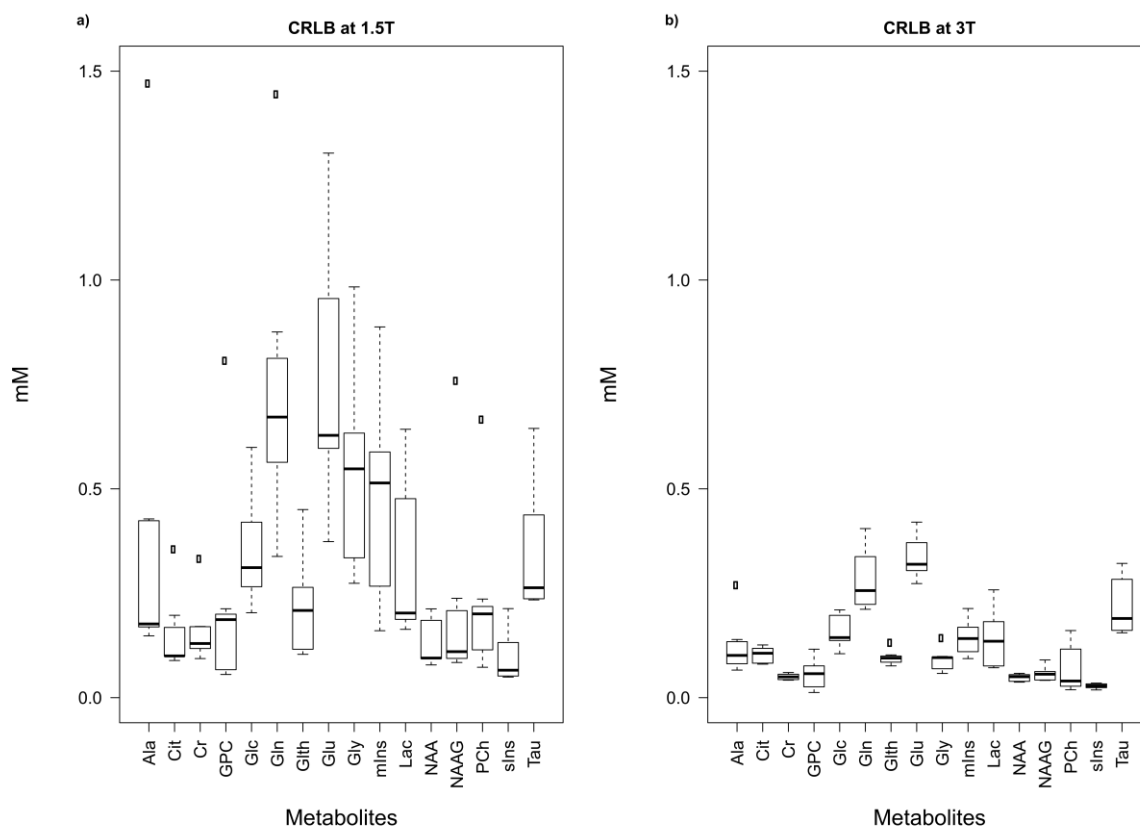
Figure 9.2 Box and whisker plots demonstrating the differences between CRLB at 1.5 T and 3 T for 16 metabolites.

An increase in SNR and SNR max was seen from 1.5 T to 3 T (Figure 9.1 a) and b) and Table 9.2). Significantly higher SNR with an overall increase of 48% equivalent to a 13% increase per unit acquisition time was found. Although both SNR per unit acquisition time (5.4 vs. 6.2, *P*>0.05) and SNR max per unit acquisition time (10.1 vs. 12.1, *P*>0.05) were higher at 3 T, these differences were not found to be statistically significantly. Significantly higher water linewidth in Hz at 3 T and water linewidth in ppm at 1.5 T was found (Figure 9.1 c) and d) and Table 9.2) resulting in an improved spectral resolution as seen in Figure 9.3. No difference was seen in Q fit between the two field strengths (Figure 9.1 e) and Table 9.2).

Table 9.3 Estimated metabolite concentrations and CRLB (SD) comparing 1.5 T vs. 3 T using a Wilcoxon signed rank test.

	Metabolite concentrations		CRLB (SD)	
Metabolites	p values	1.5 T vs. 3 T (mM)	P values	1.5 T vs. 3 T (mM)
Ala	n.s	0.33 vs. 0.11	*	0.43 vs. 0.12
Cit	n.s	0.57 vs. 0.23	n.s	0.15 vs. 0.10
Cr	n.s	4.79 vs. 5.82	*	0.16 vs. 0.05
GPC	n.s	1.23 vs. 1.33	n.s	0.23 vs. 0.06
Glc	n.s	4.25 vs. 1.96	*	0.36 vs. 0.16
Gln	n.s	2.03 vs. 0.23	*	0.74 vs. 0.29
Glth	*	0.66 vs. 1.96	*	0.22 vs. 0.10
Glu	n.s	5.28 vs. 6.68	*	0.77 vs. 0.34
Gly	n.s	1.16 vs. 0.15	*	0.53 vs. 0.09
mIns	n.s	1.89 vs. 2.48	*	0.47 vs. 0.14
Lac	n.s	0.10 vs. 0.49	*	0.33 vs. 0.14
NAA	n.s	5.70 vs. 5.94	*	0.35 vs. 0.05
NAAG	n.s	0.73 vs. 0.54	*	0.22 vs.0.06
PCh	n.s	0.09 vs. 0.21	n.s	0.23 vs. 0.07
sIns	n.s	0.08 vs. 0.05	*	0.10 vs. 0.03
Tau	n.s	1.35 vs. 1.09	n.s	0.36 vs. 0.22

Note: - n.s not significant, * $P < 0.05$

Glutathione was the only significant different metabolite between the two field strengths (Table 9.3). CRLB were shown to be lower at 3 T than 1.5 T (Figure 9.1) and this was significant ($P < 0.05$) for 12 out of 16 metabolites (Table 9.3). These included Cr, Glu, Gln, Gly, mIns and tNAA, metabolites known to be important in brain pathology.

9.4   Cohort 2: Medulloblastoma (MB)

Table 9.4 Core summary protocol for MB cohort.

MB	1.5 T protocol	3 T protocol
TE (ms)	30	37-40
TR (ms)	1500	2000
NSA	128-256	128
Voxel volume range (cm^3)	3.4-8	3.4-8
Average voxel volume (cm^3)	6.7	5.7

Cohort 2 consisted of 41 MB patients (Table 9.1) scanned at 1.5 T (12 female, 29 male, age range: 1.7-15 years, mean age: 6.8 years) compared with seven different cases at 3 T (four female, three male, age range: 1.2-8.3 years, mean age: 4.6 years) scanned at five centres. The core acquisition protocol at 1.5 T and 3 T for the MB is shown in Table 9.4. The ROI for each acquisition varied depending on protocol specified by the radiologist and the size of lesion to ensure that the voxel contained only the lesion of interest. All voxels were located over the primary tumour lesion. Six cases were excluded from the analysis of spectra acquired from MB patients.

9.4.1 Results

Comparison of quality control parameters between 1.5 T and 3 T demonstrated a significantly increased water linewidth in Hz (6.43 vs. 8.31 respectively, $P<0.01$) and decreased water linewidth in ppm at 3 T (0.1 vs. 0.07 respectively, $P<0.001$). A trend towards greater SNR and SNR max was seen at 3 T although this was not found to be significant. No difference was found in Q fit. No significant difference between SNR and SNR MAX per unit acquisition time was found. SNR per unit voxel (3.8 vs. 5.2, $P=0.05$) and SNR max per unit voxel volume (5.5 vs. 8.8, $P<0.01$) were found to be significantly higher at 3 T. SNR per unit voxel volume per unit time (1.0 vs. 1.2, $P>0.05$) was not significantly different but SNR max per unit voxel volume per unit time (1.5 vs. 2.0, $P=0.05$) was significantly higher at 3 T.

14 out of the 16 metabolites analysed were well determined at either both or one of the two field strengths. Out of those 14 metabolites, 12 were better determined at 3 T than 1.5 T however, this was only significant for three metabolites, Cr, Glutathione and Gly.

9.5 Cohort 3: Pilocytic Astrocytoma (PA)

Table 9.5 Core summary protocol for PA cohort.

PA	1.5 T protocol	3 T protocol
TE (ms)	30	37-40
TR (ms)	1500	2000
NSA	128-256	128
Voxel volume range (cm^3)	3.4-8	2.7-6
Average voxel volume (cm^3)	6.3	4

Cohort 3 consisted of 34 PA patients (Table 9.1) scanned at 1.5 T (16 female, 18 male, age range: 0.2-16.4 years, mean age: 7.4 years) compared with eight different cases at 3 T (four female, four male, age range: 6.9-11.6 years, mean age: 8.4 years) scanned at five centres. The core acquisition protocol is given in Table 9.5. Voxel was located over the primary tumour lesion. 40 patients were excluded from the analysis of spectra acquired from PAs.

9.5.1 Results

The only significant QC parameter was linewidth in Hz found to be higher at 3 T than at 1.5 T (7.97 vs. 6.47, $P<0.01$). No significant difference between SNR or SNR max per unit acquisition time was found however, SNR per unit voxel volume (1.7 vs. 2.5, $P<0.05$), SNR max per unit voxel volume (2.3 vs. 3.1, $P<0.05$), SNR per unit voxel volume per unit time (0.4 vs. 0.6, $P<0.05$) and SNR max per unit voxel volume per unit time (0.5 vs. 0.7, $P<0.05$) were all significantly lower at 1.5 T than 3 T.

Out of the 16 metabolites analysed, 11 metabolites were well determined at either both or one of the two field strengths. However out of the 11 metabolites only two were better determined at 3 T and neither of these were significant.

9.6 Cohort 4: Low grade gliomas (LGG)

Table 9.6 Core summary protocol for LGG cohort.

LGG	1.5 T protocol	3 T protocol
TE (ms)	30	36-40
TR (ms)	1500	2000
NSA	128-256	96-128
Voxel volume range (cm^3)	3.4-8	2.2-8
Average voxel volume (cm^3)	5.7	4.7

Cohort 4 consisted of six paediatric patients with LGG (Table 9.1) all scanned at BCH (three female, three male) at both 1.5 T and 3 T. The core acquisition protocol is given in Table 9.6. The voxel was located over the same lesion of interest at the two field strengths. 12 patients were excluded from the analysis of LGGs.

9.6.1 Results

No significant differences in quality control parameters between spectra acquired from LGG patients at 1.5 T and 3 T were found. A trend in increased SNR was seen at 3 T, however with a large standard error. No significant differences between SNR, SNR max per unit acquisition time, SNR per unit voxel volume or SNR max per unit voxel volume were seen. However, SNR per unit voxel volume per unit time (0.3 vs. 1.0, $P<0.05$) and SNR max per unit voxel volume per unit time (0.4 vs. 1.1, $P<0.05$) were all significantly higher at 3 T than 1.5 T.

12 out of 16 metabolites were better determined at either both or one of the two field strengths. Seven of these were better determined at 3 T and two demonstrated no difference. However, none of the differences were found to be significant

9.7   Discussion

Whilst the use of higher field strengths theoretically has many benefits for spectroscopy including increased spectral resolution, there are few studies that have demonstrated this within a clinical environment and none in children to our knowledge. A 13% increase in SNR per unit acquisition time at short echo time found in cohort 1 provides evidence for the improvement in metabolite quantitation which can be achieved at higher field strength in children with neurological disorders. Using equal voxel volumes and number of averages between both field strengths (cohort 1) provides a more robust comparison of the spectra. Cohorts 2-4 consist of the three most common brain tumour groups that present in children and demonstrate the same trends in quality control parameters.

A number of adult spectroscopy studies have been published comparing 1.5 T and 3 T. Barker et al. (Barker et al., 2001) compared the spectroscopy of normal brain in adult volunteers and stated a 28% increase in SNR of the tNAA peak at 3 T. Kim et al. (Kim et al., 2006) compared the spectroscopy of brain tumours reporting a 49.4-72.6% increase in SNR for the most important metabolites in brain pathology (mIns, tCho, Cr, tNAA). Sjobakk *et al.* (Sjøbakk et al., 2006), however, found only minor improvements in SNR for short echo time and saw greater improvements in long echo time (20-50%). The overall consensus from these studies and the results presented in this chapter is that although

SNR increases with field strength it does not reach the expected theoretical gain of 100%

for a two fold increase in field strength.
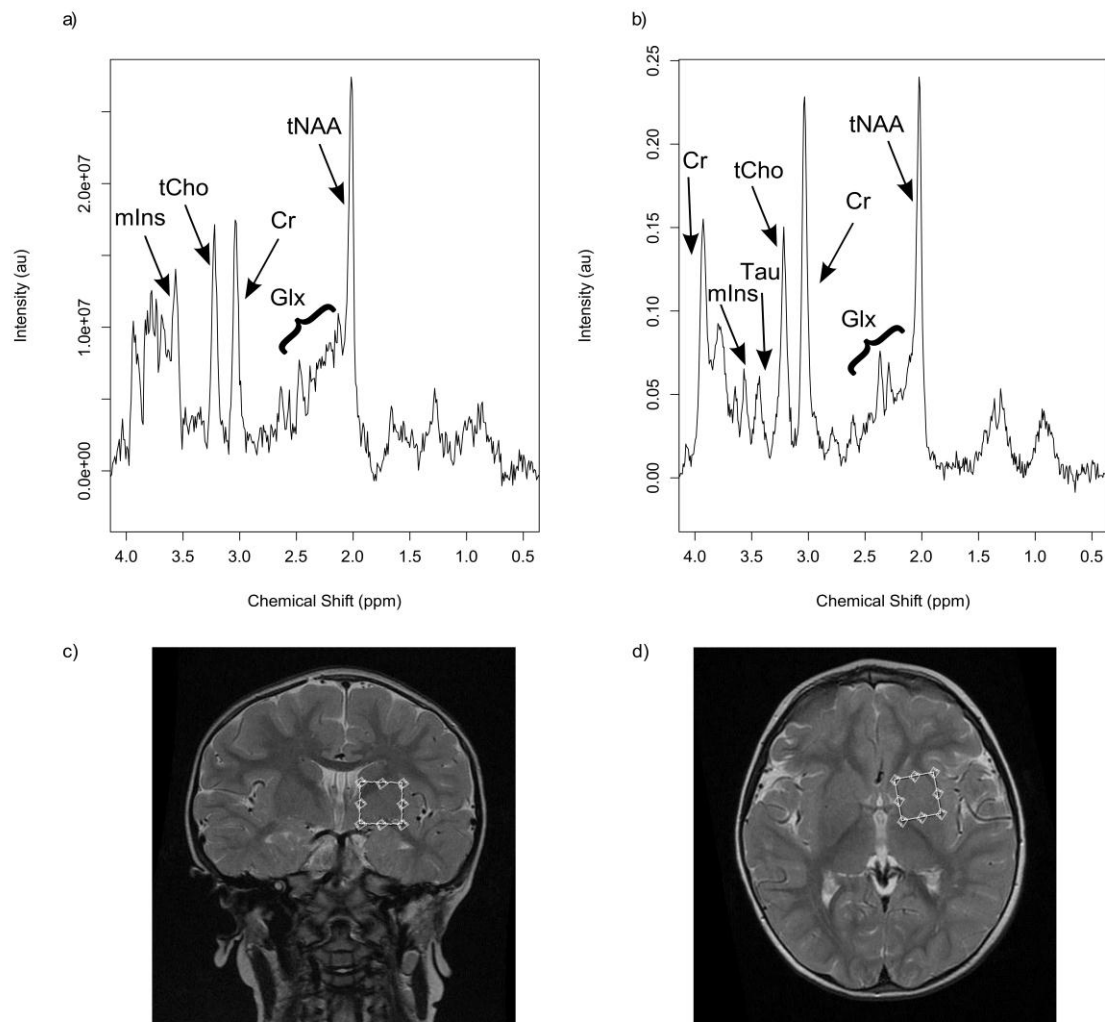
Figure 9.3 Comparison of spectra from 1.5 T and 3 T acquired from case 1 a) MRS acquired from the left basal ganglia at 1.5 T b) MRS acquired from the left basal ganglia at 3 T c) coronal T2 weighted imaging and d) axial T2 weighted imaging showing voxel location which was the same at both field strengths.

Figure 9.3 illustrates spectra from case 1 at 1.5 T and 3 T with the corresponding voxel

positions. Qualitative analysis of the example case shows differences in the spectra that

would be beneficial for assessing brain pathology validating the findings. Peaks tNAA and

Glx are better resolved on the 3 T spectrum and the peaks seen between tCho and 2nd Cr

peak (3.9 ppm) including the Cr peak itself are better resolved at 3 T. This is explained by

the narrower linewidth of the residual water peak in ppm.
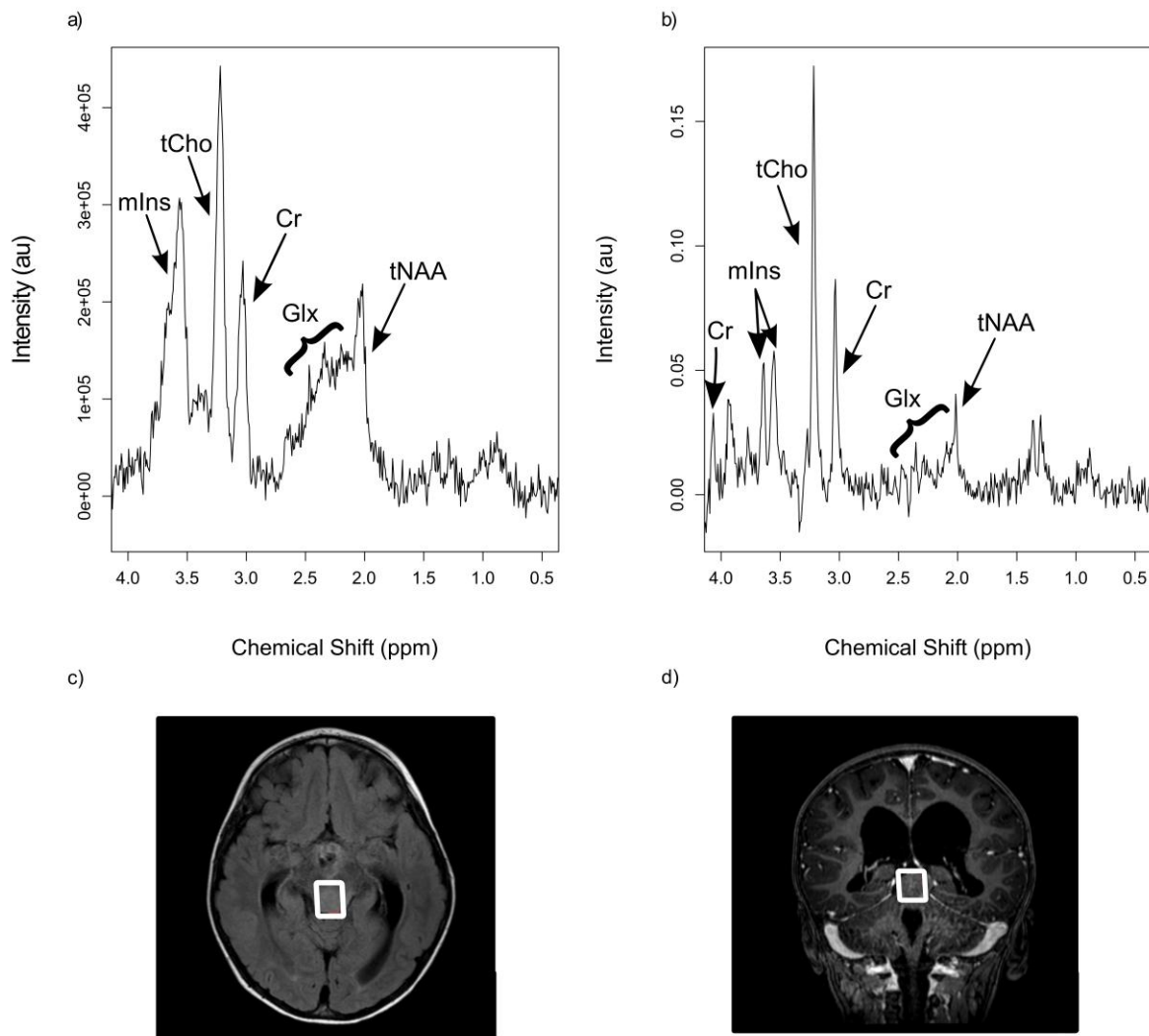
Figure 9.4 Comparison of spectra from 1.5 T and 3 T acquired from a patient with a tectal plate glioma
a) MRS acquired at 1.5 T b) MRS acquired at 3 T c) axial FLAIR imaging and d) axial STEALTH imaging
showing voxel location which was the same at both field strengths.

Figure 9.4 illustrates spectroscopy acquired from a patient with a low grade brain tumour. The spectra demonstrate a difference in the basis functions for mIns between the field strengths with a single feature seen at 1.5 T and two distinct peaks at 3 T. The few differences seen in metabolite concentrations imply the basis functions are able to allow for the differences in spectral appearance due to field strength. The separation between tNAA and Glx is seen to be greater at 3 T providing promise for aiding in brain tumour diagnosis and prognosis particularly where spectra overlap greatly (Davies et al., 2008, Wilson et al., 2013).

The significant decrease in CRLB seen at 3 T for cohort 1 demonstrates an improvement in spectral quantitation which is in agreement with the increased spectral dispersion, shown by the reduction in linewidth and increase in SNR (Tkáč et al., 2009, Posse et al., 2007). Metabolites such as mIns which has been demonstrated as marker of good prognosis and glycine, a marker of poor prognosis could potentially be better resolved (Davies et al., 2009). Scyllo-inositol which has been identified as a marker of poor prognosis closely overlaps with Tau at 3.3 ppm and likewise glutamine and tNAA have been identified as markers of good prognosis but are closely overlapping at 1.5 T (Wilson et al., 2013). The increased spectral resolution achieved in the cohorts allows a better discrimination between the closely overlapping metabolites, mIns and Gly, sIns and Tau and tNAA and Glx.

Experience of acquiring spectroscopy data in a clinical setting has demonstrated that on average smaller volumes are selected. The use of smaller and more custom voxel sizes is often used taking advantage of the theoretical benefits of increased SNR as a result of increased field strength. This works well in clinical scenarios where the tumour volume at presentation may be smaller than 1.5 cm^3, or consists of heterogeneous components, for example a tumour consists of a small solid component with predominantly cystic elements or small residual tumour at follow-up. Acquiring data from smaller voxels will ensure it does not contain normal brain and as a result is representative of the lesion of interest. Ensuring the data is acquired fully from within the lesion of interest is important for the interpretation of spectra.

The confounding variables which include different voxel volumes and different numbers of averages acquired make it difficult to formally demonstrate the theoretical improvements of performing spectroscopy at 3 T for both unpaired and paired analysis in paediatric brain tumours patients (cohorts 2-4). The unexpected lack of difference seen between the field strengths for SNR and SNR max in the tumour cohorts (cohorts 2-4) can be explained by this. To allow for these differences SNR/SNR max per voxel volume and SNR/SNR max per unit voxel volume per unit time were calculated and have demonstrated a significant increase from 1.5 to 3 T for all the cohorts. Despite the differences in echo time between the two field strengths in particular slightly longer TE at 3T, a 6-10 ms difference is likely to have very little impact on the spectral decay. It should be noted the differences in echo time between 1.5 T and 3 T are accounted for by

TARQUIN using the simulated basis set. The analysis has also demonstrated that good quality MRS data can be acquired from small lesions at 3 T.

Despite the expected advantages of higher field strengths, an increase in magnetic field heterogeneity and susceptibility artefacts hinders the ability to obtain the expected theoretical 100% gain in SNR. A reduction in T2 explains the increased metabolite linewidth in Hz seen at 3 T (Wardlaw et al., 2012).

The promising results seen in this cohort of paediatric patients where equivalent protocols were used and QC parameters compared, provides evidence for the advantages of using this technique at higher field strength. A close review of the 3 T data has shown that acquiring MRS from small lesions is of greater importance than reducing acquisition times in a clinical setting. This explains the reasoning behind the limited increase in spectral resolution seen. With ever-improving access to advanced processing MRS should become more widely used in non-specialist centres in the future.

9.8 Conclusion

1H MRS acquired at 3 T from a cohort of paediatric patients with neurological disorders shows an overall increase of 48% equivalent to a 13% increase per unit acquisition time as well as an increase in spectral resolution. For inherited metabolic disorders where the same patient was scanned on two scanners, an improvement in spectral resolution, SNR and metabolite determination is seen at 3 T. For brain tumours where different patients are compared at 1.5 T and 3 T there is an improvement in resolution and determination

of some metabolites but not SNR. At 3 T, the current practice shows a trend towards the use of smaller voxels to acquire metabolic information from smaller lesions of interest. As a consequence, the expected advantages of increased spectral quality and SNR are not observed.

CHAPTER 10: CONCLUSIONS AND FUTURE WORK

CHAPTER 10

10 CONCLUSIONS AND FUTURE WORK

This thesis has systematically demonstrated multi-centre spectroscopy data acquired from paediatric brain tumours can aid in their characterisation. Mean spectra, metabolite concentrations and classifier analysis constructed using statistical analysis methods provide diagnostic information that can be used with conventional MRI sequences. It has also been shown for the first time that MRS metabolite profiles of grade II-IV brain tumours at first relapse are not significantly different to those at diagnosis, aiding in the confirmation of tumour presence on follow-up MRI. Subtype specific prognostic markers in MB were also established. The key differences in metabolite profiles between tumours of the brain stem were identified and able to aid in characterisation. With conventional MRI providing no markers of prognosis for DIPG, Tau was found to be significantly associated with a better prognosis in these tumours. Data acquired at 3 T showed improved resolution and determination of metabolites in paediatric patients.

The conclusions drawn from this work and future directions include:

1) Qualitative and quantitative analysis of metabolite profiles shows differences between paediatric brain tumours that can aid in characterisation in a multi-scanner cohort. It has been established that *in vivo* concentrations of metabolites differ between brain tumours and variations in these metabolite pathway intermediates are likely to be explained by tumour biology. However, the number

of metabolites quantified *in vivo* is limited and although the links to metabolic pathways and cancer pathogenesis have been preliminarily explored, further validation is required. Performing *in vitro* tumour tissue analysis using higher field strength methods such as magic angle spinning can provide a greater spectral resolution. Using a combination of *in vivo*, *ex-vivo* and genetic subtyping information, these findings can be validated and probed further. Understanding the underlying biological reasons and mechanisms for these differences is currently of great interest.

2) Mean metabolite profiles differ between tumour types but no discrimination can be made between tumours based on individual metabolites. Using MRS as a diagnostic tool with mean metabolite profiles, classifiers and metabolite ratios is promising but the added value of this in clinical practice requires formally testing. This can be performed by providing a small group of radiologists with test cases firstly with MRI alone to provide a diagnosis, followed by the addition of MRS and MRS analysis results to provide a diagnosis and comparing this with the 'gold standard' histopathology results. This could be performed both retrospectively and prospectively.

3) Finding no significant differences in metabolite profiles of children's brain tumours (grade II-IV) at diagnosis and first relapse revealed that spectroscopy can aid in the confirmation of the tumour on follow-up MRI. Having now established

for the first time that diagnostic and relapse tumour spectra exhibit similar characteristics, it would be beneficial to test this on a prospectively on a larger cohort of patients and compare with other methods which may be useful in tumour detection such as diffusion and perfusion imaging. With a great interest in diffusion and perfusion methods to explore lesion cellularity and blood supply respectively, it is hoped quantitative analysis of imaging characteristics comparing diagnosis and follow-up may provide complementary information. These techniques are likely to be more beneficial to small lesions as they are not limited by voxel size like MRS. The optimum combination of imaging techniques is yet to be formally established. More detailed metabolite analysis is required to detect more subtle differences that may occur between diagnosis and relapse and this would be aided by paired tumour tissue analysis from local and national tumour tissue banks.

4) The search for prognostic markers in tumour subgroup medulloblastoma showed increased levels of Cr and tCho and a feature around 2.0 ppm attributed to macromolecules to be associated with a good prognosis. Brain tumour subtype specific markers of prognosis have not been previously reported. However, this is particularly intriguing as many recent publications have provided evidence that although these tumours are diagnosed as the same histopathological entity, they consist of heterogeneous molecular subgroups that differ in prognosis. This provides promise that spectroscopy would be able to identify this information

non-invasively. The accurate assignment of the prognostic markers particularly in the region of 2.0 ppm will be best determined in tissue samples from tumour tissue banks using *in vitro* high-resolution spectroscopy methods. Since molecular subtypes of MB can be determined on paraffin embedded tumour tissue, combining this with *in vitro* HR-MAS would be intriguing to explore. Confirming *in vivo* findings and identifying metabolites that may correlate and mapping these with the preferred metabolic networks being utilised by these tumours is of great interest. It would also be beneficial to correlate spectroscopy findings with genetic subgroup information.

5) Spectroscopy is able to identify key differences between tumours of the brain stem for example Cit, mIns and low lipids seen in DIPG. This provides further evidence for the technique as a useful tool for characterisation. This is particularly pertinent for these tumours as they are often diagnosed without a biopsy thereby making them clinically challenging to diagnose. Taurine was found to be associated with a significantly better prognosis in DIPG identifying cases which become long term survivors. With the increasing interest in biopsying DIPG and understanding the underlying biology of brain tumours HR-MAS may be able to confirm the presence of taurine and differences in long term survivors. This could be explored by obtaining archived tumour tissue samples from local and national banks of either biopsied DIPGs and/or tumours at autopsy. Another possible

source of tumour tissue would be histopathological diagnoses that match autopsy samples so anaplastic astrocytomas and high grade gliomas.

6) Single voxel spectroscopy at 3 T has shown an improvement in spectral resolution and metabolite determination for some metabolites when compared to 1.5 T. SNR shows improvement when comparing the same patients on the same scanner but not when comparing different patients at the two field strengths. To the best of our knowledge, this is the first study comparing spectroscopy at different field strengths in paediatric patients. The advantages of the theoretical increase in SNR with increasing field strength have been used to acquire metabolic information from smaller lesions of interest to answer clinical questions rather than save scanner protocol time as originally envisaged. Establishing if obtaining more pre-treatment spectroscopy data on paediatric patients at 3 T can demonstrate further differentiation of tumour types and whether it can eliminate the use of two echo times for metabolite determination would be an approach to explore.

10.1 Summary of findings

This thesis demonstrates why single voxel magnetic resonance spectroscopy is a valuable adjunct to conventional MRI sequences in the evaluation of childhood brain tumours. The additional information provided by this technique is summarised in Figure 10.1
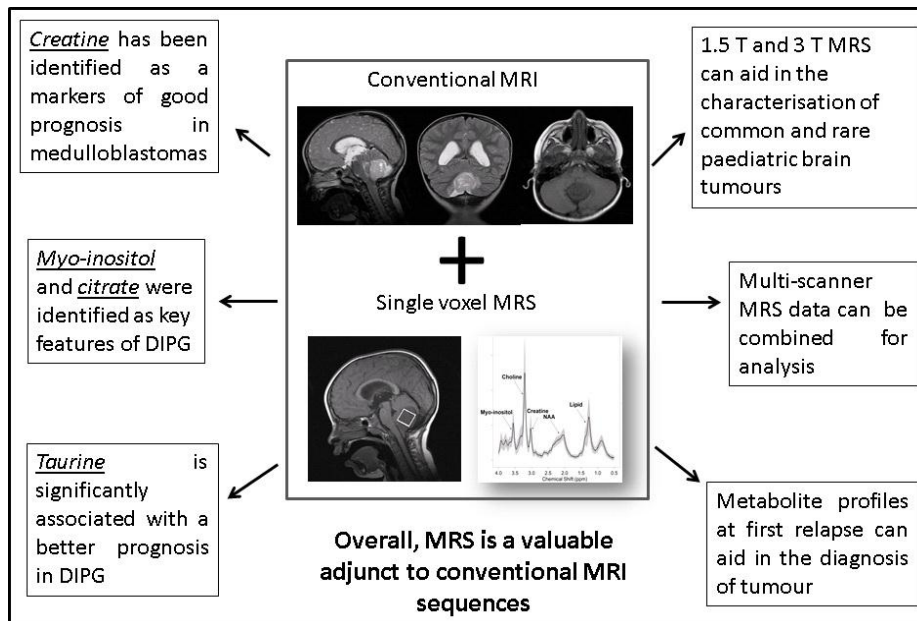
Figure 10.1 Summary of results

REFERENCES

ALBERS, M. J., KRIEGER, M. D., GONZALEZ-GOMEZ, I., GILLES, F. H., MCCOMB, J. G., NELSON, M. D. & BLÜML, S. 2005. Proton-decoupled 31P MRS in untreated pediatric brain tumors. *Magn Reson Med,* 53**,** 22-29.

ANASTAS, J. N. & MOON, R. T. 2013. WNT signalling pathways as therapeutic targets in cancer. *Nat Rev Cancer,* 13**,** 11-26.

ARTHURS, O. & GALLAGHER, F. 2011. Functional and molecular imaging with MRI: potential applications in paediatric radiology. *Pediatr Radiol,* 41**,** 185-198.

ASTRAKAS, L. G., ZURAKOWSKI, D., TZIKA, A. A., ZARIFI, M. K., ANTHONY, D. C., DE GIROLAMI, U., TARBELL, N. J. & BLACK, P. M. 2004. Noninvasive Magnetic Resonance Spectroscopic Imaging Biomarkers to Predict the Clinical Grade of Pediatric Brain Tumors. *Clin Cancer Res,* 10**,** 8220-8228.

BAKER, E. H., BASSO, G., BARKER, P. B., SMITH, M. A., BONEKAMP, D. & HORSKÁ, A. 2008. Regional apparent metabolite concentrations in young adult brain measured by 1H MR spectroscopy at 3 Tesla. *Journal of Magnetic Resonance Imaging,* 27**,** 489-499.

BALSS, J., MEYER, J., MUELLER, W., KORSHUNOV, A., HARTMANN, C. & DEIMLING, A. 2008. Analysis of the IDH1 codon 132 mutation in brain tumors. *Acta Neuropathol.,* 116**,** 597-602.

BARKER, P. & GILLARD, J. 2005. MR spectroscopy in stroke. *In:* GILLARD, J., WALDMAN, A. & BARKER, P. (eds.) *Clinical MR Neuroimaging - Diffusion, Perfusion and Spectroscopy.* 1st ed. Cambridge: Cambridge University Press.

BARKER, P. B., HEARSHEN, D. O. & BOSKA, M. D. 2001. Single-voxel proton MRS of the human brain at 1.5T and 3.0T. *Magn Reson Med,* 45**,** 765-769.

BARKHUIJSEN, H., DE BEER, R. & VAN ORMONDT, D. 1987. Improved algorithm for noniterative time-domain model fitting to exponentially damped magnetic resonance signals. *J Magn Reson,* 73**,** 553-557.

BATCHELOR, T. T., SORENSEN, A. G., DI TOMASO, E., ZHANG, W.-T., DUDA, DAN G., COHEN, K. S., KOZAK, K. R., CAHILL, D. P., CHEN, P.-J., ZHU, M., ANCUKIEWICZ, M., MRUGALA, M. M., PLOTKIN, S., DRAPPATZ, J., LOUIS, D. N., IVY, P., SCADDEN, DAVID T., BENNER, T., LOEFFLER, J. S., WEN, P. Y. & JAIN, R. K. 2007. AZD2171, a Pan-VEGF Receptor Tyrosine Kinase Inhibitor, Normalizes Tumor Vasculature and Alleviates Edema in Glioblastoma Patients. *Cancer cell,* 11**,** 83-95.

BIANCHI, M. C., TOSETTI, M., BATTINI, R., LEUZZI, V., ALESSANDRI', M. G., CARDUCCI, C., ANTONOZZI, I. & CIONI, G. 2007. Treatment Monitoring of Brain Creatine Deficiency Syndromes: A 1H- and 31P-MR Spectroscopy Study. *American Journal of Neuroradiology,* 28**,** 548-554.

BLAND, J. M. & ALTMAN, D. G. 1995. Multiple significance tests: the Bonferroni method. *BMJ,* 310**,** 170.

BLANEY, S., KUN, L. E., HUNTER, J., RORKE-ADAMS, L., LAU, C., STROTHER, D. & POLLACK, I. F. 2006. Tumors of the Central Nervous System. *In:* PIZZO, A. P. & POPLACK, D. G. (eds.) *Principles and Practise of Pediatric Oncology.* 5th ed. Philadelphia: Lippincott Williams and Wilkins.

BLANKENBERG, F. G., KATSIKIS, P. D., STORRS, R. W., BEAULIEU, C., SPIELMAN, D., CHEN, J. Y., NAUMOVSKI, L. & TAIT, J. F. 1997. Quantitative Analysis of Apoptotic Cell Death Using Proton Nuclear Magnetic Resonance Spectroscopy. *Blood,* 89**,** 3778-3786.

BLEYER, W. A. 1999. Epidemiologic impact of children with brain tumors. *Childs Nerv Syst,* 15**,** 758-763.

BLÜML, S., PANIGRAHY, A., LASKOV, M., DHALL, G., KRIEGER, M. D., NELSON, M. D., FINLAY, J. L. & GILLES, F. H. 2011. Elevated citrate in pediatric astrocytomas with malignant progression. *Neuro-Oncology,* 13**,** 1107-1117.

BLÜML, S., WISNOWSKI, J. L., NELSON, M. D., PAQUETTE, L., GILLES, F. H., KINNEY, H. C. & PANIGRAHY, A. 2013. Metabolic Maturation of the Human Brain From Birth Through Adolescence: Insights From In Vivo Magnetic Resonance Spectroscopy. *Cerebral Cortex,* 23**,** 2944-2955.

BOTTOMLEY, P. A. 1987. Spatial Localization in NMR Spectroscopy in Vivo. *Annals of the New York Academy of Sciences,* 508**,** 333-348.

BROCKER, C., THOMPSON, D. & VASILIOU, V. 2012. The role of hyperosmotic stress in inflammation and disease. *BioMolecular Concepts,* 3**,** 345–364.

BRONISCER, A., BAKER, S. J., WEST, A. N., FRASER, M. M., PROKO, E., KOCAK, M., DALTON, J., ZAMBETTI, G. P., ELLISON, D. W., KUN, L. E., GAJJAR, A., GILBERTSON, R. J. & FULLER, C. E. 2007. Clinical and Molecular Characteristics of Malignant Transformation of Low-Grade Glioma in Children. *Journal of Clinical Oncology,* 25**,** 682-689.

BRUHN, H., FRAHM, J., GYNGELL, M. L., MERBOLDT, K. D., HÄNICKE, W., SAUTER, R. & HAMBURGER, C. 1989. Noninvasive differentiation of tumors with use of localized H-1 MR spectroscopy in vivo: initial experience in patients with cerebral tumors. *Radiology,* 172**,** 541-548.

BRYANT, S., CHA, S. & BARKOVICH, J. 2010. Modern Neuroimaging of Pediatric Brain Tumors. *In:* GUPTA, N., BANERJEE, A. & HAAS-KOGAN, D. (eds.) *Pediatric CNS Tumors.* Berlin: Springer.

BURKHARD, C., DI PATRE, P.-L., SCHÜLER, D., SCHÜLER, G., YAŞARGIL, M. G., YONEKAWA, Y., LÜTOLF, U. M., KLEIHUES, P. & OHGAKI, H. 2003. A population-based study of the incidence and survival rates in patients with pilocytic astrocytoma. *Journal of Neurosurgery,* 98**,** 1170-1174.

CALLOT, V., GALANAUD, D., LE FUR, Y., CONFORT-GOUNY, S., RANJEVA, J. P. & COZZONE, P. J. 2008. 1H MR spectroscopy of human brain tumours: a practical approach. *Eur J Radiol,* 67**,** 268-274.

CANCER RESEARCH UK. Available: http://www.cancerresearchuk.org/cancer-info/cancerstats/childhoodcancer/survival/ [Accessed 18th February 2013].

CARAPELLA, C., CARPINELLI, G., KNIJN, A., RAUS, L., CAROLI, F. & PODO, F. 1997. Potential Role of in vitro 1H Magnetic Resonance Spectroscopy in the Definition of Malignancy Grading of Human Neuroepithelial Brain Tumours. *Advances in Stereotactic and Functional Neurosurgery 12,* 68**,** 127-132.

CARLOTTI, C. G., JR., SMITH, C. & RUTKA, J. T. 2008. The molecular genetics of medulloblastoma: an assessment of new therapeutic targets. *Neurosurg Rev,* 31**,** 359-68; discussion 368-9.

CASTILLO, M. 1998. Gangliogliomas: ubiquitous or not? *AJNR Am J Neuroradiol,* 19**,** 807-9.

CASTILLO, M., KWOCK, L. & MUKHERJI, S. K. 1996. Clinical applications of proton MR spectroscopy. *AJNR Am J Neuroradiol,* 17**,** 1-15.

203

CASTILLO, M., SMITH, J. K. & KWOCK, L. 2000. Correlation of Myo-inositol Levels and Grading of Cerebral Astrocytomas. *AJNR Am J Neuroradiol,* 21**,** 1645-1649.

CATALAA, I., HENRY, R., DILLON, W. P., GRAVES, E. E., MCKNIGHT, T. R., LU, Y., VIGNERON, D. B. & NELSON, S. J. 2006. Perfusion, diffusion and spectroscopy values in newly diagnosed cerebral gliomas. *NMR Biomed,* 19**,** 463-475.

CAVASSILA, S., DEVAL, S., HUEGEN, C., VAN ORMONDT, D. & GRAVERON-DEMILLY, D. 2001. Cramér–Rao bounds: an evaluation tool for quantitation. *NMR in Biomedicine,* 14**,** 278-283.

CHANG, Y.-W., YOON, H.-K., SHIN, H.-J., ROH, H. & CHO, J. 2003. MR imaging of glioblastoma in children: usefulness of diffusion/perfusion-weighted MRI and MR spectroscopy. *Pediatr Radiol,* 33**,** 836-842.

CHOI, C., GANJI, S. K., DEBERARDINIS, R. J., HATANPAA, K. J., RAKHEJA, D., KOVACS, Z., YANG, X.-L., MASHIMO, T., RAISANEN, J. M., MARIN-VALENCIA, I., PASCUAL, J. M., MADDEN, C. J., MICKEY, B. E., MALLOY, C. R., BACHOO, R. M. & MAHER, E. A. 2012. 2-hydroxyglutarate detection by magnetic resonance spectroscopy in IDH-mutated patients with gliomas. *Nat Med,* 18**,** 624-629.

CIRAK, B., HORSKÁ, A., BARKER, P. B., BURGER, P. C., CARSON, B. S. & AVELLINO, A. M. 2005. Proton magnetic resonance spectroscopic imaging in pediatric pilomyxoid astrocytoma. *Childs Nerv Syst.,* 21**,** 404-409.

CLARKE, J. & CHANG, S. 2009. Pseudoprogression and pseudoresponse: Challenges in brain tumor imaging. *Current Neurology and Neuroscience Reports,* 9**,** 241-246.

COSTELLO, L., FRANKLIN, R. & NARAYAN, P. 1999. Citrate in the diagnosis of prostate cancer. *Prostate,* 38**,** 237-245.

COX, D. R. 1972. Regression Models and Life-Tables. *Journal of the Royal Statistical Society. Series B (Methodological),* 34**,** 187-220.

DAGIA, C. & DITCHFIELD, M. 2008. 3T MRI in paediatrics: Challenges and clinical applications. *Eur J Radiol,* 68**,** 309-319.

DANG, C. V. 2012. Links between metabolism and cancer. *Genes & Development,* 26**,** 877-890.

DAVIES, N. P., WILSON, M., HARRIS, L. M., NATARAJAN, K., LATEEF, S., MACPHERSON, L., SGOUROS, S., GRUNDY, R. G., ARVANITIS, T. N. & PEET, A. C. 2008. Identification and characterisation of childhood cerebellar tumours by in vivo proton MRS. *NMR Biomed,* 21**,** 908-18.

DAVIES, N. P., WILSON, M., NATARAJAN, K., SUN, Y., MACPHERSON, L., BRUNDLER, M. A., ARVANITIS, T. N., GRUNDY, R. G. & PEET, A. C. 2009. Non-invasive detection of glycine as a biomarker of malignancy in childhood brain tumours using in-vivo (1)H MRS at 1.5 Tesla confirmed by ex-vivo high-resolution magic-angle spinning NMR. *NMR Biomed,* 23**,** 80-7.

DAYE, D. & WELLEN, K. E. 2012. Metabolic reprogramming in cancer: Unraveling the role of glutamine in tumorigenesis. *Seminars in Cell & Developmental Biology,* 23**,** 362-369.

DE GRAAF, R. A. 2007a. Basic Principles. *In Vivo NMR Spectroscopy - Principles and Techniques.* 2 ed.: John Wiley & Sons, Ltd.

DE GRAAF, R. A. 2007b. *In Vivo NMR Spectroscopy - Principles and Techniques*, John Wiley & Sons, Ltd.

DE GROOT, J. & SONTHEIMER, H. 2011. Glutamate and the biology of gliomas. *Glia,* 59**,** 1181-1189.

DE HAAS, T., HASSELT, N., TROOST, D., CARON, H., POPOVIC, M., ZADRAVEC-ZALETEL, L., GRAJKOWSKA, W., PEREK, M., OSTERHELD, M.-C., ELLISON, D., BAAS, F., VERSTEEG, R. &

KOOL, M. 2008. Molecular Risk Stratification of Medulloblastoma Patients Based on Immunohistochemical Analysis of MYC, LDHB, and CCNB1 Expression. *Clin Cancer Res,* 14**,** 4154-4160.

DEBERARDINIS, R. & CHENG, T. 2010. Q's next: the diverse functions of glutamine in metabolism, cell biology and cancer**.** *Oncogene,* 29**,** 313-24.

DEBERARDINIS, R. J., MANCUSO, A., DAIKHIN, E., NISSIM, I., YUDKOFF, M., WEHRLI, S. & THOMPSON, C. B. 2007. Beyond aerobic glycolysis: Transformed cells can engage in glutamine metabolism that exceeds the requirement for protein and nucleotide synthesis. *Proceedings of the National Academy of Sciences,* 104**,** 19345-19350.

DONALDSON, S., LANINGHAM, F. & FISHER, P. 2006. Advances toward an understanding of brainstem gliomas. *J Clin Oncol,* 24**,** 1266-72.

DONOVAN, L., POTTER, N. E., WARR, T. & PILKINGTON, G. J. 2012. A Prominin-1-Rich Pediatric Glioblastoma: Biologic Behavior Is Determined by Oxygen Tension-Modulated CD133 Expression but Not Accompanied by Underlying Molecular Profiles. *Transl Oncol.,* 5**,** 141-54.

DOWNES, C. P. & MACPHEE, C. 1991. Review myo-Inositol metabolites as cellular signals. *In:* CHRISTEN, P. & HOFMANN, E. (eds.) *EJB Reviews 1990.* Springer Berlin Heidelberg.

DUBUC, A., NORTHCOTT, P., MACK, S., WITT, H., PFISTER, S. & TAYLOR, M. 2010. The Genetics of Pediatric Brain Tumors. *Current Neurology and Neuroscience Reports,* 10**,** 215-223.

DUE-TØNNESSEN, B., HELSETH, SKULLERUD, K. & LUNDAR, T. 2001. Choroid plexus tumors in children and young adults: report of 16 consecutive cases. *Childs Nerv Syst,* 17**,** 252-6.

DUFOUR, C., BEAUGRAND, A., PIZER, B., MICHELI, J., AUBELLE, M.-S., FOURCADE, A., COUANET, D., LAPLANCHE, A., KALIFA, C. & GRILL, J. 2012. Metastatic Medulloblastoma in Childhood: Chang's Classification Revisited. *International Journal of Surgical Oncology,* 2012.

ECHEVARRÍA, M. E., FANGUSARO, J. & GOLDMAN, S. 2008. Pediatric Central Nervous System Germ Cell Tumors: A Review. *The Oncologist,* 13**,** 690-699.

EGAN, J. 1975. *Signal detection theory and ROC-analysis,* New York, Academic Press.

ERNST, T., KREIS, R. & ROSS, B. D. 1993. Absolute Quantitation of Water and Metabolites in the Human Brain. I. Compartments and Water. *Journal of Magnetic Resonance, Series B,* 102**,** 1-8.

FAWCETT, T. 2006. An introduction to ROC analysis. *Pattern Recogn. Lett.,* 27**,** 861-874.

FISCHBACH, F. & BRUHN, H. 2008. Assessment of in vivo 1H magnetic resonance spectroscopy in the liver: a review. *Liver International,* 28**,** 297-307.

FISHER, R. A. 1936. The use of Multiple Measurements in Taxonomic Problems. *Annals of Eugenics,* 7**,** 179-188.

GAN, G. & HAAS-KOGAN, D. 2010. Low-Grade Gliomas. *In:* GUPTA, N., BANERJEE, A. & HAAS-KOGAN, D. (eds.) *Pediatric CNS Tumors.* Berlin: Springer.

GARCÍA-GÓMEZ, J., LUTS, J., JULIÀ-SAPÉ, M., KROOSHOF, P., TORTAJADA, S., ROBLEDO, J., MELSSEN, W., FUSTER-GARCÍA, E., OLIER, I., POSTMA, G., MONLEÓN, D., MORENO-TORRES, À., PUJOL, J., CANDIOTA, A.-P., MARTÍNEZ-BISBAL, M. C., SUYKENS, J., BUYDENS, L., CELDA, B., HUFFEL, S., ARÚS, C. & ROBLES, M. 2009. Multiproject–multicenter evaluation of automatic brain tumor classification by magnetic resonance spectroscopy. *Magnetic Resonance Materials in Physics, Biology and Medicine,* 22**,** 5-18.

GARNETT, M., PUGET, S., GRILL, J. & SAINTE-ROSE, C. 2007. Craniopharyngioma. *Orphanet Journal of Rare Diseases,* 2**,** 18.

GASPAROVIC, C., SONG, T., DEVIER, D., BOCKHOLT, H. J., CAPRIHAN, A., MULLINS, P. G., POSSE, S., JUNG, R. E. & MORRISON, L. A. 2006. Use of tissue water as a concentration reference for proton spectroscopic imaging. *Magnetic Resonance in Medicine,* 55**,** 1219-1226.

GEISSER, S. 1975. The Predictive Sample Reuse Method with Applications. *Journal of the American Statistical Association,* 70.

GILBERTSON, R., WICKRAMASINGHE, C., HERNAN, R., BALAJI, V., HUNT, D., JONES-WALLACE, D., CROLLA, J., PERRY, R., LUNEC, J., PEARSON, A. & ELLISON, D. 2001. Clinical and molecular stratification of disease risk in medulloblastoma. *Br J Cancer,* 85**,** 705-12.

GILHEENEY, S., SAAD, A., CHI, S., TURNER, C., ULLRICH, N., GOUMNEROVA, L., SCOTT, R. M., MARCUS, K., LEHMAN, L., GIROLAMI, U. & KIERAN, M. 2008. Outcome of pediatric pineoblastoma after surgery, radiation and chemotherapy. *Journal of Neuro-Oncology,* 89**,** 89-95.

GILL, S., PANIGRAHY, A., ARVANITIS, T. & PEET, A. 2013. Magnetic Resonance Spectroscopy of Pediatric Brain Tumors. *In:* BLÜML, S. & PANIGRAHY, A. (eds.) *MR Spectroscopy of Pediatric Brain Disorders.* Springer New York.

GILLIES, R. J., RAGHUNAND, N., KARCZMAR, G. S. & BHUJWALLA, Z. M. 2002. MRI of the tumor microenvironment. *Journal of Magnetic Resonance Imaging,* 16**,** 430-450.

GLUNDE, K., BHUJWALLA, Z. M. & RONEN, S. M. 2011. Choline metabolism in malignant transformation. *Nat Rev Cancer,* 11**,** 835-848.

GOTTARDO, N. G. & GAJJAR, A. 2008. Chemotherapy for Malignant Brain Tumors of Childhood. *J Child Neurol,* 23**,** 1149-1159.

GOVINDARAJU, V., YOUNG, K. & MAUDSLEY, A. A. 2000. Proton NMR chemical shifts and coupling constants for brain metabolites. *NMR Biomed,* 13**,** 129-53.

GRAAF, M. 2010. In vivo magnetic resonance spectroscopy: basic methodology and clinical applications. *European Biophysics Journal,* 39**,** 527-540.

GRAVES, E. E., NELSON, S. J., VIGNERON, D. B., VERHEY, L., MCDERMOTT, M., LARSON, D., CHANG, S., PRADOS, M. D. & DILLON, W. P. 2001. Serial proton MR spectroscopic imaging of recurrent malignant gliomas after gamma knife radiosurgery. *AJNR Am J Neuroradiol,* 22**,** 613-24.

GUESSOUS, F., LI, Y. & ABOUNADER, R. 2008. Signaling pathways in medulloblastoma. *J Cell Physiol,* 217**,** 577-83.

GUJAR, S., MAHESHWARI, S., BJORKMAN-BURTSCHER, I. & SUNDGREN, P. 2005. Magnetic resonance spectroscopy. *J Neuroophthalmol,* 2**,** 217-26.

GULINO, A., ARCELLA, A. & GIANGASPERO, F. 2008. Pathological and molecular heterogeneity of medulloblastoma. *Curr Opin Oncol,* 20**,** 668-75.

GUPTA, R., CLOUGHESY, T., SINHA, U., GARAKIAN, J., LAZAREFF, J., RUBINO, G., RUBINO, L., BECKER, D., VINTERS, H. & ALGER, J. 2000. Relationships Between Choline Magnetic Resonance Spectroscopy, Apparent Diffusion Coefficient and Quantitative Histopathology in Human Glioma. *Journal of Neuro-Oncology,* 50**,** 215-226.

GURNEY, J. & BONDY, M. 2006. Epidemiology of Childhood Cancer. *In:* PIZZO, A. P. & POPLACK, D. G. (eds.) *Principles and Practise of Pediatric Oncology.* 5th ed. Philadelphia: Lippincott Williams and Wilkins.

HAGBERG, G. 1998. From magnetic resonance spectroscopy to classification of tumors. A review of pattern recognition methods. *NMR Biomed,* 11**,** 148-156.

HAJEK, M. & DEZORTOVA, M. 2008. Introduction to clinical in vivo MR spectroscopy. *Eur J Radiol,* 67**,** 185-93.

HAO, J., ZOU, X., WILSON, M. P., DAVIES, N. P., SUN, Y., PEET, A. C. & ARVANITIS, T. N. 2009. A comparative study of feature extraction and blind source separation of independent component analysis (ICA) on childhood brain tumour 1H magnetic resonance spectra. *NMR Biomed,* 22**,** 809-18.

HARGRAVE, D., BARTELS, U. & BOUFFET, E. 2006. Diffuse brainstem glioma in children: critical review of clinical trials. *Lancet Oncology,* 7**,** 241-248.

HARGRAVE, D., CHUANG, N. & BOUFFET, E. 2008. Conventional MRI cannot predict survival in childhood diffuse intrinsic pontine glioma. *Journal of Neuro-Oncology,* 86**,** 313-319.

HARRIS, L. M., DAVIES, N., MACPHERSON, L., FOSTER, K., LATEEF, S., NATARAJAN, K., SGOUROS, S., BRUNDLER, M. A., ARVANITIS, T. N., GRUNDY, R. G. & PEET, A. C. 2007. The use of short-echo-time 1H MRS for childhood cerebellar tumours prior to histopathological diagnosis. *Pediatr Radiol,* 37**,** 1101-9.

HARRIS, L. M., DAVIES, N. P., MACPHERSON, L., LATEEF, S., NATARAJAN, K., BRUNDLER, M. A., SGOUROS, S., ENGLISH, M. W., ARVANITIS, T. N., GRUNDY, R. G. & PEET, A. C. 2008. Magnetic resonance spectroscopy in the assessment of pilocytic astrocytomas. *Eur J Cancer,* 44**,** 2640-7.

HARRIS, L. M., DAVIES, N. P., WILSON, S., MACPHERSON, L., NATARAJAN, K., ENGLISH, M. W., BRUNDLER, M.-A., ARVANITIS, T. N., GRUNDY, R. G. & PEET, A. C. 2011. Short echo time single voxel 1H magnetic resonance spectroscopy in the diagnosis and characterisation of pineal tumours in children. *Pediatr Blood Cancer,* 57**,** 972-977.

HATTINGEN, E., MAGERKURTH, J., PILATUS, U., MOZER, A., SEIFRIED, C., STEINMETZ, H., ZANELLA, F. & HILKER, R. 2009. Phosphorus and proton magnetic resonance spectroscopy demonstrates mitochondrial dysfunction in early and advanced Parkinson's disease. *Brain,* 132**,** 3285-3297.

HATTINGEN, E., RAAB, P., FRANZ, K., LANFERMANN, H., SETZER, M., GERLACH, R., ZANELLA, F. E. & PILATUS, U. 2008a. Prognostic value of choline and creatine in WHO grade II gliomas. *Neuroradiology,* 50**,** 759-67.

HATTINGEN, E., RAAB, P., FRANZ, K., ZANELLA, F., LANFERMANN, H. & PILATUS, U. 2008b. Myo-inositol: a marker of reactive astrogliosis in glial tumors? *NMR Biomed,* 21**,** 233-41.

HATTON, B. A., VILLAVICENCIO, E. H., TSUCHIYA, K. D., PRITCHARD, J. I., DITZLER, S., PULLAR, B., HANSEN, S., KNOBLAUGH, S. E., LEE, D., EBERHART, C. G., HALLAHAN, A. R. & OLSON, J. M. 2008. The Smo/Smo Model: Hedgehog-Induced Medulloblastoma with 90% Incidence and Leptomeningeal Spread. *Cancer Research,* 68**,** 1768-1776.

HATTORI, N., ABE, K., SAKODA, S. & SAWADA, T. 2002. Proton MR spectroscopic study at 3 Tesla on glutamate/glutamine in Alzheimer's disease. *Neuroreport,* 13**,** 183-6.

HECK, J. E., LOMBARDI, C. A., COCKBURN, M., MEYERS, T. J., WILHELM, M. & RITZ, B. 2013. Epidemiology of rhabdoid tumors of early childhood. *Pediatr Blood Cancer,* 60**,** 77-81.

HEKMATYAR, S. K., WILSON, M., JEROME, N., SALEK, R. M., GRIFFIN, J. L., PEET, A. & KAUPPINEN, R. A. 2010. 1H nuclear magnetic resonance spectroscopy characterisation of metabolic phenotypes in the medulloblastoma of the SMO transgenic mice. *Br J Cancer,* 103**,** 1297-1304.

HELMS, G. 2008. The principles of quantification applied to in vivo proton MR spectroscopy. *Eur J Radiol,* 67**,** 218-229.

HIPP, S. J., STEFFEN-SMITH, E., HAMMOUD, D., SHIH, J. H., BENT, R. & WARREN, K. E. 2011. Predicting outcome of children with diffuse intrinsic pontine gliomas using multiparametric imaging. *Neuro-Oncology,* 13**,** 904-909.

HIRSCHHAEUSER, F., SATTLER, U. G. A. & MUELLER-KLIESER, W. 2011. Lactate: A Metabolic Key Player in Cancer. *Cancer Res,* 71**,** 6921-6925.

HORSKÁ, A., ULUG, A. M., MELHEM, E. R., FILIPPI, C. G., BURGER, P. C., EDGAR, M. A., SOUWEIDANE, M. M., CARSON, B. S. & BARKER, P. B. 2001. Proton magnetic resonance spectroscopy of choroid plexus tumors in children. *Journal of Magnetic Resonance Imaging,* 14**,** 78-82.

HOURANI, R., HORSKÁ, A., ALBAYRAM, S., BRANT, L. J., MELHEM, E., COHEN, K. J., BURGER, P. C., WEINGART, J. D., CARSON, B., WHARAM, M. D. & BARKER, P. B. 2006. Proton magnetic resonance spectroscopic imaging to differentiate between nonneoplastic lesions and brain tumors in children. *Journal of Magnetic Resonance Imaging,* 23**,** 99-107.

HOWE, F., BARTON, S., CUDLIP, S., STUBBS, M., SAUNDERS, D., MURPHY, M., WILKINS, P., OPSTAD, K., DOYLE, V., MCLEAN, M., BELL, B. & GRIFFITHS, J. 2003. Metabolic profiles of human brain tumors using quantitative in vivo 1H magnetic resonance spectroscopy. *Magn Reson Med,* 49**,** 223-232.

HOWE, F. A. & OPSTAD, K. S. 2003. H MR spectroscopy of brain tumours and masses. *NMR Biomed,* 16**,** 123-131.

HYGINO DA CRUZ, L. C., RODRIGUEZ, I., DOMINGUES, R. C., GASPARETTO, E. L. & SORENSEN, A. G. 2011. Pseudoprogression and Pseudoresponse: Imaging Challenges in the Assessment of Posttreatment Glioma. *AJNR Am J Neuroradiol,* 32**,** 1978-1985.

ICARD, P., POULAIN, L. & LINCET, H. 2012. Understanding the central role of citrate in the metabolism of cancer cells. *Biochimica et Biophysica Acta (BBA) - Reviews on Cancer,* 1825**,** 111-116.

ISD SCOTLAND 2011. Information and Statistics Division NHS Scotland.

JANSEN, J. F. A., BACKES, W. H., NICOLAY, K. & KOOI, M. E. 2006. 1H MR Spectroscopy of the Brain: Absolute Quantification of Metabolites. *Radiology,* 240**,** 318-332.

JEUN, S., KIM, M., KIM, B., LEE, J., CHUNG, S., OH, C., LEE, S. & CHOE, B. 2005. Assessment of malignancy in gliomas by 3T 1H MR spectroscopy . *Clin Imaging,* 29**,** 10-5.

JOHNSON, D., BROWN, P., GALANIS, E. & HAMMACK, J. 2012. Pilocytic astrocytoma survival in adults: analysis of the Surveillance, Epidemiology, and End Results Program of the National Cancer Institute. *Journal of Neuro-Oncology,* 108**,** 187-193.

JONES, D., MULHOLLAND, S., PEARSON, D., MALLEY, D., OPENSHAW, S., LAMBERT, S., LIU, L., BACKLUND, L., ICHIMURA, K. & COLLINS, V. 2011. Adult grade II diffuse astrocytomas are genetically distinct from and more aggressive than their paediatric counterparts. *Acta Neuropathol.,* 121**,** 753-761.

JULIÀ-SAPÉ, M., CORONEL, I., MAJÓS, C., CANDIOTA, A. P., SERRALLONGA, M., COS, M., AGUILERA, C., ACEBES, J. J., GRIFFITHS, J. R. & ARÚS, C. 2012. Prospective diagnostic performance evaluation of single-voxel 1H MRS for typing and grading of brain tumours. *NMR Biomed,* 25**,** 661-673.

KAISER, L. G., SCHUFF, N., CASHDOLLAR, N. & WEINER, M. W. 2005. Scyllo-inositol in normal aging human brain: 1H magnetic resonance spectroscopy study at 4 Tesla. *NMR Biomed,* 18**,** 51-55.

KANOWSKI, M., KAUFMANN, J., BRAUN, J., BERNARDING, J. & TEMPELMANN, C. 2004. Quantitation of simulated short echo time 1H human brain spectra by LCModel and AMARES. *Magnetic Resonance in Medicine,* 51**,** 904-912.

KAPLAN, E. L. & MEIER, P. 1958. Nonparametric Estimation from Incomplete Observations. *Journal of the American Statistical Association,* 53**,** 457-481.

KATZ-BRULL, R., ROFSKY, N. M., MORRIN, M. M., PEDROSA, I., GEORGE, D. J., MICHAELSON, M. D., MARQUIS, R. P., MARIL, M., NOGUERA, C. & LENKINSKI, R. E. 2005. Decreases in free cholesterol and fatty acid unsaturation in renal cell carcinoma demonstrated by breath-hold magnetic resonance spectroscopy. *American Journal of Physiology - Renal Physiology,* 288**,** F637-F641.

KENDI, T., HUVAJ, S., HUVAJ, S., BADEMCI, G., KENDI, M. & ALPARSLAN, S. 2004. Suprasellar germ cell tumor with subarachnoid seeding MRI and MR spectroscopy findings. *Clinical Imaging,* 28**,** 404-407.

KILDAY, J.-P., RAHMAN, R., DYER, S., RIDLEY, L., LOWE, J., COYLE, B. & GRUNDY, R. 2009. Pediatric Ependymoma: Biological Perspectives. *Molecular Cancer Research,* 7**,** 765-786.

KIM, J.-H., CHANG, K.-H., NA, D. G., SONG, I. C., KIM, S. J., KWON, B. J. & HAN, M. H. 2006. Comparison of 1.5T and 3T 1H MR Spectroscopy for Human Brain Tumors. *Korean J Radiol,* 7**,** 156-161.

KIM, W., CHOY, W., DYE, J., NAGASAWA, D., SAFAEE, M., FONG, B. & YANG, I. 2011. The tumor biology and molecular characteristics of medulloblastoma identifying prognostic factors associated with survival outcomes and prognosis. *Journal of Clinical Neuroscience,* 18**,** 886-890.

KLOMP, D. W. J., VAN DER GRAAF, M., WILLEMSEN, M. A. A. P., VAN DER MEULEN, Y. M., KENTGENS, A. P. M. & HEERSCHAP, A. 2004. Transmit/receive headcoil for optimal 1H MR spectroscopy of the brain in paediatric patients at 3 T. *Magnetic Resonance Materials in Physics, Biology and Medicine,* 17**,** 1-4.

KLOSE, U. 2008. Measurement sequences for single voxel proton MR spectroscopy. *Eur J Radiol,* 67**,** 194-201.

KOMOTAR, R., MOCCO, J., CARSON, B., SUGHRUE, M., ZACHARIA, B., SISTI, A., CANOLL, P., KHANDJI, A., TIHAN, T., BURGER, P. & BRUCE, J. 2004. Pilomyxoid astrocytoma: A Review. *Medscape General Medicine,* 6**,** 42.

KONOVALOV, A. N. & PITSKHELAURI, D. I. 2003. Principles of treatment of the pineal region tumors. *Surgical Neurology,* 59**,** 252-270.

KOVANLIKAYA, A., PANIGRAHY, A., KRIEGER, M. D., GONZALEZ-GOMEZ, I., GHUGRE, N., MCCOMB, J. G., GILLES, F. H., NELSON, M. D. & BLUML, S. 2005. Untreated Pediatric Primitive Neuroectodermal Tumor in Vivo: Quantitation of Taurine with MR Spectroscopy. *Radiology,* 236**,** 1020-1025.

KRUSKAL, W. & WALLIS, A. 1952. Use of Ranks in One-Criterion Variance Analysis. *Journal of the American Statistical Association,* 47**,** 583-621.

KUPERMAN, V. 2000. Introduction. *In:* MAYERGOYZ, I. (ed.) *Magnetic Resonance Imaging.* San Diego: Academic Press.

KWOCK, L. 1998. Clincal Proton Magnetic Resonance Spectroscopy: Basic Principles. *In:* MUKHERJI, S. (ed.) *Clincal applications of MR Spectroscopy.* New York: Wiley-Liss.

LANGKOWSKI, J. H., WIELAND, J., BOMSDORF, H., LEIBFRITZ, D., WESTPHAL, M., OFFERMANN, W. & MAAS, R. 1989. Pre-operative localized in vivo proton spectroscopy in cerebral tumors at 4.0 Tesla—First results. *Magnetic Resonance Imaging,* 7**,** 547-555.

LAPRIE, A., PIRZKALL, A., HAAS-KOGAN, D. A., CHA, S., BANERJEE, A., LE, T. P., LU, Y., NELSON, S. & MCKNIGHT, T. R. 2005. Longitudinal multivoxel MR spectroscopy study of pediatric diffuse brainstem gliomas treated with radiotherapy. *Int J Radiat Oncol Biol Phys,* 62**,** 20-31.

LAW, M., YANG, S., WANG, H., BABB, J. S., JOHNSON, G., CHA, S., KNOPP, E. A. & ZAGZAG, D. 2003. Glioma Grading: Sensitivity, Specificity, and Predictive Values of Perfusion MR Imaging and Proton MR Spectroscopic Imaging Compared with Conventional MR Imaging. *AJNR Am J Neuroradiol,* 24**,** 1989-1998.

LE, A., LANE, ANDREWÂ N., HAMAKER, M., BOSE, S., GOUW, A., BARBI, J., TSUKAMOTO, T., ROJAS, CAMILIOÂ J., SLUSHER, BARBARAÂ S., ZHANG, H., ZIMMERMAN, LISAÂ J., LIEBLER, DANIELÂ C., SLEBOS, ROBBERTÂ J. C., LORKIEWICZ, PAWELÂ K., HIGASHI, RICHARDÂ M., FAN, TERESAÂ W. M. & DANG, CHIÂ V. 2012. Glucose-Independent Glutamine Metabolism via TCA Cycling for Proliferation and Survival in B Cells. *Cell Metabolism,* 15**,** 110-121.

LEACH, P. A., ESTLIN, E. J., COOPE, D. J., THORNE, J. A. & KAMALY-ASL, I. D. 2008. Diffuse brainstem gliomas in children: should we or shouldn't we biopsy? *British Journal of Neurosurgery,* 22**,** 619-624.

LEHNHARDT, F. G., BOCK, C., RÖHN, G., ERNESTUS, R. I. & HOEHN, M. 2005. Metabolic differences between primary and recurrent human brain tumors: a 1H NMR spectroscopic investigation. *NMR Biomed,* 18**,** 371-382.

LEITNER, A. A., HOCHHAUS, A. & MÜLLER, M. C. 2011. Current treatment concepts of CML. *Curr Cancer Drug Targets.,* 11**,** 31-43.

LEVIT, M. 2001. *Spin Dynamics: Basics of Nuclear Magnetic Resonance*, Wiley.

LI, B. S. Y., WANG, H. & GONEN, O. 2003. Metabolite ratios to assumed stable creatine level may confound the quantification of proton brain MR spectroscopy. *Magnetic Resonance Imaging,* 21**,** 923-928.

LI, K., LAU, K. & NG, H. K. 2013. Signaling pathway and molecular subgroups of medulloblastoma. *Int J Clin Exp Pathology,* 6**,** 1211-22.

LINNET, K., BOSSUYT, P. M. M., MOONS, K. G. M. & REITSMA, J. B. 2012. Quantifying the Accuracy of a Diagnostic Test or Marker. *Clinical Chemistry,* 58**,** 1292-1301.

LISTERNICK, R., FERNER, R. E., LIU, G. T. & GUTMANN, D. H. 2007. Optic pathway gliomas in neurofibromatosis-1: Controversies and recommendations. *Annals of Neurology,* 61**,** 189-198.

LIU, A., BRANDON, J., FOREMAN, N. & FENTON, L. 2009. Conventional MRI at presentation does not predict clinical response to radiation therapy in children with diffuse pontine glioma. *Pediatr Radiol,* 39**,** 1317-1320.

LOCASALE, J. W., GRASSIAN, A. R., MELMAN, T., LYSSIOTIS, C. A., MATTAINI, K. R., BASS, A. J., HEFFRON, G., METALLO, C. M., MURANEN, T., SHARFI, H., SASAKI, A. T., ANASTASIOU, D., MULLARKY, E., VOKES, N. I., SASAKI, M., BEROUKHIM, R., STEPHANOPOULOS, G., LIGON, A. H., MEYERSON, M., RICHARDSON, A. L., CHIN, L., WAGNER, G., ASARA, J. M., BRUGGE, J. S., CANTLEY, L. C. & VANDER HEIDEN, M. G. 2011. Phosphoglycerate dehydrogenase diverts glycolytic flux and contributes to oncogenesis. *Nat Genet,* 43**,** 869-874.

LOENING, N., CHAMBERLIN, A., ZEPEDA, A., GONZALEZ, R. & CHENG, L. 2005. Quantification of phosphocholine and glycerophosphocholine with 31P edited 1H NMR spectroscopy. *NMR Biomed,* 18**,** 413-20.

LONGO, N., ARDON, O., VANZO, R., SCHWARTZ, E. & PASQUALI, M. 2011. Disorders of creatine transport and metabolism. *American Journal of Medical Genetics Part C: Seminars in Medical Genetics,* 157**,** 72-78.

LOUIS, D., OHGAKI, H., WIESTLER, O., CAVENEE, W., BURGER, P., JOUVET, A., SCHEITHAUER, B. & KLEIHUES, P. 2007. The 2007 WHO classification of tumours of the central nervous system. *Acta Neuropathol.,* 114**,** 97-109.

LU, W., PELICANO, H. & HUANG, P. 2010. Cancer Metabolism: Is Glutamine Sweeter than Glucose? *Cancer Cell,* 18**,** 199-200.

MACDONALD, D. R., CASCINO, T. L., SCHOLD, S. C. & CAIRNCROSS, J. G. 1990. Response criteria for phase II studies of supratentorial malignant glioma. *J Clin Oncol,* 8**,** 1277-80.

MACK, S. & TAYLOR, M. 2009. The genetic and epigenetic basis of ependymoma. *Childs Nerv Syst,* 25**,** 1195-1201.

MANDAL, P. K. 2012. In vivo proton magnetic resonance spectroscopic signal processing for the absolute quantitation of brain metabolites. *European Journal of Radiology,* 81**,** e653-e664.

MANN, H. & WHITNEY, D. 1947. On a Test of Whether one of Two Random Variables is Stochastically Larger than the Other. *The Annals of Mathematical Statistics,* 18**,** 50-60.

MANSSON, S., JOHANSSON, E., MAGNUSSON, P., CHAI, C. M., HANSSON, G., PETERSSON, J. S., STAHLBERG, F. & GOLMAN, K. 2006. 13C imaging-a new diagnostic platform. *Eur Radiol,* 16**,** 57-67.

MANTEL, N. 1966. Evaluation of survival data and two new rank order statistics arising in its consideration. *Cancer Chemother Rep,* 50**,** 163-70.

MANTEL, N. 1967. Evaluation of survival data and two new rank order statistics arising in its consideration. *Cancer Chemotherapy Rep,* 50**,** 163-170.

MARCUS, K., ASTRAKAS, L., ZURAKOWSKI, D., ZARIFI, M., MINTZOPOULOS, D., POUSSAINT, T., ANTHONY, D., DE GIROLAMI, U., BLACK, P., TARBELL, N. & TZIKA, A. 2007. Predicting survival of children with CNS tumors using proton magnetic resonance spectroscopic imaging biomarkers. *Int J Oncol,* 30**,** 651-7.

MARTINEZ-BISBAL, M. & CELDA, B. 2009. Proton magnetic resonance spectroscopy imaging in the study of human brain cancer. *Q J Nucl Med Mol Imaging,* 53**,** 618-630.

MCKINNEY, P. A. 2004. Brain tumours: incidence, survival, and aetiology. *J Neurol Neurosurg Psychiatry,* 75**,** ii12-ii17.

MCKNIGHT, T. R., LAMBORN, K. R., LOVE, T. D., BERGER, M. S., CHANG, S., DILLON, W. P., BOLLEN, A. & NELSON, S. J. 2007. Correlation of magnetic resonance spectroscopic and growth characteristics within Grades II and III gliomas. *Journal of Neurosurgery,* 106**,** 660-666.

MEHTA, A. I., KANALY, C. W., FRIEDMAN, A. H., BIGNER, D. D. & SAMPSON, J. H. 2011. Monitoring Radiographic Brain Tumor Progression. *Toxins,* 3**,** 191-200.

MOESTUE, S. A., ENGEBRAATEN, O. & GRIBBESTAD, I. S. 2011. Metabolic effects of signal transduction inhibition in cancer assessed by magnetic resonance spectroscopy. *Molecular Oncology,* 5**,** 224-241.

MOFFETT, J. R., ROSS, B., ARUN, P., MADHAVARAO, C. N. & NAMBOODIRI, A. M. A. 2007. N-Acetylaspartate in the CNS: From neurodiagnostics to neurobiology. *Progress in Neurobiology,* 81**,** 89-131.

MONJE, M., BEACHY, P. A. & FISHER, P. G. 2011. Hedgehogs, Flies, Wnts and MYCs: The Time Has Come for Many Things in Medulloblastoma. *Journal of Clinical Oncology,* 29**,** 1395-1398.

MORENO-TORRES, A., MARTINEZ-PEREZ, I., BAQUERO, M., CAMPISTOL, J., CAPDEVILA, A., ARUS, C. & PUJOL, J. 2004. Taurine detection by proton magnetic resonance spectroscopy in medulloblastoma: contribution to noninvasive differential diagnosis with cerebellar astrocytoma. *Neurosurgery,* 55**,** 829.

211

MORSE, D., CARROLL, D., DAY, S., GRAY, H., SADARANGANI, P., MURTHI, S., JOB, C., BAGGETT, B., RAGHUNAND, N. & GILLIES, R. 2009. Characterization of breast cancers and therapy response by MRS and quantitative gene expression profiling in the choline pathway. *NMR Biomed,* 22**,** 114-27.

MUKHERJI, S. 1998. *Clincal applications of MR Spectroscopy,* New York, Wiley-Liss.

MULLER, H. L. 2008. Childhood Craniopharyngioma. *Hormone Research in Paediatrics,* 69**,** 193-202.

MUNOZ-PINEDO, C., EL MJIYAD, N. & RICCI, J. E. 2012. Cancer metabolism: current perspectives and future directions. *Cell Death and Dis,* 3**,** e248.

NASRALLAH, F., FEKI, M. & KAABACHI, N. 2010. Creatine and Creatine Deficiency Syndromes: Biochemical and Clinical Aspects. *Pediatr Neurol,* 42**,** 163-171.

NORTHERN IRELAND CANCER REGISTRY 2011. Cancer Incidence and Mortality.

OFFICE FOR NATIONAL STATISTICS 2010. Cancer Statistics registrations: Registrations of cancer diagnosed in 2008, England. *Series MB1 no.39.* London: National Statistics,.

OPSTAD, K., BELL, B., GRIFFITHS, J. & HOWE, F. 2009. Taurine: a potential marker of apoptosis in gliomas. *Br J Cancer,* 100**,** 789-94.

OPSTAD, K. S., LADROUE, C., BELL, B. A., GRIFFITHS, J. R. & HOWE, F. A. 2007. Linear discriminant analysis of brain tumour 1H MR spectra: a comparison of classification using whole spectra versus metabolite quantification. *NMR Biomed,* 20**,** 763-770.

ORPHANIDOU-VLACHOU, E., AUER, D., BRUNDLER, M. A., DAVIES, N. P., JASPAN, T., MACPHERSON, L., NATARAJAN, K., SUN, Y., ARVANITIS, T. N., GRUNDY, R. G. & PEET, A. C. 2013. 1H magnetic resonance spectroscopy in the diagnosis of paediatric low grade brain tumours. *Eur J Radiol* [Online]. Available: http://www.sciencedirect.com/science/article/pii/S0720048X13000703.

PACKER, R. J., COHEN, B. H. & COONEY, K. 2000. Intracranial Germ Cell Tumors. *The Oncologist,* 5**,** 312-320.

PANIGRAHY, A. & BLUML, S. 2009. Neuroimaging of Pediatric Brain Tumors: From Basic to Advanced Magnetic Resonance Imaging (MRI). *J Child Neurol,* 24**,** 1343-1365.

PANIGRAHY, A., BORZAGE, M. & BLUML, S. 2010a. Basic principles and concepts underlying recent advances in magnetic resonance imaging of the developing brain. *Semin Perinatol,* 34**,** 3-19.

PANIGRAHY, A., KRIEGER, M., GONZALEZ-GOMEZ, I., LIU, X., MCCOMB, J., FINLAY, J. L., NELSON, M., GILLES, F. & BLUML, S. 2006. Quantitative short echo time 1H-MR spectroscopy of untreated pediatric brain tumors: preoperative diagnosis and characterization. *AJNR Am J Neuroradiol,* 27**,** 560-72.

PANIGRAHY, A., NELSON, M., NELSON, J., FINLAY, J., SPOSTO, R., KRIEGER, M., GILLES, F. & BLUML, S. 2008. Metabolism of diffuse intrinsic brainstem gliomas in children. *Neuro-oncology,* 10**,** 32-44.

PANIGRAHY, A., NELSON, M. D., JR. & BLUML, S. 2010b. Magnetic resonance spectroscopy in pediatric neuroradiology: clinical and research applications. *Pediatr Radiol,* 40**,** 3-30.

PATRA, S., GHOSH, A., ROY, S., BERA, S., DAS, M., TALUKDAR, D., RAY, S., WALLIMANN, T. & RAY, M. 2012. A short review on creatine–creatine kinase system in relation to cancer and some experimental results on creatine as adjuvant in cancer therapy. *Amino Acids,* 42**,** 2319-2330.

PEARSON, K. 1901. On lines and planes of closest fit to systems of points in space. *Philosophical Magazine,* 2**,** 559-572.

PEELING, J. & SUTHERLAND, G. 1992. High-Resolution 1H NMR spectroscopy studies of extracts of human cerebral neoplasms. *Magn Reson Med,* 24**,** 123-136.

PEET, A. C., ARVANITIS, T. N., LEACH, M. O. & WALDMAN, A. D. 2012. Functional imaging in adult and paediatric brain tumours. *Nat Rev Clin Oncol,* 9**,** 700-711.

PEET, A. C., DAVIES, N. P., RIDLEY, L., BRUNDLER, M. A., KOMBOGIORGAS, D., LATEEF, S., NATARAJAN, K., SGOUROS, S., MACPHERSON, L. & GRUNDY, R. G. 2007a. Magnetic resonance spectroscopy suggests key differences in the metastatic behaviour of medulloblastoma. *Eur J Cancer,* 43**,** 1037-44.

PEET, A. C., LATEEF, S., MACPHERSON, L., NATARAJAN, K., SGOUROS, S. & GRUNDY, R. G. 2007b. Short echo time 1 H magnetic resonance spectroscopy of childhood brain tumours. *Childs Nerv Syst,* 23**,** 163-9.

PEREZ-GOMEZ, J., RODRIGUEZ-ALVAREZ, C., MARHX-BRACHO, A. & RUEDA-FRANCO, F. 2010. Stereotactic biopsy for brainstem tumors in pediatric patients. *Childs Nerv Syst,* 26**,** 29-34.

PIETTE, C., DEPREZ, M., BORN, J., MICHOTTE, A., MUNAUT, C., CLOSON, M., RUTTEN, I., DRESSE, M., FORGET, P., SCHMITZ, V., MISSON, J. & HOYOUX, C. 2008. Management of diffuse glioma in children: a retrospective study of 27 cases and review of literature. *Acta Neurol Belg.,* 108**,** 35-43.

PODO, F. 1999. Tumour phospholipid metabolism. *NMR Biomed,* 12**,** 413-439.

POLLACK, I. F. 1999. Pediatric brain tumors. *Seminars in Surgical Oncology,* 16**,** 73-90.

POMEROY, S. L., TAMAYO, P., GAASENBEEK, M., STURLA, L. M., ANGELO, M., MCLAUGHLIN, M. E., KIM, J. Y., GOUMNEROVA, L. C., BLACK, P. M., LAU, C., ALLEN, J. C., ZAGZAG, D., OLSON, J. M., CURRAN, T., WETMORE, C., BIEGEL, J. A., POGGIO, T., MUKHERJEE, S., RIFKIN, R., CALIFANO, A., STOLOVITZKY, G., LOUIS, D. N., MESIROV, J. P., LANDER, E. S. & GOLUB, T. R. 2002. Prediction of central nervous system embryonal tumour outcome based on gene expression. *Nature,* 415**,** 436-42.

PORTO, L., KIESLICH, M., FRANZ, K., LEHRBECHER, T., PILATUS, U. & HATTINGEN, E. 2010a. Proton magnetic resonance spectroscopic imaging in pediatric low-grade gliomas. *Brain Tumor Pathol,* 27**,** 65-70.

PORTO, L., KIESLICH, M., FRANZ, K., LEHRBECHER, T., VLAHO, S., PILATUS, U. & HATTINGEN, E. 2010b. Spectroscopy of untreated pilocytic astrocytomas: do children and adults share some metabolic features in addition to their morphologic similarities? *Childs Nerv Syst,* 26**,** 801-806.

PORTO, L., KIESLICH, M., FRANZ, K., LEHRNBECHER, T., ZANELLA, F., PILATUS, U. & HATTINGEN, E. 2011. 'MR spectroscopy differentiation between high and low grade astrocytomas: A comparison between paediatric and adult tumours'. *Eur J Paediatr Neurol,* 15**,** 214-221.

POSSE, S., OTAZO, R., CAPRIHAN, A., BUSTILLO, J., CHEN, H., HENRY, P.-G., MARJANSKA, M., GASPAROVIC, C., ZUO, C., MAGNOTTA, V., MUELLER, B., MULLINS, P., RENSHAW, P., UGURBIL, K., LIM, K. O. & ALGER, J. R. 2007. Proton echo-planar spectroscopic imaging of J-coupled resonances in human brain at 3 and 4 Tesla. *Magn Reson Med,* 58**,** 236-244.

POULLET, J.-B., SIMA, D. M. & VAN HUFFEL, S. 2008. MRS signal quantitation: A review of time- and frequency-domain methods. *Journal of Magnetic Resonance,* 195**,** 134-144.

POUSSAINT, T. 2001. Magnetic resonance imaging of pediatric brain tumors: state of the art. *Top Magn Reson Imaging,* 12**,** 411-33.

POUWELS, P. J. W., BROCKMANN, K., KRUSE, B., WILKEN, B., WICK, M., HANEFELD, F. & FRAHM, J. 1999. Regional Age Dependence of Human Brain Metabolites from Infancy to Adulthood as Detected by Quantitative Localized Proton MRS. *Pediatr Res,* 46**,** 474-474.

PREUL, M. C., CARAMANOS, Z., LEBLANC, R., VILLEMURE, J. G. & ARNOLD, D. L. 1998. Using pattern analysis of in vivo proton MRSI data to improve the diagnosis and surgical management of patients with brain tumors. *NMR Biomed,* 11**,** 192-200.

PRICKETT, T. D. & SAMUELS, Y. 2012. Molecular Pathways: Dysregulated Glutamatergic Signaling Pathways in Cancer. *Clin Cancer Res,* 18**,** 4240-4246.

PROVENCHER, S. W. 2001. Automatic quantitation of localized in vivo 1H spectra with LCModel. *NMR Biomed,* 14**,** 260-264.

PUGET, S., GRILL, J., VALENT, A., BIECHE, I., DANTAS-BARBOSA, C., KAUFFMANN, A., DESSEN, P., LACROIX, L., GEOERGER, B., JOB, B., DIRVEN, C., VARLET, P., PEYRE, M., DIRKS, P. B., SAINTE-ROSE, C. & VASSAL, G. 2009. Candidate Genes on Chromosome 9q33-34 Involved in the Progression of Childhood Ependymomas. *J Clin Oncol,* 27**,** 1884-1892.

QIAO, H., ZHANG, X., ZHU, X.-H., DU, F. & CHEN, W. 2006. In vivo 31P MRS of human brain at high/ultrahigh fields: a quantitative comparison of NMR detection sensitivity and spectral resolution between 4 T and 7 T. *Magnetic Resonance Imaging,* 24**,** 1281-1286.

QUANT, E. & WEN, P. 2011. Response Assessment in Neuro-Oncology. *Current Oncology Reports,* 13**,** 50-56.

R DEVELOPMENT CORE TEAM 2011. R: A Language and Environment for Statistical Computing. Vienna, Austria: R Foundation for Statistical Computing.

RAO, P. 2008. Role of MRI in paediatric neurooncology. *Eur J Radiol,* 68**,** 259-270.

REDDY, A. 2005. Atypical teratoid/rhabdoid tumors of the central nervous system. *Journal of Neuro-Oncology,* 75**,** 309-313.

REMKE, M., HIELSCHER, T., NORTHCOTT, P. A., WITT, H., RYZHOVA, M., WITTMANN, A., BENNER, A., VON DEIMLING, A., SCHEURLEN, W., PERRY, A., CROUL, S., KULOZIK, A. E., LICHTER, P., TAYLOR, M. D., PFISTER, S. M. & KORSHUNOV, A. 2011. Adult Medulloblastoma Comprises Three Major Molecular Variants. *J Clin Oncol,* 29**,** 2717-2723.

RICCI, P. E., PITT, A., KELLER, P. J., COONS, S. W. & HEISERMAN, J. E. 2000. Effect of Voxel Position on Single-Voxel MR Spectroscopy Findings. *American Journal of Neuroradiology,* 21**,** 367-374.

RICH, J. T., NEELY, J. G., PANIELLO, R. C., VOELKER, C. C. J., NUSSENBAUM, B. & WANG, E. W. 2010. A practical guide to understanding Kaplan-Meier curves. *Otolaryngology -- Head and Neck Surgery,* 143**,** 331-336.

RIGHI, V., RODA, J., PAZ, J., MUCCI, A., TUGNOLI, V., RODRIGUEZ-TARDUCHY, G., BARRIOS, L., SCHENETTI, L., CERDAN, S. & GARCIA-MARTIN, M. L. 2009. 1H HR-MAS and genomic analysis of human tumor biopsies discriminate between high and low grade astrocytomas. *NMR Biomed,* 22**,** 629-37.

ROCCO, C. & TAMBURRINI, G. 2006. Ganglioglioma. *In:* TONN, J., WESTPHAL, M. & RUTKA, J. (eds.) *Neuro-Oncology of CNS Tumors.* 2 ed.: Springer.

RONEN, S., JACKSON, L., BELOUECHE, M. & LEACH, M. 2001. Magnetic resonance detects changes in phosphocholine associated with Ras activation and inhibition in NIH 3T3 cells. *Br J Cancer,* 84**,** 691-6.

ROSEN, Y. & LENKINSKI, R. E. 2007. Recent Advances in Magnetic Resonance Neurospectroscopy. *Neurotherapeutics,* 4**,** 330-345.

SANAI, N. & PRADOS, M. D. 2010. Brain Stem Gliomas. *In:* BANERJEE, G. & HAAS-KOGAN, D. A. (eds.) *Pediatric CNS Tumours.* 2 ed. New York: Springer.

SANDBERG, A. A. & STONE, J. F. 2008. Medulloblastoma, Primitive Neuroectodermal Tumors, and Pineal Tumors. *The Genetics and Molecular Biology of Neural Tumors.*

SCHULZE, A., HESS, T., WEVERS, R., MAYATEPEK, E., BACHERT, P., MARESCAU, B., KNOPP, M., DE DEYN, P., BREMER, H. & RATING, D. 1997. Creatine deficiency syndrome caused by guanidinoacetate methyltransferase deficiency: diagnostic tools for a new inborn error of metabolism. *J Pediatr.,* 131**,** 626-31.

SEMENZA, G. L. 2008. Tumor metabolism: cancer cells give and take lactate. *The Journal of Clinical Investigation,* 118**,** 3835-3837.

SEYMOUR, Z., PANIGRAHY, A., FINLAY, J., NELSON, M. & BLUML, S. 2008. Citrate in pediatric CNS tumors? *AJNR Am J Neuroradiol,* 29**,** 1006-11.

SIBTAIN, N., HOWE, F. & SAUNDERS, D. 2007a. The clinical value of proton magnetic resonance spectroscopy in adult brain tumours. *Clinical Radiology,* 62**,** 109-19.

SIBTAIN, N. A., HOWE, F. A. & SAUNDERS, D. E. 2007b. The clinical value of proton magnetic resonance spectroscopy in adult brain tumours. *Clinical Radiology,* 62**,** 109-119.

SIEVERT, A. J. & FISHER, M. J. 2009. Pediatric Low-Grade Gliomas. *J Child Neurol,* 24**,** 1397-1408.

SJØBAKK, T. E., LUNDGREN, S., KRISTOFFERSEN, A., SINGSTAD, T., SVARLIAUNET, A. J., SONNEWALD, U. & GRIBBESTAD, I. S. 2006. Clinical 1H magnetic resonance spectroscopy of brain metastases at 1.5T and 3T. *Acta Radiologica,* 47**,** 501-508.

SLAVC, I. 2011. CNS tumours in children and adolescents - differences to adult patients. *memo - Magazine of European Medical Oncology,* 4**,** 3-5.

SMITH, E. A., CARLOS, R. C., JUNCK, L. R., TSIEN, C. I., ELIAS, A. & SUNDGREN, P. C. 2009. Developing a Clinical Decision Model: MR Spectroscopy to Differentiate Between Recurrent Tumor and Radiation Change in Patients with New Contrast-Enhancing Lesions. *AJR Am J Roentgenol,* 192**,** W45-52.

SMYTH, M. D. & RUBIN, J. 2010. Ependymoma. *Pediatric CNS Tumors.* Berlin: Springer.

SONTHEIMER, H. 2008. A role for glutamate in growth and invasion of primary brain tumors. *Journal of Neurochemistry,* 105**,** 287-295.

SPAMPINATO, M., SMITH, J., KWOCK, L., EWEND, M., GRIMME, J., CAMACHO, D. & CASTILLO, M. 2007. Cerebral blood volume measurements and proton MR spectroscopy in grading of oligodendroglial tumors. *AJR Am J Roentgenol,* 188**,** 204-12.

SPEED, T. P. 1987. What is an analysis of variance? (with discussion). *Annals of Statistics***,** 885-941.

STEFFEN-SMITH, E., SHIH, J., HIPP, S., BENT, R. & WARREN, K. 2011. Proton magnetic resonance spectroscopy predicts survival in children with diffuse intrinsic pontine glioma. *Journal of Neuro-Oncology,* 105**,** 365-373.

STEFFEN-SMITH, E. A., VENZON, D. J., BENT, R. S., HIPP, S. J. & WARREN, K. E. 2012. Single- and Multivoxel Proton Spectroscopy in Pediatric Patients With Diffuse Intrinsic Pontine Glioma. *Int J Radiat Oncol Biol Phys,* 84**,** 774-779.

STILLER C 2007. *Childhood Cancer in Britain: Incidence, survival, mortality*, Oxford University Press;.

STREINER, D. L. & NORMAN, G. R. 2011. Correction for multiple testing: Is there a resolution? *CHEST Journal,* 140**,** 16-18.

STUDENT 1908. The Probable Error of a Mean. *Biometrika,* 6**,** 1-25.

SUNDGREN, P. C. 2009. MR Spectroscopy in Radiation Injury. *AJNR Am J Neuroradiol,* 30**,** 1469-1476.

SUTTON, L. N., WANG, Z., GUSNARD, D., LANGE, B., PERILONGO, G., BOGDAN, A. R., DETRE, J. A., RORKE, L. & ZIMMERMAN, R. A. 1992. Proton Magnetic Resonance Spectroscopy of Pediatric Brain Tumors. *Neurosurgery,* 31**,** 195-202.

SWANSON, M. G., VIGNERON, D. B., TABATABAI, Z. L., MALES, R. G., SCHMITT, L., CARROLL, P. R., JAMES, J. K., HURD, R. E. & KURHANEWICZ, J. 2003. Proton HR-MAS spectroscopy and quantitative pathologic analysis of MRI/3D-MRSI-targeted postsurgical prostate tissues. *Magn Reson Med,* 50**,** 944-954.

TATE, A. R., UNDERWOOD, J., ACOSTA, D. M., JULIÀ-SAPÉ, M., MAJÓS, C., MORENO-TORRES, À., HOWE, F. A., VAN DER GRAAF, M., LEFOURNIER, V., MURPHY, M. M., LOOSEMORE, A., LADROUE, C., WESSELING, P., LUC BOSSON, J., CABAÑAS, M. E., SIMONETTI, A. W., GAJEWICZ, W., CALVAR, J., CAPDEVILA, A., WILKINS, P. R., BELL, B. A., RÉMY, C., HEERSCHAP, A., WATSON, D., GRIFFITHS, J. R. & ARÚS, C. 2006. Development of a decision support system for diagnosis and grading of brain tumours using in vivo magnetic resonance single voxel spectra. *NMR Biomed,* 19**,** 411-434.

TATE, M., SUGHRUE, M. E., RUTKOWSKI, M. J., KANE, A. J., ARANDA, D., MCCLINTON, L., MCCLINTON, L., BARANI, I. J. & PARSA, A. T. 2012. The long-term postsurgical prognosis of patients with pineoblastoma. *Cancer,* 118**,** 173-179.

TAYLOR, M., NORTHCOTT, P., KORSHUNOV, A., REMKE, M., CHO, Y.-J., CLIFFORD, S., EBERHART, C., PARSONS, D., RUTKOWSKI, S., GAJJAR, A., ELLISON, D., LICHTER, P., GILBERTSON, R., POMEROY, S., KOOL, M. & PFISTER, S. 2012. Molecular subgroups of medulloblastoma: the current consensus. *Acta Neuropathol.,* 123**,** 465-472.

TEICHER, B. A., LINEHAN, W. M. & HELMAN, L. J. 2012. Targeting Cancer Metabolism. *Clin Cancer Res,* 18**,** 5537-5545.

TKÁČ, I., ÖZ, G., ADRIANY, G., UĞURBIL, K. & GRUETTER, R. 2009. In vivo 1H NMR spectroscopy of the human brain at high magnetic fields: Metabolite quantification at 4T vs. 7T. *Magn Reson Med,* 62**,** 868-879.

TONG, Z., YAMAKI, T., HARADA, K. & HOUKIN, K. 2004. In vivo quantification of the metabolites in normal brain and brain tumors by proton MR spectroscopy using water as an internal standard. *Magn Reson Imaging,* 22**,** 735-42.

TZIKA, A., ASTRAKAS, L., ZARIFI, M., PETRIDOU, N., YOUNG-POUSSAINT, T., GOUMNEROVA, L., ZURAKOWSKI, D., ANTHONY, D. & BLACK, P. 2003. Multiparametric MR assessment of pediatric brain tumors. *Neuroradiology,* 45**,** 1-10.

TZIKA, A. A., ASTRAKAS, L., CAO, H., MINTZOPOULOS, D., ANDRONESI, O. C., MINDRINOS, M., ZHANG, J., RAHME, L. G., BLEKAS, K. D., LIKAS, A. C., GALATSANOS, N. P., CARROLL, R. S. & BLACK, P. M. 2007. Combination of high-resolution magic angle spinning proton magnetic resonance spectroscopy and microscale genomics to type brain tumor biopsies. *Int J Mol Med,* 20**,** 199-208.

TZIKA, A. A., ASTRAKAS, L. G., ZARIFI, M. K., ZURAKOWSKI, D., POUSSAINT, T. Y., GOUMNEROVA, L., TARBELL, N. J. & BLACK, P. M. 2004. Spectroscopic and perfusion magnetic resonance imaging predictors of progression in pediatric brain tumors. *Cancer,* 100**,** 1246-1256.

TZIKA, A. A., ZARIFI, M. K., GOUMNEROVA, L., ASTRAKAS, L. G., ZURAKOWSKI, D., YOUNG-POUSSAINT, T., ANTHONY, D. C., SCOTT, R. M. & BLACK, P. M. 2002. Neuroimaging in Pediatric Brain Tumors: Gd-DTPA-enhanced, Hemodynamic, and Diffusion MR Imaging Compared with MR Spectroscopic Imaging. *AJNR Am J Neuroradiol,* 23**,** 322-333.

TZIKA, A. A., ZURAKOWSKI, D., POUSSAINT, T. Y., GOUMNEROVA, L., ASTRAKAS, L. G., BARNES, P. D., ANTHONY, D. C., BILLETT, A. L., TARBELL, N. J., SCOTT, R. M. & BLACK, P. M. 2001.

Proton magnetic spectroscopic imaging of the child's brain: the response of tumors to treatment. *Neuroradiology,* 43**,** 169-177.

USENIUS, J.-P., VAINIO, P., HERNESNIEMI, J. & KAUPPINEN, R. A. 1994. Choline-Containing Compounds in Human Astrocytomas Studied by 1H NMR Spectroscopy In Vivo and In Vitro. *Journal of Neurochemistry,* 63**,** 1538-1543.

VALONEN, P. K., GRIFFIN, J. L., LEHTIMÄKI, K. K., LIIMATAINEN, T., NICHOLSON, J. K., GRÖHN, O. H. J. & KAUPPINEN, R. A. 2005. High-resolution magic-angle-spinning 1H NMR spectroscopy reveals different responses in choline-containing metabolites upon gene therapy-induced programmed cell death in rat brain glioma. *NMR Biomed,* 18**,** 252-259.

VAN DEN BENT, M. J., WEFEL, J. S., SCHIFF, D., TAPHOORN, M. J. B., JAECKLE, K., JUNCK, L., ARMSTRONG, T., CHOUCAIR, A., WALDMAN, A. D., GORLIA, T., CHAMBERLAIN, M., BAUMERT, B. G., VOGELBAUM, M. A., MACDONALD, D. R., REARDON, D. A., WEN, P. Y., CHANG, S. M. & JACOBS, A. H. 2011. Response assessment in neuro-oncology (a report of the RANO group): assessment of outcome in trials of diffuse low-grade gliomas. *The Lancet Oncology,* 12**,** 583-593.

VÉZINA, L.-G. 2005. Neuroradiology of Childhood Brain Tumors: New Challenges. *Journal of Neuro-Oncology,* 75**,** 243-252.

VICENTE, J., FUSTER-GARCIA, E., TORTAJADA, S., GARCÍA-GÓMEZ, J. M., DAVIES, N., NATARAJAN, K., WILSON, M., GRUNDY, R. G., WESSELING, P., MONLEÓN, D., CELDA, B., ROBLES, M. & PEET, A. C. 2013. Accurate classification of childhood brain tumours by in vivo 1H MRS – A multi-centre study. *Eur J Cancer* 49**,** 658-667.

VIGNERON, D., BOLLEN, A., MCDERMOTT, M., WALD, L., DAY, M., MOYHER-NOWOROLSKI, S., HENRY, R., CHANG, S., BERGER, M., DILLON, W. & NELSON, S. 2001. Three-dimensional magnetic resonance spectroscopic imaging of histologically confirmed brain tumors. *Magn Reson Imaging,* 19**,** 89-101.

VITVITSKY, V., GARG, S. K. & BANERJEE, R. 2011. Taurine Biosynthesis by Neurons and Astrocytes. *Journal of Biological Chemistry,* 286**,** 32002-32010.

WALDMAN, A. 2010. Magnetic resonance imaging of brain tumors- time to quantify. *Discov Med,* 9**,** 7-12.

WALLIS, L. I., GRIFFITHS, P. D., RITCHIE, S. J., ROMANOWSKI, C. A. J., DARWENT, G. & WILKINSON, I. D. 2007. Proton Spectroscopy and Imaging at 3T in Ataxia-Telangiectasia. *AJNR Am J Neuroradiol,* 28**,** 79-83.

WANG, Z., SUTTON, L. N., CNAAN, A., HASELGROVE, J. C., RORKE, L. B., ZHAO, H., BILANIUK, L. T. & ZIMMERMAN, R. A. 1995. Proton MR spectroscopy of pediatric cerebellar tumors. *AJNR Am J Neuroradiol,* 16**,** 1821-1833.

WARDLAW, J., BRINDLE, W., CASADO, A., SHULER, K., HENDERSON, M., THOMAS, B., MACFARLANE, J., MUÑOZ MANIEGA, S., LYMER, K., MORRIS, Z., PERNET, C., NAILON, W., AHEARN, T., MUMUNI, A., MUGRUZA, C., MCLEAN, J., CHAKIROVA, G., TAO, Y., SIMPSON, J., STANFIELD, A., JOHNSTON, H., PARIKH, J., ROYLE, N., DE WILDE, J., BASTIN, M., WEIR, N., FARRALL, A., VALDES HERNANDEZ, M. & GROUP, T. S. C. 2012. A systematic review of the utility of 1.5 versus 3 Tesla magnetic resonance brain imaging in clinical practice and research. *Eur Radiol***,** 1-9.

WARREN, K. E., FRANK, J. A., BLACK, J. L., HILL, R. S., DUYN, J. H., AIKIN, A. A., LEWIS, B. K., ADAMSON, P. C. & BALIS, F. M. 2000. Proton Magnetic Resonance Spectroscopic Imaging in Children With Recurrent Primary Brain Tumors. *J Clin Oncol,* 18**,** 1020-6.

WARREN, K. E., POUSSAINT, T. Y., VEZINA, G., HARGRAVE, D., PACKER, R. J., GOLDMAN, S., WEN, P. Y., POLLACK, I. F., ZURAKOWSKI, D., KUN, L. E., PRADOS, M. D., RUTKOWSKI, S. & KIERAN, M. W. 2013. Challenges With Defining Response to Antitumor Agents in Pediatric Neuro-Oncology: A Report From the Response Assessment in Pediatric Neuro-Oncology (RAPNO) Working Group. *Pediatr Blood Cancer*.

WELSH CANCER INTELLIGENCE AND SURVEILLANCE UNIT 2011. Cancer Registrations in Wales 2008.

WEN, P. Y., MACDONALD, D. R., REARDON, D. A., CLOUGHESY, T. F., SORENSEN, A. G., GALANIS, E., DEGROOT, J., WICK, W., GILBERT, M. R., LASSMAN, A. B., TSIEN, C., MIKKELSEN, T., WONG, E. T., CHAMBERLAIN, M. C., STUPP, R., LAMBORN, K. R., VOGELBAUM, M. A., VAN DEN BENT, M. J. & CHANG, S. M. 2010. Updated Response Assessment Criteria for High-Grade Gliomas: Response Assessment in Neuro-Oncology Working Group. *J Clin Oncol,* 28**,** 1963-1972.

WESSELS, P. H., WEBER, W. E. J., RAVEN, G., RAMAEKERS, F. C. S., HOPMAN, A. H. N. & TWIJNSTRA, A. 2003. Supratentorial grade II astrocytoma: biological features and clinical course. *The Lancet Neurology,* 2**,** 395-403.

WEYBRIGHT, P., SUNDGREN, P. C., MALY, P., HASSAN, D. G., NAN, B., ROHRER, S. & JUNCK, L. 2005. Differentiation Between Brain Tumor Recurrence and Radiation Injury Using MR Spectroscopy. *AJR Am J Roentgenol,* 185**,** 1471-1476.

WILCOXON, F. 1945. Individual Comparisons by Ranking Methods. *Biometrics Bulletin,* 1**,** 80-83.

WILSON, M., CUMMINS, C. L., MACPHERSON, L., SUN, Y., NATARAJAN, K., GRUNDY, R. G., ARVANITIS, T. N., KAUPPINEN, R. A. & PEET, A. C. 2013. Magnetic resonance spectroscopy metabolite profiles predict survival in paediatric brain tumours. *Eur J Cancer,* 49**,** 457-464.

WILSON, M., DAVIES, N. P., BRUNDLER, M. A., MCCONVILLE, C., GRUNDY, R. G. & PEET, A. C. 2009a. High resolution magic angle spinning 1H NMR of childhood brain and nervous system tumours. *Mol Cancer,* 8**,** 6.

WILSON, M., DAVIES, N. P., GRUNDY, R. G. & PEET, A. C. 2009b. A quantitative comparison of metabolite signals as detected by in vivo MRS with ex vivo 1H HR-MAS for childhood brain tumours. *NMR Biomed,* 22**,** 213-9.

WILSON, M., DAVIES, N. P., SUN, Y., NATARAJAN, K., ARVANITIS, T. N., KAUPPINEN, R. A. & PEET, A. C. 2010. A comparison between simulated and experimental basis sets for assessing short-TE in vivo1H MRS data at 1.5 T. *NMR Biomed,* 23**,** 1117-1126.

WILSON, M., REYNOLDS, G., KAUPPINEN, R. A., ARVANITIS, T. N. & PEET, A. C. 2011. A constrained least-squares approach to the automated quantitation of in vivo 1H magnetic resonance spectroscopy data. *Magn Reson Med,* 65**,** 1-12.

WOLF, A., AGNIHOTRI, S. & GUHA, A. 2010. Targeting Metabolic Remodeling in Glioblastoma Multiforme. *Oncotarget,* 1.

WREDE, B., HASSELBLATT, M., PETERS, O., THALL, P., KUTLUK, T., MOGHRABI, A., MAHAJAN, A., RUTKOWSKI, S., DIEZ, B., WANG, X., PIETSCH, T., KORTMANN, R.-D., PAULUS, W., JEIBMANN, A. & WOLFF, J. A. 2009. Atypical choroid plexus papilloma: clinical experience in the CPT-SIOP-2000 study. *Journal of Neuro-Oncology,* 95**,** 383-392.

WYMANN, M. P. & SCHNEITER, R. 2008. Lipid signalling in disease. *Nat Rev Mol Cell Biol,* 9**,** 162-176.

YAMASAKI, F., KURISU, K., KAJIWARA, Y., WATANABE, Y., TAKAYASU, T., AKIYAMA, Y., SAITO, T., HANAYA, R. & SUGIYAMA, K. 2011. Magnetic resonance spectroscopic detection of

lactate is predictive of a poor prognosis in patients with diffuse intrinsic pontine glioma. *Neuro-Oncology,* 13**,** 791-801.

YAN, H., PARSONS, D. W., JIN, G., MCLENDON, R., RASHEED, B. A., YUAN, W., KOS, I., BATINIC-HABERLE, I., JONES, S., RIGGINS, G. J., FRIEDMAN, H., FRIEDMAN, A., REARDON, D., HERNDON, J., KINZLER, K. W., VELCULESCU, V. E., VOGELSTEIN, B. & BIGNER, D. D. 2009. IDH1 and IDH2 Mutations in Gliomas. *N Engl J Med,* 360**,** 765-773.

YANG, L., LIN, C., WANG, L., GUO, H. & WANG, X. 2012. Hypoxia and hypoxia-inducible factors in glioblastoma multiforme progression and therapeutic implications. *Experimental Cell Research,* 318**,** 2417-2426.

YERLI, H., AGILDERE, A., OZEN, O., GEYIK, E., ATALAY, B. & ELHAN, A. 2007. Evaluation of cerebral glioma grade by using normal side creatine as an internal reference in multi-voxel 1H-MR spectroscopy. *Diagn Interv Radiol,* 13**,** 3-9.

ZACHAROULIS, S. & MORENO, L. 2009. Ependymoma: an update. *J Child Neurol,* 24**,** 1431-1438.

ZOU, K. H., O'MALLEY, A. J. & MAURI, L. 2007. Receiver-Operating Characteristic Analysis for Evaluating Diagnostic Tests and Predictive Models. *Circulation,* 115**,** 654-657.

APPENDIX 1 METABOLITE BASIS FUNCTIONS USED IN TARQUIN

<u>1.5 T</u>

Ala

group	independance	T1		lineshape	alpha	beta			
1		1	0	l	2.5	0			
2		2	0	l	2.5	0			

group	symmetry	spin		chemical shift					
1		1	0.5	3.7746	0				
2		1	0.5	1.4667	7.234	0			
2		1	0.5	1.4667	7.234	-14.366	0		
2		1	0.5	1.4667	7.234	-14.366	-14.366	0	

Asp

group	independance	T1		lineshape	alpha	beta		
1		1	0	l	2.5	0		
2		2	0	l	2.5	0		
3		3	0	l	2.5	0		

group	symmetry	spin		chemical shift				
1		1	0.5	3.8914	0			
2		1	0.5	2.8011	3.647	0		
3		1	0.5	2.6533	9.107	-17.426	0	

Cr

group	independance	T1		lineshape	alpha	beta
1		1	0	l	2.5	0
2		2	0	l	2.5	0

group	symmetry	spin		chemical shift	
1		3	0.5	3.027	0

group	symmetry	spin		chemical shift	
2		2	0.5	3.913	0

Cit

group	independance	T1		lineshape	alpha	beta
1		1	0	l	2.5	0
2		2	0	l	2.5	0

group	symmetry	spin		chemical shift		
1		1	0.5	2.6735	0	
2		1	0.5	2.5265	16.1	0

-CrCH2

group	independance	T1		lineshape	alpha	beta
1		1	0	l	2.5	0

group	symmetry	spin		chemical shift	
1		-2	0.5	3.913	0

GABA

group	independance	T1		lineshape	alpha	beta
1		1	0	l	2.5	0
2		2	0	l	2.5	0

group	symmetry	spin	chemical shift						
3	3	0	l	2.5	0				
1	1	0.5	3.0128	0					
1	1	0.5	3.0128	-12.021	0				
2	1	0.5	1.889	5.372	10.578	0			
2	1	0.5	1.889	7.127	6.982	-13.121	0		
3	1	0.5	2.284	0	0	7.755	6.173	0	
3	1	0.5	2.284	0	0	7.432	7.933	-10.744	0

Glc

group	independance	T1	lineshape	alpha	beta
1	1	0	l	2.5	0
2	1	0	l	2.5	0
3	1	0	l	2.5	0
4	1	0	l	2.5	0
5	1	0	l	2.5	0
6	1	0	l	2.5	0
7	1	0	l	2.5	0

group	symmetry	spin	chemical shift					
1	0	0.5	5.216	0				
2	1	0.5	3.519	3.8	0			
3	1	0.5	3.698	0	9.6	0		
4	1	0.5	3.395	0	0	9.4	0	
5	1	0.5	3.822	0	0	0	9.9	0
6	1	0.5	3.826	0	0	0	0	1.5	0

7		1	0.5	3.749	0	0	0	0	6	-12.1	0

Gln

group	independance	T1		lineshape	alpha	beta	
1	1	0	l		2.5	0	
2	2	0	l		2.5	0	
3	2	0	l		2.5	0	
4	2	0	l		2.5	0	
5	2	0	l		2.5	0	

group	symmetry	spin	chemical shift					
1	1	0.5	3.753	0				
2	1	0.5	2.129	5.847	0			
3	1	0.5	2.19	6.5	-14.504	0		
4	1	0.5	2.432	0	9.165	6.324	0	
5	1	0.5	2.454	0	6.347	9.209	-15.371	0

Glu

group	independance	T1		lineshape	alpha	beta	
1	1	0	l		2.5	0	
2	2	0	l		2.5	0	
3	2	0	l		2.5	0	
4	2	0	l		2.5	0	
5	2	0	l		2.5	0	

group	symmetry	spin	chemical shift		
1	1	0.5	3.7433	0	
2	1	0.5	2.0375	7.331	0

3	1	0.5	2.12	4.651	-14.849	0		
4	1	0.5	2.3378	0	6.413	8.478	0	
5	1	0.5	2.352	0	8.406	6.875	-15.915	0

Gly

group	independance	T1	lineshape	alpha	beta
1	1	0	l	2.5	0

group	symmetry	spin	chemical shift	
1	1	0.5	3.5480	0

GPC

group	independance	T1	lineshape	alpha	beta
1	1	0	l	2.5	0
2	2	0	l	2.5	0
3	3	0	l	2.5	0
4	3	0	l	2.5	0
5	3	0	l	2.5	0
6	4	0	l	2.5	0
7	2	0	l	2.5	0
8	4	0	l	2.5	0
9	4	0	l	2.5	0

group	symmetry	spin	chemical shift	
1	9	0.5	3.212	0

group	symmetry	spin	chemical shift	
2	1	0.5	3.605	0
2	1	0.5	3.672	-14.78	0

group	symmetry	spin	chemical shift						
3	1	0.5	3.903	5.77	4.53	0			
4	1	0.5	3.871	0	5.77	0	0		
4	1	0.5	3.946	0	4.53	0	-14.78	0	
5	0	0.5	0	0	0	0	6.03	6.03	0

group	symmetry	spin	chemical shift						
6	0	0.5	4.312	0					
6	0	0.5	4.312	-9.32	0				
7	1	0.5	3.659	3.1	5.9	0			
7	1	0.5	3.659	5.9	3.1	-9.32	0		
8	0	1	0	2.67	2.67	0	0	0	
9	0	0.5	0	6.03	6.03	0	0	0	0

Gua

group	independance	T1	lineshape	alpha	beta
1	1	0	l	2.5	0

group	symmetry	spin	chemical shift	
1	2	0.5	3.78	0

mIns

group	independance	T1	lineshape	alpha	beta
1	1	0	l	2.5	0
2	1	0	l	2.5	0
3	1	0	l	2.5	0
4	1	0	l	2.5	0

group	symmetry	spin	chemical shift	
1	1	0.5	3.5217	0

2	0	0.5	4.0538	2.889	0				
1	1	0.5	3.5217	0	3.006	0			
3	1	0.5	3.6144	0	0	9.997	0		
4	1	0.5	3.269	0	0	0	9.485	0	
3	1	0.5	3.6144	9.998	0	0	0	9.482	0

Lac

group	independance	T1	lineshape	alpha	beta
1	1	0	l	2.5	0
2	2	0	l	2.5	0

group	symmetry	spin	chemical shift			
1	0	0.5	4.0974	0		
2	1	0.5	1.3142	6.933	0	
2	1	0.5	1.3142	6.933	0	0
2	1	0.5	1.3142	6.933	0	0	0

Lip09

group	independance	T1	lineshape	alpha	beta
1	1	0	g	0	283.4

group	symmetry	spin	chemical shift
1	3	0.5	0.89	0

Lip13a

group	independance	T1	lineshape	alpha	beta
1	1	0	g	0	325.2

group	symmetry	spin	chemical shift
1	2	0.5	1.28	0

Lip13b

group	independance	T1	lineshape	alpha	beta
1	1	0	g	0	114.5

group	symmetry	spin	chemical shift		
1	2	0.5	1.28	0	

Lip20

group	independance	T1	lineshape	alpha	beta
1	1	0	g	0	325.3
2	1	0	g	0	578.3

group	symmetry	spin	chemical shift			
1	1.33	0.5	2.04	0		
1	0.67	0.5	2.25	0	0	
2	0.87	0.5	2.8	0	0	0

MM09

group	independance	T1	lineshape	alpha	beta
1	1	0	g	0	283.4

group	symmetry	spin	chemical shift		
1	3	0.5	0.91	0	

MM12

group	independance	T1	lineshape	alpha	beta
1	1	0	g	0	325.3

group	symmetry	spin	chemical shift		
1	2	0.5	1.21	0	

MM14

group	independance	T1	lineshape	alpha	beta
1	1	0	g	0	417.8

group	symmetry	spin	chemical shift		
1	2	0.5	1.43	0	

MM17

group	independance	T1	lineshape	alpha	beta
1	1	0	g	0	325.3

group	symmetry	spin	chemical shift		
1	2	0.5	1.67	0	

MM20

group	independance	T1	lineshape	alpha	beta
1	1	0	g	0	325.3
2	1	0	g	0	578.3

group	symmetry	spin	chemical shift				
1	1.33	0.5	2.08	0			
2	0.33	0.5	2.25	0	0		
1	0.33	0.5	1.95	0	0	0	
2	0.4	0.5	3	0	0	0	0

NAA

group	independance	T1	lineshape	alpha	beta
1	1	0	l	2.5	0
2	2	0	l	2.5	0
3	3	0	l	2.5	0

group	independance	T1	lineshape	alpha	beta
4	3	0	l	2.5	0

group	symmetry	spin	chemical shift			
1	3	0.5	2.008	0		

group	symmetry	spin	chemical shift			
2	0	0.5	4.3817	0		
3	1	0.5	2.6727	3.861	0	
4	1	0.5	2.4863	9.821	-15.592	0

NAAG

group	independance	T1	lineshape	alpha	beta
1	1	0	l	2.5	0

group	symmetry	spin	chemical shift	
1	3	0.5	2.042	0

PCh

group	independance	T1	lineshape	alpha	beta
1	1	0	l	2.5	0
2	2	0	l	2.5	0
3	2	0	l	2.5	0
4	3	0	l	2.5	0
5	3	0	l	2.5	0
6	3	0	l	2.5	0
7	3	0	l	2.5	0

group	symmetry	spin	chem shift	
1	9	0.5	3.208	0

group	symmetry	spin	chem shift

group	symmetry	spin	chem shift						
2	0	0.5	4.2805	0					
3	0	0.5	4.2805	-14.89	0				
4	1	0.5	3.641	2.284	7.326	0			
5	1	0.5	3.641	7.231	2.235	-14.19	0		
6	0	1	0	2.68	2.772	0	0	0	
7	0	0.5	0	6.298	6.249	0	0	0	0

sIns

group	independance	T1	lineshape		alpha	beta	
1	1	0	l		2.5	0	

group	symmetry	spin	chem shift	
1	6	0.5	3.34	0

Tau

group	independance	T1	lineshape		alpha	beta	
1	1	0	l		2.5	0	
2	1	0	l		2.5	0	

group	symmetry	spin	chem shift				
1	1	0.5	3.4206	0			
1	1	0.5	3.4206	-12.438	0		
2	1	0.5	3.2459	6.742	6.403	0	
2	1	0.5	3.2459	6.464	6.792	-12.93	0

Ala

group	independance	T1	lineshape	alpha	beta
1	1	0	l	2.5	0
2	2	0	l	2.5	0

group	symmetry	spin	chemical shift				
1	1	0.5	3.7746	0			
2	1	0.5	1.4667	7.234	0		
2	1	0.5	1.4667	7.234	-14.366	0	
2	1	0.5	1.4667	7.234	-14.366	-14.366	0

Asp

group	independance	T1	lineshape	alpha	beta
1	1	0	l	2.5	0
2	2	0	l	2.5	0
3	3	0	l	2.5	0

group	symmetry	spin	chemical shift			
1	1	0.5	3.8914	0		
2	1	0.5	2.8011	3.647	0	
3	1	0.5	2.6533	9.107	-17.426	0

Cit

group	independance	T1	lineshape	alpha	beta
1	1	0	l	2.5	0
2	2	0	l	2.5	0

group   symmetry   spin   chemical shift

group	symmetry	spin	chemical shift		
1	1	0.5	2.6735	0	
2	1	0.5	2.5265	16.1	0

Cr

group	independance	T1	lineshape	alpha	beta
1	1	0	l	2.5	0
2	2	0	l	2.5	0

group	symmetry	spin	chemical shift	
1	3	0.5	3.027	0

group	symmetry	spin	chemical shift	
2	2	0.5	3.913	0

-CrCH2

group	independance	T1	lineshape	alpha	beta
1	1	0	l	2.5	0

group	symmetry	spin	chem shift	
1	-2	0.5	3.913	0

GABA

group	independance	T1	lineshape	alpha	beta
1	1	0	l	2.5	0
2	2	0	l	2.5	0
3	3	0	l	2.5	0

group	symmetry	spin	chemical shift			
1	1	0.5	3.0128	0		
1	1	0.5	3.0128	-12.021	0	
2	1	0.5	1.889	5.372	10.578	0

group	symmetry	spin	chemical shift							
2	1	0.5	1.889	7.127	6.982	-13.121	0			
3	1	0.5	2.284	0	0	7.755	6.173	0		
3	1	0.5	2.284	0	0	7.432	7.933	-10.744	0	

Glc

group	independance	T1	lineshape	alpha	beta
1	1	0	l	2.5	0
2	1	0	l	2.5	0
3	1	0	l	2.5	0
4	1	0	l	2.5	0
5	1	0	l	2.5	0
6	1	0	l	2.5	0
7	1	0	l	2.5	0

group	symmetry	spin	chemical shift							
1	0	0.5	5.216	0						
2	1	0.5	3.519	3.8	0					
3	1	0.5	3.698	0	9.6	0				
4	1	0.5	3.395	0	0	9.4	0			
5	1	0.5	3.822	0	0	0	9.9	0		
6	1	0.5	3.826	0	0	0	0	1.5	0	
7	1	0.5	3.749	0	0	0	0	6	-12.1	0

Gln

group	independance	T1	lineshape	alpha	beta
1	1	0	l	2.5	0
2	2	0	l	2.5	0

group	independance	T1	lineshape	alpha	beta				
3	2	0	l	2.5	0				
4	2	0	l	2.5	0				
5	2	0	l	2.5	0				

group	symmetry	spin	chem shift					
1	1	0.5	3.753	0				
2	1	0.5	2.129	5.847	0			
3	1	0.5	2.19	6.5	-14.504	0		
4	1	0.5	2.432	0	9.165	6.324	0	
5	1	0.5	2.454	0	6.347	9.209	-15.371	0

Glu

group	independance	T1	lineshape	alpha	beta
1	1	0	l	2.5	0
2	2	0	l	2.5	0
3	2	0	l	2.5	0
4	2	0	l	2.5	0
5	2	0	l	2.5	0

group	symmetry	spin	chemical shift					
1	1	0.5	3.7433	0				
2	1	0.5	2.0375	7.331	0			
3	1	0.5	2.12	4.651	-14.849	0		
4	1	0.5	2.3378	0	6.413	8.478	0	
5	1	0.5	2.352	0	8.406	6.875	-15.915	0

Gly

group	independance	T1	lineshape	alpha	beta
1	1	0	l	2.5	0

group	symmetry	spin	chemical shift	
1	1	0.5	3.5480	0

GPC

group	independance	T1	lineshape	alpha	beta
1	1	0	l	2.5	0
2	2	0	l	2.5	0
3	3	0	l	2.5	0
4	3	0	l	2.5	0
5	3	0	l	2.5	0
6	4	0	l	2.5	0
7	2	0	l	2.5	0
8	4	0	l	2.5	0
9	4	0	l	2.5	0

group	symmetry	spin	chemical shift		
1	9	0.5	3.212	0	

group	symmetry	spin	chemical shift					
2	1	0.5	3.605	0				
2	1	0.5	3.672	-14.78	0			
3	1	0.5	3.903	5.77	4.53	0		
4	1	0.5	3.871	0	5.77	0	0	
4	1	0.5	3.946	0	4.53	0	-14.78	0

group	symmetry	spin	chemical shift						
5	0	0.5	0	0	0	0	6.03	6.03	0
6	1	0.5	4.312	0					
6	1	0.5	4.312	-9.32	0				
7	1	0.5	3.659	3.1	5.9	0			
7	1	0.5	3.659	5.9	3.1	-9.32	0		
8	0	1	0	2.67	2.67	0	0	0	
9	0	0.5	0	6.03	6.03	0	0	0	0

Gua

group	independance	T1	lineshape	alpha	beta
1	1	0	l	2.5	0

group	symmetry	spin	chemical shift	
1	2	0.5	3.78	0

mIns

group	independance	T1	lineshape	alpha	beta
1	1	0	l	2.5	0
2	1	0	l	2.5	0
3	1	0	l	2.5	0
4	1	0	l	2.5	0

group	symmetry	spin	chemical shift				
1	1	0.5	3.5217	0			
2	1	0.5	4.0538	2.889	0		
1	1	0.5	3.5217	0	3.006	0	
3	1	0.5	3.6144	0	0	9.997	0

4	1	0.5	3.269	0	0	0	9.485	0	
3	1	0.5	3.6144	9.998	0	0	0	9.482	0

Lac

group	independance	T1	lineshape	alpha	beta		
1	1	0	l	2.5	0		
2	2	0	l	2.5	0		

group	symmetry	spin	chemical shift				
1	1	0.5	4.0974	0			
2	1	0.5	1.3142	6.933	0		
2	1	0.5	1.3142	6.933	0	0	
2	1	0.5	1.3142	6.933	0	0	0

Lip09

group	independance	T1	lineshape	alpha	beta
1	1	0	g	0	1139

group	symmetry	spin	chemical shift	
1	3	0.5	0.89	0

Lip13a

group	independance	T1	lineshape	alpha	beta
1	1	0	g	0	1307

group	symmetry	spin	chemical shift	
1	2	0.5	1.28	0

Lip13b

group	independance	T1	lineshape	alpha	beta
1	1	0	g	0	460.4

group	symmetry	spin	chemical shift		
1	2	0.5	1.28	0	

Lip20

group	independance	T1	lineshape	alpha	beta
1	1	0	g	0	1307
2	1	0	g	0	2325

group	symmetry	spin	chemical shift			
1	1.33	0.5	2.04	0		
1	0.67	0.5	2.25	0	0	
2	0.87	0.5	2.8	0	0	0

MM09

group	independance	T1	lineshape	alpha	beta
1	1	0	g	0	1139

group	symmetry	spin	chemical shift	
1	3	0.5	0.91	0

MM12

group	independance	T1	lineshape	alpha	beta
1	1	0	g	0	1307

group	symmetry	spin	chemical shift	
1	2	0.5	1.21	0

MM14

group	independance	T1	lineshape	alpha	beta
1	1	0	g	0	1679

group	symmetry	spin	chemical shift		
1	2	0.5	1.43	0	

MM17

group	independance	T1	lineshape	alpha	beta
1	1	0	g	0	1307

group	symmetry	spin	chemical shift		
1	2	0.5	1.67	0	

MM20

group	independance	T1	lineshape	alpha	beta
1	1	0	g	0	1307
2	1	0	g	0	2325

group	symmetry	spin	chemical shift				
1	1.33	0.5	2.08	0			
2	0.33	0.5	2.25	0	0		
1	0.33	0.5	1.95	0	0	0	
2	0.4	0.5	3	0	0	0	0

NAA

group	independance	T1	lineshape	alpha	beta
1	1	0	l	2.5	0
2	2	0	l	2.5	0
3	3	0	l	2.5	0
4	3	0	l	2.5	0

group	symmetry	spin	chemical shift	
1	3	0.5	2.008	0

239

group	symmetry	spin	chemical shift			
2	1	0.5	4.3817	0		
3	1	0.5	2.6727	3.861	0	
4	1	0.5	2.4863	9.821	-15.592	0

NAAG

group	independance	T1	lineshape	alpha	beta
1	1	0	l	2.5	0

group	symmetry	spin	chemical shift	
1	3	0.5	2.042	0

PCh

group	independance	T1	lineshape	alpha	beta
1	1	0	l	2.5	0
2	2	0	l	2.5	0
3	2	0	l	2.5	0
4	3	0	l	2.5	0
5	3	0	l	2.5	0
6	3	0	l	2.5	0
7	3	0	l	2.5	0

group	symmetry	spin	chemical shift	
1	9	0.5	3.208	0

group	symmetry	spin	chemical shift			
2	1	0.5	4.2805	0		
3	1	0.5	4.2805	-14.89	0	
4	1	0.5	3.641	2.284	7.326	0

5	1	0.5	3.641	7.231	2.235	-14.19	0		
6	0	1	0	2.68	2.772	0	0	0	
7	0	0.5	0	6.298	6.249	0	0	0	0

sIns

group	independance	T1	lineshape	alpha	beta
1	1	0	l	2.5	0

group	symmetry	spin	chem shift	
1	6	0.5	3.34	0

Tau

group	independance	T1	lineshape	alpha	beta
1	1	0	l	2.5	0
2	1	0	l	2.5	0

group	symmetry	spin	chem shift				
1	1	0.5	3.4206	0			
1	1	0.5	3.4206	-12.438	0		
2	1	0.5	3.2459	6.742	6.403	0	
2	1	0.5	3.2459	6.464	6.792	-12.93	0

APPENDIX 2 LOW GRADE VS. HIGH GRADE

Mean metabolite concentrations (mM) ± SD of short echo time pre-treatment low grade tumours (I+II) vs. high grade brain tumours (III +IV) at 1.5 T with p values determined using Mann-Whitney U-test.

Metabolites concs (mM± SD)	*P* values	LG (n=65)	HG(n=58)
Ala	n.s	0.36±0.63	0.41±0.73
Asp	****	**0.85±1.26**	**0.61±2.07**
Cit	**	**0.44±0.38**	**0.64±0.57**
Cr	***	**1.67±1.84**	**2.43±1.52**
GABA	*	**0.95±1.28**	**1.53±1.59**
tCho	****	**1.25±0.84**	**2.89±1.69**
Glc	****	**2.25±1.81**	**1.03±1.73**
Gln	n.s	3.25±1.83	3.02±2.48
Glu	*	**1.86±1.46**	**2.78±2.20**
Glx	n.s	5.11±2.34	5.80±3.19
Gly	****	**1.17±2.01**	**2.68±2.27**
Gua	****	**0.34±0.52**	**0.99±1.20**
mIns	*	**2.18±3.77**	**1.36±2.78**
Lac	*	**2.18±1.78**	**3.08±2.45**
LMM0.9	****	**4.31±2.76**	**7.32±3.83**
LMM1.3	****	**6.68±6.17**	**17.90±15.4**
LMM2.0	****	**7.67±4.62**	**10.86±3.22**
NAA	n.s	1.46±0.81	1.20±0.82
sIns	****	**0.14±0.25**	**0.36±0.41**
Tau	**	**0.66±0.93**	**1.94±2.25**

Note: - n.s not significant * *P*<0.05 ** *P*<0.01 *** *P*<0.001 **** *P*<0.00001

APPENDIX 3 CONFERENCE ABSTRACTS

Abstracts submitted to conferences and accepted as either a first author oral presentations or first author poster presentations are included in the pages below.

First Author Oral Presentation Abstracts

16thAnnual Scientific Meeting of the British Chapter of the ISMRM, Nottingham, September 2010

A multi-centre study of [1]H-Magnetic Resonance Spectroscopy in the diagnosis and prognosis of brain stem tumours in children

SK Gill[1,2],LM Harris[1,2], NP Davies[1,2], YSun[1,2] , K Natarajan[1,2], L MacPherson[1,2], TN Arvanitis[1,2],D Hargrave[3,4], GS Payne[3,4] , MO Leach[3,4] , FA Howe[5] , P Morgan[6] , D Saunders[7] , DP Auer[6] , T Jaspan[6] , RG Grundy[6], AC Peet [1,2]

[1]Cancer Sciences, University of Birmingham, Birmingham, [2]Birmingham Children's Hospital, Birmingham, [3]Royal Marsden Hospital, Sutton, [4]Institute of Cancer Research, Sutton, [5]St. Georges, University of London, [6]Children's Brain Tumour Research Centre, Nottingham University Hospitals, [7]Great Ormond Street Hospital, London, United Kingdom
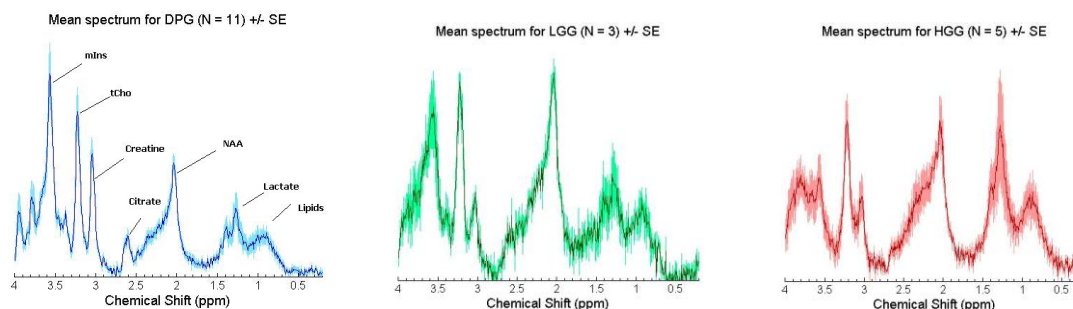
Introduction

Brain stem tumours in children pose particularly difficult management challenges. Tumours can be either diffuse or focal. Diffuse Pontine Gliomas (DPG) are usually diagnosed on clinical and imaging grounds alone with no biopsy being performed and have a particularly poor prognosis with a median survival of 9 months. There are a few long term survivors of DPGs but there are no imaging characteristics which can identify this good prognostic group at diagnosis and the lack of biopsy material reduces the opportunity to determine biological markers of good prognosis. The establishment of novel imaging biomarkers which can aid with the diagnosis and characterization of childhood brain stem tumours and identify diffuse tumours with a good prognosis would be a significant clinical advance. However, the comparative rarity of these tumours mandates a multi-centre approach. This study investigates metabolite differences in childhood brain stem tumours from a multi-centre cohort which is large compared with previous studies and has follow-up of the patients to determine length of survival.

Patients and Methods

A multi-centre study was performed using single voxel MRS (1.5 T or 3 T, PRESS, TE 30 or TE 38ms, TR 1500ms) on 30 children during routine MRI scans prior to treatment from 4 centres across the UK. Diagnosis was made on the basis of central pathology review where tissue was available or central radiology review. The cohort consists of 15 DPGs, 5 high grade gliomas (HGGs), 4 low grade gliomas (LGGs) and 6 tumours with no definitive consensus diagnosis. Spectra were processed using LCModel with a stimulated citrate component incorporated into the standard basis set of 16 metabolites and 9 lipids and macromolecules (LMM) components. 24 spectra met quality control and were analysed. All statistical analysis was performed using R Statistical Software and quantitation was relative to a water reference spectrum and normalised to sum of all metabolites. Two-tailed t-tests were performed to investigate significant differences between diffuse vs. focal tumours (where focal tumours are defined as HGGs and LGGs) and between HGGs vs. LGGs. ANOVA was performed to investigate significant differences between DPGs, HGGs and LGGs. Principal Component analysis was performed and also used for dimension reduction prior to linear discriminant analysis (LDA) for classification of undiagnosed cases. Survival data was available for 22 out of the 30 cases with a minimum follow-up of 3 years.

Results

Mean spectrum for DPG (N = 11) +/- SE · Mean spectrum for LGG (N = 3) +/- SE · Mean spectrum for HGG (N = 5) +/- SE

From the figure, DPGs differ from HGG and LGG mean spectra showing high myo-inositol (mIns) and a prominent peak around 2.6ppm assigned to citrate. T-tests showed diffuse tumours had significantly higher mIns (6 vs 3, p= 0.01); scyllo-inositol (0.2 vs 0.06, p=0.003) and citrate (0.7 vs 0.3, p=0.003) but significantly lower LMM at 0.9ppm (4.2 vs 6.5, p= 0.05) and 2.0 ppm (7 vs 11, p=0.05). There were no significant differences between focal HGG and LGG. PCA of all brain stem tumours demonstrated that the loadings were dominated by lipids and mIns. LDA showed that diffuse and focal tumours could be separated with the largest linear discriminant co-efficient being citrate. Of those who were biopsied, there was no correlation between grade of astrocytoma and survival. In the group of DPG, LMM were significantly higher at 0.9, 1.3 and 2.0ppm in those surviving less than 1 year. Out of all the DPGs the only survivor, now at 3 years, had the highest mIns in the group. Another patient who is still alive more than 5 years after diagnosis with a diffuse tumour of the pons had a markedly different MRS from the DPG group, confirmed by being an outlier on the PCA. Biopsy confirmed this case to be a diffuse astrocytoma which is consistent with the know histology of DPG.

Conclusions

MRS shows significant differences in the metabolite profiles between diffuse and focal tumours of the brain stem and this may be useful in aiding the non-invasive diagnosis of these tumours. The presence of a peak at 2.6ppm assigned to citrate and high myoinositol are spectral characteristics of DPGs which could be readily identified in a clinical setting. Of particular interest is that two patients who were thought to have a very poor prognosis but are currently doing well had spectral characteristics which set them apart from the group of DPG. The higher LMM in the DPGs surviving less than a year provides further evidence that lipids are bio-markers of poor prognosis. MRS is a useful adjunct to the characterisation of brain stem tumours and more widespread clinical evaluation of the method is warranted.

Acknowledgements

1H Magnetic Resonance Spectroscopy for characterising medulloblastomas in children

SK Gill[1,2], M Wilson[1,2], NP Davies[1,2,3], YSun[1,2], K Natarajan[1,2,3], L MacPherson[1,2], TN Arvanitis[2,4], AC Peet [1,2]
[1]Cancer Sciences, University of Birmingham, Birmingham, [2]Birmingham Children's Hospital, Birmingham [3]Medical Imaging and Physics, University Hospital Birmingham. [4]Electrical, Electronic and Computer Engineering, University of Birmingham

Introduction

Medulloblastomas (MBs) are highly aggressive tumours arising from the cerebellum accounting for 10-20% of all brain tumours in children. These tumours are staged through the Chang classification, from M0 to M4 where increasing stage corresponds to degree of disease spread and poorer prognosis. However, not all patients with localised disease (M0) survive and identifying these patients at diagnosis is a key challenge in medulloblastoma research. In this study we hypothesise that MRS can distinguish between different stages of medulloblastoma and provide prognostic markers to identify patients with poor prognosis.

Patients and Methods

Single voxel MRS (1.5 T, TE 30, TR 1500ms) was performed on 30 children during routine MRI scans for a suspected brain tumour prior to treatment at the Birmingham Children's Hospital where tumour diagnosis was made by histopathology. The cohort consists of Chang stages M0 to M3 , M0 (n=14),M1 (n=4), M2 (n=4) and M3 (n=8). Spectra were analysed using TARQUIN with a stimulated citrate and glycine component incorporated into the standard basis set. Quality control measures were met by all cases. All statistical analysis was performed using R Statistical Software and quantitation was relative to a water reference spectrum. Two-tailed t-tests were performed to investigate differences between metabolite profiles of localised M0 MBs and metastatic (M1 to M3) MBs. Lipid and metabolite profiles were used as the input to a Principal Component Analysis which was also used for dimension reduction prior to linear discriminant analysis (LDA). Survival data was available for 28 out of the 30 cases, with follow-up being up to 7 years.
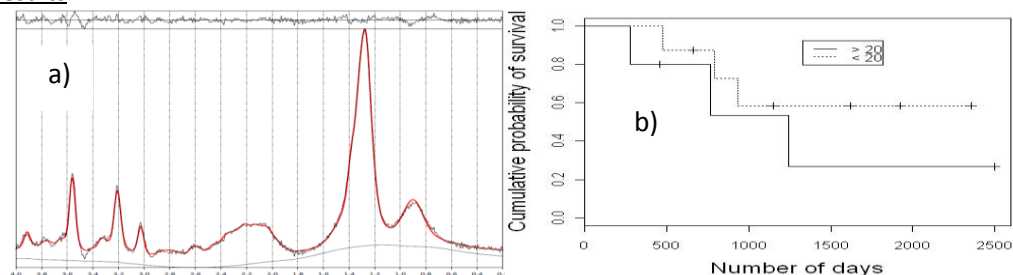
Results

Figure 1 a) An example spectrum of a patient with very high lipids that survived less than a year following diagnosis b) Kaplan Meier curves for patients with M0 MB comparing those high (> 20) and low lipid and MMs levels at 1.3ppm.

Mean spectra generated from the four Chang Stages showed very little variability in metabolite profiles except in the lipid and macromolecular (MM) peak at 1.3ppm. Univariate analysis (T-test) between M0 and M1-M3 revealed that levels of lipids and MM at 1.3ppm were the only statistically significant difference between the two groups. High variability in these lipids and MMs was a strong feature of the M0 MBs not seen in the other Chang stages (fig 1a). Principal Component analysis and linear discriminant analysis were dominated by Lipids at 1.3ppm and cases with extremely high lipids were seen as large outliers to the main group of patients. For the M0 cases, 4 out of the 5 patients who were outliers on the LDA died whilst only 2 of the remaining 8 patients died. A log rank test using only lipids at 1.3ppm for the M0 MB patients failed to reach statistical significance for the difference in survival (fig 1b).

Conclusions

Significant differences have been found in lipid and MM levels between localised (M0) and metastatic (M1-3) medulloblastoma at diagnosis. A subset of the localised tumours have metabolite profiles which distinguish them from the other tumours mainly due to their very high lipid levels and this group is

associated with poor survival. MRS is a non-invasive tool that can improve characterisation of tumours and provides potential biomarkers of prognosis in M0 medulloblastomas.

Acknowledgements

[1]H Magnetic Resonance Spectroscopy: Do metabolite profiles of brain tumours in children differ at diagnosis to those at first tumour relapse?

SK Gill[1,2], M Wilson[1,2], NP Davies[1,2,3], L MacPherson[1,2], TN Arvanitis[2,4], AC Peet [1,2]

[1]Cancer Sciences, University of Birmingham, Birmingham, [2]Birmingham Children's Hospital, Birmingham [3]Medical Imaging and Physics, University Hospital Birmingham. [4]Electrical, Electronic and Computer Engineering, University of Birmingham

Introduction

Brain tumours are the most common solid tumour diagnosed in children. Whilst some brain tumours have a good prognosis, others have continued to present major challenges and are now the leading cause of death in children. Difficulties arise when trying to accurately diagnose abnormalities detected during tumour surveillance. Currently tumour assessment of high grade tumours is performed using the RANO criteria, where increases of 2D measurements on consecutive MRI scans and clinical factors help determine the presence of tumour recurrence. In addition influences the decision of a tumour biopsy being performed. However, there are limitations to these criteria as not all changes are tumour growth specific and tumour biopsies are rarely performed at relapse. This study investigates how metabolite profiles of brain tumours analysed using TARQUIN software differ from diagnosis to first relapse of a tumour including clinical course of all patients to provide confirmation of tumour behaviour. Correct characterisation of tumour relapse is crucial to the management of brain tumours.

Patients and Methods

Single voxel 1H MRS (1.5 T, PRESS, TE 30ms, TR 1500ms) was performed on 20 children during routine MRI scans for a suspected high grade brain tumour prior to treatment at the Birmingham Children's Hospital. Following MRI, 19 patients underwent either a tumour resection or biopsy and all patients underwent either focal or craniospinal radiotherapy and/or chemotherapy. Diagnosis was made on histopathology where tissue was available or on the basis of MR imaging alone (1 case). The inclusion criteria for the cohort was high grade tumours only with the exception of diffuse astrocytomas. The cohort consists of 7 different tumours types including 4 glioblastoma multiforme, 4 medulloblastomas, 4 diffuse astrocytomas, 3 ependymomas , 2 CNS primitive neuroectodermal tumours, 1 atypical teratoid rhabdoid tumour and 1case with gliomatosis cereberi. 19 cases met quality control (38 spectra from 19 cases). Spectra were processed using TARQUIN with a basis set of 18 metabolites and 9 lipids and macromolecules (LMM) including citrate and glycine with quantitation relative to a water reference spectrum. All statistical analysis was performed using R Statistical Software. Paired Student's t-tests were performed between metabolite profiles at diagnosis and those at radiologically confirmed first relapse. This consisted of comparing all, comparing local first relapses only and distant first relapses only. Box and whisker plots were constructed to compare differences between metabolites, lipid and macromolecules at diagnosis and first relapse. Line plots were constructed to compare differences between levels of four variables choline, myo-inositol, NAA and lipids at 1.3ppm at diagnosis and first relapse.

Results

Paired Student's t-test analysis between pre-diagnostic metabolite profiles and those at first relapse (n=19) demonstrated no significant differences in metabolites or combined and individual lipid and macromolecules components at 0.9, 1.3 and 2.0ppm ($p> 0.05$). Analysis of pre-diagnostic metabolite profiles and those at first local relapse (n=12) demonstrated no significant differences in metabolites or combined and individual macromolecules and lipid components at 0.9, 1.3 and 2.0ppm ($p> 0.05$). Paired t-test analysis between pre-diagnostic metabolite profiles and those at first distant relapse (n=7) also demonstrated no significant differences in metabolites or combined and individual macromolecules and lipid components at 0.9, 1.3 and 2.0ppm ($p> 0.05$). However, Lipids at 1.3ppm were close to significance ($p=0.07$, 6.5 vs. 12.9). Box and whisker plot demonstrated no specific tumour type trends, however lipids and MMs&lipids at 1.3ppm demonstrated a large range of differences with 13 out of the 19 cases demonstrating higher levels at first relapse. Line plots of the 4 variables demonstrated relatively stable

levels between diagnosis and first relapse with only a few cases showing considerable change (of either increase or decrease).

Conclusions

MRS demonstrated no significant difference between pre-diagnostic metabolite profiles and those at first relapse (P>0.05). This study shows the metabolite profile of a tumour can aid the confirmation of tumour progression if the metabolite profile appears to be comparable to the diagnostic spectrum as opposed to post treatment effects. However, caution needs to be taken when interpreting the spectra. It is important that spectra meet the quality control criteria in particular ensuring the voxel does not contain normal brain. Interestingly there were a number of patients who, when compared on an individual case basis by qualitative analysis, demonstrated differences in metabolite profiles (particularly those with MRS over subsequent relapses). MRS is useful in characterising tumour progression. However, these findings need to be confirmed by a large multi-centre study, which ideally needs to be performed with cases grouped by tumour subtypes rather than grouped as a whole. Comparisons with MRS of post treatment related changes are also required as a comparator group to strengthen the analysis.

Acknowledgements

Single-voxel proton MRS in the brain shows improved metabolite quantification at 3 T in paediatric patients

Simrandip Kaur Gill 1,2, Martin Wilson1,2, Lesley MacPherson 2, Nigel P Davies1,2, Theodoros N Arvanitis 2,3, and Andrew C Peet 1,2

1 Cancer Sciences, University of Birmingham, Birmingham, 2 Birmingham Children's Hospital, Birmingham, 3 School of Electronic, Electrical and Computer Engineering, University of Birmingham, Birmingham

Introduction: In vivo 1H single voxel (SV) MRS is a promising technique used in characterising brain pathology in adults and children at 1.5 T. However, there are limited studies performed at 3T particularly in paediatric patients. The aim of this study was to determine whether higher field strength of 3T demonstrates an improvement in metabolite determination and quality of data acquired in paediatric patients.

Methods: SV MRS was performed on 5 paediatric patients with inherited metabolic disorders on both a 1.5 T Siemens and 3T Phillips Achieva TX, using the PRESS sequence. Patients within the cohort were matched for voxel locations on both scanners. The core acquisition protocol at 1.5 T comprised of a TE/TR/NSA of 30ms/1500ms/128 and at 3T 38ms/2000ms/128. All spectra passed QC criteria. Raw data was taken from the scanner and analysed with TARQUIN (Version 4.2.10), fitting to a linear combination of metabolite basis functions generated at the correct field strength and echo time [1].
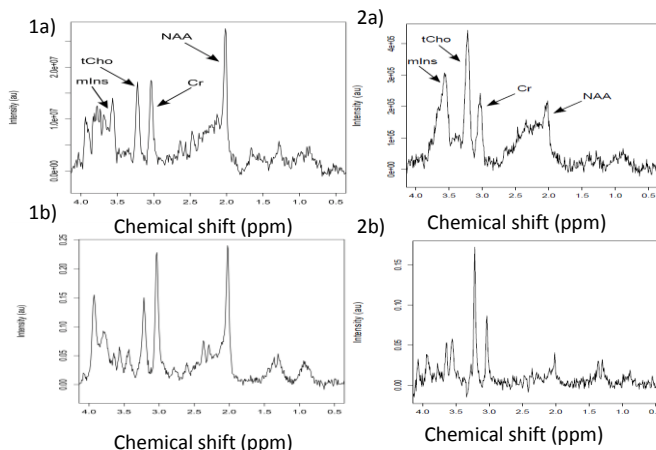
Results

Figure 1 Spectra and TARQUIN fit obtained from the left basal ganglia in a patient with an inherited metabolic disorder at a) 1.5 T and b) at 3T

Figure 2 Spectra and TARQUIN fit obtained from a patient with a tectal plate glioma at a) 1.5 T and b) at 3 T

Comparing MRS at 3 T and 1.5 T demonstrated significantly (t-test, $p < 0.05$) higher signal-to-noise ratio (SNR) with an overall increase of 76% equivalent to a 32% increase per unit acquisition time. An improved spectral resolution was shown by a significant reduction in water line width (0.078 vs. 0.053 ppm, t-test, $p < 0.05$). Comparing mean metabolite concentrations demonstrated no significant differences between metabolite concentrations at 1.5 T and 3 T (Wilcoxon signed rank test). Cramer-Rao Lower Bounds (CRLBs) were significantly lower in 15 out of 27 metabolites at 3 T confirming improved metabolite quantification. These included creatine (Cr), glutamate (Glu), glutamine (Gln), glycine, myo-inositol (mIns) and N-acetyl-aspartate(NAA), metabolites known to be important in brain pathology. Figure 1 shows an example case.

Discussion: Whilst the use of higher field strengths theoretically has many benefits for MRS including increased spectral resolution, there are few studies that have demonstrated this within a clinical environment and none published in children to our knowledge. This study shows the improvement in metabolite profile quantification which can be achieved at a higher field strength of 3T in children with neurological disorders. The increased spectral resolution allows a better discrimination between closely overlapping metabolites for example myo-inositol and glycine. This distinction is particularly important in

brain tumours since myo-inositol has been demonstrated to be a marker of good prognosis and glycine, a marker of poor prognosis [2]. Figure 2 demonstrates a case from a child with a brain tumour that was scanned pre-treatment at 1.5 T and 3 T. In this example the resonances are shown to be readily distinguishable only at the higher field strength.

Conclusion: This study provides a promising initial indication of improvement in short echo time proton spectroscopy at 3T compared with 1.5 T in paediatric patients. Improved metabolite profile determination should lead to better tissue characterization encouraging the implementation of spectroscopy at 3T in a clinical environment.

References: 1. Wilson M et al. 2011 MRM 65(1): 1-12. 2. Davies N. et al. 2009 NMR Biomed **23**(1): 80-87.

First Author Poster Presentation Abstracts

A multi-centre study of ^{1}H-Magnetic Resonance Spectroscopy in the characterisation of brain stem tumours in children compared with focal tumours in other parts of the brain using TARQUIN software

SK Gill[1,2], LM Harris[1,2], NP Davies[1,2], YSun[1,2] , K Natarajan[1,2], L MacPherson[1,2], TN Arvanitis[1,2], D Hargrave[3,4], GS Payne[3,4] , MO Leach[3,4] , FA Howe[5] , P Morgan[6], D Saunders[7], DP Auer[6] , T Jaspan[6] , RG Grundy[6] , AC Peet
[1,2][1]Cancer Sciences, University of Birmingham, Birmingham, [2]Birmingham Children's Hospital, Birmingham, [3]Royal Marsden Hospital, Sutton, [4]Institute of Cancer Research, Sutton, [5]St. Georges, University of London, [6]Children's Brain Tumour Research Centre, Nottingham University Hospitals, [7]Great Ormond Street Hospital, London, United Kingdom

Introduction

Brain stem tumours in children are clinically difficult tumours to manage. Tumours can be either diffuse or focal. One subtype, Diffuse Pontine Gliomas (DPG) is usually diagnosed on clinical and imaging grounds alone with no biopsy being performed. They have a particularly poor prognosis, with a median survival of 9 months. However, the group yields occasional long-term survivors with no current method of identifying these at diagnosis. As biopsies are rarely performed, no biological markers of prognosis can be determined. Novel imaging biomarkers are required to aid diagnosis and characterisation of brain stem tumours and identify good prognostic indicators at diagnosis. As these tumours are extremely rare, a multi-centre approach is required to obtain enough cases for robust statistical analysis. This multicentre study investigates potential diagnostic and prognostic metabolite differences in childhood brain stem tumours by comparison with diffuse and focal tumours elsewhere in the brain, TARQUIN software was used to quantify metabolite profiles allowing differences in echo time and field strength to be conveniently accounted for by simulation of appropriate basis sets.

Patients and Methods

A multi-centre study was performed using single voxel MRS (1.5 T or 3 T, PRESS, TE 30 or TE 38ms, TR 1500ms) on 79 children during routine MRI scans prior to treatment at 4 centres across the UK. Diagnosis was made on the basis of central pathology review where tissue was available or central radiology review. The cohort consists of 15 DPGs, 12 high grade gliomas (HGGs), 52 pilocytic astrocytoma (PAs) and 6 tumours with no definitive consensus diagnosis. Spectra were processed using TARQUIN with citrate (Cit) and glycine (Gly) in the basis set of 18 metabolites and 9 lipids and macromolecules (LMM) components. 59 spectra met quality control criteria and were analysed. All statistical analysis was performed using R Statistical Software and quantitation was relative to a water reference spectrum and normalised to sum of all metabolites. Two-tailed t-tests were performed to investigate significant differences between diffuse vs. focal tumours (where focal tumours are defined as HGGs and PAs) and between HGGs vs. PAs. ANOVA was performed to investigate significant differences between DPGs, HGGs and PAs. Principal Component analysis was performed and also used for dimension reduction prior to linear discriminant analysis (LDA) for classification of undiagnosed cases. Within the DPG group, potential prognostic indicators were explored using two-tailed t-tests to compare between patients surviving more than and less than 1 year with follow-up data available for up to three years.

Results

ANOVA demonstrated diffuse tumours to have significantly higher levels of myo-inositol (mIns) (0.9 vs.0.7 vs. 0.3 ,$p < 0.01$), total NAA (2.3 vs. 1.2 vs. 1.5,$p < 0.01$) and Creatine (Cr) (3 vs 1.42 vs. 0.9 ,$p < 0.01$) as well as Citrate ($p < 0.01$) , Gly ($p < 0.01$) and scyllo-inositol ($p < 0.01$) as shown in a previous study of brainstem tumours. Significantly higher levels of Gly (0.3 vs.0.6, $p=0.04$) and LMM at 0.9 ppm (4 vs 8, $p=0.02$), 1.3 ppm (6.5 vs 14, $p<0.01$) and 2.0 ppm (6 vs. 11, $p<0.01$) were found in HGGs when compared to PAs. PCA of all the tumours demonstrated loadings dominated by lipids, glutamate and glutamine (Glx) and mIns. LDA

demonstrated scyllo-inositol to separate diffuse and focal tumours. DPGs surviving less than 1 year demonstrated significantly higher levels of glutamine (Gln) (3 vs.0.7, p=0.007), lactate (1 vs.0.3, p=0.05), LMM at 2.0ppm (6vs. 4, p=0.05), tNAA (2.6 vs.1.7, p=0.05) and significantly lower levels of taurine (0.1 vs.1.2, p=0.03) when compared to those surviving over 1 year. Of the DPG cohort only one survivor remains, now at 3 years, had the highest mIns in the group. Another patient who is still alive more than 5 years after diagnosis with a diffuse tumour of the pons had a markedly different MRS from the DPG group, confirmed by being an outlier on the PCA. Biopsy confirmed this case to be a diffuse astrocytoma which is consistent with the known histology of DPG.

Discussion and Conclusions

MRS shows significant differences in the metabolite profiles between diffuse and focal tumours of the brain stem and this may be useful in aiding the non-invasive diagnosis of these tumours. The presence of a peak at 2.6ppm assigned to citrate and high myo-inositol are spectral characteristics of DPGs which could be readily identified in a clinical setting. Of particular interest is that two patients who were thought to have a very poor prognosis but are currently doing well had spectral characteristics which set them apart from the group of DPG. mIns is shown to be a marker of good prognosis. MRS is a useful adjunct to the characterisation of brain stem tumours and more widespread clinical evaluation of the method is warranted.

Acknowledgements

[1]H Magnetic Resonance Spectroscopy Biomarkers of Prognosis for Localised Medulloblastoma in Children

SK Gill[1,2], M Wilson[1,2], NP Davies[1,2,3], L MacPherson[1,2], TN Arvanitis[2,4], AC Peet [1,2]

[1]Cancer Sciences, University of Birmingham, Birmingham, [2]Birmingham Children's Hospital, Birmingham [3]Medical Imaging and Physics, University Hospital Birmingham. [4]Electrical, Electronic and Computer Engineering, University of Birmingham

Introduction
Magnetic resonance spectroscopy (MRS) is known to provide non-invasive biomarkers of tumour aggressiveness but studies are lacking in elaborating on specific tumour types and with long term follow-up for survival. Medulloblastomas (MB) are the most common malignant brain tumours of childhood and in this study we investigate whether MRS metabolite profiles can identify prognostic subgroups of this tumour.

Patients and Methods
Single voxel MRS (1.5 T, TE 30ms, TR 1500ms) was performed on 17 children with localised MB prior to treatment; patients were followed-up for a median of 3 years, 6 had died by the end of the study period. MRS was analysed using TARQUIN to provide metabolite concentrations. Principal component and linear discriminant analysis (PCA-LDA) were employed to determine metabolite profiles for good and poor prognosis groups. Kaplan Meier survival curves were constructed and pairwise correlation analysis (Pearson's) performed on metabolite values.

Results
Metabolite profiles defined good and poor prognosis groups with 9/9 and 2/8 being alive at the end of the study, respectively. There was a significant difference in Kaplan Meier survival between the two groups (log rank test, p=0.03). The poor prognosis group had a higher tumour lipid/choline ratio (t-test, p = 0.03). Citrate levels correlated positively with glutamate+glutamine levels (Pearson's correlation analysis p=0.001) in the good prognosis group but not in the poor prognosis group (p=0.5).

Conclusions
MRS metabolite profiles can be constructed that correspond to good and poor prognosis groups for MB, improving our understanding of these tumours and potentially allowing treatment to be refined.

RA-15.

NON-INVASIVE MOLECULAR CHARACTERISATION OF MEDULLOBLASTOMAS IN CHILDREN

RA-15.

NON-INVASIVE MOLECULAR CHARACTERISATION OF MEDULLOBLASTOMAS IN CHILDREN

Simrandip K. Gill,[1] Martin Wilson,[1] Nigel P. Davies,[1] Lesley MacPherson,[2] Theodoros N. Arvanitis,[1] and Andrew C. Peet[1]

Abstract

INTRODUCTION: Medulloblastomas (MBs) are highly aggressive tumours and not all patients with localised disease survive. Molecular markers from tumour tissue can define different prognostic groups and there is evidence that metabolism particularly related to glutamate could be important. This finding gives the opportunity to identify MB tumour subgroups non-invasively using magnetic resonance spectroscopy (MRS). In this study we investigate whether prognostic subgroups of M0 MB can be characterised by their MRS metabolite profiles. PATIENTS AND METHODS: Single voxel MRS (1.5 T, TE 30ms, TR 1500ms) was performed on 17 children with Chang stage M0 MB prior to treatment; patients were followed-up for a median of 3 years, 6 had died at the end of the study period. MRS data was analysed using TARQUIN software to provide metabolite concentrations and a combined principal component and linear discriminant analysis (PCA-LDA) used to determine metabolite profiles for good and poor prognostic groups. Kaplan Meier curves were constructed comparing these groups. Pair-wise correlation analysis (Pearson's) was performed on the metabolite values for the two groups. RESULTS: Metabolite profiles were constructed, which discriminated well between survivors and non-survivors with 9/9 and 2/8 being alive in the good and poor prognosis groups respectively. There was a significant difference in Kaplan Meier survival between the two groups (log rank test, $p = 0.03$). The poor prognosis group had a higher tumour lipid/choline ratio (t-test, $p = 0.03$). Citrate levels were correlated with glutamate + glutamine levels (Pearson's correlation analysis $p = 0.001$) in the group that demonstrated a better prognosis but not in the poor prognosis group ($p = 0.5$). CONCLUSIONS: Non-invasive MRS metabolite profiles can be constructed that correspond to good and poor prognosis groups for M0 MB. The biomarkers identified concur with previous findings from *in vitro* molecular profiling of MB and MRS studies.

PM057
NOVEL BIOMARKERS OF PROGNOSIS FOR MEDULLOBLASTOMA USING
1H MAGNETIC RESONANCE SPECTROSCOPY

Simrandip Kaur Gill 1,2, Martin Wilson1,2, Nigel P. Davies 1,2,3, Lesley Macpherson4,
Theodoros N. Arvanitis 2,5, Andrew C. Peet 1,2
1 Cancer Sciences, University of Birmingham; 2 Birmingham Children's Hospital; 3 Medical
Imaging and Physics, University Hospital Birmingham; 4Radiology, Birmingham Children's
Hospital; 5 Electrical, Electronic and Computer Engineering, University of Birmingham,
Birmingham, UK

Purpose: Magnetic resonance spectroscopy (MRS) is known to provide non-invasive biomarkers of tumour aggressiveness but studies are lacking in elaborating on specific tumour types and with long term follow-up for survival. Medulloblastomas (MB) are the most common malignant brain tumours of childhood and in this study we investigate whether MRS metabolite profiles can identify prognostic biomarkers of this tumour.

Methods: Single voxel MRS (1.5 T, TE 30ms, TR 1500 ms) was performed on 36 children with MB prior to treatment; patients were followed-up for a median of 4 years and 15 had died by the end of the study period. MRS was analysed using TARQUIN software to provide metabolite concentrations. Wilcoxon signed rank test analysis was used to compare metabolite profiles of those MBs currently alive compared with those that progressed and died and Cox regression analysis with overall survival was used to test each metabolite. Kaplan Meier curves were then constructed of those metabolites that demonstrated significance in the Cox regression analysis.

Results: The poor prognosis group demonstrated lower levels of Creatine (Cr) (Wilcoxon signed rank test, p=0.003) and near significant lower levels of total choline (tCho) (p=0.06). Cox regression analysis also demonstrated only Cr and tCho to be significant with a lower hazard for those subjects with higher values. Kaplan Meier curves demonstrated significant differences in survival for both Cr (p=0.001) and tCho (p=0.01).

Conclusion: Cr and tCho have been demonstrated as biomarkers of good prognosis and this may be useful for strategising treatment in MBs. The validation of these biomarkers with biological information is warranted.